Capillary Electrophoresis - Mass Spectrometry for Bioanalysis

Gleb Mironov

Thesis submitted to the
Faculty of Graduate and Postdoctoral Studies
in partial fulfillment of the requirements
for the Doctorate in Philosophy degree in Biology

Department of Biology
Faculty of Science
University of Ottawa,

Abstract

Bioanalysis is a subdivision of analytical chemistry and deals with biological analytes such as metabolites, proteins, nucleic acids, small molecules, virus particles and entire cells. The rationale of my thesis was to achieve two goals: (i) develop a set of ready to use methods (ii) which are capable providing exact concentrations of analytes as well as kinetic and thermodynamic parameters of their interactions.

CE-MS establishes a new paradigm that separation methods together with MS detection can be used as comprehensive kinetic tools. Most previous attempts to use chromatography and electrophoresis for studying nucleic acid interactions were restricted to assuming slow or no equilibrium between reactants. Kinetic CE (KCE) shows that non-zero kinetics and structural dynamics must be taken into account when separation happens. KCE-MS could be a valuable supplement to IM-MS due to the separation of ions in solution according to their size-to-charge ratio.

For the best of my knowledge, kinetic parameters for TG2 and thrombin G-quadruplex folding were reported for the first time. I developed a homogeneous method to determine k_{on}, k_{off} and K_d of fast and weak noncovalent interactions between multiple unlabeled ligands (small molecule drugs) and an oligosaccharide (α- or β-cyclodextrin) simultaneously in one capillary microreactor. It has been shown for the first time that KCE can be used to separate and detect the slowly interconverting open and closed conformations of human TG2. It allowed the first direct measurement of the K_d value for calcium binding. Sixteen new substrates were discovered for three aminotransferases (AAT, BCAT, and DAAT). In addition, Viral qCE showed a feasibility to analyse both the count of intact viral particles and sample nucleic acid contamination.

Acknowledgements

The University of Ottawa has an outstanding support team which makes all the magic possible at the very foundation of scientific research – sustaining a lab, as premises and a part of a large organization, functioning. My special gratitude to members of the Science store, machine and electronic shops

I came to Canada in 2010 to do PhD at the Berezovski lab and its members were the first people I communicated with. Among them are two very special human beings, Dr. Nasrin Khan and Dr. Victor Okhonin, who not only were my colleagues but also supported me outside workplace and helped accommodate myself to a new life. I'm glad I met many people working at Berezovski lab:

Dr. Anna Zamay, Galina Zamay, Vasilyi Mezko, Ana Gargaun, Jennifer Logie, Oguzcan Koyuturk, Shahrokh Ghobadloo, Pavel Milman, Nadia Al-Youssef,

It was my pleasure to work with the Keillor group, especially with Dr. Jeffrey Keillor and Dr. Christopher Clothier, and the Mayer group. I would like to thank Dr. Paul Mayer for all his kind support.

Two more people played a huge role in my PhD carrier: Alex Mungham and Justin Renaud. Their care and natural kindness were a constant stimulus for me to live and work.

Dr. Maxim Berezovski has been my supervisor for five years and truly deserves to be called the Teacher. Many aspects of proper lab-work management and experimental design I learned from him. I am very grateful for a chance to work under his supervision and sincerely appreciate his support and understanding.

Last but not least, I would like to say thanks to my landlord's dog, Bella, for her truly unconditional love and an exceptional ability to listen without judging.

Dedication

I dedicate this work to brave people of the first human colony on Mars.

Table of Contents

List of figures

List of tables

Abbreviations

AAT – aspartate aminotransferase

ACE – affinity capillary electrophoresis

BCA – bicinchoninic acid assay

BCAT – branched-chain amino acid aminotransferase

C – complex

CCS – collision cross section

CD – circular dichroism

CDs – β-cyclodextrins

CE – capillary electrophoresis

CIEF – capillary isoelectric focusing

CITP – capillary isotachophoresis

CZE – capillary zone electrophoresis

DAAT – D-amino acid aminotransferase

DFT – Density functional theory

DIMS – direct infusion mass spectrometry

ECEEM – equilibrium capillary electrophoresis of equilibrium mixtures

ELISA – enzyme-linked immunosorbent assay

EM – equilibrium mixture

EPR – electron paramagnetic resonance

ESI – electrospray ionization

FFA – fluorescent focus assay

FRET – Förster resonance energy transfer

GDH – L-glutamate dehydrogenase

GM-CSF – granulocyte macrophage colony-stimulating factor

GQ – G-quadruplex

HPLC – high performance liquid chromatography

HSV – herpes simplex virus

IM – ion mobility

KCE – kinetic capillary electrophoresis

L – ligand

LEKC – called liposome electrokinetic chromatography

LIF – laser induced fluorescence

MALDI – matrix-assisted laser desorption/ionization

MEEKC – micro emulsion electrokinetic chromatography

MEKC – micellar electrokinetic chromatography

MINISEP-MS – multiple interfluent nanoinjections–incubation–separation–enzyme profiling using mass spectrometry

MS – mass spectrometry

NECEEM – non-equilibrium capillary electrophoresis of equilibrium mixtures

NMR – nuclear magnetic resonance spectroscopy

nPAGE – native polyacrylamide gel electrophoresis

OV – oncolytic virus

PDA – photo diode array

pfu – plaque forming units

qCE – quantitative capillary electrophoresis

qPCR – quantitative PCR

RF – radio frequency

RRA – relative residual activity

RRKM – Rice–Ramsperger–Kassel–Marcus

SAXS – small-angle X-ray scattering

SM – small molecule

SPR – surface plasmon resonance

T – target

TBA – thrombin binding aptamer

$TCID_{50}$ – 50% Tissue Culture Infective Dose

TDLFP – transverse diffusion of laminar flow profiles

TEM – transmission electron microscopy

TG2 – human tissue transglutaminase

TOF – time of flight

UTR – untranslated region

UV – ultra violet

VSV vesicular stomatitis virus strain

VV – vaccinia virus

Chapter 1: Introduction

1.1. Capillary electrophoresis

Electrophoresis is an electrokinetic phenomenon which constitutes of the motion of charged species/particles relatively to a medium fluid when a uniformed electric field is applied. In an electrolytic cell positively charged particles (cations) move to a cathode and negatively charged particles (anions) move to an anode. There are several well-known applications of electrophoresis such as nucleic acid and protein gel electrophoresis, Western blot. Nowadays electrokinetic separation is not limited to "gel-stations" and can be performed in small nano- to micrometer channels; this technique was aptly named capillary electrophoresis (CE) [1].

There are several modes of CE, each designed for a specific task. The most widely used technique is capillary zone electrophoresis (CZE), which is basically a classic CE mode in a blank buffer. To analyze diluted samples capillary isotachophoresis (CITP), which preconcentrates analytes first, can be used. Another technique is capillary isoelectric focusing (CIEF), which utilizes a pH gradient, created by a mixture of ampholytes in the capillary, to separate analytes according to their isoelectric point and is usually applied to separate protein. In gel CE (GCE), a separation capillary is filled with a modified buffer containing dissolved polymers or a gel; this approach was previously widely used for nucleic acid sequencing. Non-ionic analytes can be separated in CE with the help of liposomes, micelles or emulsions, these techniques are called liposome electrokinetic chromatography (LEKC), micellar electrokinetic chromatography (MEKC), and micro emulsion electrokinetic chromatography (MEEKC), respectively[2]. Affinity CE (ACE) is used

to separate analytes which have different affinities to a target molecule added to the separation buffer [3]. In my work I utilized CZE and ACE.

A typical CE setup (**Figure 1.1**) consists of a fused silica capillary (inner diameter 10-100 µM, outer diameter 150-400 µM), two buffer reservoirs for inlet and outlet ends of the capillary, a high voltage power supply (usually 5-30 kV) with electrodes, and a detector (usually photo diode array (PDA), UV absorption (UV) or laser induced fluorescence (LIF)). Initially a sample is introduced in the capillary electrokinetically (by voltage) or hydrodynamicly (by pressure) and then high voltage (usually 100-300 V/cm) is applied to perform separation of analytes.

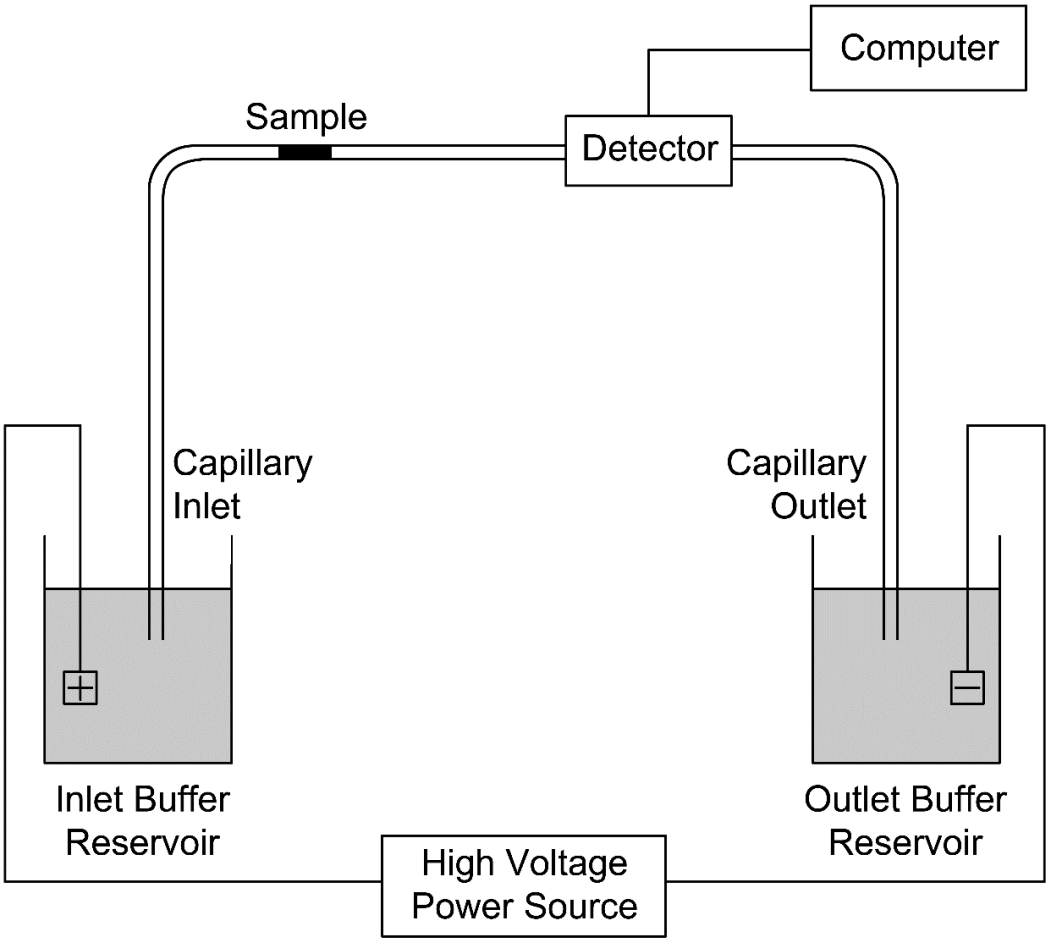

Figure 1.1. Schematic representation of a basic capillary electrophoresis setup.

High voltage causes a bulk flow of separation liquid, electroosmotic flow (EOF), in the separation capillary. This phenomenon is best explained by the release of hydrogen ions (H^+) from silanol groups (SiOH) at capillary walls (**Figure 1.2**) which makes the walls negatively charged. The hydrogen ions and other cations create two layers along the negatively charged walls. The first layer forms an electrical double-layer with the capillary walls and is semi-permanently attached, the second layer of cations is mobile and starts moving towards a cathode driven by Coulombic force and creates a drag force along the walls sustaining a bulk flow of liquid in the capillary[1]. This bulk flow has a uniformed profile in the capillary as opposed to a laminar flow created by a pressure differential **(Figure 1.3**). Because of the silanol deprotonation dependence of EOF, it is practically suppressed at pH's around 2-3 and increases with increasing pH. Adjustment of pH is one way of controlling EOF. Ionic strength of a separation buffer can also influence EOF due to the fact that high concentrations of ions decrease zeta potential (ζ), as in equation 1.1:

$$V_{EOF} = (\varepsilon\zeta/\eta)E \qquad (1.1)$$

Where V_{EOF} is the velocity of EOF, ε is dielectric constant, ζ is zeta potential, η is vescosity and E is applied electric field.

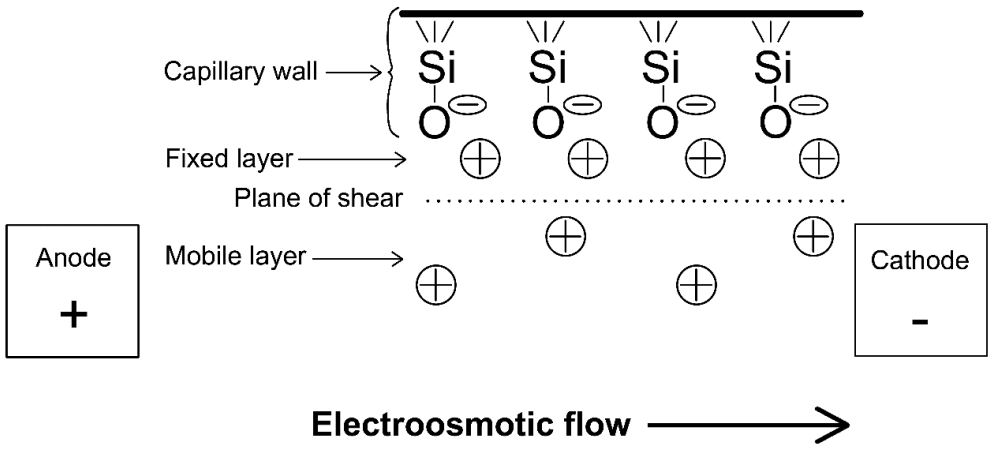

Figure 1.2. Schematic representation of EOF in a capillary. Si-O- represents a fixed layer; positively charged particles next to it represent a mobile layer which creates a bulk flow of liquid.

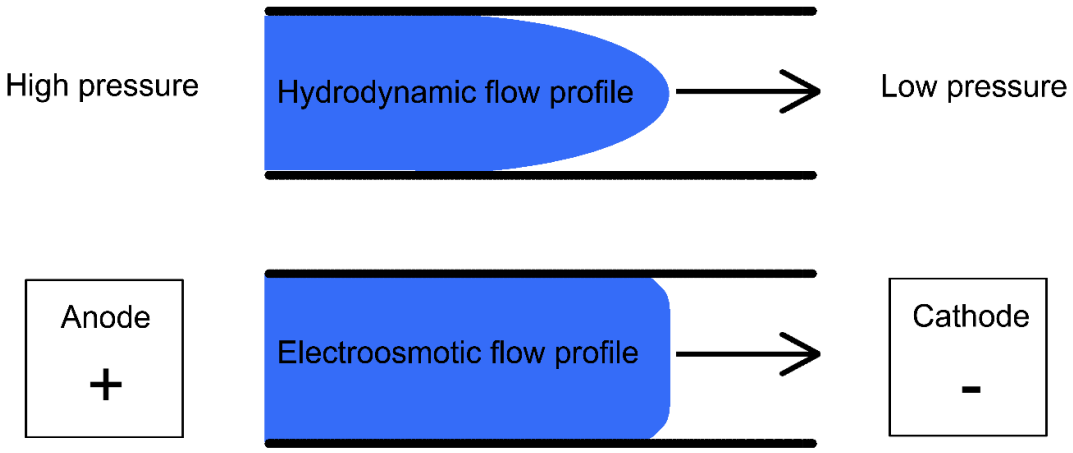

Figure 1.3. Difference in flow profiles between pressure-assisted laminar flow (upper capillary) and EOF (lower capillary).

In electrophoresis ions are separated based on their velocity (V), as in equation 1.2:

$$V = \mu_e E \tag{1.2}$$

Where μ_e is electrophoretic mobility, E is applied electric field. The mobility is determined by the ratio of electric force and drag force exerted on the particle, as in equation 1.3:

$$\mu_e \alpha = \frac{Electric\ force\ (F_E)}{Frictional\ force\ (F_F)} \tag{1.3}$$

The electric force is proportional to ion's charge (q), as in equation 1.4:

$$F_E = qE \tag{1.4}$$

The frictional force for spherical ion is proportional to its radius (r), ion velocity (V) and solution viscosity (η), as in equation 1.5:

$$F_F = -6\,\pi\,\eta\,r\,V \tag{1.5}$$

From these equations it can be concluded that in electrophoresis the slowest ions are bulky slightly charged and the fastest ions are small and highly charged.

At pH above 4, the magnitude of EOF is usually stronger than electrophoretic mobilities of analytes and it makes both cations and anions to move towards the cathode but with different velocities (**Figure 1.4**). For a smaller and more highly charged anion it is easier to resist EOF, making it to move slower, and a smaller and more highly charged cation is capable of outstriping EOF, moving faster.

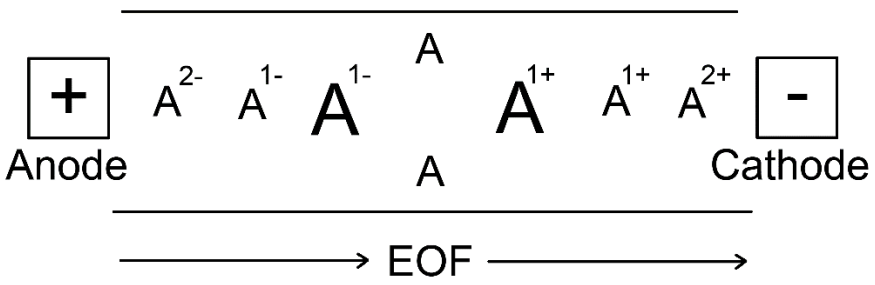

Figure 1.4. Schematic representations of analytes movement in CE base on their charge and size.

1.2. Mass spectrometry

1.2.1 Electrospray ionization

To be analyzed by mass spectrometry, molecules of interest first must be ionized and then introduced into a mass analyzer. After ionization occurres, mass spectrometry deals with ions based on their mass-to-charge ratios and abundances. It can be said that initial ionization is the key component because it determines the nature of ion-analysis techniques which may be applicable and best suitable. Two most common ionization techniques used in life-science related laboratories are matrix-assisted laser desorption/ionization (MALDI) and electrospray ionization (ESI)[4]. MALDI usually deals with samples fixed in advance (cell layers, tissue preparations, proteins) on a special carrier matrix while ESI is best suitable for on-line analysis of liquid samples.

The electrospray phenomenon, which was first noted back in 1749 [5], occurs when a strong electric field is applied on liquid forcing it to form a fine aerosol (**Figure 1.5**). A typical ESI-MS setup consists of a power supply (1-5 kV) for a sample capillary, additional

capillaries to facilitate spray formation (**Figure 1.6**) and a sample cone leading to a mass analyzer. The sequence of events can be divided into three consecutive steps:

1) Nebulization[6-8]. Initially, at low voltage a solvent drop appears spherical, then, as voltage increases, charges accumulated at the tip of the drop force the drop to elongate and form a "Taylor cone". Nebulization occurs when the electric potential applied to the sprayer capillary exceeds the surface tension of the solvent (for water = 0.073 Nm^{-2}, for methanol = 0.023 Nm^{-2}).

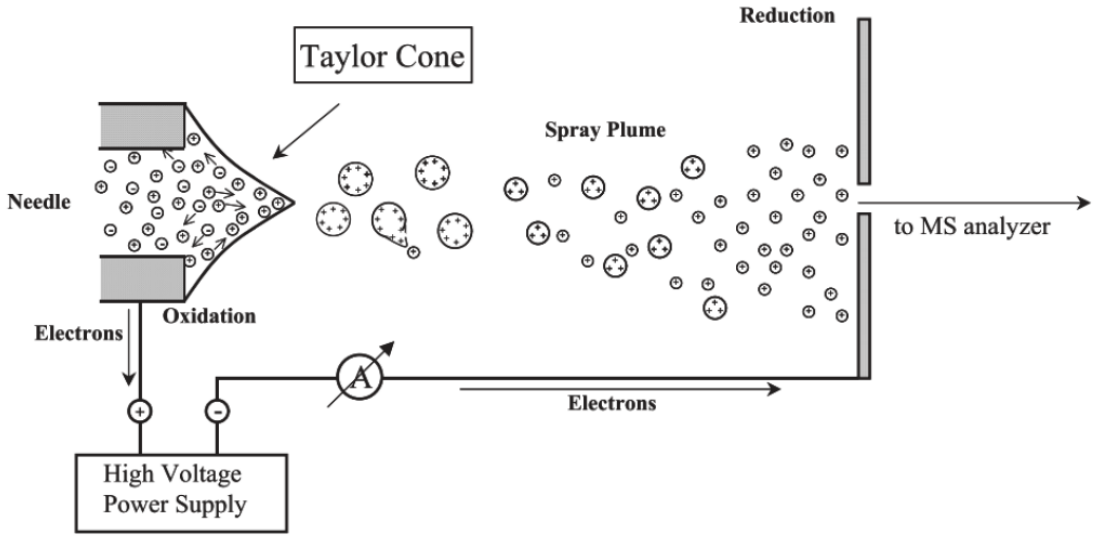

Figure 1.5. Schematic representation of ESI process. Parent droplets are formed from Taylor cone. Printed with permission of Justin Renaud, copyright Justin Renaud, 2014.

2) Droplet charging and disintegration. ESI source can be considered as a special case of an electrolytic cell[9], this electrolytic nature explains why cations (for positive mode) are accumulated at the tip of a "Taylor cone" and then are transferred to parent droplets. After a parent droplet separates from the liquid front, it starts to evaporate and shrink in size increasing electric repulsion between cations. In

addition, droplets experience shear forces while they fly throw dense gas. Both these effects cause a droplet to deform which creates an excessive electric field in the protrusion region. When deformation and Coulomb repulsion exceed the surface tension of liquid, the disintegration of a parent droplet occurs producing offspring droplets (**Figure 1.6**)[10, 11]. The process is identical for negative mode when anions are transferred into droplets.

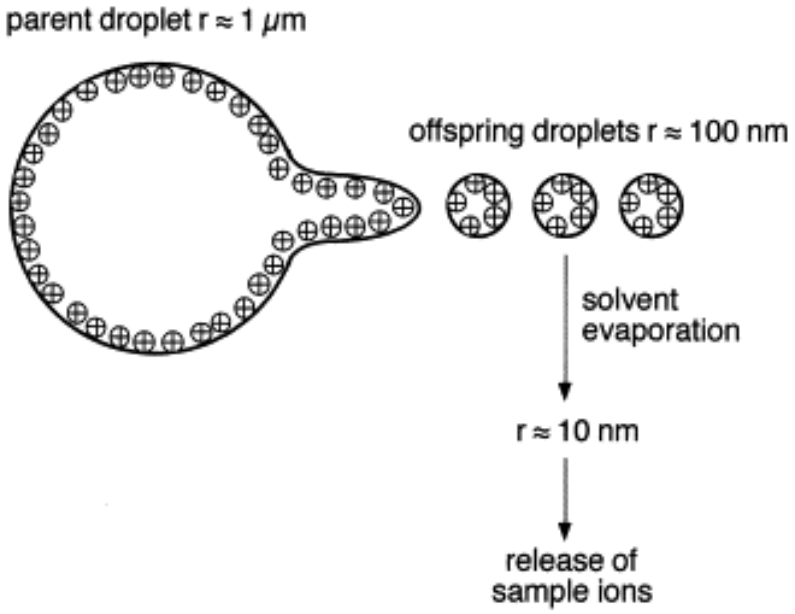

Figure 1.6. Schematic representation of droplet disintegration. Electric field causes a protrusion on a parent droplet which later forms a daughter droplet. Reprinted by permission from Elsevier, Journal of Chromatography A [12], copyright (1998).

3) Ion emission from droplets. There are two main theories how ion emission occur: ions can be emitted directly into gas phase[13], small nano-droplet can evaporate releasing ions inside of them[14]. It is highly likely that both processes co-occur.

With the development of ESI, several techniques were introduced to increase ESI efficiency and stability (**Figure 1.7**). Usually sheath liquid, sheath gas or both are introduced simultaneously with a sample.

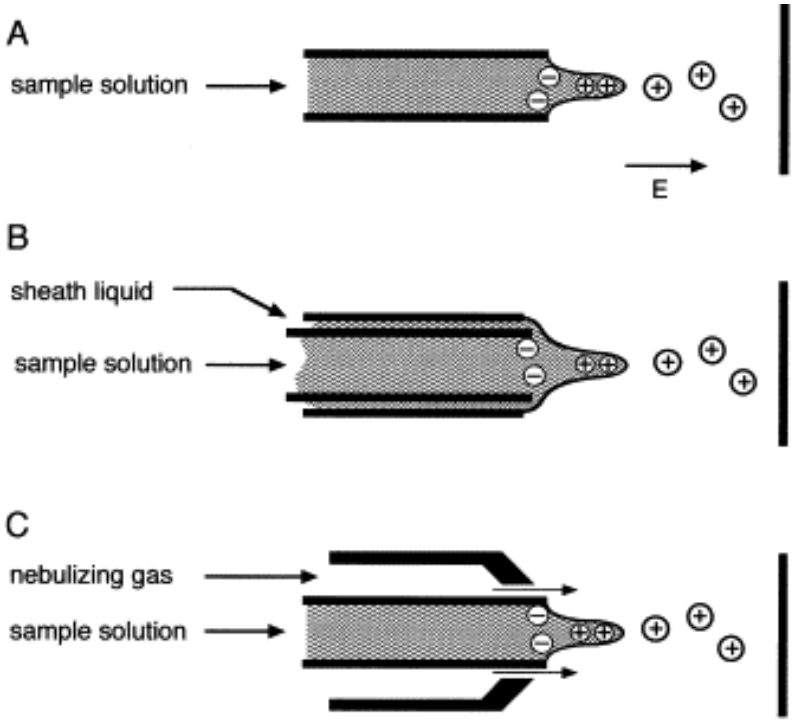

Figure 1.7. Schematic representation of ESI process. (A) Non-assisted ESI, (B) Sheath liquid-assisted ESI, (C) Pneumatically-assisted ESI. Reprinted by permission from Elsevier, Journal of Chromatography A [12], copyright (1998).

There are no strict rules on ionization efficiency for small molecules, nucleic acids, and proteins. Some general trends do exist and can be used as a guidance. Small molecules usually have a linear response in a nano- to micromolar range of concentrations and can be ionized into cations or anions depending on their structure and working pH. Proteins are usually more prone to produce cations while nucleic acids – anions. The linearity of MS response for large molecules varies greatly and severely depends on the matrix (separation buffer for CE) used in an experiment.

1.2.2 Mass analysis

After analytes undergo ionization, they need to be separated or "analyzed" according to their physical properties. In MS, mass analyzers are devices which are capable of separating ions based on their mass-to-charge ratio (m/z). It is important to note that it is not the mass of an ion which makes it unique for a mass analyzer but its mass-to-charge ratio, which can be identical for different ions possessing different masses (though there are ways to overcome this obstacle, e.g. distinguish singly charged monomers from doubly charged dimers, using isotopic distribution of analytes). Two mass analyzers were used in this study, each with its distinct features: the quadrupole and time of flight (TOF).

The quadrupole is a mass analyzer made of four parallel rods (**Figure 1.8**). Rods are arranged in pairs, one pair receives negative direct potential and radio frequency (RF) voltage on top of it, another pair receives positive direct potential and RF voltage as well. Usually direct potential magnitude is between 500 and 2000 V and RF between -3000 to +3000. As a result, both pair have direct and RF potentials and it's their superposition which makes the quadrupole work:

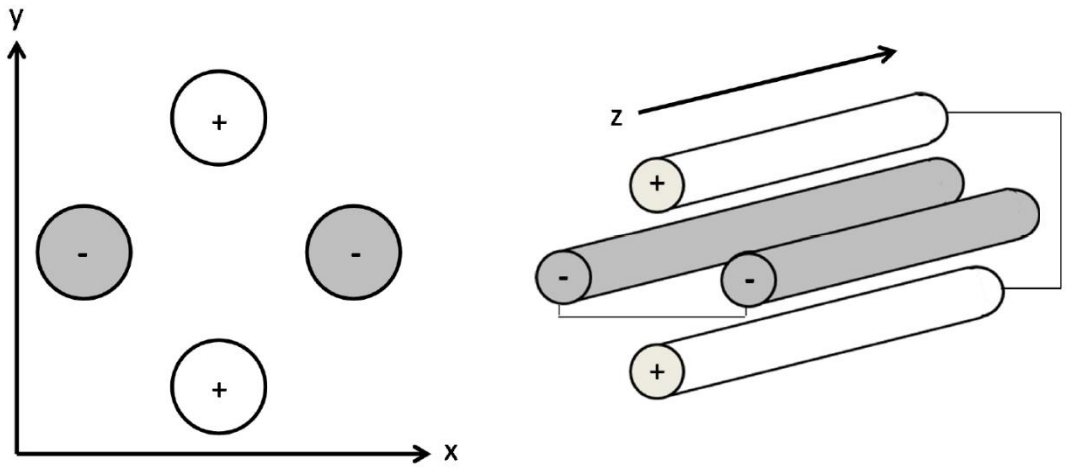

Figure 1.8. Schematic representation of a quadrupole mass analyzer. Positive and negative electrodes are mark as "+" and "-", respectively. Printed with the permission of Justin Renaud, copyright Justin Renaud, 2014.

$$\frac{d^2x}{dt^2} + \frac{2c}{mr_0^2}(U - V\ \cos\omega t)x = 0 \qquad (1.6)$$

$$\frac{d^2y}{dt^2} - \frac{2c}{mr_0^2}(U - V\ \cos\omega t)x = 0 \qquad (1.7)$$

Where x and y are x and y coordinates; m and c are the mass and charge of the ion, respectively; ω is the RF angular frequency; U is the magnitude of the direct potential; V is the magnitude of the RF potential; r_0 is the distance from the center of the axis to the surface of the rod (the trajectory of the ion is stable when the values of x and y never reach r_0, i. e. the ion never collides with the rod).

In principle, the quadrupole is a double filter: ions with m/z above a specified range are lost due to poor focusing, while ions with m/z below a specified range are propelled into unstable trajectories, thus only ions in the specified range are transmitted through the quadrupole. For cations, negative rods work as a high mass filter, they stabilize

trajectories of ions with m/z above a set value I (lower boundary) while destabilize trajectories of lower m/z. On the other hand, positive rods work as a low mass filter, they destabilize the trajectories of ions with m/z above a set value II (higher boundary). This double filtering phenomena is achieved by the superposition of direct and RF voltages[15].

Time of Flight (TOF) mass analyzers were initially described in 1946 by Stephens [16] and since then underwent numerous improvements such as the reflectron and orthogonal acceleration [17]. This type of analyzer separates ions by accelerating them with an electric field and then measuring how fast they reach a detector through a flight tube.

During acceleration, electric potential energy (E) of the ion is converted into kinetic energy (K):

$$E = qV = zeV = \frac{mv^2}{2} = K \tag{1.8}$$

where q is the total charge of the ion (ze), m is the mass of the ion, V is the accelerating potential.

Given the distance to the detector, L and time to reach the detector, t, the equation can be rearranged:

$$v = \sqrt{\frac{2qV}{m}} = \sqrt{\frac{2zeV}{m}} = \frac{L}{t} \tag{1.9}$$

And mass to charge ratio of the ion can be derived from its travel time to detector:

$$\frac{m}{z} = 2eV\,\frac{t^2}{L^2} \tag{1.10}$$

Generally speaking, the large the flight tube's length (larger L), the longer it takes for ions to reach the detector and higher is the resolution because ions are separated for a more extended period of time. Instead of utilizing very long flight tubes, many mass spectrometers rely on reflectrons which send or "reflect" ions into parabolic pathways ("V" or "W") as shown on **Figure 1.9**[15].

It is crucial to note that a mass analyzer and a detector are two separate devices. Basically speaking, a detector for quadrupole and TOF mass spectrometers is not capable of distinguishing ions with different m/z but works in tandem with an MS analyzer which spatially separates ions before they hit or excite the detector accepting or donating electrons. The detector then generates an electric current that is proportional to the ion's abundance. It can be simplified for the sake of comprehension that, ultimately, a mass spectrometer is a very sophisticated ammeter which measures the electrical current generated by each particular m/z ion.

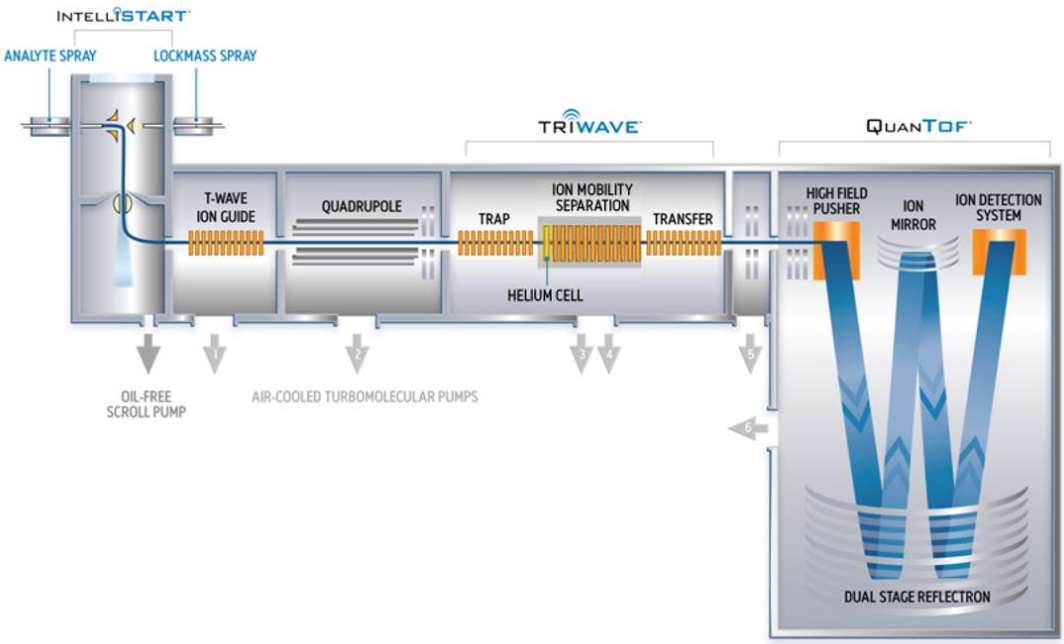

Figure 1.9. Waters Synapt G2 mass spectrometer. Courtesy of Waters Corporation, copyright Waters Corporation, 2010.

The instrument used for this thesis, Waters Synapt G2, is a hybrid mass spectrometer that utilizes two mass analyzers: the quadrupole and the TOF, with an ion mobility separation chamber between them which will be described next.

1.2.3 Ion mobility spectrometry

In principles, ion mobility separation (IMS) is very similar to separation in CE. In both techniques, an electric field creates a propelling force which moves ions through a separation fluid (liquid – in CE, gas – in IMS). It can be approximated that in CE ion mobility is proportional to charge to size ratio,

$$Mobility\ in\ CE\ \propto \frac{charge}{size} \tag{1.11}$$

while in IMS, ion mobility is proportional to charge to mass times collisional cross section (CCS),

$$Mobility\ in\ IMS \propto \frac{charge}{mass * CCS} \tag{1.12}$$

The key difference is that in CE mobility represents an apparent mobility of a moving analyte which exists in multiple co-migrating differently charged states, while in IMS mobility is assigned to an ion with a specific charge.

In more precise terms, ion mobility in IMS (K) is defined as a proportionality factor of an ion's drift velocity through a drift tube (**Figure 1.10**), V, and applied electric field of strength E,

$$K = \frac{V}{E} \tag{1.13}$$

In classical drift tubes, uniform, static, electric field is applied to move ions through a gas phase. For this type of IMS, CCS (Ω) can be calculated quite precisely[18]:

$$\Omega = \frac{3z}{16N}\left[\frac{2\pi}{\mu k_b T}\right]^{0.5}\frac{1}{K_0} \tag{1.14}$$

where N is the background gas number density, z the ionic charge, μ the reduced mass of the ion–neutral pair, k_b is Boltzmann's Constant, T the gas temperature and K_0 is the reduced mobility (=measured mobility corrected to 273.2 K and 760 Torr).

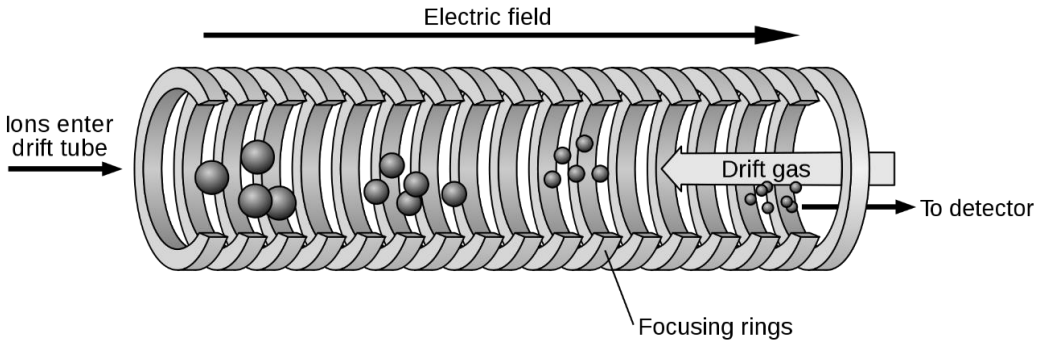

Figure 1.10. Principles of ion mobility drift tube. Reprinted with permission from Jeff Dahl under GNU Free Documentation License, copyright (2009).

In experiments performed for the thesis, traveling wave ion mobility spectroscopy (TWIMS) was used. This technique is available on commercial Waters instruments and is

different in its principles to IMS in classic drift tubes. Instead of a constant uniform electric field, a number of RF electric pulses are applied through a series of electrodes. Adjacent electrodes receive opposite RF voltages and create a radially confined effective potential barrier (**Figure 1.11**). This potential barrier propagates from one pair of electrodes to the next one carrying ions through the IMS chamber[18].

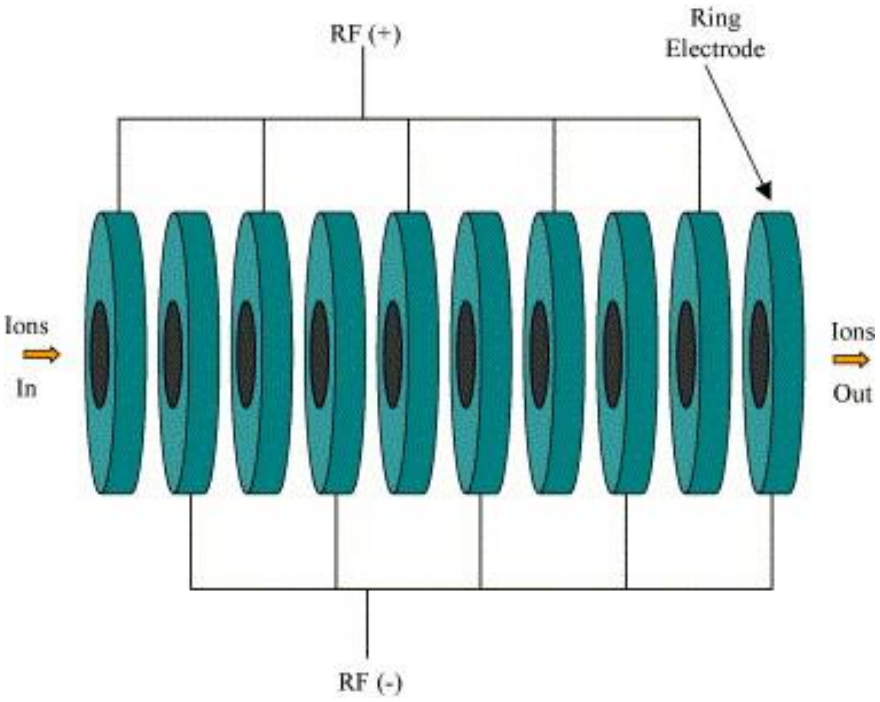

Figure 1.11. TWIMS ion guides. Reprinted by permission from Elsevier, International Journal of Mass Spectrometry[19], copyright (2007).

From my point of view, the difference between a classic drift tube (constant direct potential) and TWIMS (RF potential) can be illustrated by a "ship and wind" analogy. Ships (ions) can be moved by a constant unidirectional wind (constant direct potential) and small ships (ions with low m/z and CCS values) will move faster than large ships (ions with high m/z and CCS values) – this is a classic drift tube. On the other hand, ships can be moved by a series of wind puffs, then not only small ships will move faster they also will

be more responsive to the wind puffs compare to large ships which, due to their inertia, can even miss a puff or two and start to lag behind very soon. At the end of the day all ships will reach the opposite shore but it will take a larger distance and longer time to separate ships of different size by the constant wind than by wind puffs.

TWIMS has an advantage compare to most drift tubes: it can accumulate and radially confine ions increasing the sensitivity of a mass spectrometer[19].

To have a clearer picture about IMS I suggest to watch this very good animation (https://www.youtube.com/watch?v=i_l2egLZ5lM), created by Waters Corporation, which illustrates the TWIMS process and its benefits.

1.3. Capillary electrophoresis - mass spectrometry

Capillary electrophoresis – mass spectrometry (CE-MS) was first introduced in 1987 and evolved from home-made simple devices to sophisticated automated machines. Nowadays sheath-less and sheath-liquid assisted interfaces [20] are commercially available and can be fitted to almost any ESI-MS. All regular CE modes described above can be used for CE-MS[21].

In CE-MS system utilized for this research a path of analytes can be described as following (**Figure 1.12**): first, analytes are separated in a liquid phase in the CE capillary, second, analytes are ionized by ESI (**Figure 1.13** and **Figure 1.14**) and enter a mass spectrometer, where only ions of a specific m/z range are transferred through the quadrupole and pushed into IMS chamber to be separated based on their m/z and CCS,

and finally, ions are analyzed in a TOF tube, which provides a precise m/z number for each ion.

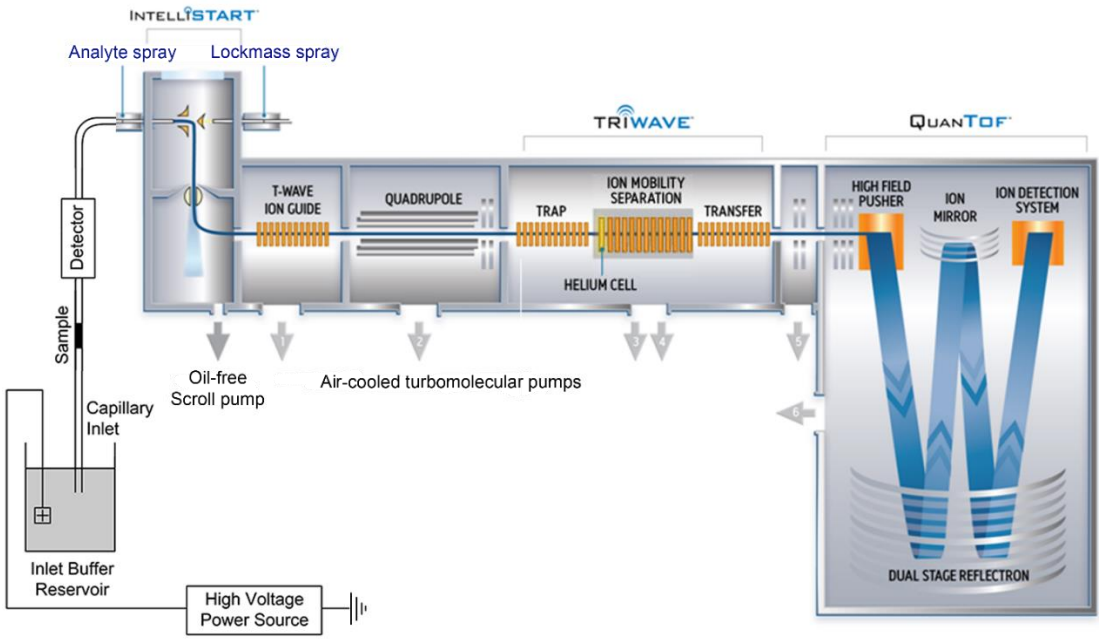

Figure 1.12. Schematic representation of Beckman PA800 plus – Waters Synapt G2, CE-MS, system. Modified from Waters Corporation. Copyright Waters Corporation, 2010.

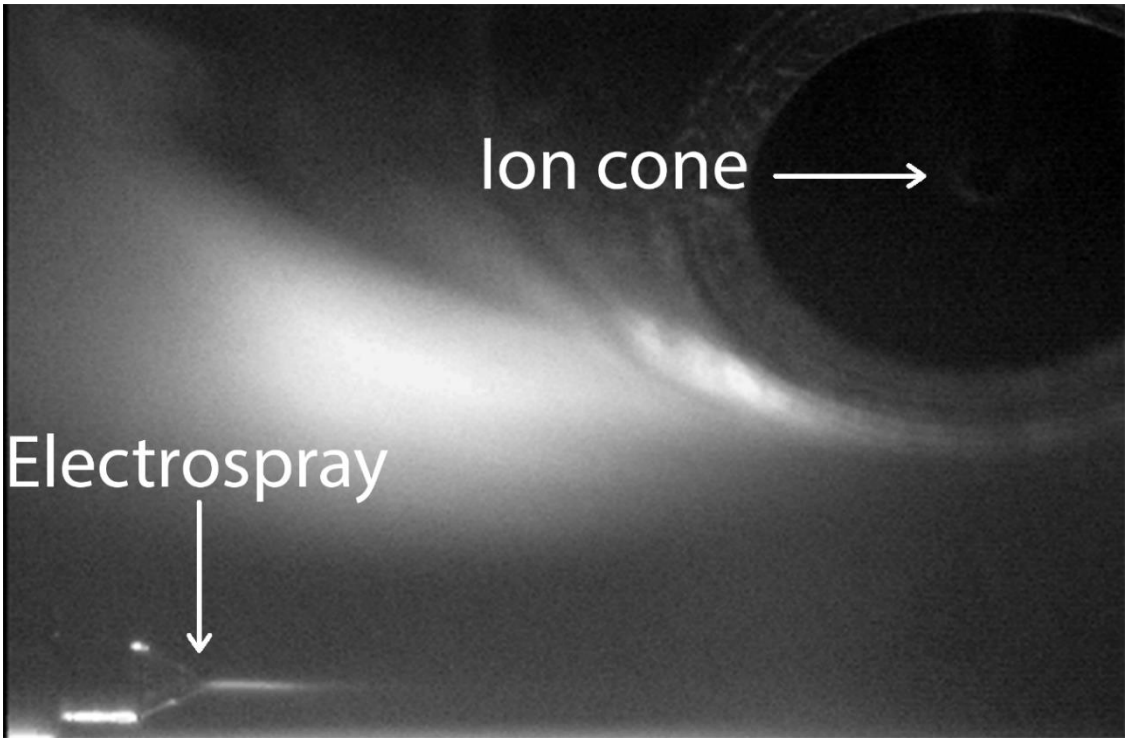

Figure 1.13. Real view of electrospray process. Bottom left – electrospray. Top right – ion extraction cone.

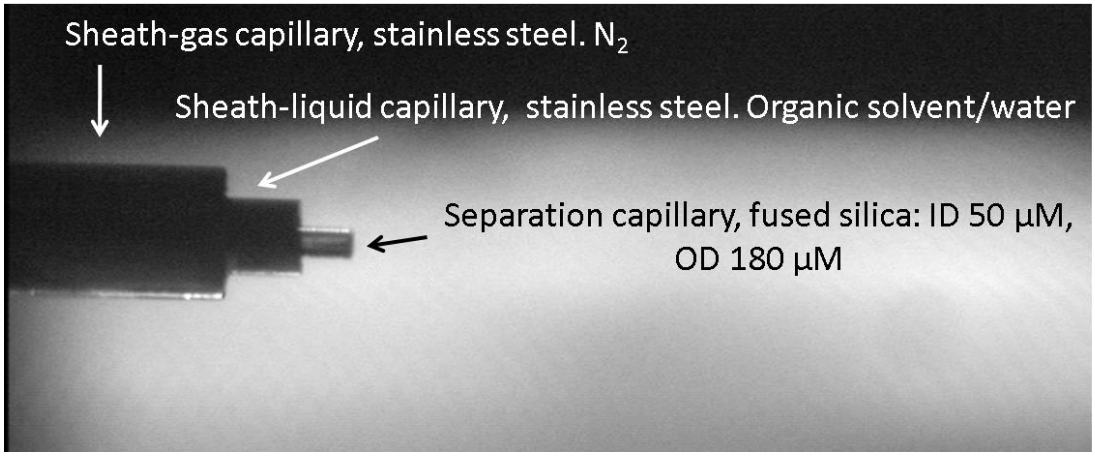

Figure 1.14. Real view of experimental ESI setup used in the thesis. ID – inner diameter, OD – outer diameter.

At this point two reasonable question may be asked. Why such a complicated path is necessary? Why not dissolve all analytes in an organic solvent and inject them with a

syringe into a mass spectrometer (i.e. DIMS)? Indeed, when a simple sample is to be analyzed for the presence of a compound of interest, DIMS can be sufficient, but a complex sample can contain isomers of the same compound which can't be resolved by MS alone. Separation before MS analysis is very often achieved by high performance liquid chromatography (HPLC). Unfortunately, it requires use of organic solvents for the liquid phase denaturing biomolecules and their complexes while the separation occurs between two phases (solid and liquid) making it hard to study interactions of bio-molecules. CE doesn't have these disadvantages: appropriate buffers can be used and the separation occurs in a single liquid phase. For CE-MS it can be said that it is not merely the fact that an analyte reached a detector matters but how it did it. **Figure 1.15** illustrates this concept. Analyzed separately, analytes A, B and C migrate in three non-overlapping bands. When the mixture of A and B is analyzed in the separation buffer containing C, only two bands can be observed. MS detection allows to track each compound separately. From MS data it is clear that the new band is a complex of B and C (it has mass of B+C and can be fragmented into daughter ions of mass B and C) and from CE data it can be concluded that B-C complex is not an ion adduct formed during ionization but a true complex which existed in the separation buffer and migrates with a velocity different from velocities of B and C. The shape of a peak also matters and will be discussed in detail in Chapter 3. More details on this subject will be provided later.

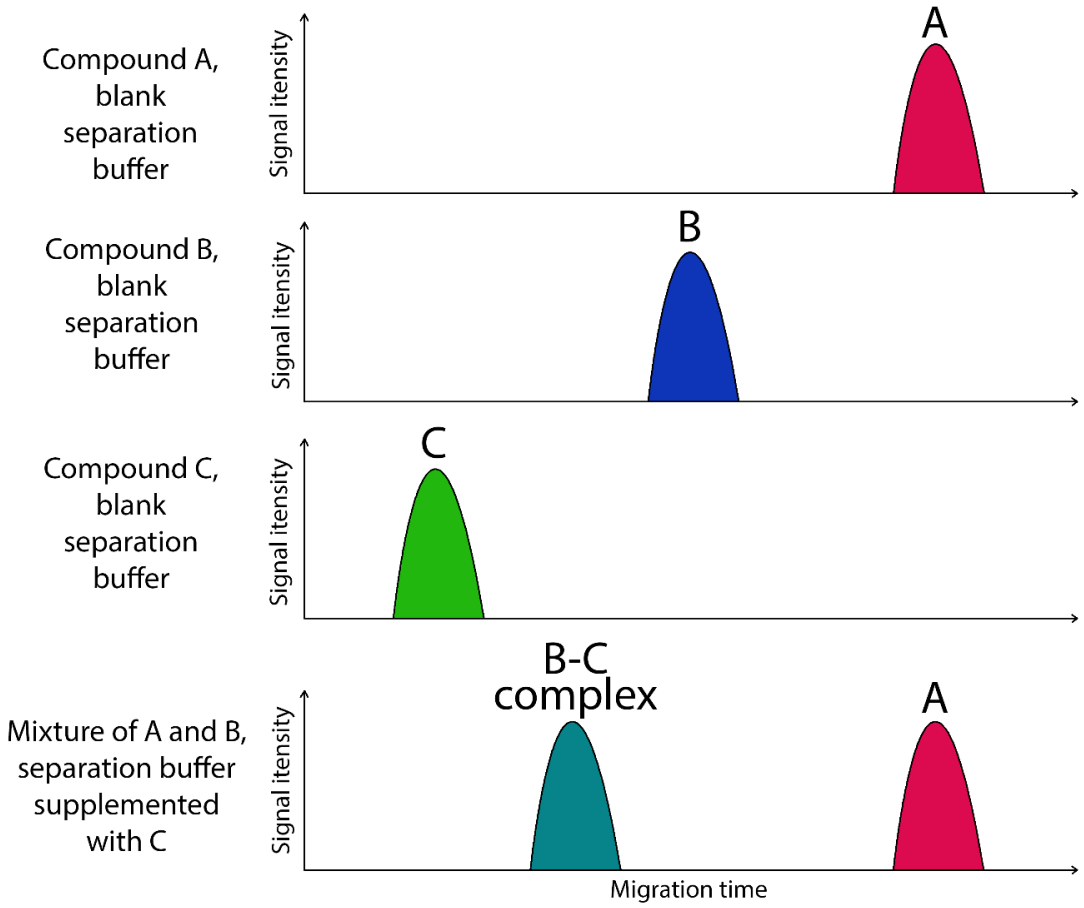

Figure 1.15. CE separation of analytes A, B, C and their mixture.

1.4. Non-covalent interactions and enzymatic activity

Non-covalent interactions, unlike covalent interactions, do not require the sharing of electrons and are sustained by the multitude of electromagnetic interactions between molecules and atoms. Two aspects of non-covalent interactions are worth to be mentioned: equilibrium distance and stabilization energy. Non-covalent interactions usually lie in the range of 1-20 kcal/mol with closest intersystem distances of 2 Å, while covalent bonds usually have binding energies around 100-200 kcal/mol and interatomic

distances of 1.5 Å. These intrinsic properties make non-covalent interactions sensitive to entropy changes, which is always negative for cluster formation[22].

Regarding the role of non-covalent interactions in bio-systems it can be speculated that life (not the life as a phenomenon in general but the life we are used to observe) would be impossible without non-covalent interactions due to the fact that the liquid state of water as well as the formation of a solution are sustained by non-covalent interactions. In more specific terms, non-covalent interactions play a crucial role in sustaining the 3D organisation of large species (proteins, nucleic acids, supramolecular clusters such as a lipid bilayer), specific recognition (antibody-antigen), enzymatic specificity, etc[22].

Non-covalent interactions can also be crudely classified as fast with lifetime in the seconds range (the beta-cyclodextrin-ibuprofen complex has a life time of 0.1 sec[23]) and slow with lifetime range in minutes and higher (antibody-lysozyme complex has a lifetime of 12 min[24]). Both types are important in biological systems and serve different functions.

The challenges of and methods for studying fast non-covalent interactions will be discussed in detail in Chapter 3.

Enzymes are biomolecules that catalyze chemical reactions. The increase in the rate of a reaction is achieved by lowering its activation energy. As conventional catalysts, enzymes do not change the equilibrium of chemical reactions and are not consumed in chemical reactions. To make an enzymatic reactions possible, the transition state of an enzyme-substrate complex is stabilized by noncovalent interactions between an enzyme

and its substrate. Once the reaction is over, the affinity of a product to an enzyme should decrease for the product to be released. This process is heavily dependent on noncovalent interactions which can alter the shape of an enzyme and vice versa[25, 26].

To characterize an enzyme, two constants are used very often: K_M and k_{cat}. K_M is the Michaelis-Menten constant, and shows the substrate concentration at which the enzyme reaches the one-half of its maximum reaction rate. k_{cat} is a turnover number which is the number of substrate molecules handled by one active site per second.

Challenges of studying enzymes include but are not limited to screening libraries of substrates, studying an enzyme transition from one conformation to another and linking its enzymatic activity to a particular conformation. Substrate screening can be difficult to perform if products are not easily detectable by UV or LIF, the screening process itself can be automated to increase the throughput of the analysis. Assigning enzymatic activity to a specific conformation is extremely difficult to perform if interconversion between conformations occurs during a reaction time. More details about specific aspects of enzymatic studies and accompanying challenges are provided in chapters 6 and 7.

1.5. Oncolytic viruses

Oncolytic viruses are a special kind of virus that can selectively infect and kill cancerous tissues while leaving healthy tissues unaffected[27]. The idea of using viruses for oncotherapy was devised from clinical reports cancer regression that occurred at the same time as natural viral infections[28]. Starting in the 1950s, oncolytic viruses were used to treat cancer in hundreds of patients with varying success. These early attempts can be

characterized by the employment of unpurified viruses and the investigation of acceptable administration routes[29]. One of the main issues of oncolytic virotherapy was the neutralization of viruses by the host immune system. Hence the most promising results were obtained in immunosuppressed patients[30]. The era of oncolytic virotherapy began in 1991 when virus genomes were modified to increase their antitumor specificity to murine glioblastoma cells by removing thymidine kinase gene from HSV[31]. Currently, oncolytic viruses are extensively genetically modified and thereby can exploit several tumour-specific abnormalities to improve the therapy: tumour specific receptors can be used for virus attachment and cell entry; active tumor-specific promoters and enhancers can be used to modulate the expression of viral genes; normal and tumour cells microRNAs profiles can be used to guide viral gene expression by inserting complimentary sequences in viral genomes; viral infection can attract immune system to target tumour-associated antigens (**Figure 1.16**). Every viral family has its unique properties which can be used to target a specific cancer type. Nowadays, there are oncolytic viruses from at least ten different families which are undergoing clinical trials[32].

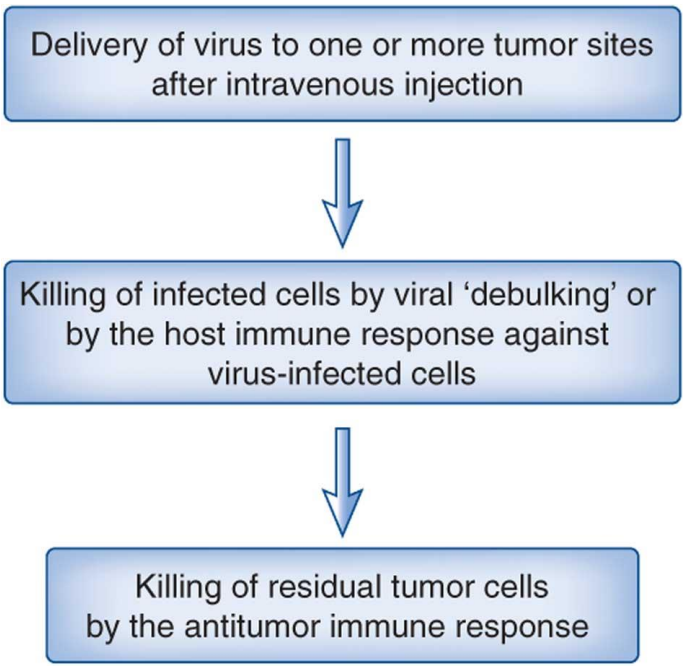

Figure 1.16. The oncolytic virotherapy paradigm. Reprinted by permission from Nature Publishing Group, Nature Biotechnology[32], copyright (2012).

Two important aspects of the oncolytic virotherapy are safety and efficiency. Overall, virotherapy has proved to be safe even at higher doses with minimal side effects[33]; but there are still concerns that oncolytic viruses can spread from a patient, mutate and regain its pathogenicity[34]. Possible negative outcomes are balanced by proved efficiency that can be illustrated by a notable example: adenovirus based Oncorine was approved for head and neck cancer in 2005 in China, Talimogene laherparepvec for melanoma successfully completed phase III trials in 2013, and JX-594 for hepatocellular carcinoma is in phase IIB clinical trials[35].

During phase 1 clinical trials one notable observation was made for vaccinia virus based vaccine, JX594 – the extravasation of oncolytic viruses from blood vessels to the tumor is concentration dependent with a concentration threshold above 10^9 infectious

units[36]. Therefore it is extremely important to monitor the concentration of virus preparations which will be used to make injection doses.

1.6. Challenges of bioanalysis

Bioanalysis is a subdivision of analytical chemistry. In the simplest form its task can be to quantify a single compound in a sample or each isomer of that compound. A more complicated task can be to quantify all analytes in a complex mixture or to investigate if one compound in that mixture can interact with another and if it can, if it is simple binding or an enzymatic reaction which converts a substrate into a product. Key questions of bioanalysis are: what are concentrations of analytes? What type of interactions is observed between analytes (covalent/non-covalent)? What are kinetic and thermodynamic parameters if these interactions?

To investigate interactions between biomolecules special conditions are required which do not interfere with the course if biomolecule interactions. Establishing these conditions and optimization of separation and detection parameters can be tedious and can take longer than actual analysis of samples. For CE key parameters include the choice of a separation buffer, its pH and ionic strength, and the composition of capillary walls. Walls can be left intact or coated to control EOF and the degree of interactions between analytes and capillary walls. It is also important to maintain an appropriate temperature to study biomolecules, e.g. for human enzymes it can be 37°C. The inner diameter of a separation capillary is important as well. Smaller diameters can increase separation efficiency but decrease the LOD. Another disadvantage of smaller diameter capillaries is that smaller is the diameter higher are chances for that capillary to be clogged.

On the MS side it is crucial to use a soft ionization technique which is capable of preserving non-covalent interactions but at the same type it should be strong enough to ionize large analytes such as proteins and nucleic acids. Optimal ionization of analytes and analysis of produced ions can be achieved by tuning capillary, sample cone and extraction cone voltages; the temperature of an ion source; cone, nano-flow and purge gas flows; CID voltage; ion mobility voltages and gas pressure.

The rationale of my thesis was to achieve two goals: (i) develop a set of ready to use methods (ii) which are capable of answering key questions of bioanalysis by providing exact concentrations of analytes as well as kinetic and thermodynamic parameters of their interactions.

1.7. Thesis outline

The research done for the thesis was performed with and relied on technical advances in capillary electrophoresis (CE) and mass spectrometry (MS) areas and the availability of fine-engineered instruments. The introduction, Chapter 1, shines light on the concepts of capillary electrophoresis (CE), mass spectrometry (MS), ion mobility separation (IMS), their coupling (CE-MS) and application for study of both fast non-covalent and covalent interactions and viral particles.

Chapters 2-7 are dedicated to the research done by me and my colleagues. To ease the transition from the introductory part to the experimental part of my thesis I would like to introduce the concept of oncolytic viruses and why their quantitative analysis is important for therapeutic applications at the end of the Introduction and from there

proceed to Chapter 2: Viral Quantitative Capillary Electrophoresis. Briefly, in the first article, Viral Quantitative Capillary Electrophoresis for Counting Intact Viruses, a method for quantitative analysis of a viral sample was developed that enabled measurement of the number of intact DNA virus particles and nucleic acid contamination, with a dynamic range of virus concentrations from 10^6 to 10^{12} ivp/mL and the sample consumption at 5 - 40 μL. In the second article, Viral Quantitative Capillary Electrophoresis for Counting and Quality Control of RNA Viruses, the method was expanded to analyze RNA viruses, with a wide dynamic range of virus quantification from 10^8 to 10^{13} ivp/mL and the sample volume from 5 μL to 40 μL.

Chapters 3 to 6 show a chronological path how studying non-covalent interactions went from utilizing CE with a UV detector (CE-UV) through CE coupled with MS (CE-MS) to tandem CE-UV-MS. Initially, a method to study fast non-covalent interactions was developed for CE-UV (Chapter 3) and was used for multiplex determination of kinetic parameters describing weak (3 mM > K_d > 80 μM) and fast (0.25s ≥ τ ≥ 0.9 ms) non-covalent interactions between four small molecule drugs (ibuprofen, s-flurbiprofen, salicylic acid and phenylbutazone) and α- and β-cyclodextrins.

Later a mass spectrometer was coupled to CE and three methods for affinity measurements were evaluated: CE-UV, CE-MS and direct infusion MS (DIMS) (Chapter 4). It was clear that CE-MS combined advantages of both techniques and was truly superior to CE-UV and DIMS. Unlike CE-UV, CE-MS doesn't require an analyte to be able to absorb UV light and provides an opportunity to detect a target, a ligand and their complex on different non-overlapping channels. Compared to DIMS, CE-MS is capable of tracking a

time-propagation pattern (which is formed during separation) of interacting species, this pattern can be used to study chemical kinetics and helps avoid false-positive interactions which are abundant during DIMS process, when molecules are forced to “interact” by a strong electric field producing ions adduct rather than real complexes. The application of CE-MS for measuring affinity constants between eight small molecule drugs (ibuprofen, s-flurbiprofen, diclofenac, phenylbutazone, naproxen, folic acid, resveratrol and 4,4’-(propane-1,3-diyl) dibenzoic acid) and β-cyclodextrin was described.

After CE-MS concept was established and validated, it was successfully applied to study nucleic acid (NA) folding induced by potassium cation into a G-quadruplex structure (Chapter 5). Kinetic CE-MS (KCE-MS) was used to separate a thrombin binding aptamer d[GGTTGGTGTGGTTGG] from mutated sequences based on affinity to potassium, and revealed the apparent equilibrium folding constant (K_F ~ 150 μM), folding rate constant (k_{on} ~ $1.70\times10^3\ s^{-1}M^{-1}$), unfolding rate constant (k_{off} ~ $0.25\ s^{-1}$), half-life time of the G-quadruplex ($t_{1/2}$ ~ 2.8 s), and relaxation time (τ ~ 3.9 ms at physiological 150 mM [K^+]). In addition, KCE-MS was used to screen for a GQ-stabilizing/destabilizing effect of DNA binding dyes and an anti-cancer drug - cisplatin.

In Chapter 6 we first utilized KCE-UV to study a transition between “open” and “closed” conformations of human tissue transglutaminase-2 (TG2). This analysis yielded a value of 38 ± 9 μM for the dissociation constant (K_d) of calcium binding, and values of (138 ± 27) × 10^{-3} min^{-1} and (49.8 ± 1.5) × 10^{-3} min^{-1} were determined for k_{open} and k_{close}, respectively. Coupling CE to MS revealed that the “biologically” small TG2 protein was “mass-spectrometrycally” enormous at mass 72 kDa. The protein didn’t equally undergo

ionization for both conformers disabling the quantitative aspect of CE-MS analysis. To overcome this obstacle, a home-made modification was introduced in the CE-MS setup that turned it into an ultimate CE-UV-MS machine capable of both multiplexing and direct quantitative analysis of protein conformers and enzymatic activity. Three competitive irreversible inhibitors, NC9, VA5 and AA10 were analyzed and EC_{50} for enzymatic activity and conformational changed were determined.

Engineering new enzymes require a method for fast and multiplex screening of substrates and their products to guide the designing process. In Chapter 7, we introduce an entirely automated enzyme assay based on capillary electrophoresis coupled to electrospray ionization mass spectrometry termed MINISEP-MS for Multiple Interfluent Nanoinjections-Incubation-Separation-Enzyme Profiling using Mass Spectrometry. MINISEP-MS requires only nanoliters of reagent solutions and uses the separation capillary as a microreactor, allowing multiple substrates to be assayed simultaneously. The method can be used to rapidly profile the substrate specificity of any enzyme and to measure steady-state kinetics in an automated fashion. We used the MINISEP-MS assay to profile the substrate specificity of three aminotransferases (*E. coli* aspartate aminotransferase, *E. coli* branched-chain amino acid aminotransferase, and *Bacillus sp.* YM-1 D-amino acid aminotransferase) for 33 potential amino acid substrates, and to measure steady-state kinetics. Using MINISEP-MS, we were able to recapitulate the known substrate specificities and to discover new amino acid substrates for these industrially-relevant enzymes. Additionally, we were able to measure the apparent K_M and k_{cat} parameters for amino acid donor substrates of these aminotransferases. Because of

its many advantages, the MINISEP-MS assay has the potential of becoming a useful tool for researchers aiming to identify or create novel enzymes for specific biocatalytic applications.

The thesis summary and future plans will be presented in the Conclusion.

Chapter 2: Viral Quantitative Capillary Electrophoresis (Viral qCE)

2.1. Objectives and contributions

My objectives were to develop a CE-based technique capable of quantitative analysis of DNA virus particles and performing CE experiments as well as mathematical analysis.

Alexey Chechik was responsible for performing NanoSight experiments. Rachel Ozer and Dr. John Bell were responsible for providing samples of oncolytic viruses. Dr. Maxim Berezovski provided technical guidelines and supervision in performing all CE experiments. Afnan Azizi was responsible for performing CE experiments for an RNA virus. Darija Muharemagic and Mohamed Wehbe supervised the RNA virus handling.

2.2. Viral Quantitative Capillary Electrophoresis for Counting Intact Viruses.

2.2.1 Introduction.

Oncolytic viruses (OVs) promise to improve cancer patient outcomes through their tumor-selective replication and multimodality attack against cancers[38]. The new hope generated by this virus-based technology, including impressive efficacy in animal tumor models, has been somewhat tempered by limited therapeutic activity in the clinic[39]. Human trials have, however, demonstrated that in general, the OV platform has an exceptional safety profile with much less toxicity, compared to standard forms of cancer therapy like chemo and radiation therapy[40]. Some viral platforms (namely vaccinia from

Jennerex Biotherapeutics, HSV from Biovex and Reovirus from Oncolytics Biotech) have entered, or are progressing into, phase III assessment, and thus approval of an OV therapeutic in North America seems to be on the horizon[41].

Quantification of OVs involves counting the number of viruses in a certain volume to find the virus concentration. It is used in commercial and academic laboratories as well as production situations where the quantity of viruses at various steps is important information. For example, the manufacturing of OVs for cancer therapy, production of viral vaccines, the expression of recombinant proteins using viral vectors and viral antigens all require virus quantification to continually adapt and monitor the process in order to optimize production yields. There are various techniques currently used to quantify viruses in liquid samples such as culture-based and instrumental methods.

The most popular culture-based method is the plaque forming assay[42]. Viral plaque assays determine the number of plaque forming units (pfu) in a virus sample, which is one measure of virus quantity. A viral plaque is formed when a virus infects a cell within the fixed cell monolayer. Plaque formation can take 3 – 14 days, depending on the virus being analyzed. In addition to the plaque assay, there is a 50% Tissue Culture Infective Dose ($TCID_{50}$)[43].

There are several traditional instrumental-based methods such as the fluorescent focus assay (FFA)[44], the protein assay[45], the bicinchoninic acid assay (BCA), and transmission electron microscopy (TEM)[46]. Quantitative TEM results will often be higher in number than results from other assays as all particles, regardless of infectivity, are quantified in the reported virus-like particles per mL (vlp/mL) result. Quantitative TEM

generally works well for virus concentrations greater than 10^6 particles/mL. Because of high instrument cost and the amount of space and support facilities needed, TEM equipment is available in a limited number of facilities.

Modern instrumental methods for virus quantification are relatively new, less time consuming, and more sensitive like the flow cytometry-based assay[47], Raman scattering based immune assay[48], ELISA[49], and quantitative PCR (qPCR)[50]. qPCR utilizes polymerase chain reaction chemistry to amplify viral DNA or RNA to produce high enough concentrations for detection and quantification by fluorescence. In general, qPCR relies on serial dilutions of standards of known concentration being analyzed in parallel with the unknown samples for calibration and reference. Since PCR amplifies all target nucleic acids, whether from an intact virion or free nucleic acids in solution, qPCR results (expressed in terms of genome copies/ml) are likely to be higher in quantity than viral plaque assay and TEM results.

Viral preparations are also contaminated with DNA from the host cells used to produce the virus. This material is a process impurity in vaccine or therapeutic production and is subject to regulatory limits. The guidance from the World Health Organization is that vaccines should contain less than 10 ng residual host cell DNA per human dose[51].

In this work, we introduce a novel method called Viral Quantitative Capillary Electrophoresis (Viral qCE). It is a separation-based technique that is able to discriminate between intact virus particles (ivp) and residual DNA with high resolution and sensitivity. Viral qCE is suitable to quantify viruses in the wide dynamic range from 10^6 to 10^{12} ivp/mL. All measurements are performed by a commercial capillary electrophoresis instrument

with laser-induced fluorescent detection (CE-LIF) without modifications, suggesting that Viral qCE can be immediately and widely practiced in academic and industrial labs.

In our experiments we used the JX-594 strain of vaccinia virus (VV). It is a member of the poxvirus family and has a large linear double-stranded DNA genome of approximately 200 kbp in length that encodes ~ 250 genes. The dimensions of the virion are roughly 360×270×250 nm, with a mass of 5-10 fg. It has several attributes that make it particularly well suited as an anticancer therapeutic[52]. JX-594 is a virus with a modification of the viral thymidine kinase gene and expression of the immunostimulatory cytokine, GM-CSF (granulocyte macrophage colony-stimulating factor). JX-594 exploits a specific genetic feature in cancer cells to become activated and lyse the cells, including the EGFR-ras signaling pathway, the cell cycle activation and the loss of cellular interferon defenses. JX-594 is designed to attack cancer through three diverse mechanisms of action: 1) the lysis of cancer cells through viral replication, 2) the reduction of the blood supply to tumors through vascular targeting and destruction, and 3) the stimulation of the body's immune response against cancer cells.

2.2.2 Materials and methods

Chemicals and Materials. Vaccinia virus samples and a purified polyclonal rabbit antivaccinia primary antibody were provided by Jennerex Inc. (Ottawa, ON, Canada). Chemicals were purchased from the following companies: λ DNA (cat. no. M6201, Biomatik Corporation, Canada), sodium borate decahydrate (cat. no. SX0355-1, EMD Chemicals, U.S.A.), YOYO-1 dye (cat. no. N7565, Invitrogen, U.S.A.), proteinase K (cat. no.

AM2546, Ambion, U.S.A.), FITC-labeled goat antirabbit antibody (cat. no. A11009, Invitrogen, U.S.A.). The bare silica capillary with an o.d. of 365 μm and an i.d. of 75 μm was purchased from Polymicro Technologies (cat. no. TSP075375, Phoenix, AZ, U.S.A.). All buffers were made using Milli-Q-quality deionized water and filtered through a 0.22 μm filter.

Preparation of Lysed Virus and DNA Standards. Proteinase K solution (1 μL of 20 mg/mL) was added to 19 μL of virus or λ DNA solution with subsequent heating at 37 °C for 2 h. The control of nonlysed samples was prepared identically, but 1 μL of 10 mM borax buffer was used instead of proteinase K. Standards of λDNA were prepared by the serial dilution (5, 5^2, 5^3, 5^4, 5^5, 5^6, 5^7, and 5^8 times) of 500 μg/mL stock solution in 10mM borax buffer. Working samples of VV were prepared from the stock solution of the virus by 5, 5^2, 5^3, 5^4 and 5^5 times stepwise dilution in 10 mM borax buffer. An amount of 0.88 μL of 10 μM YOYO-1 was added to 8 μL of each standard solution of λ DNA and working solution of the virus.

Capillary Electrophoresis. Capillary electrophoresis analyses were performed using a PA800ю pharmaceutical analysis capillary electrophoresis system (Beckman Coulter, Brea, CA, U.S.A.) with LIF detection. Fluorescence was excited with a 488 nm line of a solid-state laser and detected at 520±10 nm. Separations were carried out using a bare fused-silica capillary of 30 cm total length and 20.5 cm from an injection point to a detection window. Hydrodynamic injection of a sample (45 nL) was made by a pressure pulse of 0.5 psi for 5 s for the CE separation. The total fluorescence of the sample was measured by pushing it through the capillary as a continues plug with pressure of 5 psi for 3 min. The CE

separations were conducted by applying a voltage of 10 kV (an electric field of 333 V/cm) when a positive charge is at the inlet and the ground at the outlet. The temperature of the capillary and samples was kept constant at 20 °C. The output data was fluorescence intensity in the detection point, as a function of time passed since the application of the electric field. Data were collected and analyzed using 32 Karat version 8.0 software. The run buffer was 50 mM sodium tetraborate (borax) at pH 9.2. At the start of each run, prior to injection, the capillary was rinsed with 0.1 M HCl for 2 min, 0.1 M NaOH for 2 min, deionized water for 2 min, and the run buffer for 4 min.

NanoSight Measurements. Different concentrations (from 10^7 to 10^9 vp/mL) of VV in PBS were measured using a NanoSight LM10 system (NanoSight Ltd., U.K.). The software used for capturing and analyzing the data was the NTA 2.0. The particle numbers were counted by their scattered light spots which could be identified clearly on the video image. The mean particle number per frame was counted from 1800 frames of the videos from five measurements of each sample. The video was recorded for 60 s at 30 frames/s for each measurement. NanoSight was preliminarily calibrated with 100, 200, and 400 nm polystyrene microspheres in concentration between 10^7 and 10^9 beads/mL (Nanosphere from Thermo Scientific, Fremont, CA). Three measurements of the same sample were performed for all polystyrene beads and six measurements for virus samples. The relative average error of these measurements was about 12%.

2.2.3 Results and discussion

Viral qCE Analysis. The principle of Viral qCE is shown in **Figure 2.1.** Briefly, after virus production and storage, the viral sample contains intact viral particles as well as degraded ones with released viral DNA, and residual host cell DNA. When the mixture of the virus particles and the free DNA is injected and separated by capillary electrophoresis, two distinctive zones are observed (**Fig. 2.1 top**). The fast moving zone contains intact virus particles and is observed as a group of narrow peaks. The slow moving zone represents the free DNA visible as a wide peak. The slow mobility of the free DNA is explained by the multiple negative charges of phosphate groups. After virus lysis by heat or proteases, the fast moving zone disappears and the slow moving zone of free DNA becomes more intense (**Fig. 2.1 bottom**). The gain in peak intensity is due to the DNA release from virus particles, so it can be used to calculate the concentration of the intact particles in the original samples before lysis.

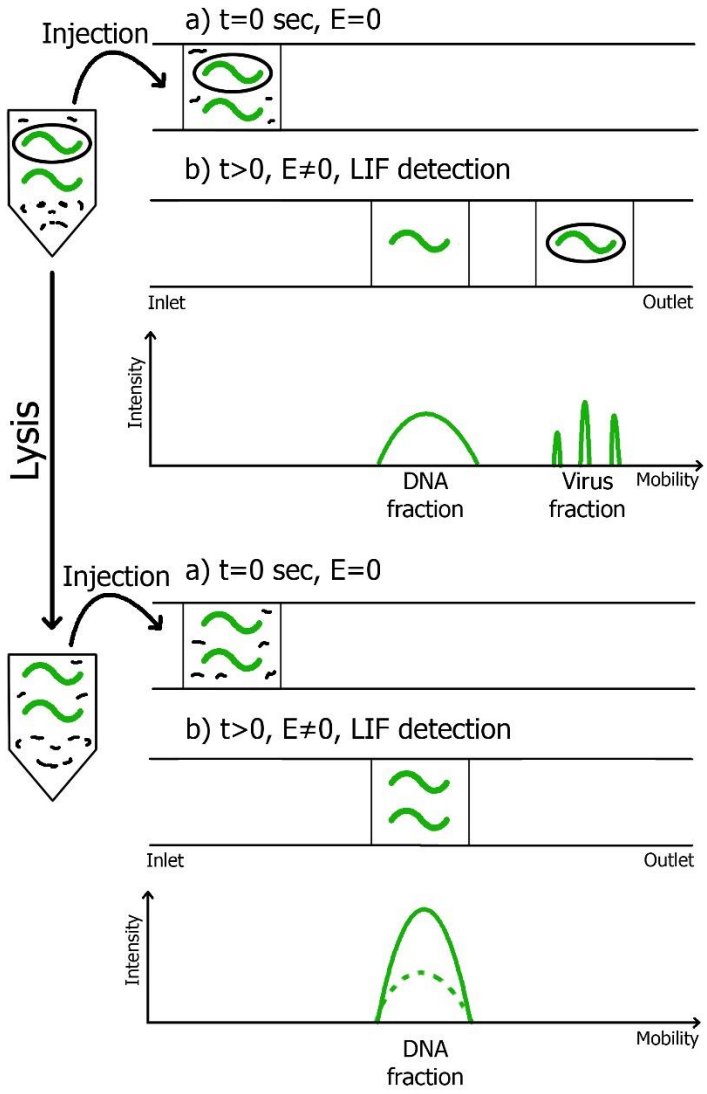

Figure 2.1. Schematic of diagram of Viral qCE analysis. A mixture of intact virus particles with encapsulated DNA (a green curve in an oval) and the free contaminated DNA (a green curve without an oval) is injected into the capillary as a short plug. When an electric field is applied (E > 0 V/cm), viruses and the free DNA are separated into two fractions. After lysis, the virus fraction disappears and the free DNA peak increases. The gain shows the amount of encapsulated DNA before lysis and is used to count intact virus particles. DNA is stained with YOYO-1 dye.

In our experiments we applied YOYO-1 intercalating dye to detect encapsulated DNA and free DNA. YOYO-1 stain shows over a thousand-fold increase in its green fluorescence when bound to dsDNA[53]. YOYO-1 stained the free and encapsulated DNA as seen on the

electropherogram at **Figure 2.2B.** An anti-VV antibody stained only virus peaks. It helped verify the position of VV peaks during CE analysis (**Fig. 2.2C**). Virus particles were degraded using proteinase K at 37˚C for 2 hours. The moderate heating accelerated proteolysis and prevented DNA denaturation. After the lysis step all viral DNA was released into solution. This was confirmed by the disappearance of the viral particle peaks and the increase of the free DNA peak (**Fig. 2.2B**). To be certain that VV and YOYO-1 did not have auto-fluorescence, we tested YOYO-1 only and VV without YOYO-1 in CE (**Fig. 2.2A**).

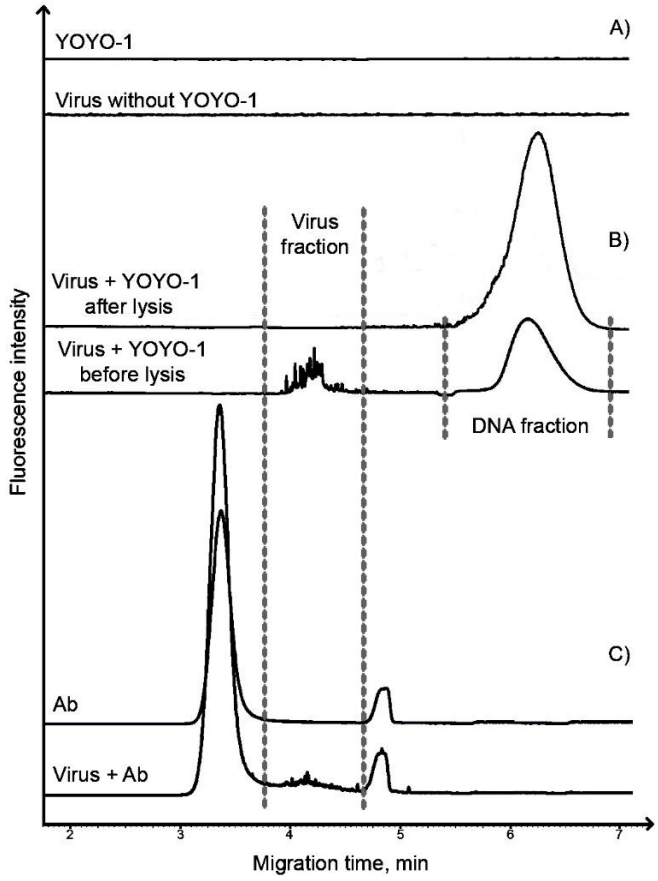

Figure 2.2. Experimental Viral qCE electropherograms. A) Control experiments: 1 µM YOYO-1 only (top), VV without YOYO-1 (bottom). B) The second lysed VV sample with YOYO-1 (top); The second intact VV sample with YOYO-1 (bottom). C) A mixture of the primary Ab and the secondary FITC-labelled Ab without VV (top); Antibodies with VV

(bottom). Peaks stained with Abs and YOYO-1 are shown as the virus fraction. Peaks stained only by YOYO-1 are marked as the DNA fraction. CE separations are performed in 30 cm-long uncoated capillary with 50 mM Borax run buffer pH 9.2 under 333 V/cm at 20˚C using LIF detection.

Quantitation of Virus Samples with CE. Calculation of the virus concentration was performed in three steps. First, the contamination level (CL) of VV was calculated as:

$$CL = A_0 / A_{Lysed} \tag{2.1}$$

Where A_0 and A_{Lysed} are free DNA peak areas before and after lysis, respectively. Second, the concentration of viral DNA in ng/ml was found using calibration curve of serial dilutions of lambda phage DNA (λ DNA). The calibration curve was built by plotting fluorescent intensities of YOYO-1 labelled λ DNA samples repeated three times versus their concentrations in ng/ml (**Fig. 2.3**). Practically, serial dilutions of λ DNA (48502 bp) with YOYO-1 were pushed through a capillary by pressure as a continuous flow and their fluorescence intensities were measured. Thereafter, a sample of the lysed virus with YOYO-1 was moved through the capillary the same way as λ DNA and its fluorescence intensity was measured and compared with the standards. In the last step, the concentration of intact virus particles [VV] in ivp/ml was calculated:

$$[VV] = \frac{(1 - CL) \times N_A \times [\lambda\ DNA]}{10^9 \times Mr(VV)} \tag{2.2}$$

Where [λ DNA] is the concentration of λ DNA in ng/ml found from the calibration curve for the lysed VV sample. N_A is the Avogadro constant (6.022×10^{23} mol^{-1}) and Mr(VV) is the molar mass of the viral DNA in g/mol and equals 135×10^6 g/mol for VV. Spiking the actual viral sample with known amounts of λ DNA and generating the standard curve in the presence of viral DNA can be useful to eliminate the influence of sample media. We

did not notice a big difference with the spiking method, because our VV samples were diluted in 10 mM borax buffer before CE analysis.

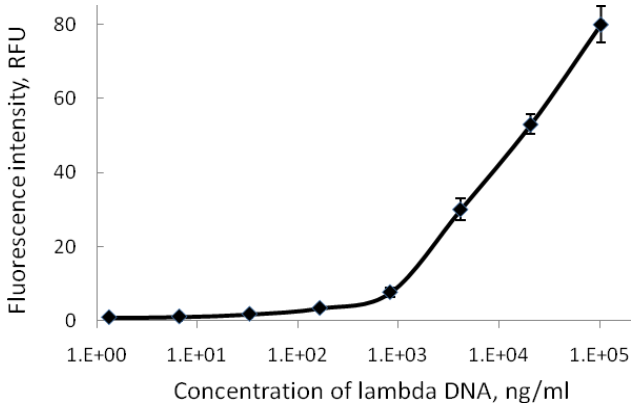

Figure 2.3. Calibration curve of YOYO-1 stained λ DNA standards for finding viral DNA concentration after lysis. 1 μM YOYO-1 was used for DNA staining.

Three samples of VV were studied. The first contained 2-month old VV, the second sample had VV from a different batch that underwent 20 freeze/thaw cycles, and the third sample contained the freshly prepared virus. The degradation and concentration was calculated to be 2% and $(4.5\pm0.4)\times10^{9}$ ivp/ml for the first sample, 30% and $(7.7\pm1.4)\times10^{9}$ ivp/ml for the second, and 10% and $(1.6\pm0.3)\times10^{10}$ ivp/ml for the third sample, respectively. The second VV sample had the significant amount of degraded or contaminated DNA, as the intensive zone of free DNA was observed in **Fig. 2.2B**. The additional Viral qCE electropherograms are shown in **Fig. 2.4** for different virus concentrations.

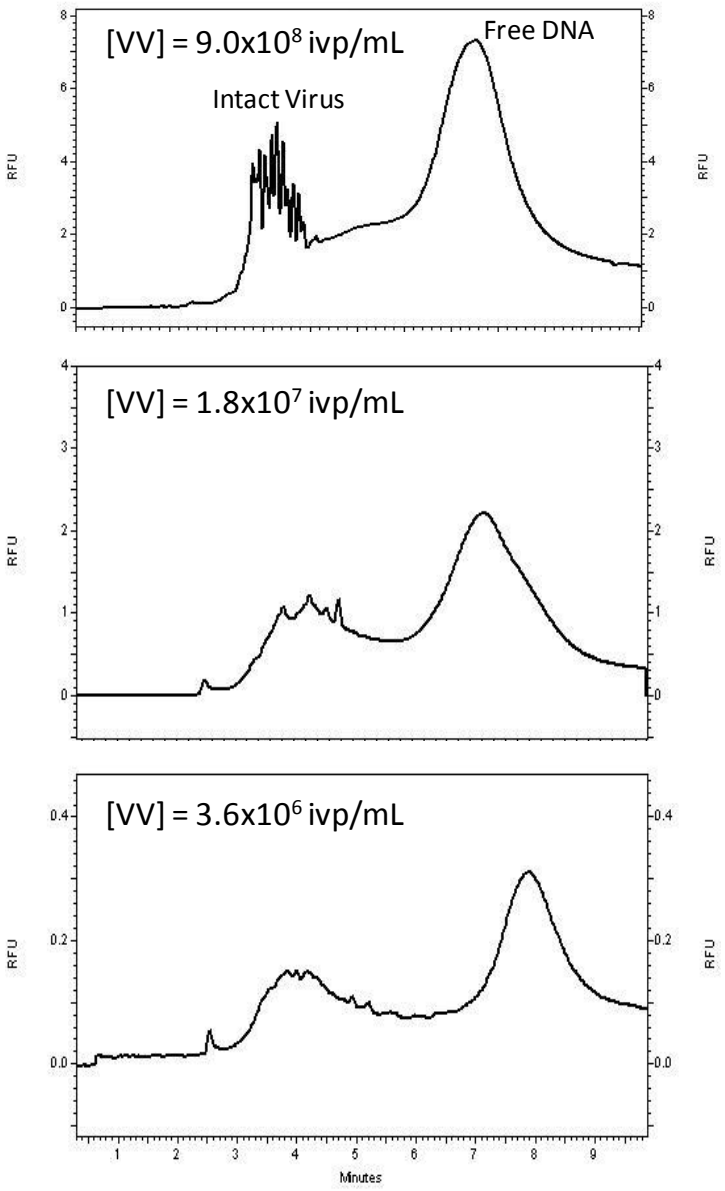

Figure 2.4. Experimental Viral qCE electropherograms of different Vaccinia Virus (VV) concentrations. VV is stained with 1 µM YOYO-1. CE separations are performed in 50 cm-long uncoated capillary with 50 mM Borax run buffer pH 9.2 under 200 V/cm at 20˚C using LIF detection.

Different methods (temperature, sonication and SDS) of virus lysis were also evaluated. We found that temperature denaturation of VV had a big disadvantage – it melted big viral DNA and prevented YOYO-1 intercalation making the assay irreproducible.

Sonication didn't give consistent results as well. The lysis with SDS worked relatively well with 5 % SDS solution and consequent 20 times dilution of the virus lysate. High concentration of SDS decreases binding of YOYO-1 to DNA. The most stable results were obtained using proteinase K. It is a broad-spectrum serine protease. The predominant site of cleavage is the peptide bond adjacent to the carboxyl group of aliphatic and aromatic amino acids with blocked alpha amino groups. Adding proteinase K to nucleic acid preparations rapidly inactivates nucleases that might otherwise degrade the DNA during sample preparation[54].

We should consider that differences in sample constituents of λ DNA and VV could influence on the precise quantification of the virus DNA due to variable behaviour of the intercalating YOYO dye in different conditions. To reduce this effect all samples and standards were prepared and diluted in the same buffer and analysed in the same run buffer. We also applied an excess of the dye (1 μM) to saturate and keep constant the dye:base pair ratio. We suggest that DNA isolated from a target virus can be used for making a calibration curve. The efficiency of the dye intercalation and proteinase digestion was tested on replicate analysis of virus samples before and after lysis (**Fig. 2.5**).

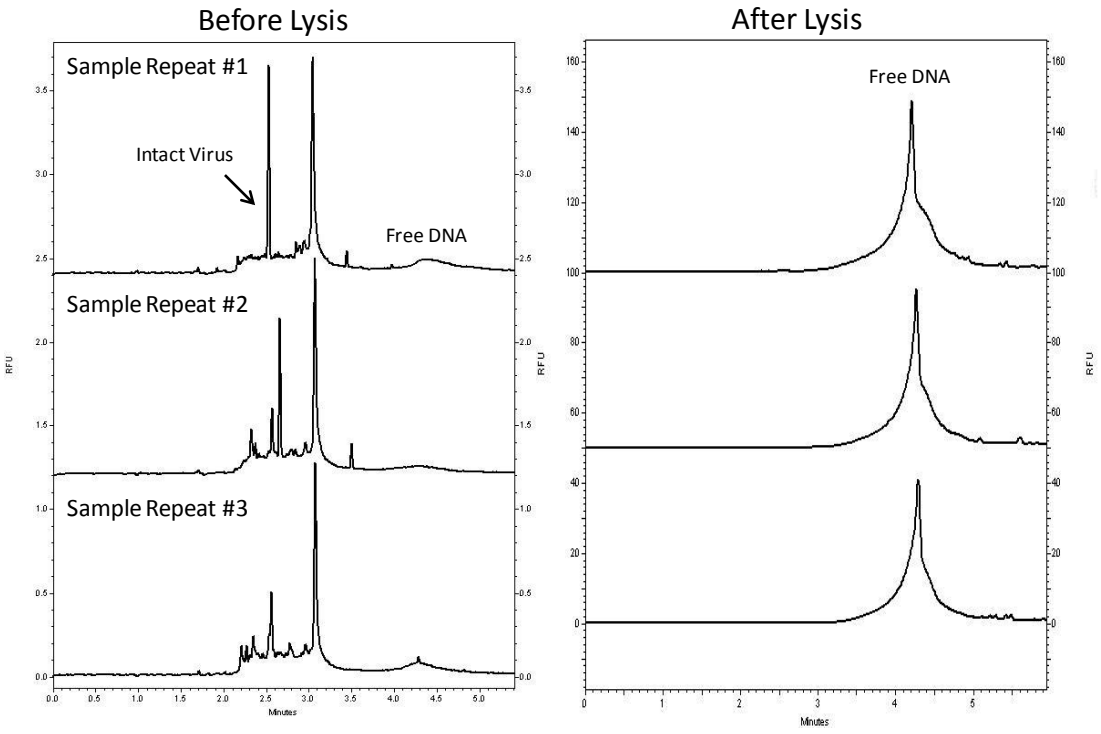

Figure 2.5. Viral qCE analysis for three replicates of a virus sample before lysis and after lysis with protease K. Stained with 1 µM YOYO-1. CE separations are performed in 30 cm-long uncoated capillary with 50 mM Borax run buffer pH 9.2 under 333 V/cm at 20˚C using LIF detection.

Quantitation of Viruses with NanoSight. To verify the quantitation of intact viral particles by Viral qCE, an additional technique called Nanoparticle Tracking Analysis (NTA) and "NanoSight" instrument were used[55]. The NTA analysis is based on a laser illuminated microscopy technique. Brownian motion of nanoparticles is analyzed in real-time by a CCD camera; each particle is being simultaneously but separately visualized and tracked by a dedicated particle tracking image analysis software. The software is capable of distinguishing bright particles captured by the CCD camera from black background and further tracking them while they are in the focus. The distance run by every single particle over a time period results in the speed value which is reversely proportional to particle

size. Depending on side scattering and the speed of the particles movement it is possible to determine their concentration and size. NanoSight is able to simultaneously visualize and analyze nanoparticles on an individual basis from heterogeneous samples in the size range of from 10 to 1000 nm, and the concentration range from 10^7 to 10^9 particles/ml[56].

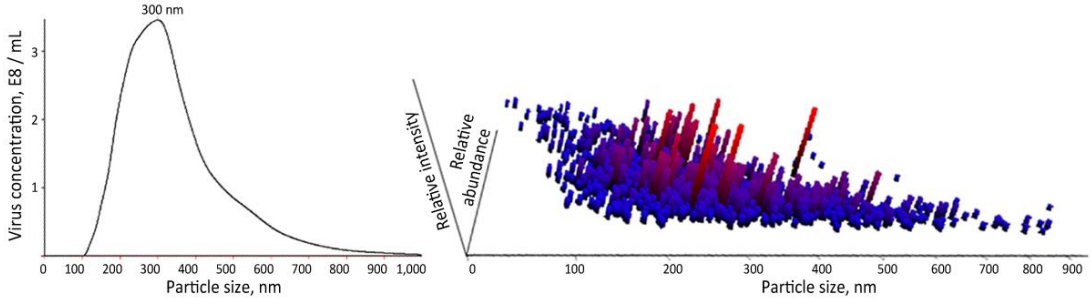

Figure 2.6. Size distribution from NTA measurement and 3D graph (size vs. intensity vs. abundance) of vaccinia virus.

We applied the NanoSight instrument to analyse the first (2-month-old) sample of VV (**Figure 2.6**). Its concentration was measured to be $(2.5 \pm 0.3)\times10^9$ ivp/ml. As seen on **Figure 2.6A**, VV has a wide size distribution with the maximum on 300 nm and a right shoulder. This maximum value is the average of linear dimensions of a virion (250×270×360 nm). The right shoulder represents self-aggregation of the virus. **Figure 2.6B** shows the distribution of particles by their size, the relative intensity of light scattering, and the abundance (or tracking stability) of the particles. The relative intensity can be used to discriminate virus particles from high scatter agglomerates (cell debris, denatured viruses and polymer beads). Contaminated host cell DNA was not detected by the NanoSight due to a very small size (<10 nm).

We confirm three major advantages of Viral qCE. First, it works in a wider dynamic range of virus concentrations from 10^6 to 10^{12} ivp/mL than NanoSight (10^7 - 10^9 ivp/mL). Second, the sample consumption is very low (5 - 40 µl for CE vs. 300-1000 µl for NanoSight). The third benefit is the ability to calculate the level of virus contamination by denatured viral DNA or residual cellular DNA impurities.

2.2.4 Conclusion

In this chapter, I demonstrated a CE-based method for reliable quantification of intact virus particles. Viral qCE can be done in 5 - 15 min and requires minimal skills for the optimization of CE separation. Viral qCE enables partitioning of intact viral particles and free DNA, measures an exact intact particle concentration and host cell DNA impurity contamination of viral samples. CE with LIF detection is very sensitive and accurate, and it has a wide dynamic range of virus quantification. It can also distinguish non-DNA impurities and exclude them from calculations. Viral qCE gives the possibility of live monitoring heat-induced aggregation, providing information about the aggregation kinetics. We foresee that the presented method can be applied for quality control in oncolytic viruses and vaccine productions.

2.2.5 Acknowledgments

This work was supported by the Natural Sciences and Engineering Research Council of Canada's Engage Grant and Ottawa Technology Transfer Network's Proof of Principle

Fund (OTTN-PoP). The authors also thank Dr. Victor Okhonin, Ms. Jennifer Logie, and Ms. Ekaterina Berezovskaia for critical reviews and valuable suggestions.

2.3. Viral Quantitative Capillary Electrophoresis for Counting and Quality Control of RNA Viruses.

2.3.1 Introduction.

Viruses as vehicles of antigens and gene therapy agents have progressed rapidly from labs to clinics[58]. Furthermore, extraordinary efforts have been taken in the field of oncolytic viral therapy culminating in a number of ongoing phase II and III clinical trials with some encouraging results in effective targeting of tumours[59, 60]. RNA oncolytic viruses (OVs) possess a large share of this novel form of cancer therapy and many families of such viruses are being developed for destruction of tumour cells[61]. In light of this exponential increase in production and use of viruses as therapeutic agents, it is necessary to improve upon current methods of quantification of viral titers to develop novel approaches that would enhance efficiency and accuracy of determination of virus concentration in a given sample.

Viral titers are usually quantified based on either infectivity or particle numbers. Plaque forming, fluorescent focus, endpoint dilution, and Pock assays belong to the former category of quantification methods[62]. Plaque-forming assay (PFA), as applied to mammalian cells by Dulbecco[63], is the most extensively used method for quantification

of viral titers[64]. It is considered by many virologists to be highly accurate and reproducible. However, this method, similar to others based on infectivity, only quantifies the number of units (which usually include more than one virus particle forming an aggregate) that are able and available to infect the cells, thus underestimating the number of viral particles present. This approach has the disadvantage of excluding all classes of non-infectious viruses, such as attenuated vaccine viruses, gene therapy vehicles, and other viruses that do not form plaques[65]. Furthermore, PFA is time consuming and requires at least three days to perform[62].

Other methods commonly employed for viral analysis are those that quantitatively yield the number of viral particles. Transmission electron microscopy (TEM), quantitative PCR (qPCR), flow cytometric counting, fluorescence correlation spectroscopy (FCS), immunostaining and detection of viral nucleic acids are among such methods. While TEM can be used to accurately find the total number of viral particles and their concentration[66], the cost per sample and high level of expertise associated with its application deem it impractical for routine use at academic laboratories with limited resources or low-budget industrial operations. FCS analysis gives the average number of fluorescent particles and average diffusion time, when the particles move in solution due to Brownian motion in a small volume (~1 μm^3). FCS enabled the measurement of both the low concentration and size of HIV-1 viruses in blood[67]. Quantitative PCR has also been broadly used for virus counting. The use of qPCR, however, not only poses intrinsic errors due to possibility of confounding effects of amplification of contaminating nucleic acids but also could be more erroneous in quantifying RNA viruses where the step of

reverse transcription has to be added to the process[68]. Moreover, approaches based on quantifying the total viral proteins or quantitative detection of viral nucleic acids are also commonly used. Nonetheless, these methods are liable to produce overestimations as a result of non-specific detection of non-viral protein or nucleic acid impurities in samples. Likewise, many of less commonly used methods suffer from lack of sufficient specificity or sensitivity, as well as long preparation and assay times.

Furthermore, while assays based on infectivity, such as PFA, are reproducible and, indeed, necessary for many therapeutic applications, often it is also important to determine the number of both infectious and non-infectious particles administered to patients. In addition, World Health Organization (WHO) has recommended that virus preparations from continuous cell lines contain no more than 10 ng per human dose of contaminating cellular DNA[69]. As a result, devising a method capable of separating virus titer from such contamination and quantifying each is highly desirable. To this end, we have tailored our previously developed method, viral quantitative capillary electrophoresis (viral qCE)[70], for RNA viruses and have used it to address these quantitative and qualitative issues.

We used a vesicular stomatitis virus strain, VSV-Δ51 (Jennerex Inc., Canada), which has been shown to possess potent oncolytic properties[71] against a large number of potential tumor types[72]. VSV is a small bullet-shaped negative-strand RNA virus from the *Rhabdoviridae* family[73]. Its genome consists of about 11.9 kb of encapsidated ssRNA encoding for five proteins[74] and is approximately 200 nm in length and 70 nm in diameter[75]. VSV selectively attacks tumor cells by taking advantage of defects to the

interferon pathway demonstrated by many such cells[76]. In fact, VSV is very sensitive to this pathway in normal cells[77] forming a basis for production of recombinant VSV strains, including VSV-Δ51, which have heightened sensitivity to innate immunity resulting in a better tumor selectivity over healthy cells[78]. Subsequently, VSV has been considered for clinical trials by the Recombinant DNA Advisory Committee of NIH at least on two occasions[79, 80]. Furthermore, VSV is being developed as a vaccine shuttle for an array of viral pathogens, such as HIV-1[81], Ebola virus[11], hepatitis B[82] and C[83]. Therefore, in view of the significant therapeutic potential of VSV and due to its widespread use and well-characterized nature as a model virus for *Rhabdoviridae*[77], we applied the viral qCE method to determine the number of intact virus particles (ivp) in viral samples, the amount of DNA contamination, and the degree of viral degradation after a number of processes frequently used during sample handling. This method provides an ideal first step in the path to full automation of virus analysis and quality control using CE coupled to liquid handling devices.

2.3.2 Materials and methods

Chemicals and Materials. Samples of purified vesicular stomatitis virus (Δ51-YFP) were originally provided by Jennerex Inc. (Ottawa, ON, Canada). More samples were subsequently produced, in house, using Vero cells (donated by the Bell lab) as described before[84]. The following chemicals were purchased: sodium borate decahydrate (cat. no. SX0355-1, EMD Chemicals, USA); anti-VSV-G antibody conjugated with DyLight™ 488 (cat. no. 600-441-386, Rockland Immunochemicals, USA); YOYO®-1 dye (cat. no. Y3601,

Invitrogen, USA); lambda DNA standard (cat. no. D1501, Promega, USA); RiboGreen® and *Escherichia coli* rRNA (16S and 23S) standard from the Quant-IT™ RiboGreen® RNA Assay Kit (cat. no. R11490, Invitrogen, USA); SYTO® RNASelect™ (cat. no. S3270, Invitrogen, USA); RNase A (cat. no. 21210, batch lot no. 4144128, Affymetrix, USA); Proteinase K (cat. no. BP1700-100, Fisher Scientific, Canada); bare silica capillary with O.D. 360 µm and I.D. 75 µm (cat. no. TSP075375, Polymicro Technologies, AZ, USA). All buffers and samples were prepared from nuclease-free de-ionized water using a Synergy UV system (cat. no. SYNSV00WW) supplied with a 13 kDa cut-off, BioPak Point-of-Use ultrafilter (cat. no. CDUFBI001, Millipore, MA, USA).

Preparation of rRNA and DNA standards, virus lysis, RNase A and NaOH treatments. Samples of rRNA were prepared by serial 5-fold dilutions starting from the 100 µg mL^{-1} stock solution in 25 mM borax buffer. Samples of DNA standard were prepared in the same manner from a 100 µg mL^{-1} dilution of the 303 µg mL^{-1} stock solution. All virus samples were diluted to 20 times the provided stock concentration using 5 mM borax buffer before further manipulation and analysis. To lyse the virus, VSV samples were incubated with 600 µg mL^{-1} of proteinase K at 50°C for two hours. Samples for RNase A treatment analysis were incubated at 60°C with 378 µg mL^{-1} of RNase A (5830 units mg^{-1}). In order to hydrolyse RNA for contaminating DNA determination, samples of proteinase K-lysed virus were incubated with a final concentration of 50 mM NaOH at 60°C for 60 minutes. DNA standard samples included a final concentration of 50 mM NaOH and were subjected to the same conditions as lysed viral samples. YOYO-1 dye and RiboGreen

reagent were diluted in 25 mM borax buffer and added to each sample to a final concentration of 2 µM.

Degradative conditions. Viral samples were exposed to the following conditions to determine the amount of loss or degradation of virus titers. Extensive vortexing: 10 µL of virus samples were continuously vortexed for 0.5, 1 or 5 minutes at highest speed using an analog vortex mixer (cat. no. 58816-121, VWR, Canada). Sonication: 10 µL of virus samples were placed in a Branson Ultrasonic Cleaner (Model 3510, Branson Ultrasonics Corporation, USA) for 0.5, 1 or 5 minutes at room temperature. Freeze-thaw cycles: 10 µL of virus samples were exposed to 1, 5 and 10 freeze-thaw cycles. The cycles were performed by freezing the samples on dry ice for 30 seconds and then allowing them to completely thaw at room temperature for 2.5 minutes.

Capillary Electrophoresis. A ProteomeLab™ PA 800 system (Beckman Coulter, CA, USA) was used to perform all capillary electrophoresis with laser-induced fluorescence detection (LIF). Fluorophores were excited using 488 nm Argon Ion Laser source (Beckman Coulter, CA, USA), whose fluorescence was detected using a 520±10 nm filter. The data were acquired and analyzed using 32 Karat Software version 8.0 (Beckman Coulter, CA, USA). The electrophoresis was performed using a fused silica capillary with a total length of 59.1 cm and an effective length of 49.0 cm from point of injection to detection window. For electrokinetic separation experiments, a plug of 40 nL sample was injected into the capillary by applying a pressure pulse of 1.0 psi for 5 seconds. The analytes in the sample were separated by applying 25.1 kV potential difference along the capillary resulting in an electric field of 424 V cm^{-1}. To measure the total fluorescence of samples, a continuous

plug was pushed through the capillary by applying 1.5 psi pressure for 10 minutes. The capillary was maintained at a temperature of 15°C at all times. The run buffer for all analyses was 25 mM borax buffer; before each run, the capillary was rinsed by applying 20.0 psi of 0.1 M HCl, 0.1 M NaOH, and ddH_2O for 2 minutes each and 25 mM borax buffer for 4 minutes. All buffers and rinsing solutions were passed through a 0.2 μm filter before use.

2.3.3 Results and discussion

Viral qCE analysis for RNA viruses. We have shown previously that viral qCE can be used to accurately determine concentration of a DNA virus and a measure of its degradation[70]. Hence, it is desirable to extend the application of this method to RNA-based viruses and improve it by integrating a method for quantification of DNA contamination from host cells. In principle, viral qCE relies on the differential mobility of negatively charged free nucleic acids and intact viral particles. The general scheme of the method is depicted in **Figure 2.7** and can be summarized as follows. A sample containing intact virus particles, DNA contamination from host cells and potential carried-over RNA is stained with YOYO-1 fluorescent dye, injected into the capillary and subjected to gel-free electrophoresis. Intact virus particles and nucleic acids are separated (**Figure 2.7A**). Virus travels faster to the cathode than nucleic acids due to its smaller charge and bigger size and migrates slightly slower than an electroosmotic flow of the buffer solution. Virus particles are difficult to quantify directly because they create multiple spikes on an electropherogram resulting in irreproducible complex patterns. Therefore, we lysed all virus particles by

proteinase K to release viral RNA in a free form (**Figure 2.7**). The resulting nucleic acid peak contains DNA from host cells, carried-over RNA and released viral RNA. Furthermore, host DNA can be detected after the additional treatment of the above sample with sodium hydroxide (**Figures 2.7C**), which hydrolyzes RNA and leaves DNA intact.

Fluorescent staining of nucleic acids. We tested three nucleic acid binding dyes, SYTO RNASelect, RiboGreen and YOYO-1 for their compatibility with CE-LIF detection of RNA viruses. Of these dyes, SYTO RNASelect, a cell-permeant cyanine dye, was deemed impractical because it maintained much lower fluorescence intensity than RiboGreen and YOYO-1. Both of these dyes have more than 1000-fold increase in fluorescence upon binding to nucleic acids. While YOYO-1 is primarily used for staining dsDNA, it can bind RNA[85] and ssDNA[86]. Both nucleic acid dyes have previously been used successfully to stain and identify encapsidated viruses in CE analysis[70, 87, 88].

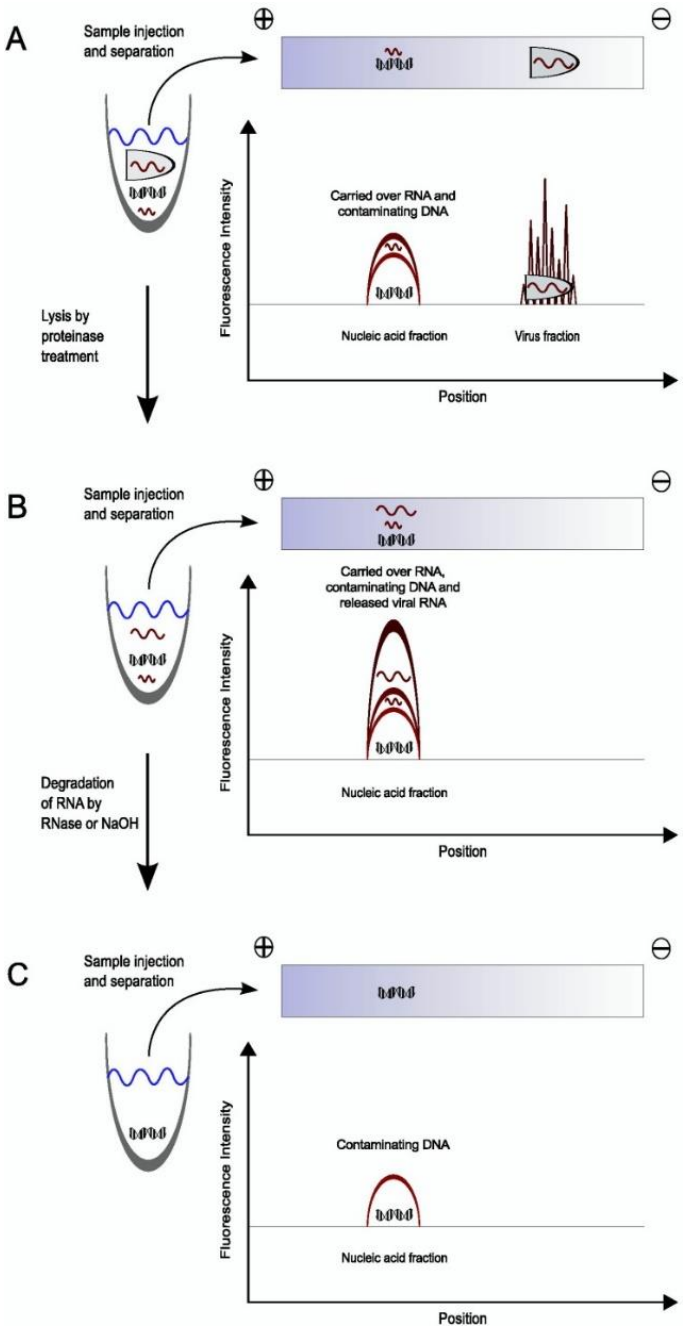

Figure 2.7. Schematic diagram of viral qCE for RNA viruses demonstrating a snapshot of the capillary during each part of the analysis. (A) A sample of intact virus particles with encapsulated RNA, released RNA and contaminating DNA is injected into a capillary and separated into two zones: virus fraction and nucleic acid fraction. (B) After proteinase K treatment, the virus fraction disappears and the nucleic acid peak increases. The gain shows the amount of released RNA and is used to count intact virus particles (C) After NaOH treatment, RNA is hydrolyzed leaving DNA only. This is used to calculate the amount of contaminating DNA from host cells. DNA and RNA are stained with YOYO-1 dye and detected by LIF.

Therefore, they were judged to be appropriate for our application since they would penetrate the viral capsid and would not dissociate or diffuse during the separation process. In our CE analysis, YOYO-1 demonstrated a slightly higher fluorescence than RiboGreen upon binding to ribosomal RNA (rRNA) standards. In addition, RiboGreen stains RNA preferentially, with little sensitivity to DNA, and is not suitable for quantification of DNA contamination. YOYO-1 intercalating cyanine dimer[89] stains both RNA and DNA, with higher signal when bound to the latter, and was selected for the following viral qCE experiments.

Lysis of the virus and RNA hydrolysis. Proteinase K, a robust serine protease, was used to break down the viral proteins and lyse the virus. The main advantage of proteinase K is its ability to digest naturally folded proteins[90] and liberate the viral RNA from nucleocapsid proteins, removing the need for introducing denaturing conditions in samples prior to treatment. Complete lysis of viral particles was confirmed by disappearance of spiked peaks corresponding to the intact virus (**Figure 2.8A**) after proteinase K treatment and the gain in the nucleic acid peak (**Figure 2.8B**). We treated the lysed sample further by Ribonuclease A (RNase A) and observed a complete disappearance of RNA portion of the nucleic acid peak leaving a small peak of the residual DNA contamination (**Figure 2.9**). If the viral RNA were in its ribonucleoprotein form and associated with nucleocapsid proteins, RNase A could not access and hydrolyze the viral RNA[91].

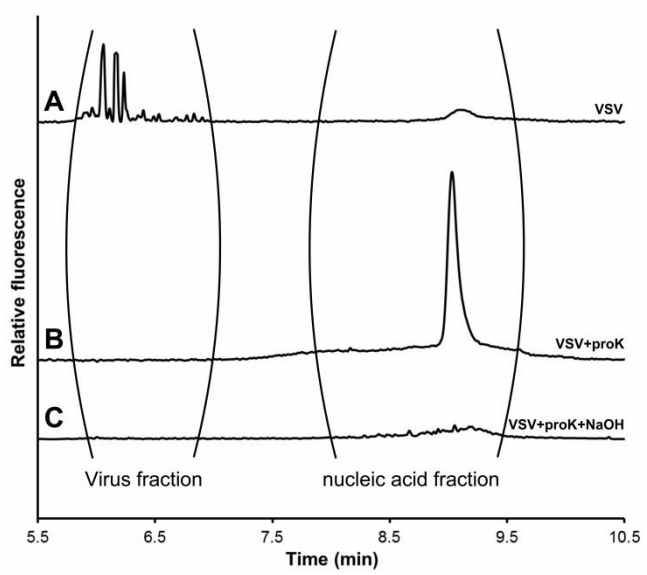

Figure 2.8. Experimental viral qCE electropherograms of vesicular stomatitis virus (VSV). A) An intact VSV sample. B) The proteinase K-lysed VSV sample; C) the lysed VSV sample after NaOH treatment. All samples were stained with 2 µM YOYO-1. CE separations are performed in 49 cm-long uncoated capillary with 25 mM Borax run buffer pH 9.2 under 424 V/cm at 20˚C using LIF detection.

Alternative to RNase A treatment, we employed NaOH-based hydrolysis of RNA to detect the DNA contamination (**Figure 2.8C**). The results with this method were more reproducible and consistent than RNase A digestion. The optimal condition for hydrolysis of RNA, while leaving DNA intact, was found to be 60 minutes incubation with 50 mM NaOH at 60°C. Smaller concentrations of NaOH and lower temperatures did not completely degrade RNA.

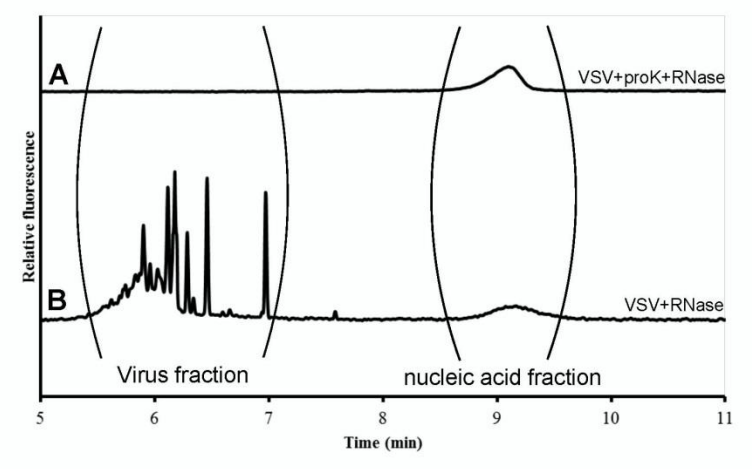

Figure 2.9. A VSV sample after proteinase K + RNase treatment (A) and RNase treatment only (B). The nucleic acid fraction contains only residual DNA contamination.

Quantification of intact RNA virus. Concentration of the intact virus was calculated in six steps. First, a VSV sample stained with YOYO-1 was separated in CE before any treatment. Second, the VSV sample was treated with proteinase K, stained with YOYO-1 and separated again. The area of a nucleic acid peak was measured before and after proteinase K treatment, A_0 and A_{proK} (**Figure 2.8 A and B**). Third, the sample of the lysed virus with YOYO-1 was pushed through a capillary by pressure as a continuous flow and its fluorescence intensity (RFU_{proK}) was recorded. Fourth, a calibration curve was built by plotting fluorescent intensities of rRNA standards bound to YOYO-1 as a function of their concentrations (**Figure 2.10A**). The fluorescent intensities of the standards were measured by a continuous flow, the same way as the viral sample. Fifth, the fluorescence intensity of the lysed sample was multiplied by a contamination coefficient k,

$$\mathbf{k} = 1 - \frac{\mathbf{A}_0}{\mathbf{A}_{\mathbf{proK}}} \qquad (2.3)$$

The resulting intensity was used to find the equivalent concentration of the viral RNA, [RNA_{VSV}], from the calibration curve. In the last step, the concentration of intact virus particles [VSV] in ivp/mL was calculated

$$[\mathbf{VSV}] = \frac{\mathbf{N}_{\mathbf{A}} \times \mathbf{D}_{\mathbf{proK}} \times [\mathbf{RNA}_{\mathbf{VSV}}]}{10^{9} \times \mathbf{MM}(\mathbf{RNA}_{\mathbf{vsv}})} \tag{2.4}$$

where N_A is Avogadro's constant, 6.02×10^{23} mol^{-1}, D_{proK} is a dilution factor (>1) due to addition of proteinase K to the virus sample, MM(RNA_{VSV}) is the molecular mass of the viral RNA, which is 3.84×10^{6} g/mol for VSV strain in use, 10^{9} is a unit conversion factor to obtain ivp/mL. Noting that differences in sample constituents of standards (rRNA and λDNA) and VSV could influence the precise quantification process due to the possibility of differential binding of the intercalating YOYO-1 dye to the nucleic acids. To reduce this effect all samples and standards were diluted and prepared under the same conditions and analysed in the same run buffer. We also applied an excess of the dye (2 μM) to saturate the nucleic acids and keep the ratio of dye to bases constant. We suggest that, alternatively, RNA isolated from a target virus can be used for making a calibration curve, when possible.

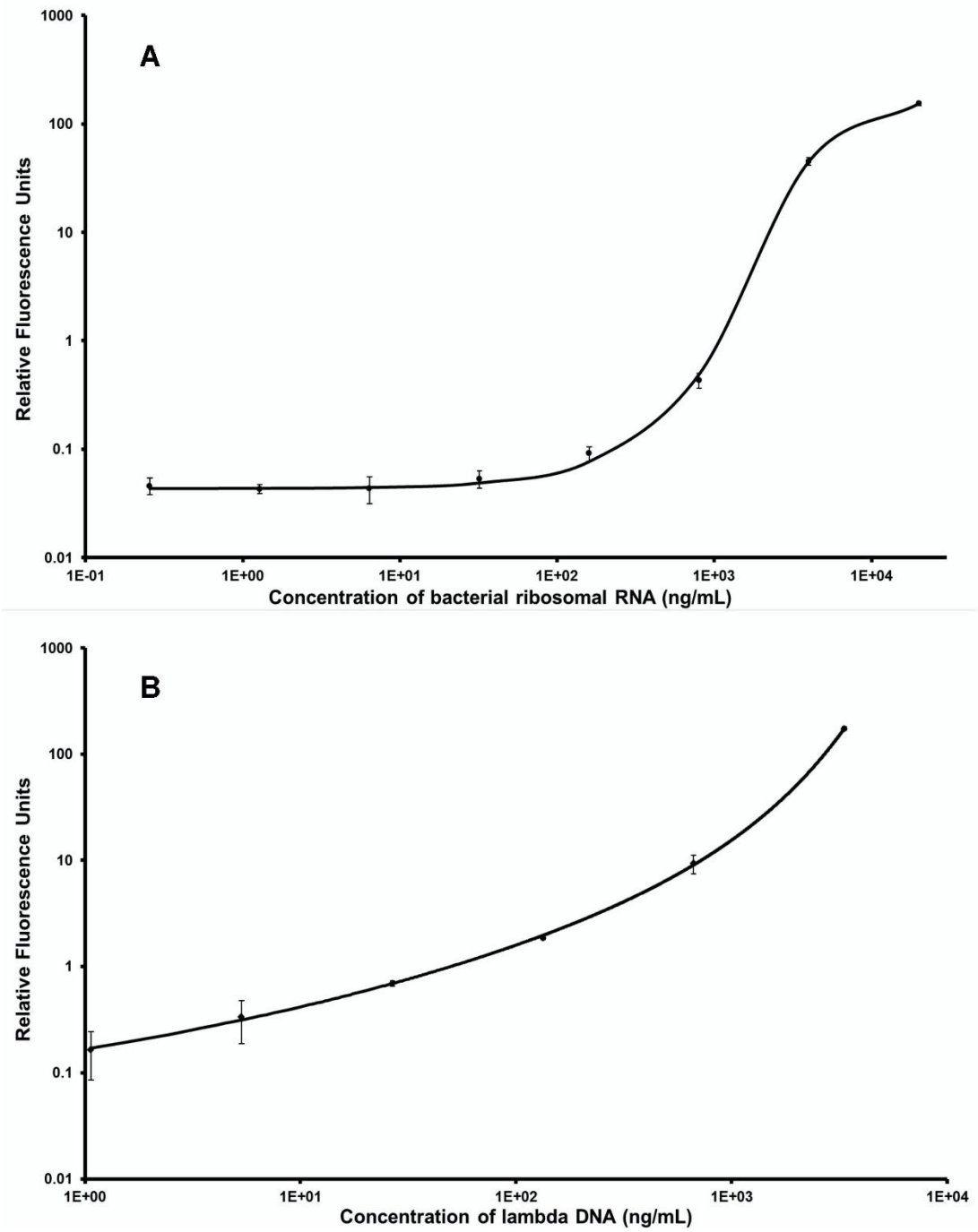

Figure 2.10. Calibration curves showing the correlation between fluorescence and concentrations of A) bacterial rRNA and B) λDNA. The concentration of YOYO-1 was 2 µM in this assay. Non-linear regression was used to fit data points and find concentrations of viral RNA and host DNA.

Three differently prepared VSV batches were studied. The results from viral qCE analysis and plaque-forming assay (PFA) are summarized in **Table 2.1.** For all three batches viral qCE yielded values two orders of magnitude higher than those obtained using PFA. This discrepancy confirms the notion that the cell-based virus infectivity method underestimates viral concentrations due to aggregation of viral particles and exclusion of non-infective ones. Specifically, non-infectious virus in the form of defective interfering particles can substantially decrease the yield of viral preparations; in particular, since the effect of these particles is compounded depending on passage frequency and multiplicity of infection[92]. In fact, it has been reported that less than 10% of VSV preparations are infectious[93]. Hence, it is reasonable that such RNA-containing non-infectious particles cause the observed difference between viral qCE and PFA results. In addition, this difference could be partly due to variations in YOYO-1 binding to viral and ribosomal RNA. However, to further investigate this issue, we used nanoparticle tracking analysis by NanoSight instrument (**Figure 2.11**). Similar to viral qCE, NanoSight counts single particles, not infective units. The concentration of batch 1 was determined using NanoSight and it was only 1.7 times higher than that found using viral qCE, which confirms the latter's efficacy in counting intact particles.

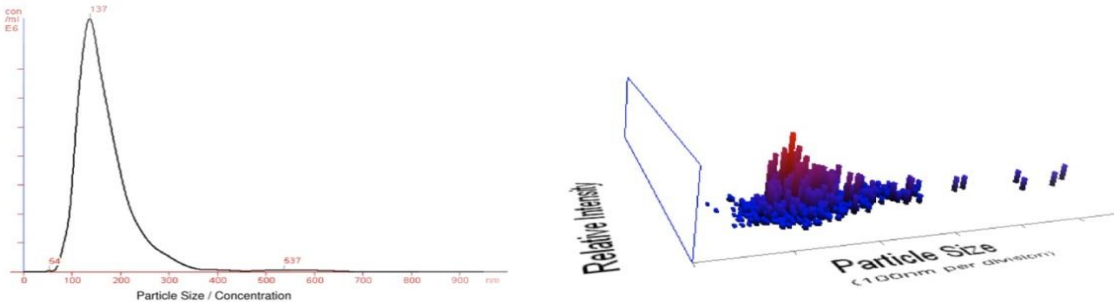

Figure 2.11. Size and concentration distribution of VSV particles in a representative sample measured by NanoSight.

Table 2.1. Experimental results with standard deviation for various analyses performed on samples from three batches of VSV prepared with slight variations

Analysis	Batch 1	Batch 2	Batch 3
Concentration			
Viral qCE (ivp/mL)	$(9.3 \pm 0.3) \times 10^{12}$	$(1.20 \pm 0.05) \times 10^{13}$	$(2.07 \pm 0.02) \times 10^{12}$
Plaque-forming assay (PFU/mL)	1.0×10^{11}	3.6×10^{10}	5.6×10^{9}
Host DNA contamination (ng/mL)	N/A	4100 ± 30	176 ± 1

N/A – not available

Quantification of DNA contamination in virus sample. Regulatory guidelines limit the amount of DNA that is allowed in human dose of viral therapeutics to 10 ng[69]. Consequently, we employed our method to determine the amount of DNA in virus samples. This process was completed in two steps. In the first step fluorescent intensity ($RFU_{proK+NaOH}$) of a viral sample after proteinase K and NaOH treatments was measured by a continuous flow through a capillary. Second, the DNA concentration was determined from a calibration curve which was constructed by plotting fluorescent intensities of λDNA standards bound to YOYO-1 as a function of their concentrations (**Figure 2.10B**). All λDNA standards were incubated with 50 mM of NaOH under the same conditions as viral samples to correct for any possible loss of DNA by hydrolysis. This curve was applied to interpolate the concentration of contaminating DNA within samples from batch 2 and

batch 3. Batch 1 was not available and had already been consumed before this assay was completely developed. Batch 2 was prepared for applications that did not require high purity of the virus. Batch 3, however, had been purified using a sucrose gradient[84] and contained much less cellular DNA. In fact, batch 2 contained 4100 $\pm$ 30 ng/mL of DNA, whereas batch 3 contained only 176 $\pm$ 1 ng/mL. Although batch 3 has a concentration almost 6 times lower than batch 2, its DNA content is approximately 23 times less indicating the ability of sucrose gradient to remove much of the contaminating DNA. Furthermore, for concentrations of virus used in therapeutic doses of 10^7 PFUs or less, which are common clinical values for oncolytic virus therapeutics[60], such viral preparations would easily satisfy WHO guidelines.

Quantification of carried-over RNA in virus samples. Viral qCE can be used to further investigate quality of the original virus preparation. The free nucleic acid peak before viral lysis may contain RNA from host cells or from virus degradation during preparation steps. Therefore, the concentration of contaminating RNA, [RNA_C], can be calculated as follows:

$$[\mathbf{RNA}_{\mathbf{C}}] = \frac{(\mathbf{A}_0 - \mathbf{A}_{\mathbf{DNA}}) \times \mathbf{D}_{\mathbf{proK}} \times \mathbf{D}_{\mathbf{NaOH}} \times [\mathbf{RNA}_{\mathbf{VSV}}]}{\mathbf{A}_{\mathbf{proK}} - \mathbf{A}_0} \tag{2.5}$$

where D_{NaOH} is a dilution factor (>1) after adding NaOH to the proteinase-treated virus sample, A_{DNA} is the area of the nucleic acid peak after NaOH treatment (**Figure 2.8C**). We investigated the amount of carried over RNA in freshly prepared viral samples and found that the RNA contamination was negligible and practically undetectable.

Degradation analysis. We also applied our method for measuring the level of viral degradation due to processes commonly encountered during viral storage or use. The percentage of viral degradation, VD, is

$$\%\mathbf{VD} = \frac{[\mathbf{RNA}_{\mathbf{C}}]}{[\mathbf{RNA}_{\mathbf{VSV}}]} = \frac{(\mathbf{A}_{0} - \mathbf{A}_{\mathbf{DNA}}) \times \mathbf{D}_{\mathbf{proK}} \times \mathbf{D}_{\mathbf{NaOH}}}{\mathbf{A}_{\mathbf{proK}} - \mathbf{A}_{0}} \times 100\% \tag{2.6}$$

In this manner, viral qCE provides a facile way to investigate the extent of viral degradation without the need for quantification of total amount of virus present in each sample due to the separation of intact virus particles from free nucleic acids. Thus, the gain in the area under the nucleic acid peak after a given degradative process can be used as a measure of the degradation level. **Figure 2.12** illustrates representative electropherograms for the three treatments.

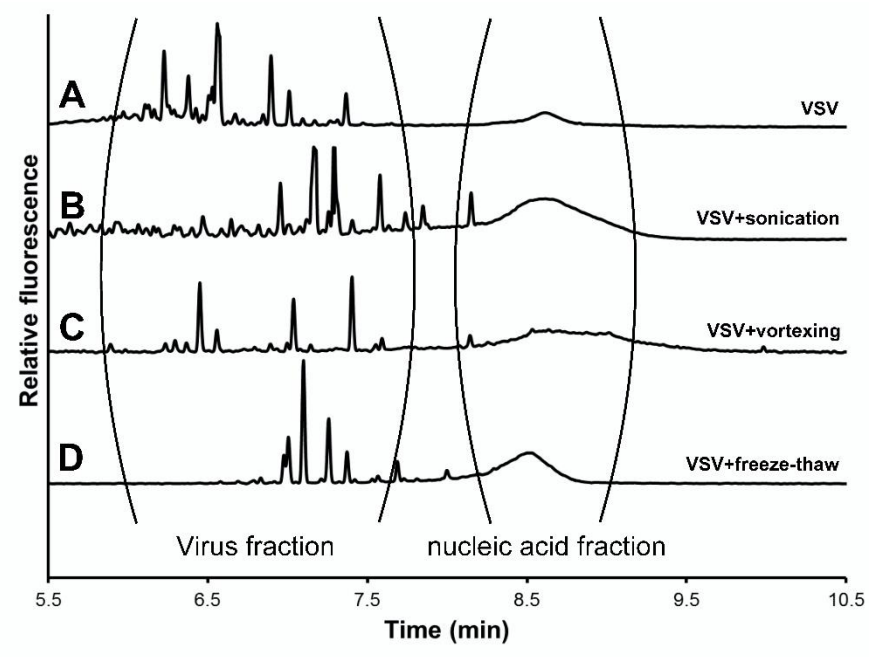

Figure 2.12. Degradation analysis. A) A fresh VSV sample, after B) 1 min ultrasonic treatment, C) 1 min vortexing and D) ten freeze-thaw cycles.

Ultrasonic treatment: Sonication or ultrasonic treatment is often used as a technique for solubilizing proteins before Western blotting[94]. Furthermore, it is desirable to increase the solubility of VSV particles prior to analysis, specifically, to break down virus aggregates that could decrease the infectivity of viral sample. Therefore, we analyzed the effects of ultrasonic treatment on viral samples using an ultrasonic bath with 40 kHz power (**Figure 2.12B**). The virus sample was degraded by 32 ± 3% and 64 ± 9% after 1 and 5 minutes of treatment, respectively.

Extensive vortexing: Vortexing is another commonly used procedure for solubilizing insoluble components or pellets after centrifugation. The same analysis as described above was applied to samples vortexed continuously for 0.5, 1 and 5 minutes. The mild treatment of 30 seconds only slightly, 1.2 ± 0.2%, degraded the virus. Yet, vortexing the sample for 1 and 5 minutes caused 12 ± 2% and 52 ± 11% viral degradation, respectively (**Figure 2.12C**).

Freeze-thaw cycles: Storage of biological samples at very low temperatures poses the risk associated with loss of activity or degradation attributed to cycles of freezing and thawing. After 10 cycles, 14 ± 2% of viral degradation was observed (**Figure 2.12D**).

It must be noted, however, that in all the aforementioned analyses, released viral RNA is used as a measure of viral degradation. This measure cannot be directly correlated to infectivity. Therefore, while the fraction of viral titer which has been deemed 'degraded' would not be infectious (due to loss of capsid), the 'non-degraded' fraction may, as well, contain agglomerated or non-infectious virions. The mechanical processes of vortexing

and sonication seem to promote RNA release much more than freezing and thawing of the sample.

2.3.4 Conclusion

In this chapter, I demonstrated a CE-based method for reliable quantification of intact RNA viruses. Viral qCE enables partitioning of intact viral particles and free nucleic acids. It measures an exact virus concentration, the level of virus degradation and host cell DNA contamination. Viral qCE can be carried out to completion in a few hours and requires minimum optimization of CE separation. Furthermore, CE-LIF detection is a very sensitive and accurate method, providing a wide dynamic range of virus quantification from 10^8 to 10^{13} ivp/mL. The sample consumption is very low and varies from 5 µL to 40 µL. It can also distinguish non-DNA impurities and exclude them from calculations. Viral qCE gives the possibility of live monitoring of virus degradation, providing information about the sample stability during storage and handling. We foresee that the presented method can be applied for quality control in oncolytic viruses and vaccine productions.

2.3.5 Acknowledgments

This work was supported by Strategic Project Grant #396508-10 for M.V.B. and Undergraduate Student Research Award for A.A. from the Natural Sciences and Engineering Research Council of Canada. The authors thank Alexey Chechik for help with NanoSight measurements.

Chapter 3: Revealing Equilibrium and Rate Constants of Weak and Fast Noncovalent Interactions

3.1. Objectives

My objectives were to develop a method for study of fast non-covalent interactions. I performed all CE experiments and analyzed data.

Dr. Victor Okhonin was responsible for creating a mathematical model for calculating rate and equilibrium constants. Dr. Serge Gorelsky was responsible for DFT calculations. Dr. Maxim Berezovski provided technical guidelines and supervision in performing all CE experiments.

3.2. Introduction

Measuring rate and equilibrium constants of molecular noncovalent interactions is important for the understanding of drug actions and cellular processes[96-98]. The dissociation rate of drug-protein complexes may be the limiting step for drug elimination and tissue distribution. Only the unbound drug is available for diffusion from plasma into organs and for reaction with cellular targets [97, 99]. For example, fast binding rates allow ligands to activate immune T cells more effectively than slow ligands and demonstrate a strong stimulatory effect[96].

The determination of rate constants is very difficult for a fast binary reaction where a ligand (L) binds reversibly to a target (T) forming a complex (C):

$$\mathrm{L} + \mathrm{T} \underset{k_{off}}{\overset{k_{on}}{\rightleftharpoons}} \mathrm{C} \qquad K_d = k_{off} / k_{on} \tag{3.1}$$

where k_{on} and k_{off} are rate constants of forward and reverse processes, respectively, and K_d is the equilibrium dissociation constant. The relaxation time τ to equilibrium for weak (K_d > 1 μM) reactions is usually less than a second and depends on rate constants, ligand (*L*) and target (*T*) concentrations:

$$\tau = 1/(k_{on}(L+T)+k_{off}) \tag{3.2}$$

The major existing methods studying noncovalent molecular interaction kinetics are Stopped-Flow (SF) and Surface Plasmon Resonance (SPR) with the minimum τ of 0.001 and 0.1 s, respectively [100, 101]. These methods fail to measure faster rates because of mixing dead-time and re-dissociation of reagents for SF as well as mass transport to and heterogeneity of the surface of a SPR chip[102, 103]. The kinetics of such interactions in SF and SPR are studied by monitoring the changes in the reactant/product concentration after the reaction is significantly perturbed from an equilibrium[104].

In our work, we introduce the first homogeneous approach to determine k_{on}, k_{off} and K_d of weak and fast kinetics in quasi-equilibrium for multiple unlabeled ligands simultaneously in one microreactor. At the conceptual level, an equilibrium mixture (EM) of L, T and C is prepared. The mixture is introduced into the beginning of a long and narrow capillary reactor filled with T. Afterward, differential mobility of L, T and C along the reactor is induced by an external action such as an electric field. The combination of differential mobility of reactants and their interaction leads to a change of the EM peak position and shape. The change is a function of rate constants, so that the rate and

equilibrium constants are directly determined from the analysis of the propagation pattern and the shape of the EM peak along the reactor.

In this work, we apply a method called Equilibrium Capillary Electrophoresis of Equilibrium Mixtures (ECEEM)[105]. It is a member of Kinetic Capillary Electrophoresis (KCE), a platform for kinetic homogeneous affinity methods in which molecules interact with each other during electrophoretic separation[106]. Previously, ECEEM was used only for determination of K_d and selection of "smart" affinity probes (aptamers and DNA-tagged small molecules) with desirable K_d values [105, 107, 108]. The quasi-equilibrium nature of ECEEM allows us to find an approximated analytical solution of mass transfer equations. We use this solution to simulate and study spatial and temporal propagation patterns of L and C for different T concentrations. We then develop a parameter-based method for finding the rate constants of complex formation and dissociation from experimental electropherograms. Finally, we demonstrate the use of ECEEM for determining kinetic parameters of non-covalent interactions between four small molecule drugs (ibuprofen, s-flurbiprofen, salicylic acid and phenylbutazone) as ligands and α- and β-cyclodextrins as targets. A long silica capillary is used as a microreactor, a diode-array detector is used for detection of the unlabeled small molecules, and an electric field is used to induce differential mobility. The measurements are performed by a commercial capillary electrophoresis instrument without modifications, suggesting that ECEEM can be immediately and widely practiced.

3.3. Materials and methods

Chemicals and Materials. Chemicals were purchased from the following companies: salicylic acid (Santa Cruz Biotechnology, USA, cat. # sc-203374), (S)-flurbiprofen (Cayman Chemical, USA, cat. # 10004207), ibuprofen (Sigma Aldrich, Canada, cat. # I4883), phenylbutazone (Santa Cruz Biotechnology, cat. #sc-204843), R-cyclodextrin (USB Corporation, USA, cat.#13979), and β-cyclodextrin (Sigma Aldrich, Canada, cat.#c4767). For all experiments, 50 mM Tris-Acetate, pH 7.85, was used as an incubation/run buffer. The buffer was prepared by dilution from 200 mM Tris-Acetate stock buffer. The stock buffer was made by dissolving 12.11 g of Tris-base Bio Basic Inc., Canada, cat.# 77-86-1) and 2.86 mL of acetic acid (Bio Basic Inc., Canada, cat.# C1000) in 500 mL of ddH2O.

Equilibrium mixtures of drugs and cyclodextrins were prepared in the incubation buffer with the following concentrations of small molecules: 30 µM S-flurbiprofen, 30 µM ibuprofen, 30 µM phenylbutazone, 50 µM salicylic acid, and cyclodextrins: 25 µM-5 mM β-cyclodextrin and 250 µM-100 mM R-cyclodextrin. Stock solutions (10 mM) of small molecules (except phenylbutazone) were prepared by directly dissolving a weighed amount of the drugs in 10 mL of the incubation buffer. For phenylbutazone, a 10 mM stock solution was prepared in 95% ethanol and then diluted in the incubation buffer. All solutions were filtered through 0.22 µm pore size membrane filters (Millipore, Nepean, ON, Canada).The bare-silica capillary was purchased from Polymicro (Phoenix, AZ, USA).

Experimental Conditions of ECEEM. All ECEEM experiments were performed with the following instrumentation, settings, and operations unless otherwise stated. ECEEM was carried out with a PA800 Pharmaceutical Analysis CE system (Beckman Coulter, USA)

equipped with PDA and UV detectors. We used the following conditions: the sample storage and capillary temperature maintained at 25 (0.5 C, an electric field of 303 V/cm (172 V/cm for the individual β-CD/ibuprofen pair) with a positive electrode at the injection end, the run buffer with one of the cyclodextrins in the inlet reservoir, and the incubation/run buffer in the outlet reservoir. The concentration of the cyclodextrin in the equilibrium mixture and the run buffer was the same for individual ECEEM experiments. For all experiments, the capillary was 89 cm long (80 cm to the detection window; for individual ibuprofen 29 and 20 cm, respectively) with an inner diameter of 75 µm and an outer diameter of 360 µm. An approximately 15 mm long plug (29 nL) of the equilibrium mixture was injected into the capillary from the inlet end by a pressure pulse of 8 s^{-1} 0.5 psi. Before each experiment, the capillary was rinsed by 20 psi pressure with 0.1 M HCl for 3 min, 0.1 M NaOH for 3 min, ddH2O for 3 min, 50mM tris-acetate buffer for5min, and the incubation/run buffer with cyclodextrin for 1 min. The output data was absorbance intensity in the detection point, as a function of time passed since the application of the electric field.

3.4. Results

Principle of ECEEM

Practically, in ECEEM, an equilibrium mixture of a target with one or multiple ligands is prepared and equilibrated. A plug of EM is injected into a capillary pre-filled with a run buffer containing T with a total concentration identical to EM (**Figure 3.1A**). Components of EM are separated by capillary electrophoresis while quasi-equilibrium is maintained

between T, L and C inside the capillary. There are three unique features of ECEEM: (i) the migration time of the EM peak depends on concentration of T in the run buffer, so ligands with different K_d values migrate with different velocities, (ii) L and C migrate as a single EM peak due to fast exchange between them and (iii) EM peak broadening is dependent on concentration of T, relaxation time τ and characteristic separation time. The characteristic separation time, t_{sep}, is the time required for L and C to separate from each other and can be defined as:

$$t_{\text{sep}} = w / \left(2 \left| V_C - V_L \right| \right) \tag{3.3}$$

where w is the width of the initial EM peak, V_C and V_L are the velocities of C and L, respectively. If $\tau > t_{sep}$, the zones of L and C are separated before the re-equilibration in reaction (1) proceeds to a significant extent. Thus, L and C are moving as separate peaks. If $\tau \sim t_{sep}$, re-equilibration in reaction (3.1) and separation proceed with comparable rates. Therefore, L and C are moving as two peaks with some overlap between them. Finally, if $\tau < t_{sep}$, the re-equilibration in reaction (3.1) occurs much faster than peaks separation, and, as a result, L and C will be moving as a single peak. The last case of fast molecular interactions conceptually illustrated in **Figure 3.1**. The figure shows spatial propagation patterns of L and C for the three different concentrations of T ($T = 0, 0.5K_d$ and $10K_d$).

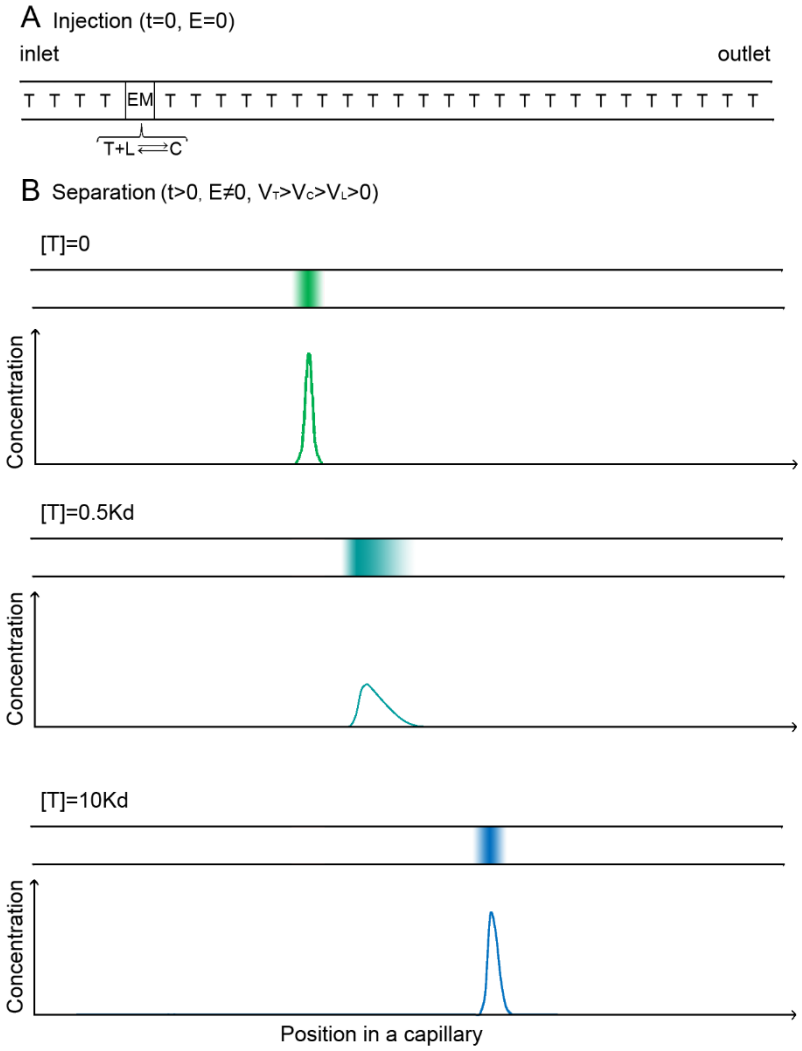

Figure 3.1. (A) Schematic representation of ECEEM setup in its initial condition. (**B**) Illustration of spatial propagation patterns of a ligand (L, green) and a complex (C, blue) in a single-dimensional reactor at different target concentrations (T, white).

When T = 0 (**Fig. 3.1B top panel**), C completely dissociates in the first seconds, so EM migrates as a Gaussian symmetrical peak with the velocity of free L. When $T = 0.5K_d$ (**Fig. 3.1B middle panel**), EM contains L and C in a 1:2 ratio and moves as a single peak with an intermediate velocity V_{EM} ($V_C > V_{EM} > V_L$). At the same time, the peak becomes asymmetrical and wider than free L. The asymmetry of the peak is caused by the

nonlinear effect of complex formation due to the gradient of *T* inside the EM peak. In **Figure 3.1B bottom panel**, the concentration of T is so high ($T = 10K_d$) that the majority of L presents in C and migrates with V_C. The shape of the peak becomes symmetrical again and the width is similar with free L.

Analytical Solutions of Mass Transfer Equations in ECEEM

The ECEEM separation of three reactants in capillary electrophoresis is described by the system of mass transfer equations:

$$\frac{\partial L}{\partial t} + V_L \frac{\partial L}{\partial x} - D_L \frac{\partial^2 L}{\partial x^2} = \frac{\partial T}{\partial t} + V_T \frac{\partial T}{\partial x} - D_T \frac{\partial^2 T}{\partial x^2} = k_{off} C - k_{on} LT = \\ = -\frac{\partial C}{\partial t} - V_C \frac{\partial C}{\partial x} + D_C \frac{\partial^2 C}{\partial x^2} \quad (3.4)$$

where *L, T* and *C* are the concentrations of a ligand, target, and complex, respectively, V_L, V_T and V_C are the migration velocities, D_L, D_T, D_C are the coefficients of diffusion, *t* is the time, *x* is the spatial coordinate, k_{off} is the decay constant, and k_{on} is the rate constant of complex formation.

The general analytical solution of these nonlinear differential equations in partial derivatives is not known. In some cases like (i) formation or decay rate constants are negligible or zero[109, 110], (ii) $V_C = V_L$ or $V_C = V_T$, the equations (3.4) become linear directly or after the Cole-Hopf substitution[111, 112]. For our case of fast molecular exchange ($\tau < t_{sep}$) and $L < T + K_d$, the following approximated equation can be used:

$$\partial_t L + \left(V_{EM} - \frac{2k_{on} D_{CID}}{V_T - V_{EM}} L \right) \partial_x L \approx \left(D_{CID} + D_{EM} \right) \partial_x^2 L \quad (3.5)$$

where V_{EM} is the velocity of EM peak, D_{EM} is a physical diffusion coefficient for EM peak and D_{CID} is a chemically induced coefficient of diffusion. They can be described as:

$$V_{EM} \equiv \frac{K_d V_L + T V_C}{K_d + T}, \quad D_{EM} \equiv \frac{K_d D_L + T D_C}{K_d + T}, \quad D_{CID} \equiv \frac{T K_d^2 \left(V_C - V_L\right)^2}{k_{off} \left(K_d + T\right)^3} \tag{3.6}$$

Equation (3.5) is well known in mathematics as Burgers' equation. The special exact solution of Burgers' equation is following

$$\Delta \equiv \sqrt{\Delta_0^2 + 4t\left(D_{EM} + D_{CID}\right)}, \quad L + C = \\ = \frac{\left(1 + \frac{D_{EM}}{D_{CID}}\right)\left(K_d + T\right)\frac{\left|V_T - V_{EM}\right|}{k_{off}\Delta}\exp\left(-\left(\frac{x - V_{EM}t}{\Delta}\right)^2\right)}{\sqrt{\pi} \Big/ \left(\exp\left(\frac{k_{off} D_{CID} L_0 \times l}{\left|V_T - V_{EM}\right|\left(K_d + T\right)\left(D_{CID} + D_{EM}\right)}\right) - 1\right) + \int\limits_{-\infty \cdot sign(V_T - V_{EM})}^{\frac{x - V_{EM}t}{\Delta}} \exp(-y^2)dy} \tag{3.7}$$

Where Δ and Δ_0 are a Gaussian half-width (STDv2) of the EM peak at $t > 0$ and $t = 0$, respectively, after the Cole-Hopf transformation which "linearizes" Burgers' equation. In other words, an asymmetrical peak becomes a symmetrical after the Cole-Hopf transformation. L_0 is the total concentration of the ligand in EM and l is a plug length of the EM injection. Solution (3.7) corresponds to initial conditions when the initial EM peak is sharp or the peak becomes a Gaussian after the Cole-Hopf transformation. In a case, when L_0 is very low and $L_0 \times l << \left|V_T - V_{EM}\right|\left(K_d + T\right)/k_{off}$, solution (3.7) becomes close to Gaussian distribution and does not require the Cole-Hopf transformation.

The asymmetry of the EM peak, J is defined by a factor r, a ratio of the bigger area (A_1) to the smaller area (A_2) of the EM peak divided at its maximum (**Fig. 3.2C**). There is an approximated connection between r and the rate and equilibrium constants:

$$J \equiv \frac{k_{off} D_{CID} L_0 \times l}{\left|V_T - V_{EM}\right|\left(K_d + T\right)\left(D_{CID} + D_{EM}\right)} \approx$$
$$\approx 5.499 \cdot \left(r-1\right)^{0.87925} \cdot \exp\left(\left(r-1\right) \cdot 0.0289\right) \tag{3.8}$$

K_d can be found from the expression:

$$K_d \approx \sum_i \frac{\left(V_{EM}^i - V_L\right)^3 \left(V_C - V_{EM}^i\right)}{T_i} \Big/ \sum_i \frac{\left(V_L - V_{EM}^i\right)^4}{T_i^2} \tag{3.9}$$

When J, V_C, V_L, V_T, D_C, D_L, and K_d are known, k_{off} can be determined from equation (3.8). For the low asymmetry case (r ~ 1), k_{off} can be found from the EM peak widening using equation (3.7).

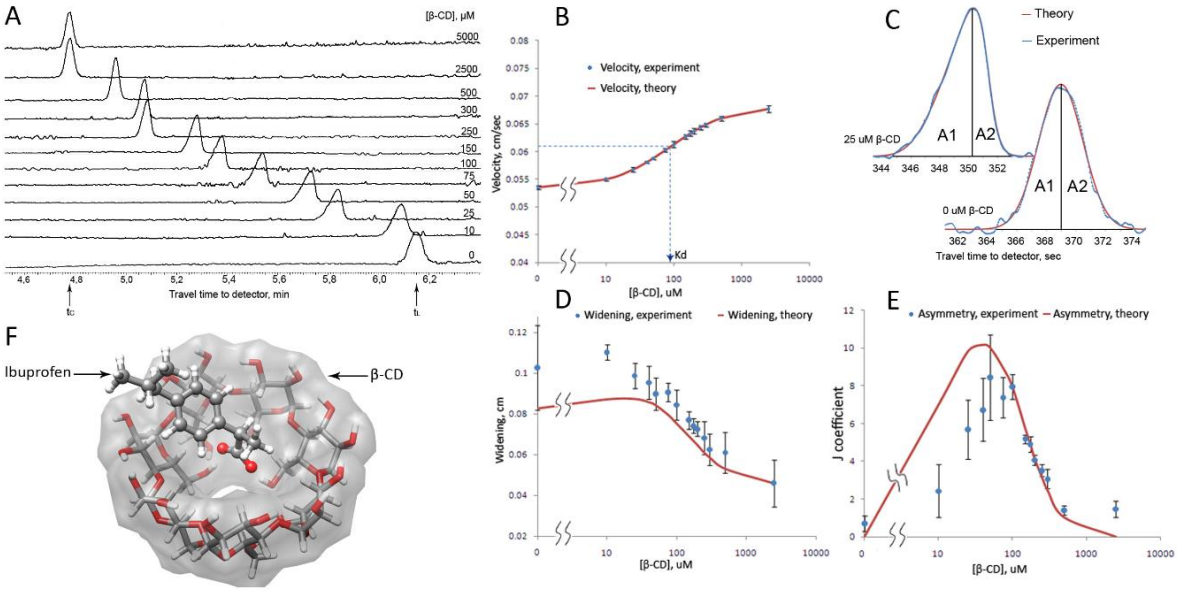

Figure 3.2. Determination of equilibrium and rate constants of β-CD/ibuprofen. (**A**) Representative ECEEM electropherograms of ibuprofen (30 μM) for varying concentration of β-CD. (**B**) The plot of EM velocity as a function of β-CD concentration for K_d determination. (**C**) Representative shapes of free ligand and EM peaks (theoretical and experimental). (**D**) Dependence of EM peak widening $(\Delta - \Delta_0)$ on the concentration of β-CD. (**E**) Dependence of EM peak asymmetry, J, on the concentration of β-CD. (**F**) The visualization of a DFT calculated β-CD/ibuprofen complex.

Experimental Model

An experimental model involving the formation of inclusion complexes between α- and β-cyclodextrins (CDs) and small organic molecules (SMs) was chosen as a representative and important example of weak and fast affinity non-covalent interactions. Four well-known anti-inflammatory drugs: ibuprofen, s-flurbiprofen, salicylic acid and phenylbutazone form a host-guest complex with cyclodextrins. Visual structures of the complexes are presented in **Figures 3.2F** (for β-CD/ ibuprofen) **and Figure 3.3** (for α- and β-CD/SMs).

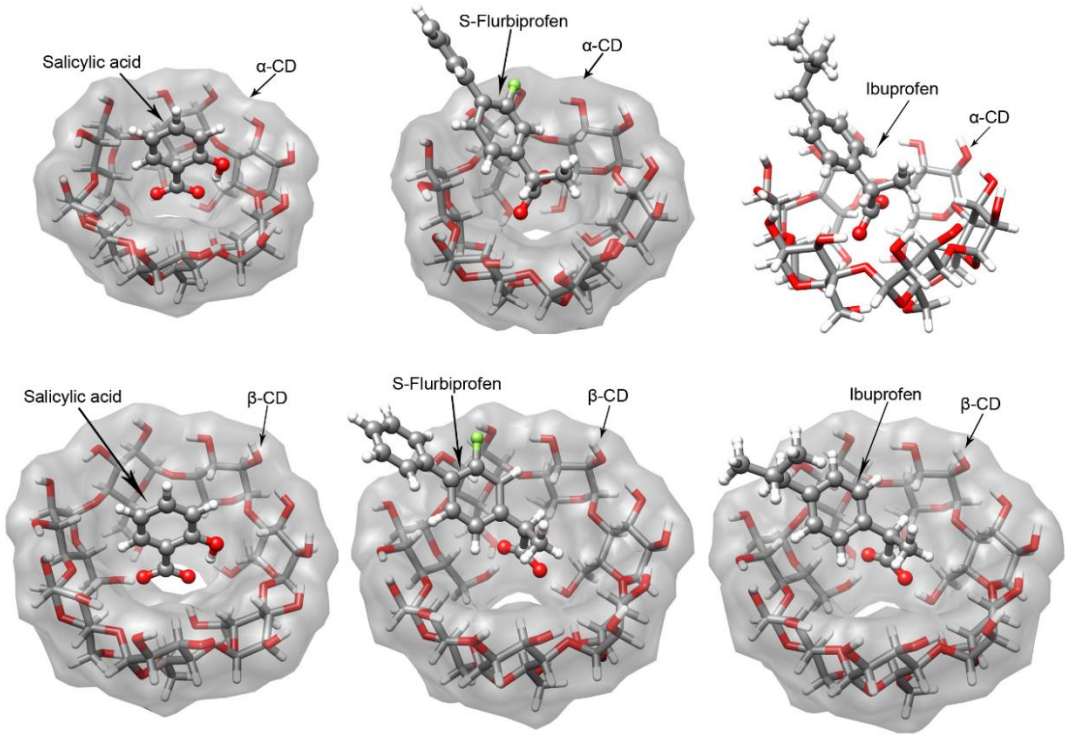

Figure 3.3. DFT-calculated structures of complexes of α- and β-cyclodextrins and small molecule drugs.

The formation of inclusion complexes modifies the physical and chemical properties of guest small molecules and significantly increases their water solubility. This is the reason why CDs attract interest in pharmaceutical applications[113]. CDs enhance the bioavailability of poorly soluble drugs by delivering a hydrophobic drug to a lipid cell membrane, where the drug can penetrate inside a cell[114]. Therefore, measuring kinetics of complex dissociation and association between CDs and drugs is extremely important for understanding drug actions. Fast kinetics with high affinity increases the drug activity by enhancing its solubility and the fraction of an administered dose of the drug that reaches the systemic circulation. Reciprocally, slow kinetics and low affinity decrease its activity. In this proof-of-principle work, we conducted the study in a narrow (inner diameter of 75 μm) and long 89 cm (29 cm for ibuprofen) capillary reactor. We chose an electric field to induce differential mobility of L and C. Radial gradients of concentrations and radial mass transfer are negligible in such a 1-dimensional capillary reactor. To exclude boundary effects in a finite-length capillary reactor, the ends of the capillary were placed into reservoirs with the running buffer containing T. Advantageously, commercial capillary electrophoresis instruments with UV or photodiode array (PDA) detection can be used for such experiments. They are typically equipped with single-point detectors (located close to the end of the capillary) recording temporal label-propagation patterns. In this work, we used one such instrument without any modifications.

To stay consistent with the terminology used in the theoretical consideration, α- and β-cyclodextrins are called T, while the small molecules are called L. Their complexes are called C.

We have a few important notes on the choice of experimental conditions. The experimental conditions for the CD/SM system were chosen to minimize the potential effect of the formation of a complex of a small molecule with two molecules of CD. We used a range of concentrations of β-CD (10 μM to 5 mM) well below concentrations of β-CD (> 10 mM) at which the formation of 2:1 β-CD/SM complex was observed[115].

Experimental Parameter-Based Method for Determination of Kd, kon and koff for One Interaction Pair

Time propagation profiles of C and L propagation for the experimental model β-CD/ibuprofen was studied for varying concentrations of β-CD (**Fig. 3.2A**). CD molecules are bulky and neutral, so electroosmotic flow moves them faster than SM molecules. The mobility of the complex is between CD and SM and can be found by the mobility of the EM peak at high concentration of CD using the dependence on EM velocity and concentration of β-CD **(Fig. 3.2B)**. A notable shift of the EM zone was observed with the increase of *T*.

To determine k_{on} and k_{off} for our experimental model, we used the parameter-based method the theory of which was described earlier. The process of finding binding constants can be divided into four steps: (i) measuring velocities of L, C and T, (ii) calculating K_d, (iii) finding *J* (EM peak asymmetry) and (iv) finally calculating k_{off}.

Rate and equilibrium constants were determined for the ibuprofen/β-CD system: k_{off} = 12.7 ± 1.7 s^{-1}, K_d = 86.1 ± 1.4 μM and k_{on} = (14.8 ± 2.3) ×10^4 $M^{-1}s^{-1}$. To the best of our knowledge, this is the first report on the kinetic parameters for the fast (τ ~ 1.9 ms) small

organic molecule/cyclodextrin interaction. This molecular pair also has prominent pharmacological importance [113]. The constants were calculated based on fifteen experiments repeated three times each with a fixed concentration of ibuprofen (30 µM) and varying concentrations of β-CD from 10 µM to 5 mM. Experiments carried out with *T* in the range of (0.1 - 3)×K_d provide the most confident results of rate and equilibrium constants. In this range the EM contains both L and C in comparable amounts. The behavior of the confidence for β-CD/Ibuprofen complex formation is presented in **Fig. 3.4**.

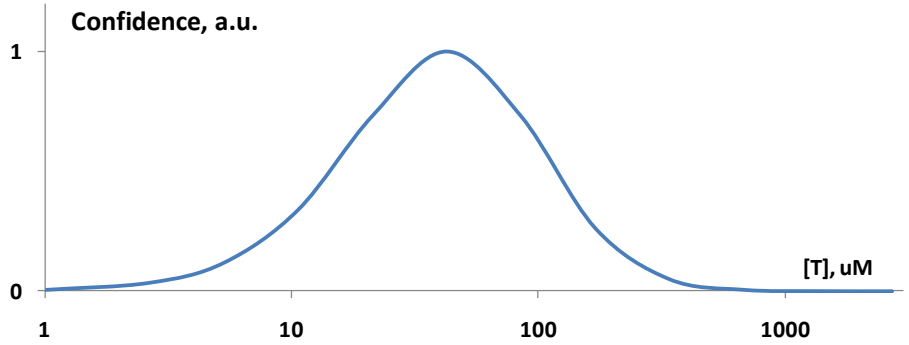

Figure 3.4. The behavior of the confidence for β-CD/Ibuprofen complex formation. [T] – concentration of β-CD.

It should be mentioned that molecular diffusion can contribute to zone widening in a similar way as molecular interaction. Moreover, in our case, the zone became broader with decreasing migration time – the phenomenon opposite to that could be caused by diffusion. Nevertheless, we found diffusion coefficients for L and C by a CE method described elsewhere[116]. Briefly, we measured the change of either L (at *T* = 0 in the run buffer) or C (at high *T*) peak profiles in the same CE experiment: before dispersion and after dispersion of an injected plug. This was achieved by first moving an analyte in one direction to pass the detector and record the initial concentration profile. The analyte was

then stopped to allow for its diffusion. Finally, the analyte was moved back to pass the detector for the second time and record the final concentration profile. The diffusion coefficients for free ibuprofen and its complex were 4.6×10^{-6} and 1.7×10^{-6} cm^2sec^{-1}, respectively.

A computer simulated model of the complex between ibuprofen and β-CD is shown in **Fig. 3.2F**. According to this DFT-calculated model, CD holds ibuprofen inside the cavity by two hydrogen bonds between a terminal carboxyl group of ibuprofen and two hydroxyl groups on the bottom of the cyclic oligosaccharide.

Simultaneous Determination of K_d, k_{on} and k_{off} for Multiple Interaction Pairs

The experimental setup and calculation procedures of finding rate and equilibrium constants for multiple CD/SM pairs were the same as for the previously described β-CD/ibuprofen pair. The only differences were the longer length of the capillary (89 cm) and the injected EM contained all four SMs. As long as electropherograms provide necessary information (a velocity, area and shape) about all peaks it is possible to measure binding constants, so the maximum number of compounds studied with this methods is limited only by resolution of the CE separation, which was ~60.

We studied time profiles of peak propagation for two experimental models - a mixture of phenylbutazone, ibuprofen, S-flurbiprofen and salicylic acid with either α-CD or β-CD. The experimental electropherograms for varying concentrations of α-CD and β-CD are shown in **Figs. 3.5C** and **3.5A**, respectively. The increase of CD concentration decreases the migration times of SMs and the change of their peak shapes. For example, peak 2

(ibuprofen) and peak 3 (S-flurbiprofen) in **Fig. 3.5B** are asymmetrical and wider than the symmetrical and narrow peak 1 (phenylbutazone) in the presence of 50μM β-CD, because phenylbutazone does not form a complex.

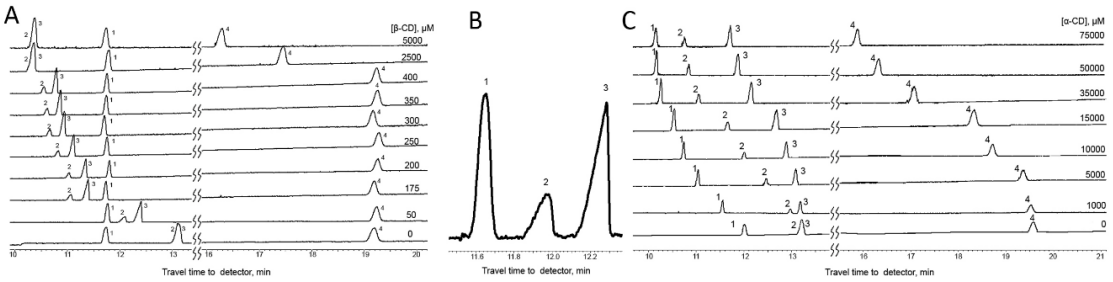

Figure 3.5. ECEEM of mixture of 30 μM phenylbutazone (1), 30 μM ibuprofen (2), 30 μM S-flurbiprofen (3) and 50 μM salicylic acid (4) in 50 mM Tris-Acetate buffer with various concentrations of β-CD (A) and α-CD (C). Observed peak shapes for 30 μM phenylbutazone (1), 30 μM ibuprofen (2) and 30 μM S-flurbiprofen (3) in 50 mM Tris-Acetate buffer with 50 μM β-CD (B).

We calculated all rate and equilibrium constants and presented them in **Table 3.1** except for the β-CD/phenylbutazone pair. Phenylbutazone did not show any affinity to β-CD. Binding affinities of drugs to β-CD are higher than to α-CD by a factor of 145 for ibuprofen, 121 for S-flurbiprofen and 8 for salicylic acid. Structural diversity between α-CD and β-CD causes the variation in rate constants of complex formation. The inner cavity of α-CD (3.9 Å at the bottom and 5.3 Å at the top) is smaller than that of β-CD (5.3 Å×7.0 Å), so it takes longer for drugs to fit in and to form an inclusion complex with α-CD than β-CD. The dissociation of complexes happens very quickly and the life-time of the complexes varies from 31 ms to 233 ms. We were able to measure the rate and equilibrium constants for very fast interactions with the relaxation time varying from 230 ms to 0.9 ms and K_d varying from 80 μM to 3mM.

Table 3.1. Rate and equilibrium constants between small molecules and cyclodextrins measured in multiplex experiments.

α-CD (β-CD)	S-Flurbiprofen	Ibuprofen	Salicylic acid	Phenylbutazone
K_d, μM	19000±4000 (155±2)	12000±1500 (80±17)	26000±3000 (3200±700)	4500±800 -
$k_{on,}$ $\times 10^3$ $M^{-1}s^{-1}$	0.3±0.1 (210±30)	0.8±0.4 (102±9)	0.3±0.1 (1.3±0.4)	1.2±0.3 -
$k_{off,}$ s^{-1}	6.0±0.7 (33±5)	9.5±2.8 (8.4±1.2)	6.5±0.9 (4.3±1.7)	5.4±0.7 -
Complex's life-time, ms	166±16 (31±5)	104±24 (119±15)	155±18 (230±7)	185±22 -

Cyclodextrins have a shape of a torus with a less hydrophilic cavity than the outside environment. To enter into the cavity ibuprofen, S-flurbiprofen and salicylic acid have to overcome steric hindrances and exclude water molecules from the inner space, but the formation of new hydrogen bonds between SM and the bottom of the cavity stabilizes these complexes. In our experiments, we observed a high affinity of ibuprofen and s-flurbiprofen binding to β-CD. S-flurbiprofen with two aromatic rings is bigger than ibuprofen which has only one ring. Interesting to note is that k_{on} for s-flurbiprofen is twice as high as for ibuprofen, but the complex's life-time is four times shorter. The big size of S-flurbiprofen probably makes it difficult to stay inside CD, so the complex dissociates very fast.

In addition, we performed DFT calculations for complexes between three drugs (ibuprofen, S-flurbiprofen and salicylic acid) and cyclodextrins to find their structures (**Fig.**

3.3). The calculated electronic binding energies (ΔE without entropy and thermal correlation) depend linearly with the Gibbs free energies (ΔG) obtained from experimentally determined equilibrium dissociation constants (**Fig. 3.6**).

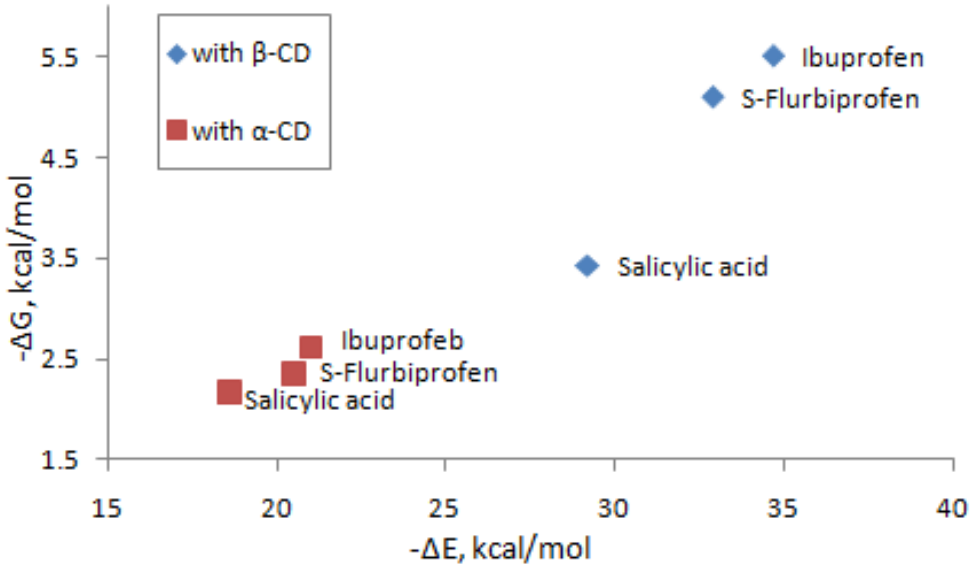

Figure 3.6. Correlation between experimental binding free energies, ΔG, obtained from Kds and DFT-calculated electronic binding energies, ΔE, for α-CD/SM (red squares) and β-CD/SM (blue diamonds) complexes.

3.5. Discussion

Kinetic Capillary Electrophoresis (KCE)[106], which started with pioneering work of Whitesides on Affinity Capillary Electrophoresis (ACE)[117-119], establishes a new homogeneous platform for studying kinetics and thermodynamics of molecular interactions. In KCE, differential mobility of T and L is used to create conditions for measuring rate and equilibrium constants of their interactions. Most of the seven KCE methods (NECEEM, SweepCE, plug-plug KCE, etc.) are perturbations and not suitable for measuring reactions with fast re-equilibration ($\tau < t_{sep}$). This makes the perturbation

methods inapplicable to fast reactions. For example, in NECEEM, if the dissociation of a complex happens quickly, it is almost impossible to measure $k_{off} > 0.1\ s^{-1}$.

In contrast, ECEEM considers both the forward and reverse process in reaction (3.1). ECEEM is a quasi-equilibrium method, in which a target fills the reactor and the propagation of one or multiple ligands through the target is followed while maintaining fast equilibrium. The method was originally used to find K_d only. However, Whitesides and co-authors suggested it for finding rate and equilibrium constants through a relatively complicated numerical approach of fitting reactant-propagation profiles[118, 119]. The complexity of the analysis and the method's applicability to intermediate rates of equilibration ($\tau \sim 10$ sec) likely explain why the method has never been utilized thereafter for 18 years.

In this study, we applied a simple experimental method, ECEEM, and revealed that peak's shift, its asymmetry and widening can be used for the precise determination of rate constants for weak molecular interactions. There is no labeling procedure necessary. The equilibrium mixture of the unlabeled ligand and the target is injected into a "long" capillary and separated in the buffer containing the same concentration of the target. "Long" means there are no boundary effects at the entrance and exit points of the reactor and "narrow" means there are no radial concentration gradients and mass transfer. For practical consideration, capillaries typically used in capillary electrophoresis and capillary chromatography have a length of 20-80 cm and an inner diameter of 20-75 μm, and can be used as "long and narrow" reactors in all foreseeable experimental models.

In addition, ECEEM has a unique "accumulation" property. It accumulates the effect of molecular interactions through the change of peak shapes during the electrophoretic separation. Experiments in extra long capillaries could potentially reveal rates of extremely fast interactions by measuring width and asymmetry of EM peaks, if $D_{CID} > D_{EM}$.

While in our experimental demonstration of ECEEM we used an electric field, other means of inducing differential mobility can be used like chromatography or centrifugation. It is difficult to hypothesize on advantages and limitations of different ways of separation *a priori* but some general considerations can be made. An external action used in ECEEM to induce the differential mobility can potentially affect the reaction kinetics. We performed our separation experiments at different electric fields and found small variations (<25%) of binding constants. Nevertheless, the possibility of such an influence cannot be completely excluded and could be experimentally studied by varying an electric field and extrapolating the results to zero voltage. A similar concern exists for chromatography. The interaction of the reaction components with the chromatographic stationary phase can also affect the reaction kinetics. While PDA detection was used in our study, ECEEM is compatible with other types of detectors: fluorescent, electrochemical, and mass spectrometric.

3.6. Conclusion

We developed a homogeneous method to determine k_{on}, k_{off} and K_d of fast and weak noncovalent interactions between multiple unlabeled ligands (small molecule drugs) and an oligosaccharide (α- or β-cyclodextrin) simultaneously in one capillary microreactor. The

availability of commercial instrumentation for capillary electrophoresis and high-performance liquid chromatography with all of the previously listed detection approaches suggests that ECEEM can be practiced immediately. ECEEM can potentially facilitate kinetic studies of noncovalent interactions with complicated stoichiometry (different from 1:1) involving proteins and nucleic acids.

3.7. Acknowledgments

This work was supported by Natural Sciences and Engineering Research Council of Canada

Chapter 4: Comparative Study of Three Methods for Affinity Measurements Capillary Electrophoresis Coupled with UV Detection and Mass Spectrometry, and Direct Infusion Mass Spectrometry

4.1. Objectives

My objectives were to compare three different methods for affinity measurements. I designed and performed all CE-MS and DIMS experiments and compiled and analyzed experimental data.

Jennifer Logie CE-UV experiments. Dr. Victor Okhonin was responsible for creating a mathematical model for calculating equilibrium constants. Dr. Justin Renaud and Dr. Paul Mayer were responsible for RRKM modeling and gas phase experiments. Dr. Maxim Berezovski provided technical guidelines and supervision in performing all CE experiments.

4.2. Introduction

Kinetic Capillary Electrophoresis (KCE) [121] is a separation of species that interact during electrophoresis and is applied for measuring rate and equilibrium constants of molecular noncovalent interactions [122, 123], assessing thermodynamics[124], and performing affinity purification of both DNA aptamers[125] and DNA-tagged drugs[126]. The development of KCE started with pioneering work of Whitesides on Affinity Capillary

Electrophoresis (ACE)[127-129] and established a new paradigm that separation can be used as comprehensive kinetic tool for the study of drug actions and screening[119].

While UV absorption and laser-induced fluorescence detection have been successfully used in conjunction with capillary electrophoresis (CE), the ability to acquire accurate molecular mass and structural information about interacting molecules is highly desirable. Applications of capillary electrophoresis coupled with mass spectrometry (CE-MS) started over twenty years ago[130] and made significant advancements in the field of analytical chemistry. The mass spectrometer can provide information regarding the structure of known and unkno wn components present in a complex mixture with high specificity and high sensitivity.

The study of noncovalent molecular interactions is a great interest for design and screening new drugs. Recently, several reviews were published on this topic[131, 132]. While there are different techniques for affinity measurements: MS[133], NMR[134], spectroscopy[135], SPR[136], stop-flow[137], and HPLC[138], only CE provides a possibility to study simultaneously multiple analytes in a liquid and homogenous phase due to their spatial separation.

In this work, we coupled on-line ACE with MS to combine separation and binding capability of ACE together with molecular weight and structural elucidation of MS in one system. The potential advantages of ACE-MS are that (i) analytes interact with each other in a homogeneous reaction at near physiological conditions (pH and ionic strength), and binding parameters are measured in solution; (ii) analytes don’t require special labeling

for the MS detection; and (iii) interactions of multiple analytes are studied together in one capillary microreactor.

To understand the benefits of ACE-MS, we compare three methods: Direct Infusion Mass Spectrometry (DIMS), ACE with UV detection (ACE-UV) and ACE-MS for finding the affinity constants of noncovalent interactions between β-cyclodextrin (CD) and eight small molecule drugs (SMs) in the following equilibrium reaction:

$$\mathrm{SM+CD} \rightleftarrows \mathrm{Complex}$$

where SM denotes the drug, CD is the cyclodextrin, and Complex is the drug-cyclodextrin complex. The apparent dissociation constant of drug-cyclodextrin complex, K_d, is defined according to the mass action law for the reaction above:

$$K_d = \frac{[SM] \times [CD]}{[SM]_0 - [SM]} \tag{4.1}$$

where $[SM]_0$ and [SM] are the total and unbound drug concentrations, respectively. [CD] is the unbound cyclodextrin concentration. SMs are five non-steroidal anti-inflammatory drugs: ibuprofen, s-flurbiprofen, diclofenac, phenylbutazone, naproxen, as well as three other small molecules: folic acid, resveratrol and 4,4'-(propane-1,3-diyl) dibenzoic acid (PDDA).

The experimental model involving the formation of inclusion complexes between CD and SMs is chosen as an important example of fast affinity non-covalent interactions[139]. It is also a complicated model due to high stoichiometry of complexes and different ionization levels for SM, CD and their complexes. SMs form a host-guest complex with CD. The formation of inclusion complexes modifies the physical and chemical properties of

guest SMs and significantly increases their water solubility. This is the reason why CDs have attracted interest in pharmaceutical applications[140]. CDs enhance the bioavailability of poorly soluble drugs by delivering a hydrophobic drug to a lipid cell membrane, where the drug can penetrate inside a cell[141]. Only the unbound (free) drug is available for diffusion across membranes, which results in absorption and distribution, and eventually in reaching the activity site. The unbound drug fraction, $F_u(SM)$, is defined as the ratio of the unbound drug concentration, [SM], to the total drug concentration, $[SM]_0$ and depends on the apparent dissociation constant.

$$F_u(SM) = \frac{[SM]}{[SM]_0} = \frac{1}{1+[CD]_0/K_d} \qquad (4.2)$$

when $[CD]_0 >> [SM]_0$

In DIMS, ion intensities of free SMs are used for finding apparent dissociation constants in several titration experiments with different CD concentrations (**Figure 4.1**). This is the simplest method, but its major problem is the difference in electrospray ionisation efficiency of each compound in a mixture when they are injected all together without prior spatial separation.

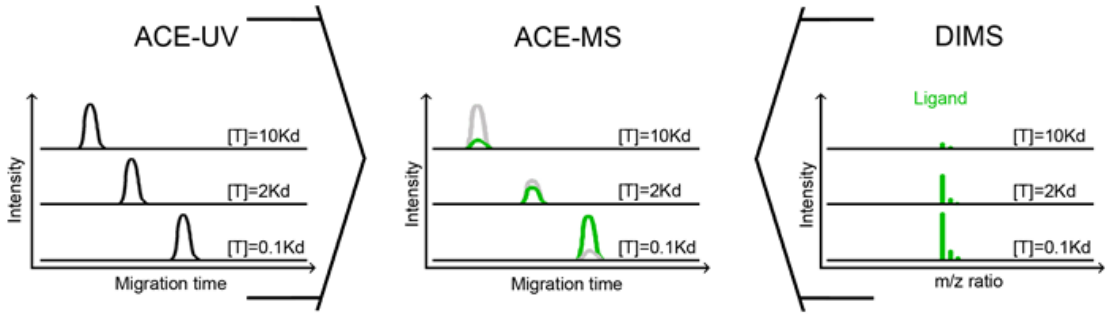

Figure 4.1.Schematic representation of titration experiments using three methods for affinity measurement: ACE-UV, ACE-MS and DIMS. Grey color represents the complex between a small molecule ligand and cyclodextrin as a target (T). Green color represents

the free ligand. Concentration of the target varies from 0.1 K_d to 10 K_d. In DIMS experiments, only ion intensity of a free ligand is used for calculation of K_ds. In ACE-UV, migration times of an equilibrium mixture between the ligand and the target are used. ACE-MS combines the information from migration times and ion intensities.

ACE-UV is a CE-based separation technique with a universal and nonspecific UV detection. We applied a ACE method called Equilibrium Capillary Electrophoresis of Equilibrium Mixtures (ECEEM)[142]. In ECEEM, an equilibrium mixture (EM) of β-cyclodextrin with all small molecules is prepared and equilibrated. A plug of EM is injected into a capillary pre-filled with a run buffer containing CD with a total concentration identical to EM and is subject to a high electric field along the capillary (**Figure 4.1**). EM is separated while quasi-equilibrium is maintained between CD, SMs and their complexes inside the capillary during electrophoresis. Two features are characteristic for ECEEM: (i) the migration time of the EM peak depends on the concentration of CD in the run buffer, therefore, SMs with different K_ds migrate with different velocities (**Figure 4.2**), and (ii) a free SM and its complex migrate as a single EM peak due to fast exchange between them.

When ACE is combined with MS detection (**Figure 4.1**), it tracks abundance of all SMs and determines dissociation constants for more small molecules than ACE-UV and DIMS. In this work, we show that this label-free, homogeneous and multiplexed method, ACE-MS, significantly reduces the error in all K_d measurements and calculates K_d for a non-shifting drug as well.

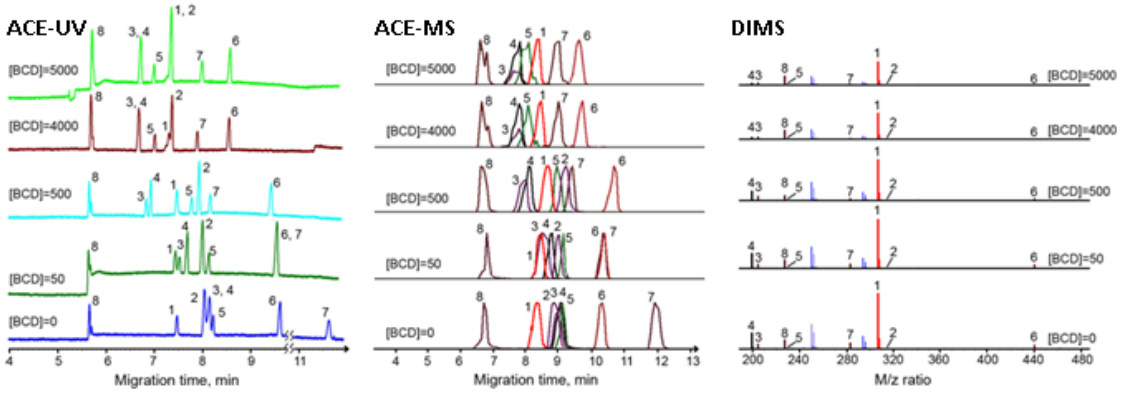

Figure 4.2. Experimental data from three methods for affinity measurements. Small molecule compounds: 1-phenylbutazone, 2 - diclofenac, 3 - ibuprofen, 4 - s-flurbiprofen, 5 - naproxen, 6 – folic acid, 7 – PDDA, 8 – resveratrol. Titration experiments were performed with a fixed concentration of a SM (15 µM each) and different concentrations of β-cyclodextrin (BCD) from 0 to 5000 µM.

4.3. Materials and methods

Reagents and chemicals. Reagents were purchased from Sigma-Aldrich (Canada) unless otherwise noted. 100 mM ammonium acetate buffer pH 6.5 was prepared by dissolving 1.92 g of ammonium acetate powder in 250 ml of distilled deionized water (ddH2O). 10 mM ammonium acetate was used as a running/incubation buffer in all experiments. First all SMs were dissolved in methanol (HPLC grade) to create a stock solution with a concentration of 10 mM. Final equilibrium mixtures of SMs and CD were prepared in the incubation buffer with the following concentrations of all SMs: 15, 50 and 100 µM, and CD in a range of 10 µM – 15 mM. All solutions were filtered through 0.22-µm pore size membrane filters (Millipore, Nepean, ON, Canada).The bare-silica capillary was purchased from Polymicro (Phoenix, AZ, USA).

All MS experiments were done in negative polarity mode. For integration the following m/z ratios were used with 0.02 Da window: ibuprofen – 205.12, s-flurbiprofen – 243.08,

resveratrol – 227.07, PDDA – 283.09, folic acid – 440.13, naproxen – 229.08, diclofenac – 315.99, phenylbutazone – 307.14 (Fig. S1).

Experimental Conditions for ACE-UV. ACE-UV experiments were carried out with a PA800 plus Pharmaceutical Analysis CE system (Beckman Coulter, USA) equipped with either a UV or PDA detector. The sample storage and capillary temperature was maintained at 25 ± 0.5 °C. An electric field of 325 V/cm was applied inside the capillary with a positive electrode at the injection end (an inlet) and a ground electrode at the detection end (an outlet). The inlet vial was filled with the run buffer containing one of the cyclodextrins, and the outlet vial contained the run buffer only. The concentration of CD in the equilibrium mixture and the run buffer was the same for individual ACE-UV experiments. The capillary was 89 cm long (80 cm to the detection window) with an inner diameter of 50 μm and an outer diameter of 360 μm. The equilibrium mixture was injected into the capillary from the inlet end by a pressure pulse of 8 s × 0.5 psi. Before each experiment, the capillary was rinsed by 20 psi pressure with: 0.1 M HCl for 3 min, 0.1 M NaOH for 3 min, ddH2O for 3 min, 10 mM ammonium acetate buffer for 5 min, and the incubation/run buffer with CD for 1 min. The output data was absorbance intensity in the detection point, as a function of time passed since the application of the electric field.

Experimental Conditions for ACE-MS. SYNAPT G2 High Definition Mass Spectrometer from Waters (UK) was coupled on-line with PA800plus Pharmaceutical Analysis CE system (Beckman Coulter, USA) through the CE-ESI sprayer from Micromass (UK). Ionization conditions were as follows: capillary voltage 3 kV, sampling cone voltage 45 V, extraction cone voltage 3 V, source temperature 100˚C, cone N2 gas 0 L/h, nano flow N2 gas 0.5 Bar,

purge N2 gas 3 L/h. Sheath liquid – 80:20 isopropanol:ddH2O 2 mM ammonium acetate – was delivered with a flow rate of 1.5 µl/min. All CE conditions were the same as for ACE-UV experiments.

Experimental Conditions for DIMS. Source and MS conditions were the same as for ACE-MS. All samples were injected into MS by applying a constant pressure (2 psi) through a capillary (89 cm long and an inner diameter of 50 µm).

Experimental Conditions for MS/MS and kinetic stability of gas phase complexes. Kinetic stabilities of β-CD/SM non-covalent complexes were measured using an ESI-MS/MS and RRKM unimolecular rate modeling method explained in detail elsewhere[24,25] . Briefly, using a Waters Q-TOF 1 with MassLynx 4.1 for analysis and data processing, (capillary voltage was 3 kV, cone voltage was 45 V) breakdown diagrams were generated by measuring the percentage of complex survival as a function collision energy.

$$k(E) = \frac{\sigma N^{\ddagger}(E - E_o)}{\hbar \rho(E)} \tag{4.3}$$

The theoretical breakdown curve is found using the unimolecular rate k(E) constant which is calculated using the transition state sum-of-states above the 0K activation energy [N‡(E-E0)] the density of states of the reactant ion [ρ(E)] at an internal energy which are themselves calculated from the molecular and transition state vibrational frequencies (Gaussian 03, AM1 level) using the direct count method. The transition state vibrational frequencies and activation energy (E_0) are scaled until the best possible theoretical-experimental match is obtained.

4.4. Results and discussion

Measuring Affinity by DIMS. Direct infusion of equilibrium mixtures of SMs with different CD concentration were performed by applying constant pressure to create stable nano-electrospray ionization (nano-ESI) of analytes and following with MS detection. No CE separation of drugs and the cyclodextrin was performed prior to ionization. Three concentrations of SMs (15 μM, 50 μM and 100 μM of each SM) and a range of CD concentrations from 10 μM to 5 mM were used.

All eight SMs were detected and identified by characteristic m/z ratios (**Figure 4.2 and Figure 4.3**). The main complex was 1SM-1CD. Nevertheless, multiple noncovalent complexes of SMs with CD were also observed with stoichiometry 1SM-2CD, 1SM-3CD, though some of them possibly were adducts formed during ionization than specific complexes. Ion mobility mass spectrometry (IM-MS) experiments confirmed inclusion nature of 1SM-1CD complex as shown in **Figure 4.4**. Complexes of CD with SM detected by MS can be inclusion complexes or adducts formed during ionization. To distinguish them we used a simple approach based on comparison of drift times of complexes and chemically modified CD, (2-Hydroxypropyl)-β-cyclodextrin. It was shown that modified CD posses the same mass as SM-CD complexes and a different drift time. Collision cross section (CCS) of the inclusion complex shouldn't greatly differ from CCS of free CD due to dwelling of SM partially inside CD. In opposite, chemically modified CD posses hydroxypropyl groups on its surface that greatly increases drift time in an ion mobility experiment. Differences in drift times of SM-CD complexes, free CD and modified CD can

be clearly seen in **Figure 4.4**. Due to these differences, we can propose that the majority of SM-CD complexes in the affinity experiments are inclusion complexes.

A) S-Flurbiprofen, $[M-1H]^{1-}$=243.0824

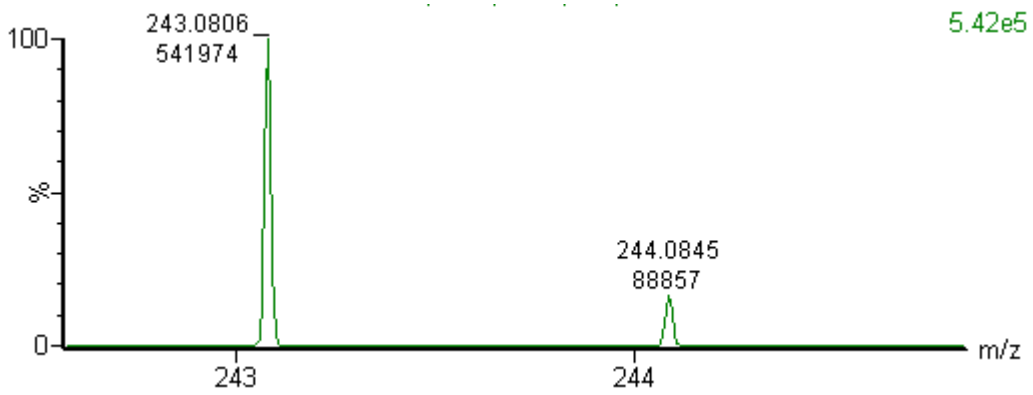

B) Ibuprofen, $[M-1H]^{1-}$=205.1229

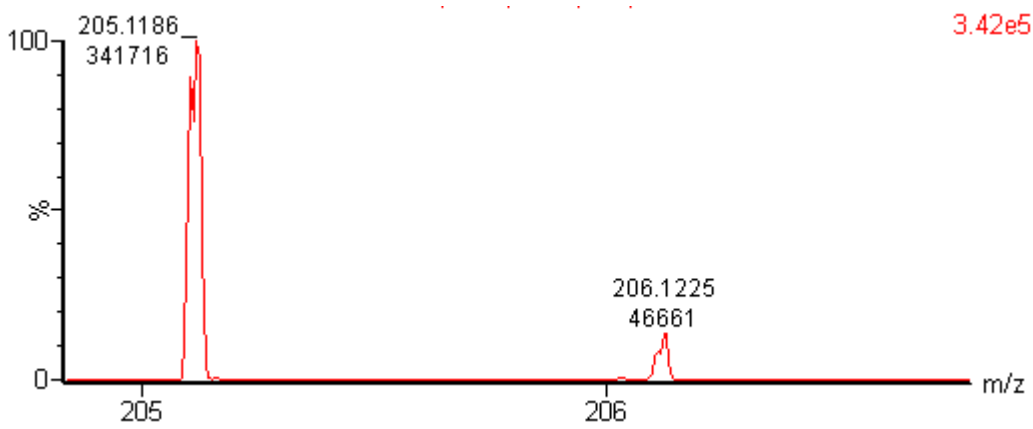

C) Resveratrol, $[M-1H]^{1-}$=227.0708

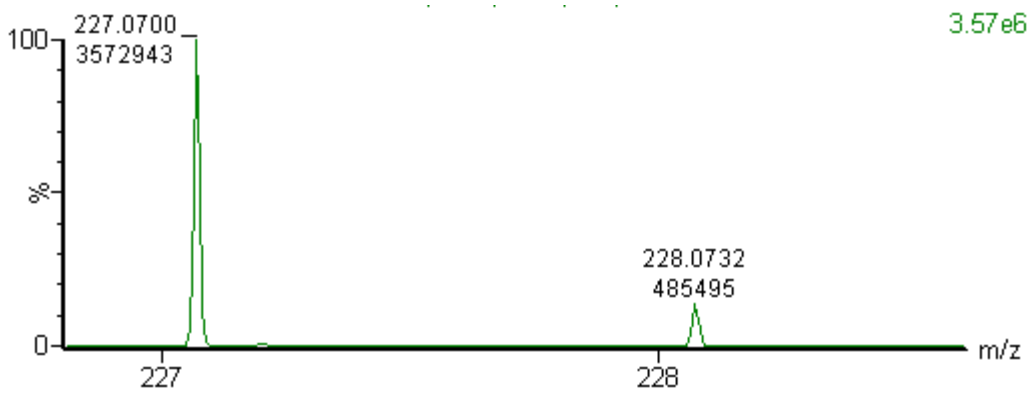

D) PDDA, $[M-1H]^{1-}$=283.097

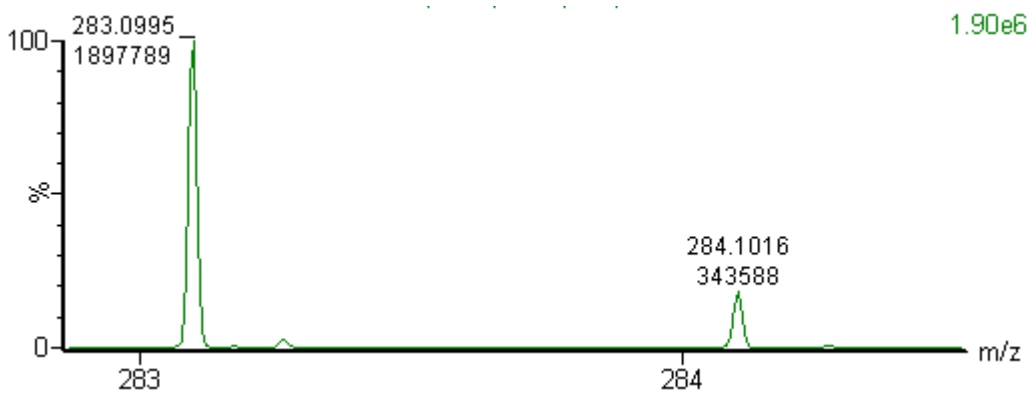

E) Folic acid, $[M-1H]^{1-}$=440.1319

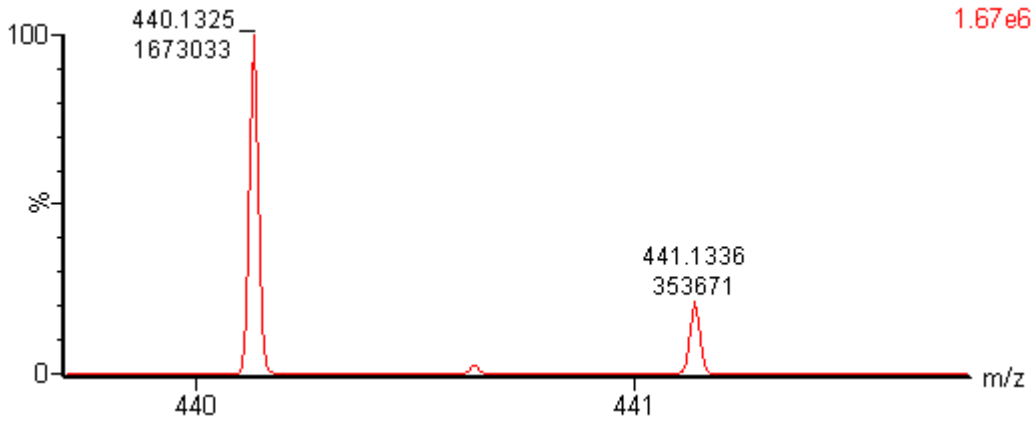

F) Naproxen, $[M-1H]^{1-}$=229.0865

G) Diclofenac, $[M-1H]^{1-}$=315.9908

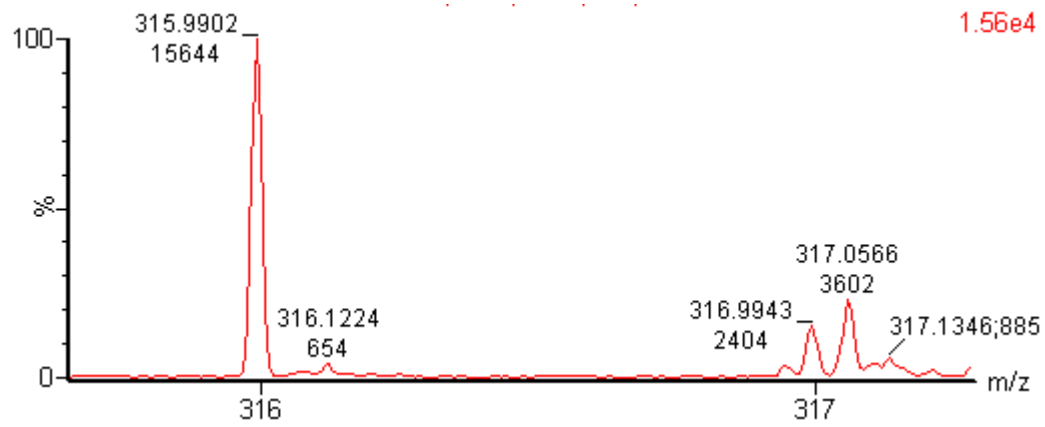

H) Phenylbutazone, $[M-1H]^{1-}$=307.1447

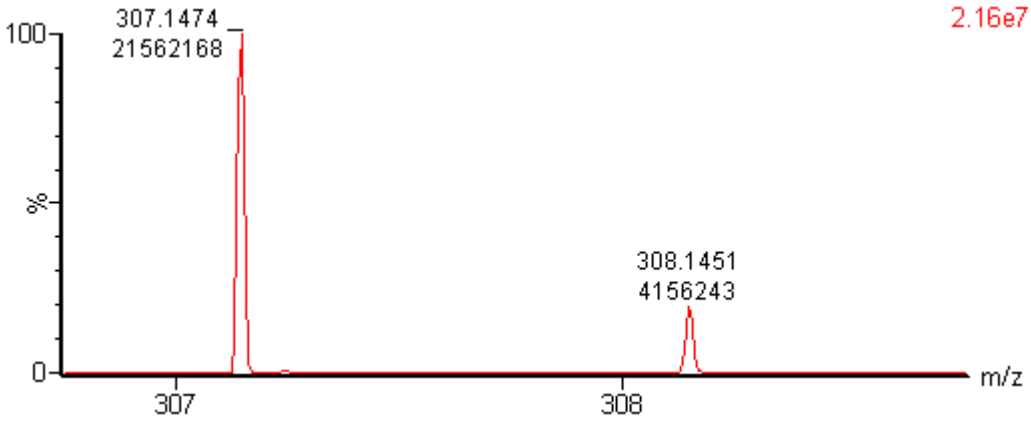

Figure 4.3. MS spectra for eight SMs: (A) s-flurbiprofen, (B) ibuprofen, (C) resveratrol , (D) PDDA, (E) folic acid, (F) naproxen, (G) diclofenac, (H) phenylbutazone.

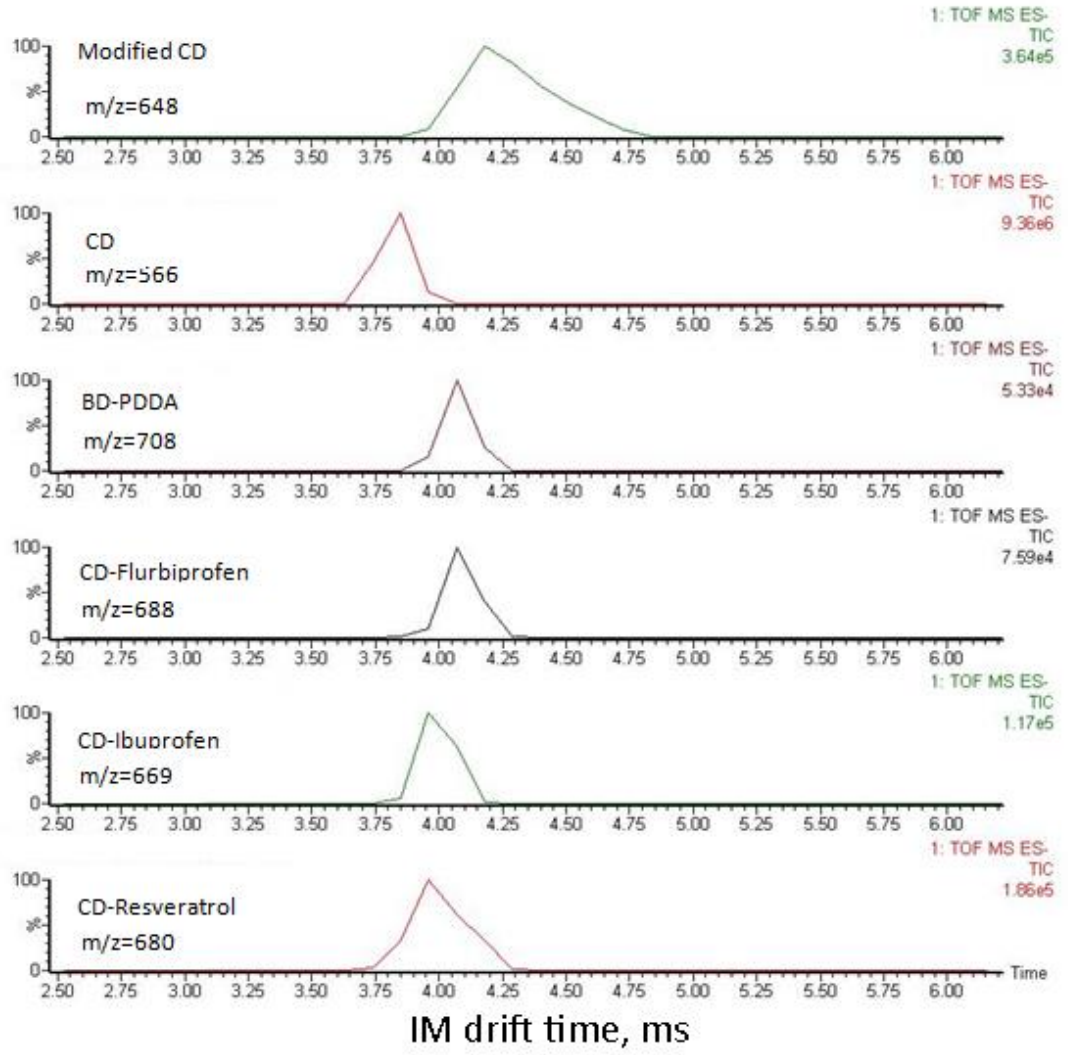

Figure 4.4. Ion mobility drift times for modified CD ((2-Hydroxypropyl)-β-cyclodextrin) and CD-SM complexes.

Due to non-simple stoichiometry, we measured the apparent constant, K_d, by using changes in ion intensity of free SMs. We plotted the unbound drug fraction, F_u(SM), versus concentration of cyclodextrin in the run buffer. F_u(SM) is defined as the ratio of the

intensity of free SM ions in the presence of CD, I(SM), to the intensity of free SMs without CD, I_0(SM):

$$F_u(SM) = \frac{I(SM)}{I_0(SM)} \tag{4.4}$$

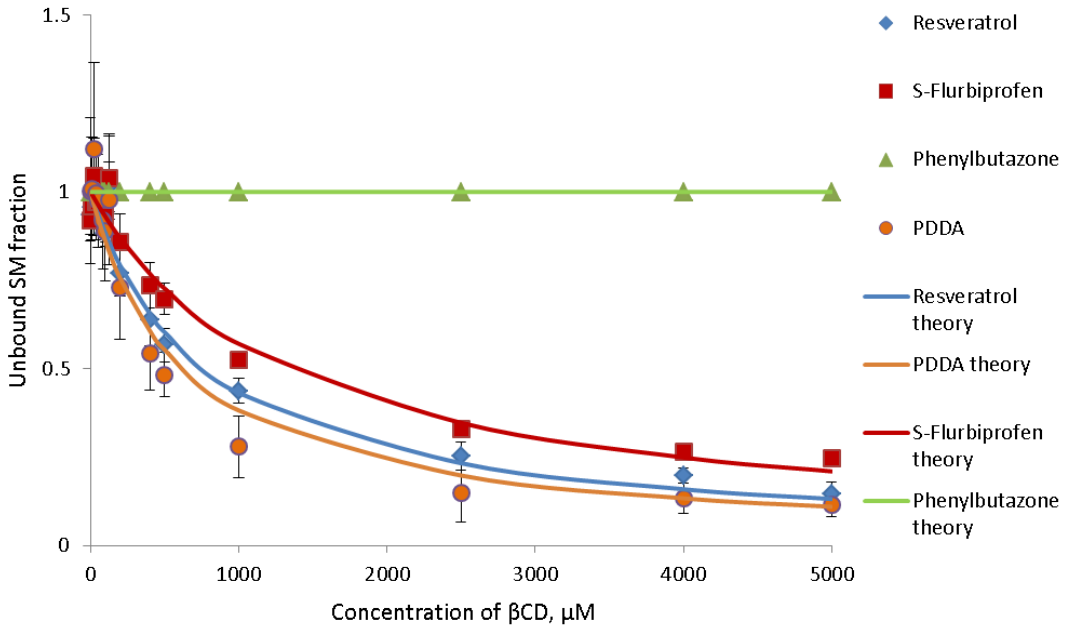

Figure 4.5. Correlation of the normalized unbound SM fraction from concentration of βCD. Normalization was done by phenylbutazone's ion intensity. Apparent K_d for SM equals the CD concentration when a half of small molecules is bound.

The DIMS detection showed ion suppression of all analytes with the increase of CD concentration (**Figure 4.6**). Even for phenylbutazone, which does not interact with CD, the ion suppression was significant at [CD] > 200 μM. It is important to note that ion intensities of SMs were in linear correlation with their concentration at zero concentration of CD. In the presence of CD it is almost impossible to distinguish complexes with different stoichiometry and salt adducts, and calculate the unbound fraction of SMs. To compensate the effect of ion suppression with increasing [CD] for

affinity calculations, we normalized F_u(SM) of all interacting SMs by the ion intensity of phenylbutazone, which does not bind CD and works as an internal standard (**Figure 4.5**). The concentration of CD when a half of small molecule's amount is bound (F_u(SM) = 0.5) gives the apparent K_d. All K_ds found by DIMS are presented in **Table 4.1**. Affinity constants only for three SMs (s-flurbiprofen, resveratrol and PDDA) out of seven reactive drugs were calculated. For folic acid, diclofenac and naproxen, K_ds lay in range of CD concentrations where ionization suppression becomes overwhelming. Ibuprofen has an impurity with the same mass what made impossible to calculate K_d without prior separation.

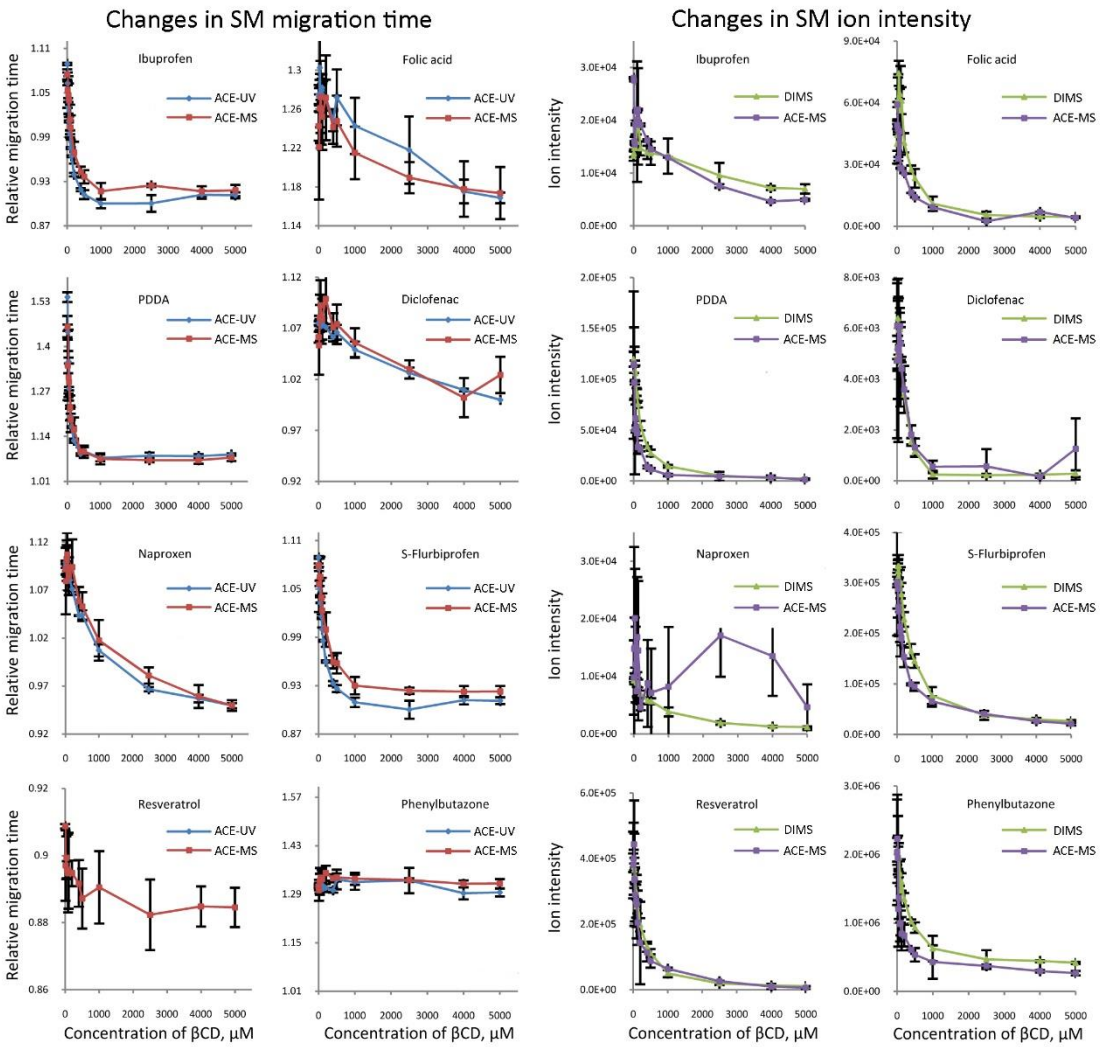

Figure 4.6. Correlation between migration time and ion intensity of SMs from the concentration of βCD based on ACE-UV, ACE-MS and DIMS experiments. Experiments were repeated three times with [SMs] = 100 μM and [CD] = 0 - 5000 μM.

Measuring Affinity by ACE-UV. In ACE-UV, the determination of the apparent dissociation constant for each small molecules is dependent on electrophoretic mobility and can be calculated using the following equation:

$$K_d = [CD]\left(\frac{t_{EM} - t_0}{t_0 - t_C}\right) \tag{4.5}$$

where [CD] is the concentration of β-cyclodextrin in the running buffer, t_{EM} is migration time of EM, t_0 and t_C are migration times of free SM and its complex, respectively. Migration time of the complex can be estimated from experiments with high concentration of CD when most of SM is bound. All migration times were normalized by the migration time of one of the internal standards such as phenylbutazone or a electroosmotic flow (EOF) peak.

The apparent K_d constant for a SM can be found by two ways. The first way is similar to the method described above for DIMS. The relative migration time of EM peak and CD concentration is plotted (**Fig. 4.6**), where K_d equals the concentration of CD at 50% of the total shift of EM peak. The second more precise method requires fitting of experimental data using **Eq. 4.6** while minimizing the error, *H*, between theoretical and experimental migration time of EM:

$$H = \sum \ln\left(1 + \frac{1}{Std\,(t)_i^2}\left(t_i^{exp} - t_i^{theory}\right)^2\right) \tag{4.6}$$

where t^{exp} - t^{theory} is the difference between experimental and theoretical migration time of SM for an experiment with i-th CD concentration, *Std(t)* is standard deviation of t^{exp}.

The constants found by fitting are presented in **Table 4.1**. They were found based on fifteen experiments repeated three times each with a fixed concentration of SMs (15 μM, 50 μM and 100 μM of each SM) and varying concentrations of CD from 10 μM to 5 mM. The representative ACE-UV electropherograms are displayed in **Figure 4.2.** Six compounds out of 8 shows a significant shift of the EM peak with an increase of CD concentration in the run buffer. Resveratrol and phenylbutazone peaks are not shifted with the increase of CD. Resveratrol is neutral at the experimental conditions thus it migrates with EOF and makes the calculation of K_d impossible by the mobility change. In addition to the problem of the neutral drug, overlapping peaks complicate the calculation of migration times of individual components and affinity constants for them.

Table 4.1. Apparent Kd values for affinity interactions between SMs and β-cyclodextrin measured by DIMS, ACE-UV and ACE-MS methods. N/R – a SM does not bind β-cyclodextrin, N/D – K_d was not determined. N/F – no data found.

	DIMS, μM	ACE-UV, μM	ACE-MS, μM	Reference values, μM
Resveratrol	760±78	N/D	559±35	520[143], 992[144]
S-Flurbiprofen	1329±161	183±14	186±14	455[145], 224[146], 167[147]
Ibuprofen	N/D	131±12	116±9	114[148], 94[149], 1170[144]
Folic Acid	N/D	1181±335	837±132	N/F
Phenylbutazone	N/R	N/R	N/R	N/F

PDDA	619±102	66±6	69±2	N/F
Naproxen	N/D	979±89	1066±244	680[149], 590[150], 475[144]
Diclofenac	N/D	2421±676	1503±111	13000[151], 9940[152]

Measuring affinity by ACE-MS. ACE-MS brings the advantages of both DIMS and ACE-UV methods, where ion intensity and CE mobility for every small molecule drug are determined. Therefore, both ion intensities and migration time shifts can be combined into one math model to measure K_d for all reacting SMs. Changes in ion intensities and migration times for each SM upon increasing CD concentration are plotted in **Figure 4.6.** Dissociation constants can be found by fitting equations 2 and 4 while minimizing the combined error, H:

$$H = \sum \ln(1 + \frac{1}{Std(I)_i^2}([SM_i] \cdot a - I(SM_i))^2) + \sum \ln(1 + \frac{1}{Std(t)_i^2}(t_i^{\exp} - t_i^{theory})^2) \quad (4.7)$$

Where $[SM_i]$ is the theoretical concentration of a SM for an experiment with i-th type of conditions, $I(SM_i)$ – an experimental ion intensity signal of the SM, $Std(I)_i$ is standard deviation of $I(SM_i)$, a is a transformation coefficient between concentration and ion intensity signal. K_ds for all seven reacting compounds were measured with better accuracy than DIMS and ACE-UV and in good agreement with references presented in **Table 4.1**. Overlapping peaks were well resolved by multiplexed MS detection of ions with different m/z ratios. Neutral resveratrol did not show a CE mobility shift, so the binding was measured by the change of its ion intensity in MS.

Small broadening of SMs' peaks was observed in ACE-MS compare to ACE-UV experiments. The peak broadening happens due to a suction effect caused by evaporation

of liquid at the outlet of the capillary and a gas flow during electrospray ionization. It creates a laminar flow with a parabolic profile inside the capillary and disperses peaks. However the peaks become wider it doesn't have any considerable effect on reproducibility of migration time of SMs. Also, the ion intensities were less reproducible in ACE-MS experiments compared to DIMS for naproxen and diclofenac due to Taylor's effect causing peak dispersion and less stable ionization by the fluctuation of an ion current in CE separation as seen in **Figure 4.4**.

Comparing an apparent dissociation constant with an activation energy of 1:1 complex in MS/MS experiments. Many different tandem mass spectrometry techniques are used to investigate stability of non-covalent complexes, and although sometimes there are examples of gas phase binding values coinciding with the relative solution phase affinities, there are a plethora of cases where they do not. A previous study ranking the gas phase stabilities of α, β and γ cyclodextrin with rutin, showed good correlation with solution phase association constants[153]. Here we employed Rice–Ramsperger–Kassel–Marcus (RRKM) based breakdown diagram modeling approach[154]; taking into account the differences in vibrational frequencies, cross sections, and degrees of freedom. All singly deprotonated, CD-SM complexes showed a single dissociation pathway involving the loss of neutral SM. There were some exceptions including folic acid, which retained the charge, and phenylbutazone which had 2 dissociation pathways where the negative charge could be retained by CD or phenylbutazone and was not included in ranking the relative activation energy (E_0). Unlike the aforementioned CD MS/MS study, we found

poor correlation between the solution phase K_d values and the gas phase complex stabilities.

Interestingly, the E_0 values for ibuprofen, PDDA, folic acid, diclofenac and naproxen were quite similar, between 0.84 and 0.91 eV. Outliers, included resveratrol, which has the lowest E_0 value of 0.69 eV and s-flurbiprofen which had the highest E_0 value of 1.01 eV. There is very little correlation between the K_d and E_0 values (**Figure 4.7**), attesting to the difference between solution phase and gas phase complexes. The E_0 measurements point to the electrostatic interactions as being the major factor in determined the gas phase stabilities of these systems. Resveratrol differs from the other SM because it lacks a carboxylic acid moiety, explaining its much lower activation energy. PDDA and folic acid possess 2 carboxylic acid groups, yet have very similar E_0 to SM which possess only 1 carboxylic acid. Because there is only 1 charge bearing site within these gas phase complexes, this suggests that ionic H-bonds are the most important influence upon the stabilities of these singly deprotonated gas phase complexes.

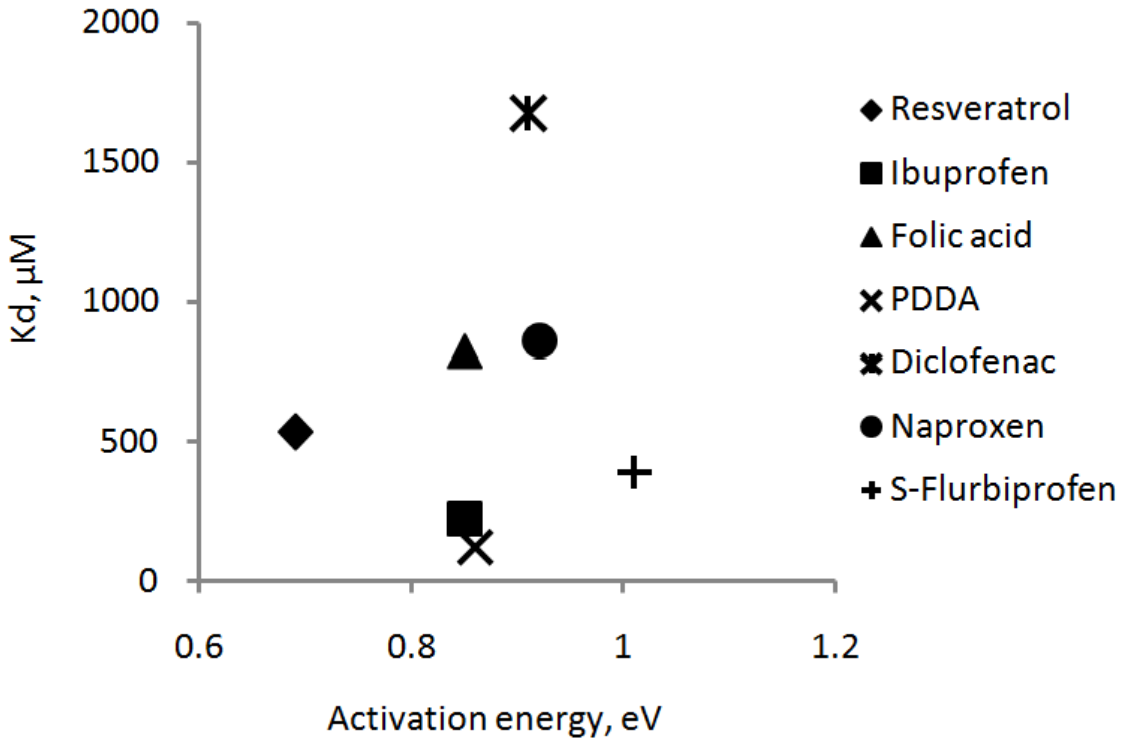

Figure 4.7. Comparative plot of activation energies for seven SMs versus their apparent Kds. The activation energy was calculated for each SM by CID experiments and RRKM theory. K_d was found from ACE-MS experiments.

4.5. Conclusion

DIMS analysis is fast and simple, and requires only a MS instrument, but the major disadvantage of DIMS is the lack of spatial separation between drugs before MS analysis. Therefore, it is impossible to eliminate competitive binding of SMs to cyclodextrin, difficult to distinguish specific binding from nonspecific, and difficult to analyze compounds with similar masses. High concentrations of CD (> 200 µM) suppress ionization of SMs. K_d values measured by DIMS differ significantly from more reliable separation-based techniques. The advantage of ACE-UV is in spatial separation of small molecules at near physiological pH with high concentration of salts and additives (up to

100 mM). The main disadvantages are that small molecules must be detectable in UV or VIS region and separated from each other as individual peaks.

Beneficially, ACE-MS provides an opportunity to estimate apparent K_d even if a SM has the same mobility as CD and its complex by tracking ionization intensity of the free SM. As is seen from experiments with resveratrol. In addition ACE-MS separates and detects analytes from impurities. Unfortunately, MS detection does not work well in high concentrations of CD (>1 mM) in the run buffer. The high concentration of CD decreases electroosmotic flow during CE separation and suppresses ionization of small molecules. The ACE-MS approach is also applicable for off-line connection CE and MS, when ACE and MS data obtained separately on two different instruments at different times[153].

To summarize, ACE-MS is a comprehensive platform for the development of label-free solution-based methods for studying the affinity of molecule interactions. This technique shows the migration profile of small molecules in ACE by multiplex MS detection. In this work, we interfaced ACE and MS on-line, which allowed us to identify all small molecules and their complexes directly by MS without any intermediate steps (desalting or buffer-exchange) between ACE and MS. The method works well with a mixture of small molecules and allows the determination of K_ds for all reacting small molecules even in cases when peaks overlap with each other during capillary electrophoresis separation. The range of K_ds that can be measured by ACE-MS will depend on the efficiency of ionization of small molecules and the MS detection limit. Instrumentation for ACE-MS used in this study can measure K_d values from 1 μM to 2.5 mM. Measuring nanomolar K_d values will require a different CE method called Nonequilibrium Capillary Electrophoresis of

Equilibrium Mixtures (NECEEM)[155] which is more suitable for stable complexes with slow dissociation rates. Advantageously, ACE-MS does not need MS detection of an intact cyclodextrin–small molecule complex, which can be very challenging due to the stoichiometry different from 1:1 and a decay of the complex during ionization. The ability of MS to rapidly scan through m/z facilitates the simultaneous analysis of the interaction between a cyclodextrin with several small molecules; this would potentially lead to high-throughput screening of panels of new binding candidates. In the future, ACE-MS can be used for a wide range of applications outside the cyclodextrin-small molecule model such as nucleic acid – metal complexes, protein and DNA/RNA conformational changes, high-throughput screening and discovery of new ligands.

4.6. Acknowledgments

This work was supported by the Natural Sciences and Engineering Research Council of Canada (NSERC), Canadian Foundation for Innovation (CFI) and Ontario Research Fund from Ministry of Research and Innovation (ORF-MRI).

Chapter 5: Conformational Dynamics of DNA G-Quadruplex in Solution Studied by Kinetic Capillary Electrophoresis Coupled On-line with Mass Spectrometry

5.1. Objectives

My objectives were to study G-quadruplex folding by CE-MS and compare kinetic data obtained by UV detection and MS detection. I designed and performed all experiments and analyzed experimental data.

Dr. Victor Okhonin was responsible for creating a mathematical model for calculating rate and equilibrium constants. Dr. Nasrin Khan was responsible for initial characterization of studied sequences by CE-UV. Dr. Christopher Clouthier assisted with CD experiments. Dr. Maxim Berezovski provided technical guidelines and supervision in performing all CE experiments.

5.2. Introduction

G-quadruplexes (GQs) are non-canonical secondary structures formed from G-rich sequences of nucleic acids, and play important roles in the regulation of gene transcription and translation. Formation of GQ in a telomere region causes inhibition of telomerase activity with subsequent obsolescence and cell death[157]. GQ structures are found in some promoters of oncogenes, such as c-MYC[158], BCL-2[159], c-KIT[160], K-ras[161], VEGF[162]. Therefore, GQs could be a key therapeutic target for anti-cancer drugs.

Quarfloxin, a GQ stabilizing drug for the treatment of neuroendocrine/carcinoid tumors has reached Phase II clinical trial[163]. Recently, a novel translation activation function of GQ in 3'-untranslated regions (3' UTR) of messenger RNA was also presented[164].

While the idea of GQ stabilizing/destabilizing compounds looks promising for switching genes on and off, it is critical to measure kinetics of GQ folding in solution for efficient drug design and high-throughput screening of drug candidates. Finding kinetic parameters can relate the GQ folding time scale with biological processes like replication and transcription. Up to now, the most common techniques for studying of GQ conformations include circular dichroism (CD)[165], UV absorption at 295/297 nm[166], non-denaturing gel electrophoresis[167], fluorescence-based single molecule methods[168], nuclear magnetic resonance (NMR)[169], surface plasmon resonance (SPR)[170] and X-ray crystallography (XRC)[171]. However, CD studies the conformational changes in anisotropic molecules and chiral super assemblies in equilibrium, and for fast interactions it measures thermodynamic constants only. NMR shows DNA's conformational dynamics in solution with atomic resolution. XRC provides a static picture of a DNA conformation. Alternatively, FRET[172, 173] measures the relative distance between fluorescent residues or labels and requires fluorescent labelling that may interfere with DNA dynamics and ligand binding. The main disadvantages of NMR techniques are a requirement for the high concentration of a sample (around mM range) and difficulties in performing a multiplex study. Other solution-based techniques do not provide direct information about the structure of a GQ making it challenging to interpret the data. The main methods for measuring kinetics of DNA folding and affinity binding are Stopped-Flow (SF)[166], and

SPR[170], both of which have the capability of calculating rate and thermodynamic constants of DNA binding to big biomolecules. They have restrictions due to mixing dead-time and re-dissociation of reagents for SF as well as mass transport to and heterogeneity of the surface of a SPR chip.

In this chapter, I demonstrate the power of kinetic capillary electrophoresis coupled on-line with mass spectrometry (KCE-MS) to monitor individual DNA conformers and reveal rate and equilibrium constants of GQ DNA folding upon binding to potassium ions. This represents an important step in deciphering fast kinetics of DNA folding, in addition to establishing KCE-MS as a real-time method for studying DNA dynamics and screening DNA binding ligands.

Conceptually, KCE-MS is defined as an electrophoretic separation of compounds, which interact inside a capillary column during electrophoresis and are detected by mass spectrometry. Usually, separated analytes are detected by UV-VIS absorption or laser-induced fluorescence (LIF). These detection modes can be problematic for screening of complex mixtures with multiple targets and ligands. Therefore, the ability to acquire accurate molecular mass and structural information about analytes is highly desirable. Capillary electrophoresis was coupled with mass spectrometry (CE-MS) over twenty years ago, which significantly advanced the field of nucleic acid and bioanalytical chemistry[174]. Here, we connect KCE with MS on-line by electrospray ionization (ESI), a soft ionization technique, which keeps non-covalent complexes intact. It combines in one system the separation and kinetic capability of KCE together with molecular weight and structural elucidation of MS. The advantages of KCE-MS are that (i) DNA interacts with a ligand and

folds at near physiological conditions, and all kinetic and thermodynamic parameters are measured in solution but not a gas phase; (ii) DNA and ligands don't need special labeling for the MS detection; and (iii) interactions/foldings of several DNAs and ligands can be studied simultaneously in one capillary microreactor. KCE-MS implicates the benefits of both ion mobility, mass spectrometry and KCE-UV(LIF), where ion intensities, masses, electrophoretic mobilities and affinity of interacting compounds are determined. Ion mobility (IM) spectrometry separates ions on the basis of their collision cross section with a buffer gas. IM is fast and simple, and requires only a MS instrument with a drift cell. Nevertheless, the competitive binding, ion suppression during ionization and formation of non-specific complexes in a gas phase could cause problems in interpretation of IM results. Fortunately, KCE can be coupled with IM directly, so that KCE separates interacting molecules based on their affinities and size-to-charge ratios in solution inside a capillary prior to the electrospray ionization (ESI), followed by IM separation in a gas phase and MS detection.

5.3. Materials and methods

Chemicals and Reagents. All DNA sequences were purchased from IDT DNA Technologies (USA). For all experiments, 12.5 mM Tris-Acetate, pH 7.85, was used as an incubation/run buffer. The buffer was prepared by dilution from 200 mM Tris-Acetate stock buffer. The stock buffer was made by dissolving 12.11 g of Tris-base (Bio Basic Inc., Canada, cat.# 77-86-1) and 2.86 mL of acetic acid (Bio Basic Inc., Canada, cat.# C1000) in 500 mL of ddH2O. 100 mM solutions of ammonium chloride (Sigma-Aldrich, USA, cat.#

254134), sodium chloride (Sigma-Aldrich, USA, cat.# S7653) and potassium chloride (Sigma-Aldrich, USA, cat.# P9541) were prepared in ddH2O. 1 mM 4,4'-(propane-1,3-diyl)dibenzoic acid (PDDA) (Sigma-Aldrich, USA, cat.# S499455,) was prepared in run buffer and used as internal standard in CE separation to normalize electrophoretic mobilities.

Equilibrium mixtures of DNA and chlorides were prepared in the incubation buffer with 10 µM concentration of all DNA sequences. Concentrations of KCl were in range 10 µM – 2.5 mM. All solutions were filtered through 0.22-µm pore size nylon membrane filters (Millipore, Nepean, ON, Canada). The bare-silica capillary was purchased from Polymicro (Phoenix, USA).

KCE Experiments. The sample storage and capillary temperature was maintained at 25 ± 0.5 °C, the electric field in KCE separation was 290 V/cm with a positive electrode at the injection end, the run buffer was with one of the coordinating ions in the inlet reservoir. The concentration of the coordinating ions in the equilibrium mixture and the run buffer was the same for individual KCE experiments. For all experiments, the capillary was 89 cm long (30 cm in KCE-UV experiment, 20 cm to window) with an inner diameter of 50 µm and an outer diameter of 360 µm. The equilibrium mixture was injected into the capillary from the inlet end by a pressure pulse of 10 s × 1 psi (0.3 psi for 3 sec in KCE-UV experiment). Before each experiment, the capillary was rinsed by 75 psi pressure with: 0.1 M HCl for 3 min, 0.1 M NaOH for 3 min, ddH2O for 3 min, 12.5 mM Tris-Acetate buffer for 5 min, and the incubation/run buffer with coordinating ions for 2 min. A Synapt G2 HDMS mass spectrometer from Waters (UK) was coupled with a PA800plus Pharmaceutical

Analysis CE system having a PDA detector (Beckman Coulter, USA) through a CE-ESI sprayer from Micromass (UK) and used in all KCE-MS experiments. Electrospray ionization conditions were as follows: capillary voltage 3 kV, negative mode, sampling cone voltage 45 V, extraction cone voltage 3 V, source temperature 100˚C, cone gas 0 L/h, nano flow gas 0.5 Bar, purge gas 3 L/h, mobility cell bias voltage 3 V. Sheath liquid (80:20 isopropanol: ddH2O 5 mM triethanolamine) was delivered with flow rate of 1.5 µl/min.

5.4. Results and discussion

Principles of KCE. KCE-based separation of GQ DNA involves two major processes. First, it includes non-covalent interactions of unfolded DNA (DNA) with a coordinating metal ion (M) leading to formation of a folded GQ complex (GQ-M) and dissociation of the complex regulated by a rate constant of complex formation (kon) and a decay constant (koff);

$$\mathrm{DNA+M} \underset{k_{off}}{\overset{k_{on}}{\rightleftharpoons}} \mathrm{GQ\text{-}M} \tag{5.1}$$

Second, there is simultaneous separation of DNA, M, and GQ-M based on differences in their electrophoretic velocities in solution. These velocities are directly proportional to a size/charge ratio of DNA, M, and GQ-M. These two processes are described by the scheme of reaction (5.1) and general system of partial differential equations (5.2):

$$\begin{aligned} &\frac{\partial[\mathrm{DNA}]}{\partial t}+V_{\mathrm{DNA}}\frac{\partial[\mathrm{DNA}]}{\partial x}-D_{\mathrm{DNA}}\frac{\partial^2[\mathrm{DNA}]}{\partial x^2}=\frac{\partial[\mathrm{M}]}{\partial t}+V_{\mathrm{M}}\frac{\partial[\mathrm{M}]}{\partial x}-D_{\mathrm{M}}\frac{\partial^2[\mathrm{M}]}{\partial x^2}= \\ &=-\frac{\partial[\mathrm{GQ\text{-}M}]}{\partial t}-V_{\mathrm{GQ\text{-}M}}\frac{\partial[\mathrm{GQ\text{-}M}]}{\partial x}+D_{\mathrm{GQ\text{-}M}}\frac{\partial^2[\mathrm{GQ\text{-}M}]}{\partial x^2}=k_{off}[\mathrm{GQ\text{-}M}]-k_{on}[\mathrm{DNA}][\mathrm{M}] \end{aligned} \tag{5.2}$$

Where [DNA], [M] and [GQ-M] are the concentrations of a unfolded DNA, metal ion, and a folded GQ-metal complex, respectively, V_{DNA}, V_M and V_{GQ-M} are the migration velocities, D_{DNA}, D_M and D_{GQ-M} are the diffusion coefficients, t is the time, x is the spatial coordinate along a capillary.

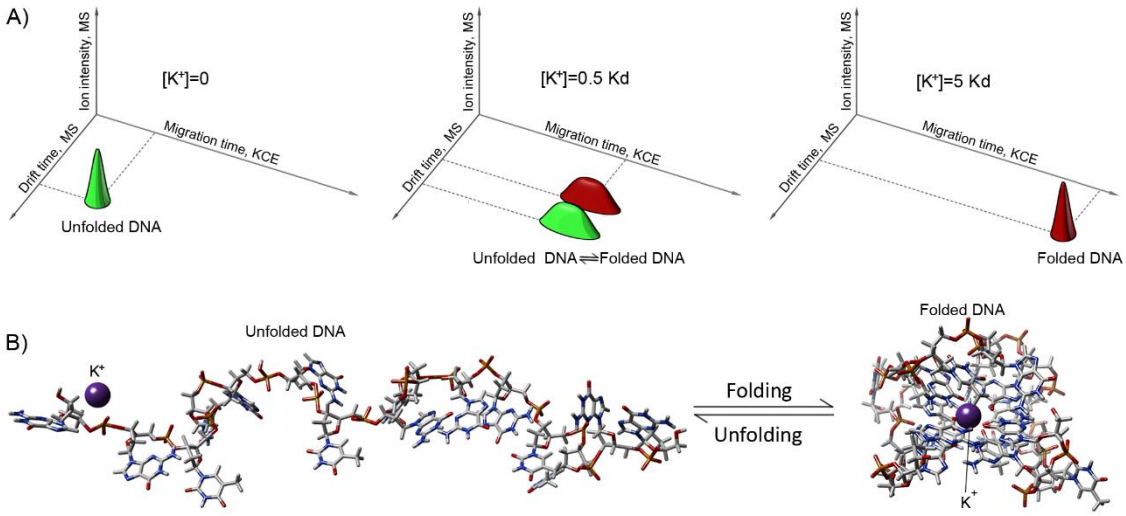

Figure 5.1. Schematic representation of two-dimensional separation (KCE vs. IM) of unfolded (green) and folded (red) forms of GQ DNA. (A) First dimension is KCE separation in solution; the second dimension is IM separation in a gas phase. (B) DNA folding in a compact GQ structure is mediated by potassium ion.

Practically, a plug of an equilibrium mixture (EM) that consists of DNA, M, and GQ-M is injected into the capillary pre-filled with the run buffer containing the metal ion with a total concentration identical to EM. Components of EM are separated by capillary electrophoresis while quasi-equilibrium is maintained between DNA, M and GQ-M complex inside the capillary (**Figure 5.1A**). This method is called Equilibrium Capillary Electrophoresis of Equilibrium Mixtures (ECEEM)[175]. It is a mode of Kinetic Capillary Electrophoresis (KCE), a platform for kinetic homogeneous affinity methods in which molecules interact with each other during electrophoretic separation[176]. The unfolded

DNA and folded GQ migrate with different velocities due to different shapes; GQ is more compact than unfolded DNA (**Figure 5.1B**), and thus migrates later than the unfolded DNA. There are three unique features of this separation: (i) DNA and GQ migrate as a single EM peak due to fast exchange between them, (ii) the migration time of the EM peak depends on concentration of M in the run buffer, so DNA sequences with different equilibrium folding constants, $K_F = k_{off}/k_{on}$, migrate with different velocities and separated from each other, and (iii) EM peak broadening is dependent on concentration of M, rate constants and characteristic separation time, t_{sep}. The characteristic separation time is the time required for DNA and GQ-M to separate from each other inside the EM plug and defined as:

$$t_{sep} = w / \left(2\left|V_{GQ\text{-}M} - V_{DNA}\right|\right) \tag{5.3}$$

where *w* is the width of the initial EM peak.

The general analytical solution of these nonlinear differential equations (5.2) in partial derivatives is not known. In some cases like (i) formation or decay rate constants are negligible or zero[177, 178], (ii) $V_{GQ\text{-}M} = V_M$ or $V_{GQ\text{-}M} = V_{DNA}$ the equations (5.2) become linear directly or after the Cole-Hopf substitution[179, 180]. In our case, the molecular exchange between an unfolded DNA and a folded GQ-M complex is very fast. The relaxation time, τ, to equilibrium for weak ($K_F > 1$ μM) and fast reactions depends on rate constants, DNA and M concentrations:

$$\tau = 1/(k_{on}([DNA]+[M])+k_{off}) \tag{5.4}$$

If $\tau > t_{sep}$, the zones of DNA and GQ-M are separated before the re-equilibration in reaction (5.1) proceeds to a significant extent. Thus, unfolded DNA and folded GQ-M are moving as individual peaks. If $\tau \sim t_{sep}$, re-equilibration in reaction (5.1) and separation proceed with comparable rates. Therefore, DNA and GQ-M are moving as two overlapping peaks. Finally, if $\tau < t_{sep}$, the re-equilibration in reaction (5.1) occurs much faster than peaks separation (our case), and, as a result, DNA and GQ-M will be moving as a single peak. The last case of fast molecular interactions experimentally illustrated in **Figure 5.2**.

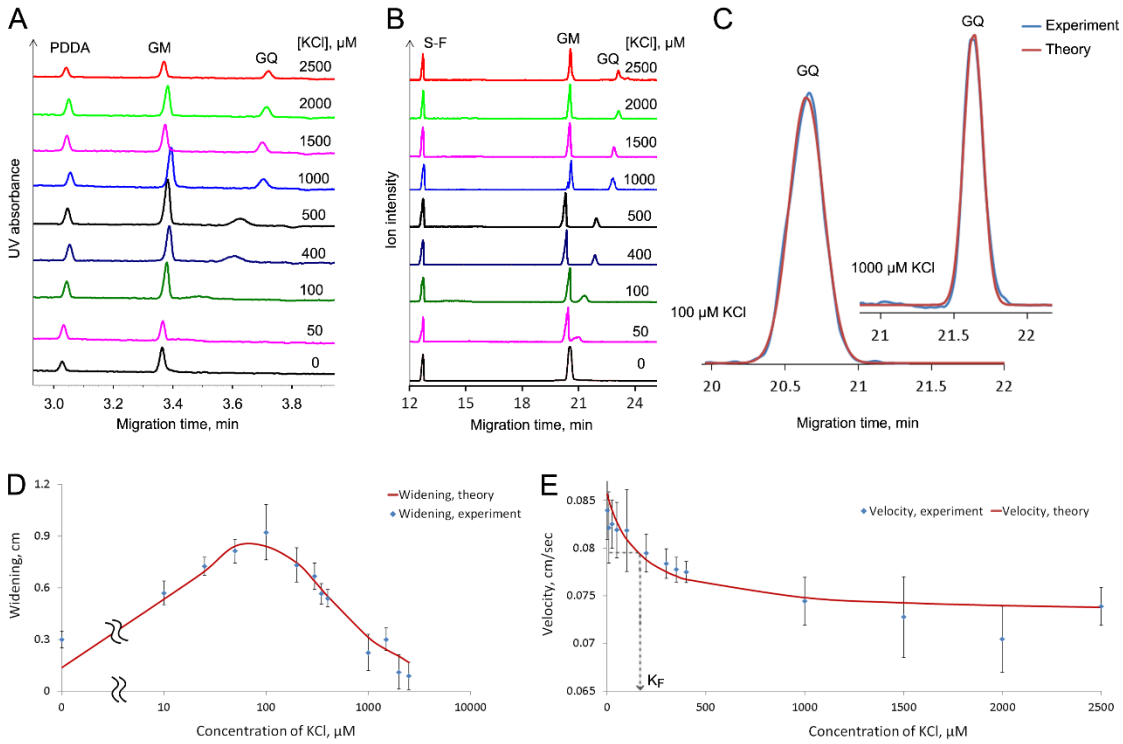

Figure 5.2. KCE-MS experiments for finding rate and equilibrium constants. Representative ECEEM electropherograms of 4 DNA strands (GM1, GM2, GM3 and GQ, 10 μM each) and varying concentration of KCl with UV-detection (panel A) and MS detection (panel B). (C) Representative shapes of a GQ peak at different concentrations of KCl with MS detection. (D) Dependence of GQ peak widening on the concentration of KCl with MS detection. (E) Plot of GQ peak velocity as a function of KCl concentration for K_F determination with MS detection. Theoretical fitting is shown as a red curve, experimental data – blue dots or a blue curve. PDDA and S-F are internal standards.

For the fast molecular exchange when $\tau << t_{sep}$ and [DNA] << [M] + K_F, the approximated equation is used:

$$\partial_t[\mathrm{DNA}]+\left(V_{\mathrm{EM}}-\frac{2k_{off}D_{\mathrm{CID}}}{K_F\left(V_{\mathrm{DNA}}-V_{\mathrm{EM}}\right)}[\mathrm{DNA}]\right)\partial_x[\mathrm{DNA}]\approx\left(D_{\mathrm{CID}}+D_{\mathrm{EM}}\right)\partial_x^2[\mathrm{DNA}] \quad (5.5)$$

where V_{EM} is the velocity of EM peak, D_{EM} is a physical diffusion coefficient for EM peak and D_{CID} is a chemical induced coefficient of diffusion. They can be described as:

$$V_{EM}\equiv\frac{K_F V_{\mathrm{DNA}}+[\mathrm{M}]V_{\mathrm{GQ\text{-}M}}}{K_F+[\mathrm{M}]},\quad D_{EM}\equiv\frac{K_F D_{\mathrm{DNA}}+[\mathrm{M}]D_{\mathrm{GQ\text{-}M}}}{K_F+[\mathrm{M}]},\quad D_{CID}\equiv\frac{[M]K_F^2\left(V_{GQ-M}-V_{DNA}\right)^2}{k_{off}\left(K_F+[M]\right)^3} \quad (5.6)$$

K_F can be found from the expression:

$$K_F\approx\sum_i\frac{\left(V_{EM}^i-V_{DNA}\right)^3\left(V_{GQ-M}-V_{EM}^i\right)}{[M]_i}\Big/\sum_i\frac{\left(V_{EM}^i-V_{DNA}\right)^4}{[M]_i^2} \quad (5.7)$$

Equation (5) is well known in mathematics as Burgers' equation and can be solved analytically if the injected EM plug is narrow (w << the length of capillary)[181]. When V_{DNA}, $V_{GQ\text{-}M}$, V_M, $D_{GQ\text{-}M}$, D_{DNA} are known, K_F is found from equation (5.7). Afterward, k_{off} is determined from equation (5.5), and $k_{on} = k_{off} / K_F$. Interesting to note, ECEEM has a unique "accumulation" property. It accumulates the effect of molecular interactions in extra long capillaries; it could reveal rates of extremely fast reactions, if $D_{CID} > D_{EM}$.

Measuring rate and equilibrium constants for GQ folding. We mixed 10 µM of GQ forming a 15-nt thrombin binding aptamer (TBA) sequence (5'GGTTGGTGTGGTTGG3') with three mutated sequences (10 µM each, the flipped bases are underlined), GM1 (GGTTGGTGTGGTGTG), GM2 (GGTTGTGGTGGTGTG), GM3 (GTGTGTGGGTGTGTG)

(equimolar mixture of GM1, GM2 and GM3 is labeled as GM), and separated in varying concentrations of K^+ from 10 μM to 2.5 mM KCl in 12.5 mM Tris-Acetate (TA) run buffer, pH 7.8. All DNA sequences have the same number of nucleotides and molecular mass (MW = 4726.1 Da). As shown in **Figure 5.2,** GQ sequence is separated well from a mixture of mutated sequences upon increasing concentration of K^+ and visualized by UV (**Fig. 5.2A**) and MS detections (**Fig. 5.2B**). Broadening of the GQ peak has a bell-shaped curve, with a maximum width at ~150 μM of KCl, when fractions of unfolded DNA and GQ are equal (**Fig. 5.2D**). Experiments carried out in the range of 15 – 450 μM of KCl, (0.1 - 3)×K_F, provide the most confident results for finding rate and equilibrium constants. In this range, the EM contains both DNA and GQ in comparable amounts.

Molecular diffusion can contribute to peak widening in a similar way as dynamic equilibrium between different DNA conformers. Moreover, in our case, the GQ peak became narrower with increasing migration time in experiments when [KCl] > 500 μM – the phenomenon opposite to that could be caused by diffusion. Nevertheless, we found diffusion coefficients for GQ and GM by a CE method as described elsewhere[182]. Briefly, we measured the change of GQ and GM peak widths with and without KCl. This was achieved by first moving an analyte in one direction to pass the UV detector and record the initial peak width. The analyte was then stopped to allow for its diffusion for 40 min. Finally, the analyte was moved back passing the detector for the second time and recording the final peak width. Diffusion coefficients for GQ and GM sequences were the same and equal to (1.4±0.1)×10^{-6} $cm^2\,sec^{-1}$ without KCl, and (4.5±0.2)×10^{-6} and (1.8±0.2)×10^{-6} $cm^2\,sec^{-1}$ in presence of 2 mM KCl, respectively. The folding of DNA to a

compact GQ structure decreases molecular cross-section and a diffusion coefficient accordingly.

The apparent folding constant (K_F) for GQ is 147±8 μM; k_{on} is (1.70±0.41)×10^3 $s^{-1}M^{-1}$; k_{off} for unfolding is 0.25±0.06 s^{-1}. Half-life time of the complex is 2.8 s; relaxation time (τ) equals 2.0 s in 150 μM KCl and 6.5 ms in 90 mM KCl. To the best of our knowledge, this is the first report on kinetic parameters for fast DNA folding/unfolding in solution measured on-line by a separation technique and mass spectrometry. To confirm the value of K_F measured by KCE-MS, we performed independent circular dichroism (CD) titration experiments and found K_F equaled 126±4 μM for GQ-potassium complex. Our results are consistent as well with that reported by Zhang and Balasubramanian[166] for hTelo sequence (GGGTTAGGGTTAGGGTTAGGG): K_F = 120±20 μM, k_{on} = (0.28±0.04)×10^3 $s^{-1}M^{-1}$ and τ = 40 ms in 90 mM KCl using UV titration and stoped-flow techniques. The hTelo sequence is 21-nt long, has 3-quartet DNA G-quadruplexes and folds with a stronger positive cooperativity than TBA with 2 quartets only, therefore, hTelo has smaller K_F and k_{on} values and longer relaxation time.

While in our experimental demonstration of KCE we used an electric field, other means of inducing differential mobility can be used like chromatography or centrifugation. An external action used in KCE to induce the differential mobility can potentially affect the folding kinetics. We performed our KCE separation at different electric fields and found small variations (<20%) of folding constants. Nevertheless, the possibility of such an influence cannot be completely excluded and could be

experimentally studied by varying an electric field and extrapolating the results to zero voltage.

Monitoring DNA folding with ion mobility mass spectrometry. The challenge for MS detection is that molecular weights and m/z ratios of all GM and GQ DNA sequences are the same due to the same nucleotide constitution. It makes these molecules unresolvable by means of MS only. Nevertheless, the differential affinity of DNA to K^+ can be observed by direct injection mass spectrometry (DIMS). The main ions in DIMS are $(GQ\text{-}4H^+)^{4-}$ for free GQ and $(GM\text{-}4H^+)^{4-}$ for free GM (**Fig. 5.3C and 5.3A**). Mixing with 2 mM KCl eliminates free GQ as well as Na^+ adduct (**Fig. 5.3D**), but brings several complexes of GQ with K^+ where $(GQ+K^+\text{-}5H^+)^{4-}$ and $(GQ+2K^+\text{-}6H^+)^{4-}$ are the main ions. The high concentration of KCl does not change significantly the amount of free GM (**Fig. 5.3B**), which confirms the absence of specific affinity of GM to K^+. In DIMS experiments, the first and second dissociation constants K_{D1} for GQ-1K and K_{D2} for GQ-2K have been previously found to be equal 119 μM and 556 μM, respectively[183]. The apparent folding constant K_F obtained in solution by KCE is inherently different from the consecutive dissociation constants K_{D1} and K_{D2} determined by mass spectrometry in a gas phase, because KCE does not resolve 1:1 and 1:2 GQ–metal complexes in solution.

Complexation of GQ with 2 potassium ions causes GQ folding in a compact structure with smaller collision cross section (CCS) that is detectable by ion mobility spectrometry (IMS). GQ has shorter migration in CE and drift time in IMS experiments than GM sequences (**Figure 5.4)**. Addition of K^+ ions to GM sequences increases a cross section and drift time as opposed to the GQ strand (**Fig. 5.4B**).

We also observed that Na^+ and NH_4^+ ions possessed weaker GQ stabilizing activity than K^+ as was previously shown[184]. Important to note, NH_4^+ based buffers (popular in mass spectrometry) should be avoided in studying coordinating effects of nucleic acids (NAs) with different ligands due to the fact that NH_4^+ would compete with the ligands to bind to GQ making it harder to interpret experimental results.

Balthasart et al[185]. studied complexation of TBA (GQ sequence) with NH_4^+ using IMS and found that the loss of NH_4^+ from the complex doesn't change the CCS of NA meaning that free TBA and TBA-NH_4^+ complex have identical CCS's. These findings also support our conclusion that K^+ is a stronger G-quadruplex stabilizing agent.

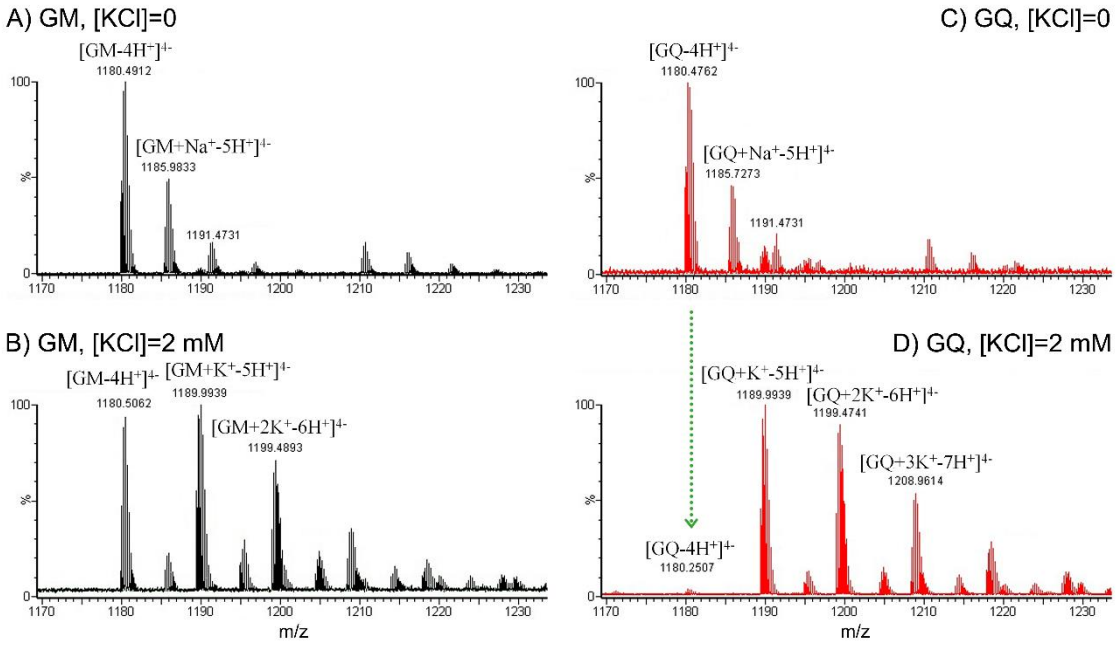

Figure 5.3. Ion patterns of GM (A and B) and GQ (C and D) in the absence (A, C) and presence (B, D) of KCl in DIMS. Free GQ is eliminated upon the binding with K^+ ions. GM – a mixture of GM1, GM2, GM3; GQ – a thrombin binding aptamer.

Screening for GQ stabilizing/destabilizing molecules. Since GQ structures can regulate a broad spectrum of different biological processes and cancer development, it's

of great importance to search for compounds altering its stability. We tested a set of compounds that could possibly stabilize/destabilize GQ: nucleic acid binding dyes: SYTO, BOBO-1 iodide, BOBO-3 iodide. POPO-1 iodide, POPO-3 iodide, TOTO-1 iodide, TOTO-3 iodide, YOYO-1 iodide, YOYO-3 iodide; and an anti-cancer drug called cisplatin or *cis*-diamminedichloroplatinum (II). The dyes were supplemented into the run buffer as well as into samples of GQ, GM1, GM2, and GM3 sequences were

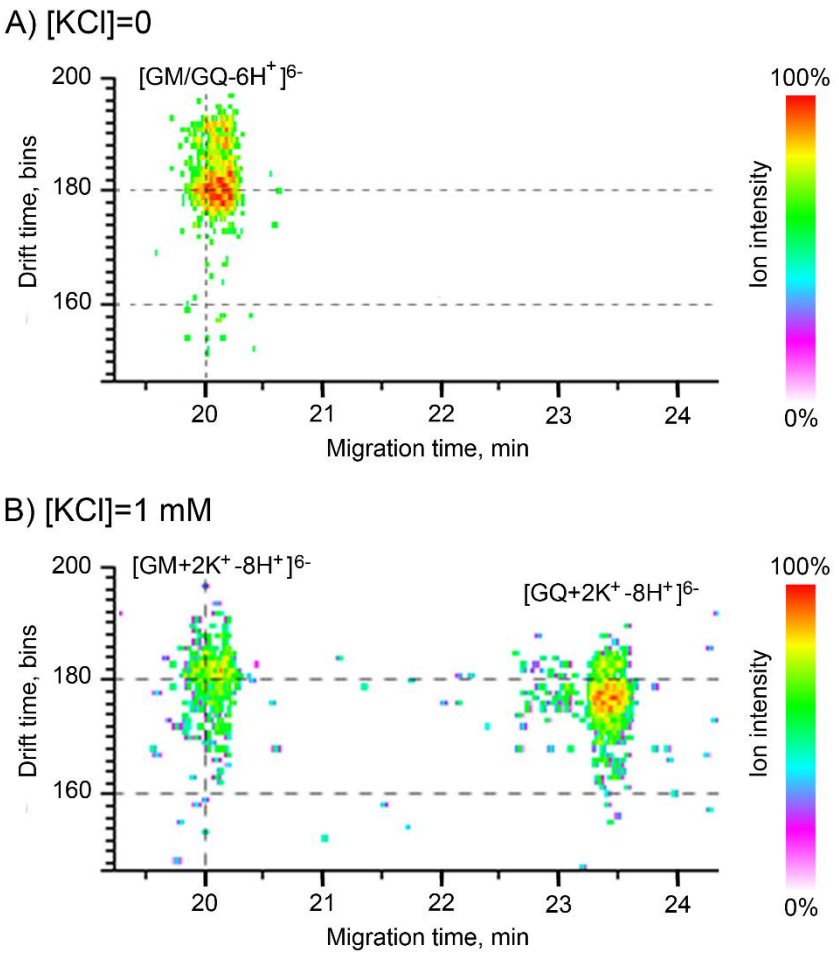

Figure 5.4. On-line KCE-IM-MS experiments for separation of GM (GM1, GM2 and GM3) and GQ DNA sequences. GMs and GQ are well resolved by KCE in solution and poorly by IMS in a gas phase with K^+ ions (B); and are not resolved without KCl (A). Migration time relates to KCE and drift time - to ion mobility spectrometry.

subjected to KCE-MS analysis. We did not observe any migration time shifts and peak widening in KCE, and did not detect GQ-dye complexes by MS in the range of dyes concentrations from 50 nM to 1.6 μM. We concluded that aforementioned DNA binding dyes did not possess any GQ stabilizing/destabilizing activity. Usually these dyes bind well to long double-stranded DNA.

Unlike the dyes cisplatin demonstrated strong GQ destabilizing activity. Cisplatin coordinates to the N7 atoms of the purine (guanine and adenine) bases and forms a covalent adduct with two adjacent bases on the same strand of DNA.

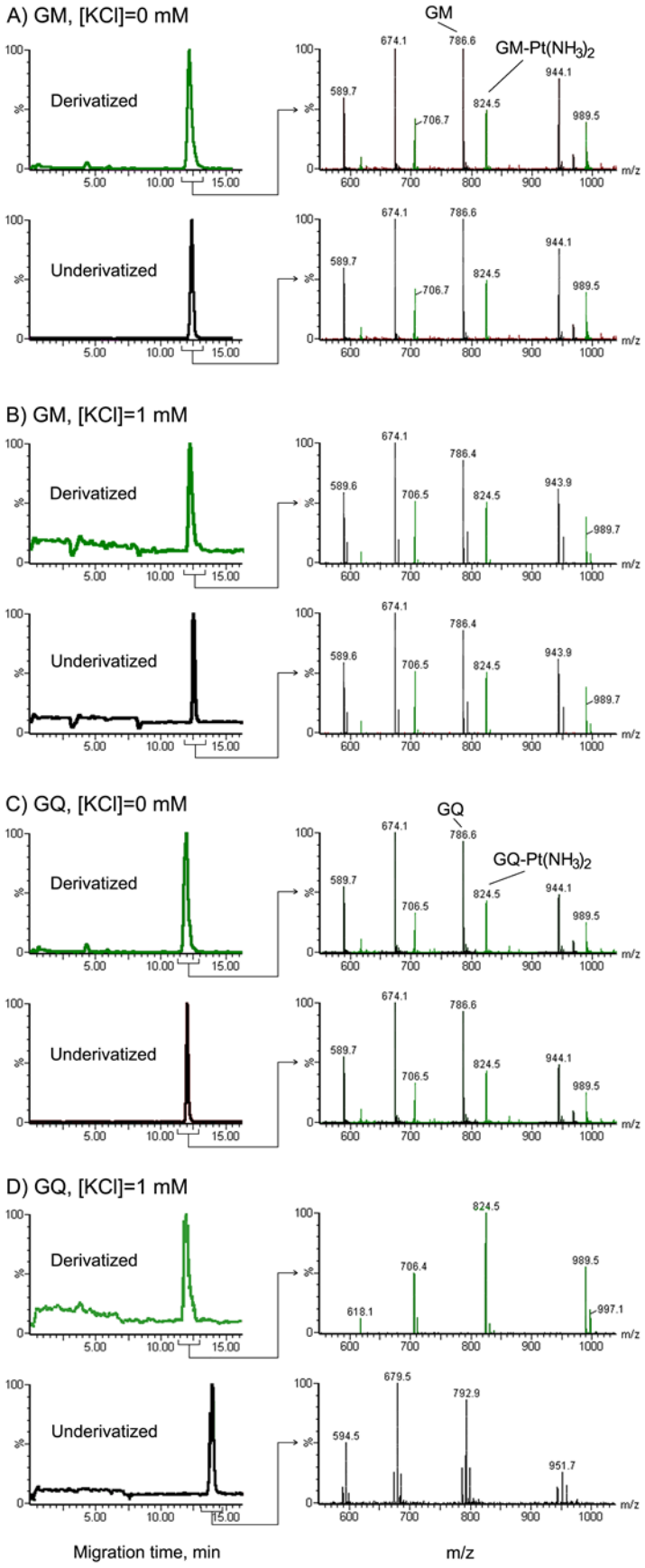

Figure 5.5. KCE-MS electropherograms and m/z ion spectra of GM and GQ sequences after cisplatin derivatization. Green color represents derivatized nucleic acid, black color represents underivatized nucleic acid.

In this experiment, GM and GQ strands were derivatized with cisplatin with and without the presence of K^+ ions (**Figure 5.5**). After derivatization, free DNA as well as monoderivatized strands were detected. Important to note that in cisplatin-DNA complexes both available bonds of cisplatin were used, which indicates intra-strand cross-linking. After cisplatin derivatization, DNA was no longer able to fold into GQ structure (**Figure 5.5D**). Therefore, cisplatin could be used as a strong and non-specific GQ destabilizing agent.

5.5. Conclusion

Whitesides and co-authors were first to apply CE for finding rate and equilibrium constants through a numerical approach of fitting reactant-propagation profiles[186, 187]. Most of the seven KCE methods (NECEEM, SweepCE, plug-plug KCE) cause irreversible perturbations in binding equilibrium and are not suitable for measuring reactions with fast re-equilibration ($\tau < t_{sep}$). For example, in NECEEM, if the dissociation of a complex happens quickly, it is almost impossible to measure $k_{off} > 0.1\ s^{-1}$. In contrast, ECEEM considers both the forward and reverse process in reaction.

In this study, we coupled on-line Kinetic Capillary Electrophoresis with Mass Spectrometry for the study of fast DNA conformations and dynamics in solution. We showed that a peak's shift in CE and its widening can be used for the precise determination of rate and equilibrium constants for DNA-metal affinity interactions and DNA folding. We confirmed DNA folding by ion mobility spectroscopy and presented two-dimensional separation (KCE vs. IM) of conformers in solution and a gas phase.

In conclusion, KCE-MS establishes a new paradigm that separation methods together with MS detection can be used as comprehensive kinetic tools with mass and structure elucidation of nucleic acids. Most previous attempts to use chromatography and electrophoresis for studying nucleic acid interactions were restricted to assuming slow or no equilibrium between reactants. KCE shows that non-zero kinetics and structural dynamics must be taken into account when separation happens. KCE-MS could be a valuable supplement to IM-MS due to the separation of ions in solution according to their size-to-charge ratio. We believe that KCE-MS will be used complementally to CD, SF, and SPR techniques for studying nucleic acid structures and functions, screening DNA/RNA binding compounds and selecting aptamers.

5.6. Acknowledgments

This work was supported by the Natural Sciences and Engineering Research Council of Canada (grant RGPIN/385739-2010) and Canada Foundation for Innovation (project # 25462). The authors also thank Dr. Jeffrey W. Keillor for providing a CD instrument and Mr. Justin Renaud for critical comments and valuable suggestions.

Chapter 6: Real-time monitoring of protein conformational dynamics in solution using kinetic capillary electrophoresis

6.1. Objectives

My objectives were to develop a CE-UV-IM-MS technique to study protein conformational changes and enzymatic activity simultaneously. I was in charge of performing some CE-UV experiments and all CE-UV-IM-MS experiments and analyzing experimental data.

Dr. Victor Okhonin was responsible for creating a mathematical model for calculating rate and equilibrium constants. Dr. Christopher Clouthier was responsible for TG2 preparation, CE-UV experiments. Dr. Jeffrey Keillor provided supervision for the experimental part. Dr. Maxim Berezovski provided technical guidelines and supervision in performing all CE experiments.

6.2. Introduction

Conformational changes represent an important means of regulating protein biological function within the complex environments found in living systems[189, 190]. The development and application of techniques able to detect these conformational changes have therefore become a vital area of biophysical research. To date, the most commonly applied methods include nuclear magnetic resonance spectroscopy (NMR), X-ray

crystallography (XRC), small-angle X-ray scattering (SAXS), Förster resonance energy transfer (FRET), and electron paramagnetic resonance (EPR) spectroscopy[191-198].

Generally speaking, the most widely employed method is X-ray crystallography. However, this method provides only a static picture of one protein conformation under certain conditions, whereas NMR, EPR, and fluorescence spectroscopy can probe dynamic conformational changes under more physiologically relevant conditions. NMR spectroscopy can provide results relating to protein conformational mobility in solution and with atomic resolution, but this technique is generally limited to smaller proteins (<25 kDa). Alternatively, fluorescence-based methods (including FRET) can measure the relative distance between intrinsically fluorescent residues or fluorescent labels, related to protein conformational changes. However, the fluorescent labelling of a protein may affect its ability to undergo a given conformational change.

Kinetic capillary electrophoresis (KCE) has emerged as a powerful bioanalytical technique for monitoring a wide range of biomolecular interactions during electrophoretic separation, including the measurement of rate and equilibrium constants associated with protein–ligand binding[199, 200]. The power of capillary electrophoresis (CE) has been illustrated through its ability to differentiate between the folded and unfolded states of a protein suggesting it may also be able to monitor, in real-time, the ability of a native, unlabelled protein to undergo large-scale conformational changes[201, 202]. This method is rapid, requires little material, and can easily accommodate the presence of allosteric regulators.

Recently, it has been shown that human tissue transglutaminase (TG2) undergoes large-scale tertiary structural changes related to the regulation of its activity. The binding of guanidine di- or triphosphate (GDP/GTP) inactivates the enzyme in a compact "closed" conformation while Ca^{2+} binding activates the enzyme in the form of an extended "open" conformation[203-205]. TG2 is a structurally and functionally complex protein that has been suggested to function as a cytosolic scaffold protein[206] in addition to its role as a calcium-dependent catalyst capable of cross-linking proteins through transamidation of protein-bound glutamine and lysine side chains[207-209]. Furthermore, unregulated TG2 activities have been implicated in a number of physiological disorders such as Huntington's disease[210, 211], Alzheimer's disease[212, 213], Celiac disease[214], and in cancer metastasis[215-217] underlining the potential of the enzyme as a therapeutic target.

TG2 comprises four structural domains: an N-terminal β-sandwich, a core domain containing the transamidase active-site catalytic triad (Cys277, His335, and Asp358), and two β-barrels (**Figure 6.1**). In its GDP-bound state, the compact structure adopted by TG2 offers restricted accessibility to its active site, in sharp contrast to the extended or open conformational form in which it was crystallized following its calcium-dependent reaction with an irreversible inhibitor[203, 218]. Correlation of structural and kinetic data suggests that the open conformational form of TG2 represents the active form of the enzyme, capable of binding the acyl donor substrate[218-220]. Several potential calcium binding sites have been tentatively identified[221], whereas the nucleotide binding pocket of TG2 associated with GTP/GDP binding has been shown by X-ray crystallography to include residues 476–482 and 580–583 of the first and last strand of β-barrel 1[203].

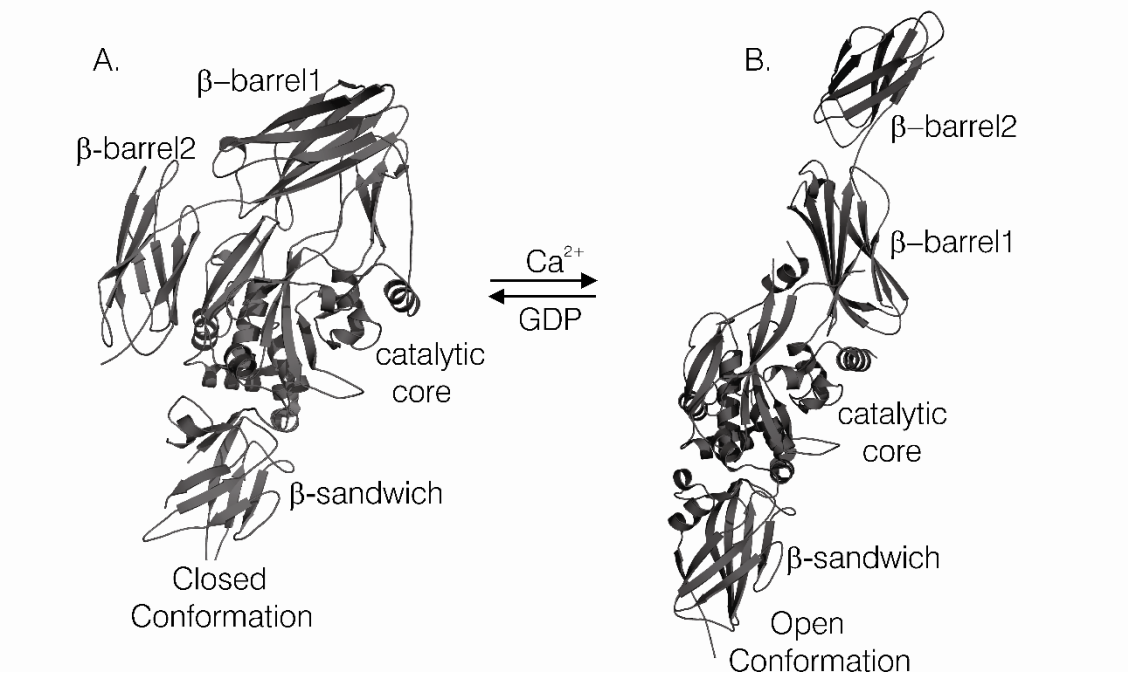

Figure 6.1. Two conformations of TG2. Explanation in the text.

In this work we demonstrate the power of using KCE to monitor the large-scale, ligand-induced conformational changes associated with the regulation of human TG2 activity. This represents an important step in assigning functional capacity to conformers of TG2 and establish KCE as a real-time method for studying protein dynamics and function in general.

After this article was published, we performed additional CE-UV-IM-MS experiments which will be discussed in the section 6.4.2.

6.3. Materials and methods

Chemicals and Materials. Calcium chloride, magnesium chloride, peptone, yeast extract, ampicillin, Tris-(2-carboxyethyl) phosphine (TCEP), ethylene glycol tetraacetic acid (EGTA), glycerol, Triton X-100, and glutathione (GSH) were purchased from

Bioshop Canada. Tris-base and acetic acid were purchased from Bio-Basic Canada. *Guanosine diphosphate* (GDP) was purchased from Sigma-Aldrich, Canada. All bare fused-silica capillary with an inner diameter of 75 μm and an outer diameter of 360 μm was purchased from Polymicro (Phoenix, AZ). Glutathione resin was purchased from GE healthcare. All buffers and capillary wash solutions were filtered through 0.22-μm pore size filters (Millipore, (Nepean, ON).

Expression and Purification of human tissue transglutaminase. Expression and purification followed a protocol recently adapted in our group[222]. In brief, *E. coli* cells harbouring the expression plasmid pGST-PSP-hTG were taken from frozen stock and used to inoculate 10 mL (2 × 5 mL) of rich Terrific Broth (TB) medium containing 100 μg/mL ampicillin, which was allowed to grow at 37°C overnight (16-18 h). This pre-culture was then used to inoculate 1 L of fresh TB media and the culture was allowed to grow at 37 °C until the A_{600nm} reached between 0.6-0.8, at which point the incubator temperature was reduced to 28°C and the culture was allowed to grow for an additional 18 to 20 h. Protein expression occurred owing to the leaky nature of the T7 promoter of the pGST-PSP-hTG plasmid, without addition of any exogenous IPTG. Cells were pelleted by centrifugation (30 min, 2000 × g, 4°C), resuspended in 30-40 mL of lysis buffer (20 mM Tris, 150 mM NaCl, 1 mM EGTA, 1 mM TCEP, and 15% glycerol at pH 8.0) and lysed in 10-mL aliquots using a cell homogenizer (Avestin Inc, Ottawa, ON). The cellular debris was removed via centrifugation (60 min, 44000 × g, 4°C) and the supernatant was filtered through a 0.22-μm filter, yielding crude lysate.

All purification procedures were carried out in a cold-room environment at 0-5 °C. Approximately 1 mL of glutathione Sepharose resin 4B in 20% ethanol was washed twice with 2 mL deionized water and twice with 2 mL lysis buffer, after which it was added to the crude lysate and placed on an orbital rocker plate for 2 h. The lysate-glutathione Sepharose resin mixture was loaded into a gravity filtration column (Bio-Rad Econo-Column 1.5 × 10 cm). After column loading the resin was washed with 10 mL of lysis buffer containing 0.5% triton X-100, 10 mL of lysis buffer, and 10 mL of elution buffer (20 mM Tris, 150 mM NaCl, 1mM EGTA, 1mM TCEP at pH 7.2) with the flow-through being retained after each wash. After washing, 1 mL of GST-tagged Prescission Pre protease (0.3 mg/mL concentration) was added to the column, incubated overnight (~12 h), and the column was eluted with 3 mL of elution buffer to liberate TG2 from the column. The presence of human TG2 was confirmed by SDS-PAGE (4% stacking gel and 10% running gel) stained with 250R Coomassie Brilliant Blue and using broad-range molecular weight markers (Biorad, Hercules, CA). Protein concentrations were quantified by Bradford assay (Biorad, Hercules, CA), using bovine serum albumin as the standard, with general protein yields in the range of 1.5 to 3 mg/L. Human TG2 activity was assayed using an established tissue transglutaminase assay[223] and found to have specific activities in the range of 0.2 to 0.3 U/mg, where one unit of activity is defined as the release of 1 µmol *p*-nitrophenolate per min. Purified protein samples were flash frozen in 500-µL aliquots (approximately 6-8 µM) and stored at -80°C.

Kinetic Capillary Electrophoresis. All capillary electrophoresis experiments were performed using a P/ACE MDQ chiral capillary electrophoresis (CE) system (Beckman

Coulter, Brea, CA, U.S.A.) equipped with a photo-diode array detector. Prior to all capillary electrophoresis experiments purified TG2 was buffer changed into double distilled water and concentrated to a final concentration of 30-40 µM using Amicon spin concentrators with a MW cut-off of 30 kDa (Millipore, Nepean, ON). Protein samples were injected without pre-incubation with conformational regulators. For all experiments in the current study protein absorbance was monitored using two channels scanning from the 200 to 300 nm region of the ultra-violet spectrum. Separations were carried out using a bare fused-silica capillary of 50 cm in total length and 40 cm from the injection point to the detector window (effective length). A hydrodynamic injection strategy was used through application of a 1-psi pressure pulse for 5 s for the CE separation. A 20-kV voltage (an electric field of 400 V/cm), with the positive charge at the inlet and the ground at the outlet, was applied to the sample-loaded capillary to facilitate the CE separations. Results were reported as UV absorbance intensity at the detection point as a function of time passed after initiation of the electric field, which was analyzed using the Beckman 32 Karat version 8.0 software. Running buffer for all experiments was 12.5 mM Tris-Acetate (TA) at pH 8.3. Prior to each experiment, a capillary rinsing procedure using 20 psi pressure was performed for 4 min, washing with 0.1M NaOH, deionized water, and 12.5 mM TA running buffer. The capillary temperature was maintained at 15 ± 0.5 °C unless otherwise stated.

Capillary Electrophoresis Titration Studies. Purified TG2 (in 20 mM Tris, 150 mM NaCl, 1 mM EGTA, 1 mM TCEP at pH 7.2) was buffer changed into double distilled water and concentrated to 30-40 µM using Amicon spin concentrators with a MW cutoff of 30 kDa

(MilliPore, Nepean, ON). TG2 conformational modulation studies were performed by supplementing the CE running buffer (12.5 mM Tris-Acetate) with the following concentrations of calcium chloride ($CaCl_2$): 50 µM, 75 µM, 100 µM, 125 µM, and 150 µM and performing CE experiments using the general capillary electrophoresis conditions. Control experiments were performed using magnesium chloride ($MgCl_2$) with concentrations in the range of 50 to 150 µM. Stock solutions of 10 mM for $CaCl_2$ and $MgCl_2$ were used to supplement the CE running buffer. Temperature ramping studies were performed by modulating the capillary temperature during the electrophoresis runs. Temperature points ranging from 15°C to 50°C were applied and CE experiments using the previously described conditions. All capillary electrophoresis experiments were done in triplicate using freshly prepared TG2 protein samples.

Kinetic Capillary Electrophoresis TG2 incubation with irreversible inhibitor. Purified TG2 (in 20 mM Tris, 150 mM NaCl, 1 mM EGTA, 1 mM TCEP at pH 7.2) was buffer exchanged into double distilled water using Amicon spin concentration with a MW cutoff of 30 kDa to remove salts and concentrate the sample to approximately 25 µM. To these concentrated TG2 samples were added 50 µM of $CaCl_2$ and 70 µM of the irreversible TG2 inhibitor NC-9[224] and samples were incubated for 1 h at 4 °C. After incubation CE experiments were performed on the inhibited TG2 samples using the general capillary electrophoresis conditions with CE buffer containing no additives (12.5 mM Tris-Acetate). All capillary electrophoresis experiments were performed in duplicate using individual freshly buffer exchanged and concentrated TG2 samples.

TG2 activation and deactivation kinetics assay. Activation and inactivation kinetic studies of purified TG2 were performed in triplicate using the colorimetric AL-5 (*N*-Cbz-Glu(γ-p-nitrophenyl ester) Gly assay[223]. The change in absorbance was monitored at 405 nm using a Cary 100 Bio UV-Vis spectrophotomer at 25 °C. TG2 activation kinetic assays were conducted using 925 µL of buffer composed of 0.1 M MOPS and 50 µM EDTA (pH 7.0), 50 µL of 8 µM TG2, and 25 µL of AL-5 in DMF (total reaction volume 1 mL). Background hydrolysis of AL-5 was monitored for 10 min after which a 3-µL aliquot of 1 M $CaCl_2$ (3 mM final) was added and the calcium-activated TG2-catalyzed hydrolysis of AL-5 was monitored until all the substrate was consumed. For TG2 inactivation studies, assays were conducted using 925 µL of buffer composed of 0.1M MOPS, 50 mM $CaCl_2$ and 50 µM EDTA (pH 7.0), 50 µL of 8 µM TG2, and 25 µL of AL-5 in DMF (total reaction volume 1 mL). The activated TG2-catalyzed hydrolysis reaction was monitored for 5 min after which 6 µL of 1 M EGTA (6 mM final) was added and the reaction monitored further. All TG2 activation and deactivations experiments were performed in triplicate.

KCE-UV-IMS-MS experiments - Chemicals and Reagents. For all experiments, 15 mM Tris-Acetate, pH 7.85, was used as an incubation/run buffer. The buffer was prepared by dilution from 200 mM Tris-Acetate stock buffer. The stock buffer was made by dissolving 12.11 g of Tris-base (Bio Basic Inc., Canada, cat.# 77-86-1) and 2.86 mL of acetic acid (Bio Basic Inc., Canada, cat.# C1000) in 500 mL of ddH2O.

Mixtures of TG2, $CaCl_2$, inhibitors and substrates drugs were prepared in the incubation buffer with (i) inhibition titration experiments: 30 µM TG2, 200 µM - $CaCl_2$, 0, 20, 50, 100 and 200 µM inhibitor, 100 µM each substrate; (ii) deactivation experiment: .

CE-UV-IMS-MS instrument. All solutions were filtered through 0.22-µm pore size nylon membrane filters (Millipore, Nepean, ON, Canada). The bare-silica capillary was purchased from Polymicro (Phoenix, USA). KCE Experiments. The sample storage and capillary temperature were maintained at 4 ± 0.5 and 15 ± 0.5 °C, respectively. An electric field in KCE separation was 330 V/cm with a positive electrode at the injection end. For all experiments, the capillary was 90 cm long (35 cm to UV detector) with an inner diameter of 50 µm and an outer diameter of 360 µm. The equilibrium mixture was injected into the capillary from the inlet end by a pressure pulse of 6 s × 5 psi. Before each experiment, the capillary was rinsed by 75 psi pressure with: 0.1 M NaOH for 3 min, ddH2O for 3 min, 15 mM Tris-Acetate buffer for 5 min. A Synapt G2 HDMS mass spectrometer from Waters (UK) was coupled with a PA800plus Pharmaceutical Analysis CE system having a PDA detector (Beckman Coulter, USA) through a CE-ESI sprayer from Micromass (UK) and used in all CE-UV-MS experiments. Liquid cooling tubing was home-modified to apply the cooling liquid to the whole capillary. Electrospray ionization conditions were as follows: capillary voltage 3.2 kV, positive mode, sampling cone voltage 80 V, extraction cone voltage 5 V, source temperature 120˚C, cone gas 50 L/h, nano flow gas 0.15 Bar, purge gas 3 L/h, mobility cell bias voltage 3 V. Sheath liquid (50:50 methanol:ddH2O 1% acetic acid) was delivered with flow rate of 1.5 µl/min.

MS data was acquired from m/z=300 Da to m/z=2700 Da. Acceptor peptide was tracked at m/z=392.28, donor peptide at m/z=854.55, product at m/z=1229.13, TG2 for IMS experiment at m/z=2430 Da.

GraphPad Prism fitting. Log(inhibitor) vs. response – variable slope with four parameters fitting. Top value constraint was set at 1 for both graphs. For relative residual activity the Hill slope was constrained at less than -3.2.

6.4. Results and discussion

6.4.1. CE-UV

Conceptually, the method is illustrated in **Figure 6.2**. Given the dramatic structural differences between the two conformational forms of TG2, we reasoned that the conformers may be separable by KCE, if their interconversion is slow relative to the separation time between two protein forms. This is illustrated in **Figure 6.2A**, where the structurally larger open form migrates faster than the more compact closed form, resulting in the observation of two quasi-separated peaks. Furthermore, this method would allow the dynamic conformational equilibrium of TG2 to be probed through supplementation of the electrophoretic running buffer with known conformational regulators of TG2 (**Figure 6.2B**). The ability to regulate TG2 conformation during separation would allow a unique kinetic analysis of the protein/regulator interaction.

Human TG2 was expressed and its purity was confirmed by sodium dodecyl sulfate polyacrylamide gel electrophoresis (SDS-PAGE; see the Supporting Information). Analysis of purified TG2 by KCE revealed the presence of two peaks, separated by an approximately 1.5-minute difference in electrophoretic migration times (**Figure 6.3A**).

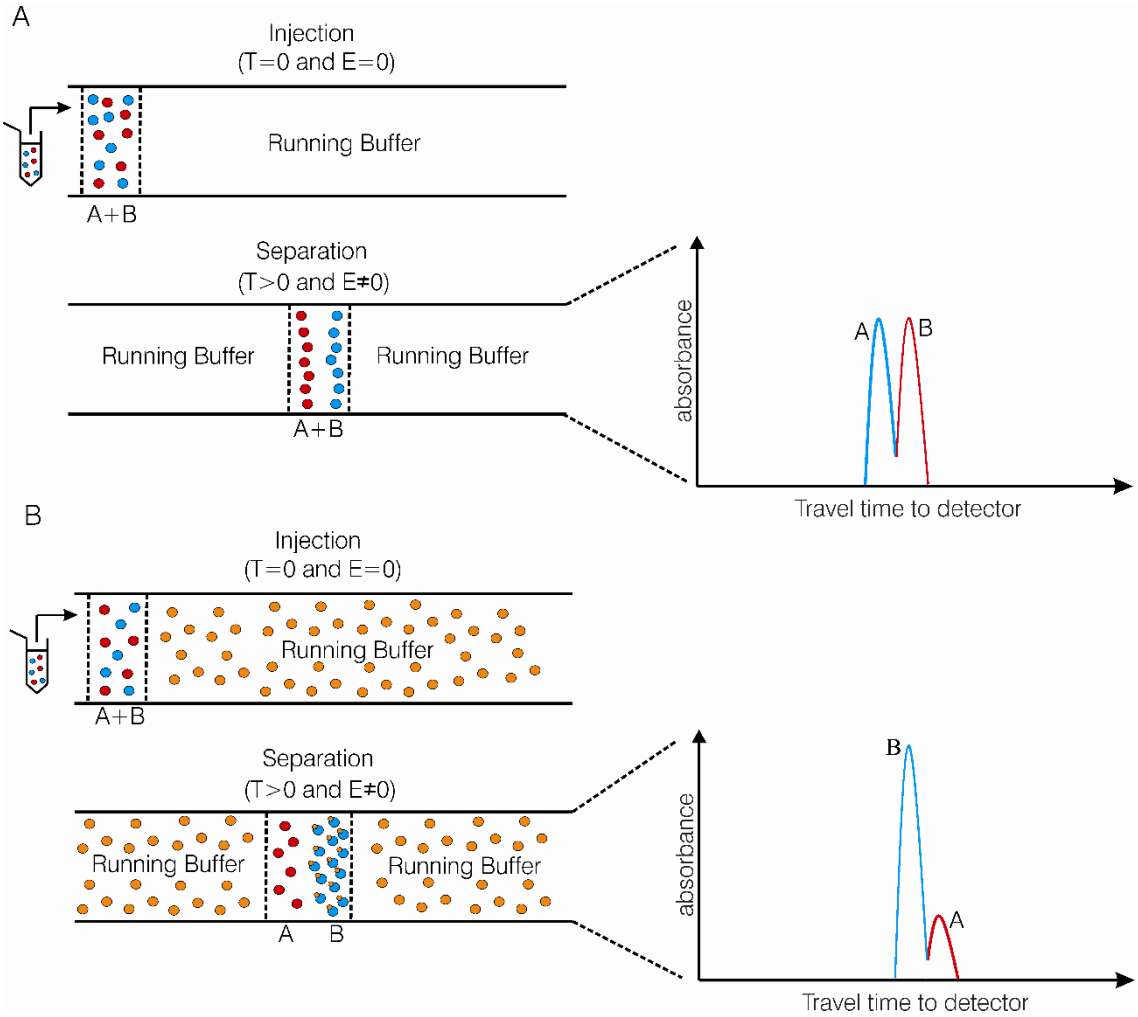

Figure 6.2. Kinetic capillary electrophoresis experiment. The open conformation of TG2 is shown as blue spheres, while the closed conformation is represented by red spheres. A) A mixture of the two conformational forms of TG2 is injected into the capillary as a short plug. Application of an electric field (E>0 V cm^{-1}) results in the migration and separation of the two forms into two fractions. B) Injection and separation of a TG2 sample in running buffer supplemented with a conformational regulator (orange spheres) results in the observation of an altered conformational distribution (T=travel time).

This observation is in excellent agreement with earlier studies wherein two forms of TG2 with different electrophoretic mobilities were observed by native polyacrylamide gel electrophoresis (nPAGE) and assigned as the open and closed conformations[218]. In the present study, both peaks migrating from the KCE were confirmed to be purified TG2 by

electrospray ionization mass spectrometry, and neither peak corresponds to denatured TG2 (see the Supporting Information). These results suggest that the two peaks correspond to natively folded conformers of TG2, or rather, to two families of closely related conformers. Just as it is naive to assume that TG2 exists only in the two conformations that have been crystallized, it is important to note that each peak observed by KCE may represent a number of similar conformers that migrate together. Minor or rapid conformational changes occurring on the microsecond to millisecond time scale, such as those that would occur during a catalytic cycle of the enzyme, would only lead to slight broadening of each peak corresponding to a conformer family.

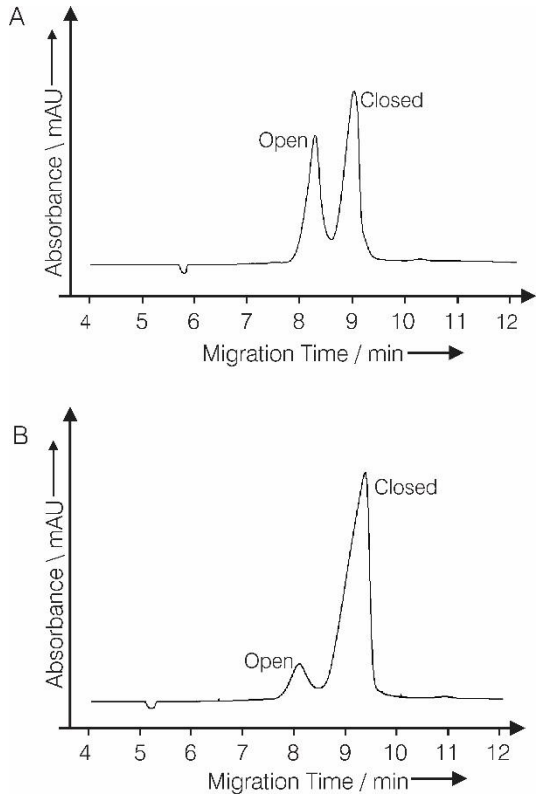

Figure 6.3. Capillary electropherograms of TG2 in 12.5 mM tris-acetate (pH 8.3). A) KCE separation in the absence of known allosteric regulators (GDP or calcium) showing the protein in the open and closed conformational forms (see labelled peaks). B) KCE separation in the presence of 20 µM GDP supplemented in the running buffer, showing a distinct shift in the conformational distribution from "open" to "closed".

This suggests that raising the temperature should increase the rate of interconversion between the conformer families and may lead to coalescence of the peaks. To test this hypothesis, purified TG2 was analyzed by CE from 15 to 50 °C through modulation of the capillary running buffer temperature (see the Supporting Information). Ramping of the capillary buffer temperature resulted in the broadening of the two peaks and their coalescence into one peak having an averaged elution time presumably due to conformers that interconvert rapidly at higher temperatures.

We then sought to assign each peak observed by KCE to a known TG2 conformation. To this end, the equilibrium capillary electrophoresis of equilibrium mixtures (ECEEM) method was employed, in which a plug of protein is injected into a capillary prefilled with running buffer containing the known conformational effector[225]. This method is based on the affinity capillary electrophoresis (ACE) approach reported by Whitesides and co-workers where a near-equilibrium is maintained between the interacting species, in this case protein and conformational regulator, during the CE run[226]. KCE separation of TG2 in running buffer supplemented with 20 µM guanosine diphosphate (GDP) resulted in a shift in conformational distribution in favor of the slower eluting peak (see **Figure 6.3B**). The closed conformation was assigned to this peak, according to several lines of evidence. Most significantly, GDP was found to be bound in the X-ray structure of the closed conformation[227]. Furthermore, early SAXS results also suggest that TG2 adopts a more compact conformation in the presence of GDP[219]. Moreover, the intensity of the faster eluting band observed by nPAGE was found to increase upon addition of GDP to the running buffer[218, 220]. The fact that the more compact conformation migrates more

slowly than the open conformer in CE is not surprising; the open conformation could easily expose more charged residues to the solvent and be subject to greater electro-osmotic force. Finally, when we incubated TG2 with NC9, an irreversible inhibitor developed previously in our group[228] that has been shown to favor a more extended conformation[229], the intensity of the faster eluting peak increased at the expense of the slower eluting peak.

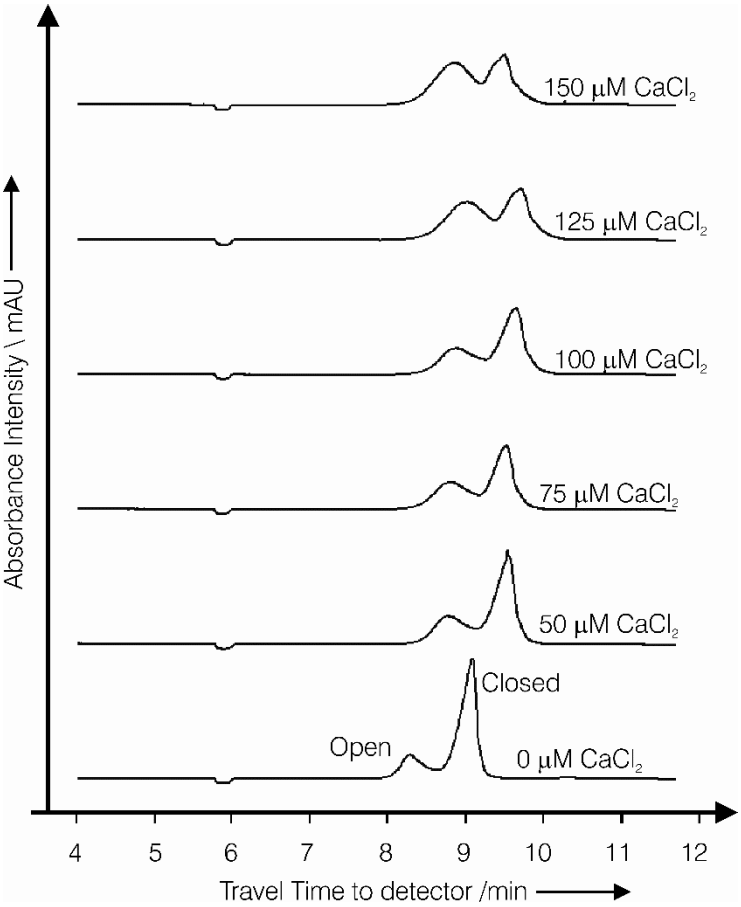

Figure 6.4. KCE of TG2 showing the influence of increasing concentrations (50 to 150 μM) of calcium chloride on the equilibrium distribution of the open and closed conformations.

Although no X-ray structures of TG2 have included bound calcium, previous SAXS, fluorescence, and dynamic CD studies have all suggested that the enzyme adopts a more

open conformation in the presence of Ca^{2+}[205, 219, 230]. Taking into account our observations described above, we predicted that we should be able to increase the proportion of the slower eluting CE peak by adding increasing amounts of divalent calcium to the running buffer. Our initial observation of two conformational peaks in the absence of added Ca^{2+} suggests that trace amounts of calcium are co-purified with TG2, as has been shown in the past[221]. To minimize the concentration of co-purified calcium, ethylene glycol tetraacetic acid (EGTA), a divalent metal ion chelator having a strong affinity for calcium, was added to the buffers used during the purification of recombinant TG2. This resulted in a significant decrease of the intensity of the faster eluting peak, with a concomitant increase in the intensity of the slower eluting peak (**Figure 6.4**). Moreover, increasing the concentration of calcium chloride in the running buffer up to 150 µM resulted in a striking shift of the relative intensity of the faster eluting peak, consistent with displacement of the conformational equilibrium to the active, open conformation (**Figure 6.4**). Admittedly the concentration range of Ca^{2+} ions used in the present study is lower than those frequently used in TG2 activity assays, because millimolar concentrations of Ca^{2+} ions resulted in severe broadening and suppression of the protein KCE signal. However, while this may represent a limitation of the experimental method, a recent study has confirmed that TG2 is active at physiological concentrations around 100 µM Ca^{2+} ions[231], suggesting that the titration range employed herein represents a valid method for probing relevant TG2 behavior. In **Figure 6.4** it can also be noted that adding a salt such as calcium chloride to the running buffer has the general effect of broadening peaks and lengthening migration times. This general salt effect was also observed when

magnesium chloride was added to the running buffer instead of calcium chloride; however, adding Mg^{2+} ions up to 150 µM does not have a significant effect on the proportion of the conformers (**Figure 6.5**). This important control experiment suggests that the effect of added calcium is due to specific ligand binding rather than a general medium effect.

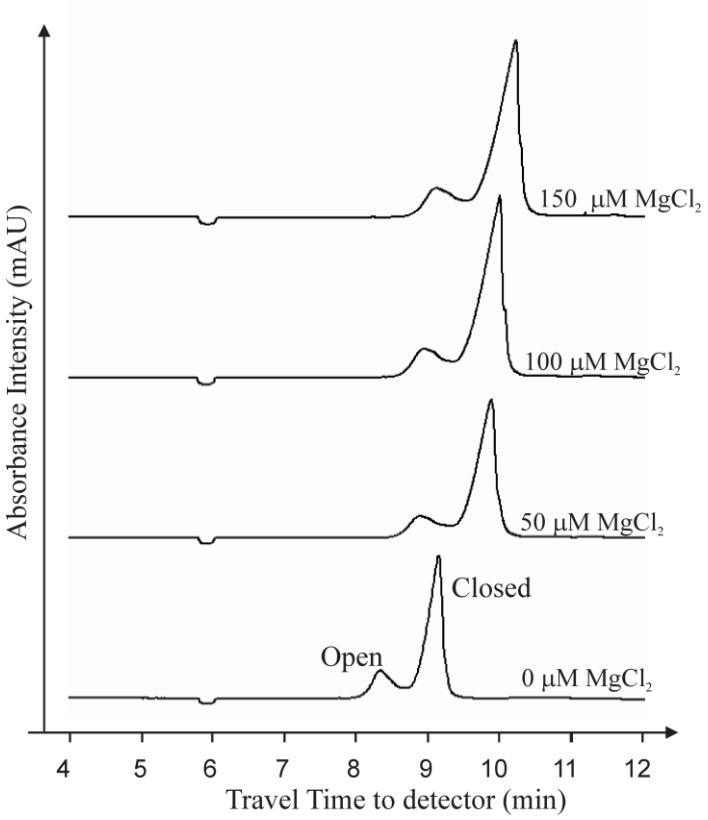

Figure 6.5. Capillary electropherograms illustrating the lack of influence of various concentrations of magnesium chloride on the equilibrium distribution of the open and closed conformations human TG2.

The relative intensities of the peaks assigned to the open and closed forms of TG2 were then analyzed as a function of added calcium concentration, using a previously developed method for studying the kinetics of biomolecular interactions at equilibrium[232]. Since little is known regarding the microscopic details of TG2 opening and

calcium binding, we cannot exclude the possible existence of a closed, calcium-bound form of TG2 that can either lose calcium or change conformation by the dashed arrows of **Scheme 6.1**. However, for simplicity, fitting was performed using the solid arrows of this scheme, based on the species observed crystallographically, shown in bold. This fitting yielded a value of (38±9) μM for the dissociation constant (K_d) of calcium binding, and values of (138±27)×10^{-3} min^{-1} and (49.8±1.5)×10^{-3} min^{-1} were determined for k_{open} and k_{close}, respectively (**Scheme 6.1**). The K_d value obtained is close to those previously measured by isothermal titration calorimetry (0.1–4.6 μM)[221] while the values for k_{open} and k_{close} represent, to our knowledge, the first reported for human TG2.

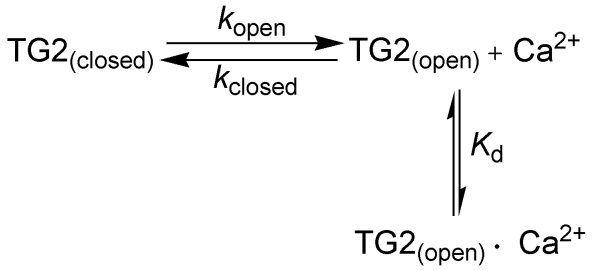

Scheme 6.1. Kinetic and thermodynamic parameters for TG2 ligand binding.

These rate constants provide half-lives of 5.0 min for opening and 13.9 min for closing. From these values one can see that limited conformational interconversion takes place on the time scale of the CE separation (8–10 min elution time). It is also instructive to compare the k_{open} and k_{close} rate constants to k_{cat} values associated with the catalytic cycle. For the reaction of the highly homologous guinea pig liver TG2 with substrate analogues, k_{cat} values in the range of 17–114 min^{-1} have been reported[225, 231]. Since the rate constants measured herein for the conformational changes associated with TG2

activation are much lower than k_{cat}, these conformational changes cannot be occurring during the catalytic cycle. This eliminates the possibility, for example, that the closed form reacts with a substrate, opens up upon acylation, and then closes up again upon the product release. Instead, it appears that a slow conformational change takes place upon activation of the enzyme, as a mechanism for functional regulation, and that once open, it then remains open throughout its catalytic cycle.

Finally, a simple kinetic experiment was performed to confirm the time scale of activation and deactivation. As shown in **Figure 6.6**, TG2 deactivation by calcium depletion was virtually instantaneous, consistent with rapid dissociation of calcium to an inactive calcium-unbound form. However, TG2 activation by calcium addition was slower, consistent with the rapid activation of existing open form TG2, followed by a slower shift in the conformational equilibrium from closed to open, on the minute time scale observed by KCE.

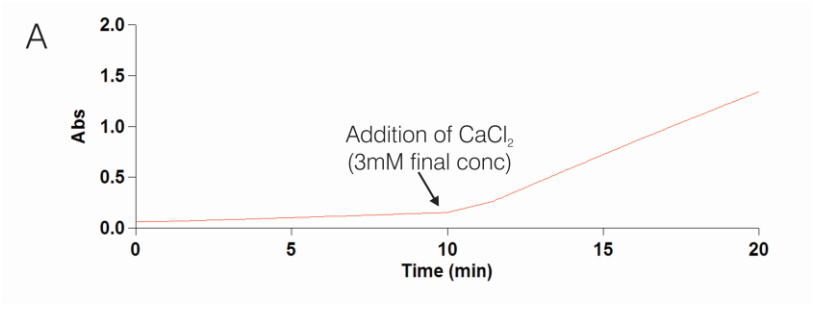

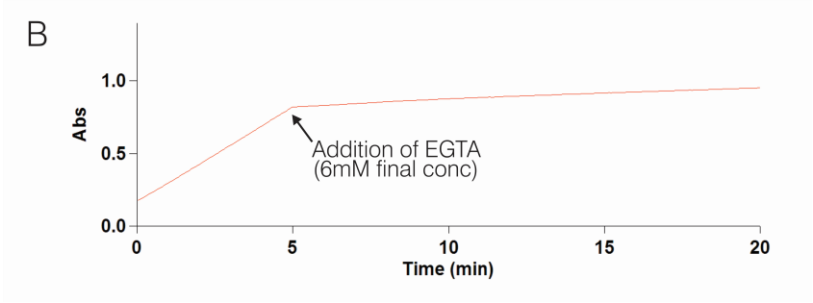

Figure 6.6. Activation and deactivation of TG2 probed via the monitoring of the UV-Visible change in absorbance at 405 nm indicative of the hydrolysis of the TG2 substrate analogue AL5[223] (400 nM TG2 and 435 µM AL5 present in each cuvette). **A**. TG2 activation study showing the slow onset of TG2-mediated AL5 hydrolysis upon addition of $CaCl_2$ to a final concentration of 3 mM. **B**. TG2 deactivation experiment showing the rapid decrease in TG2-mediated AL5 hydrolysis upon depletion of calcium by the addition of EGTA to a final concentration of 6 mM.

6.4.2. CE-UV-IM-MS

To simultaneously investigate TG2 enzymatic activity and conformation, a CE-UV-IMS-MS method was developed (in this text, the "ESI" abbreviation has been omitted for simplicity). This method combines advantages of both CE-UV and CE-MS, while eliminating some of their limitations. CE separates analytes based on their size to charge ratio. The nature of this separation method allows one to estimate the size of an analyte, if its charge is known. Unfortunately, the charge of a large biopolymer like a protein cannot be accurately estimated based solely on its sequence. UV detection also has its advantages and disadvantages. One important advantage is that UV absorption is directly proportional to the concentration of the analyte protein, which allows the concentration of each protein conformer to be determined, if they are spatially separable. The main disadvantage, however, is that small molecules are not easily detectable and identifiable by UV at low concentrations or in complex samples. Therefore, when online analysis of complex samples is required, MS is the detection technique of choice. In addition to permitting the analysis of small molecules, MS can also be used to detect proteins; furthermore, IM provides means for comparing the relative sizes of conformers bearing the same charge. Taken together in a coupled method, the separation of species in solution is accomplished by CE, on a size to charge basis, while UV provides quantitative

information about conformer concentration, MS informs on the mass of each conformer and quantifies substrates and products, and IM estimates the size of each TG2 conformer.

Figure 6.7A schematically represents the CE-UV-IM-MS approach. CE-UV indicates that a sample contains two proteins, X and Y, with relative abundance of 70% and 30%, respectively. After ionization, it is clear that the mass of protein X is identical to the mass of protein Y, but the cross-section (size) of X is smaller compared to Y. It can be concluded that proteins X and Y are two conformers of the same protein that have different behavior both in CE and IM. MS also allows the semi-quantitative monitoring of substrates and products for the enzymatic reaction, taking place in the sample solution. If titration with an irreversible inhibitor is performed, it is possible to assign enzymatic activity to a specific conformer. The overall conclusion from this experiment is depicted in **Figure 6.7B**.

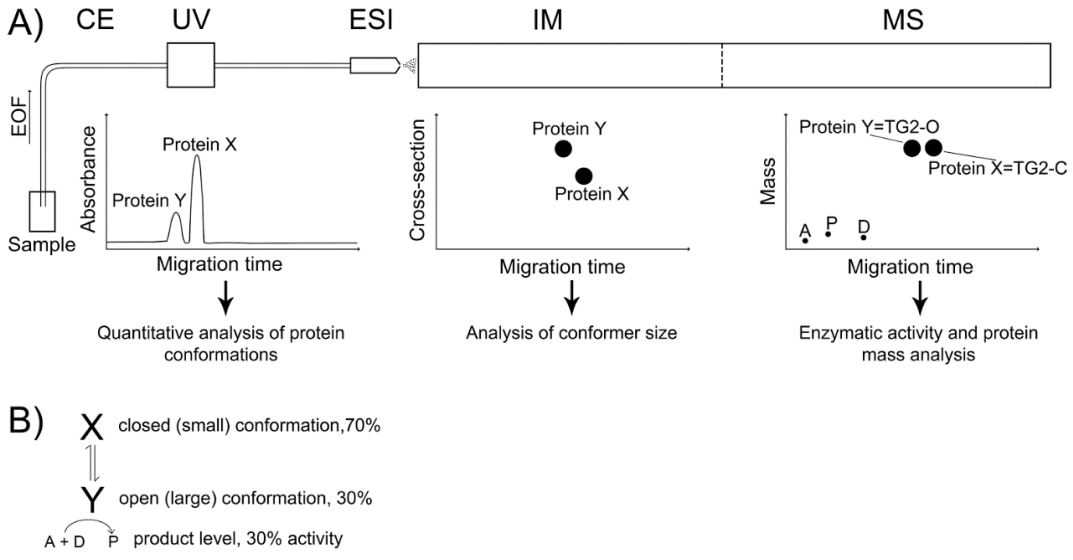

Figure 6.7. A) Schematic representation of the CE-UV-ESI-IM-MS method. A - acceptor substrate, D - donor substrate, P - product, TG2-O - open conformation of TG2, TG2-C - closed conformation of TG2. B) Conformation change and enzymatic activity model.

A single CE-UV-IM-MS experiment generates a huge amount of data. This data can be first divided into two aspects (TG2 conformational changes and TG2 enzymatic activity), then analyzed separately and finally combined together.

CE-UV-IM-MS experiments revealed that the intensity of the MS signal for TG2 did not correlate well with the intensity of its UV absorption. It can be clearly seen (**Figure 6.8A**) that in our experimental conditions in the absence of inhibitor, according to UV data, there were two distinct peaks detected for the two conformations of TG2, and the closed conformation predominates. However, according to MS data (**Figure 6.8B**), both conformations produce approximately the same MS response. This discrepancy reflects an intrinsic drawback of MS detection; namely, different species can have different ionization efficiencies and hence their responses cannot be compared directly. We believe that the ionization efficiency for the closed conformation of TG2 (TG2-C) is significantly lower than that of its open form (TG2-O), presumably due to the lower exposed ionizable surface area of the compact conformation. Another interesting aspect was that TG2-O produces an ion distribution pattern with one maximum at m/z=2288 while TG2-C yields two maxima at m/z=1994 and m/z=2288 (**Figure 6.9**), which are probably artefacts of unfolding during ionization.

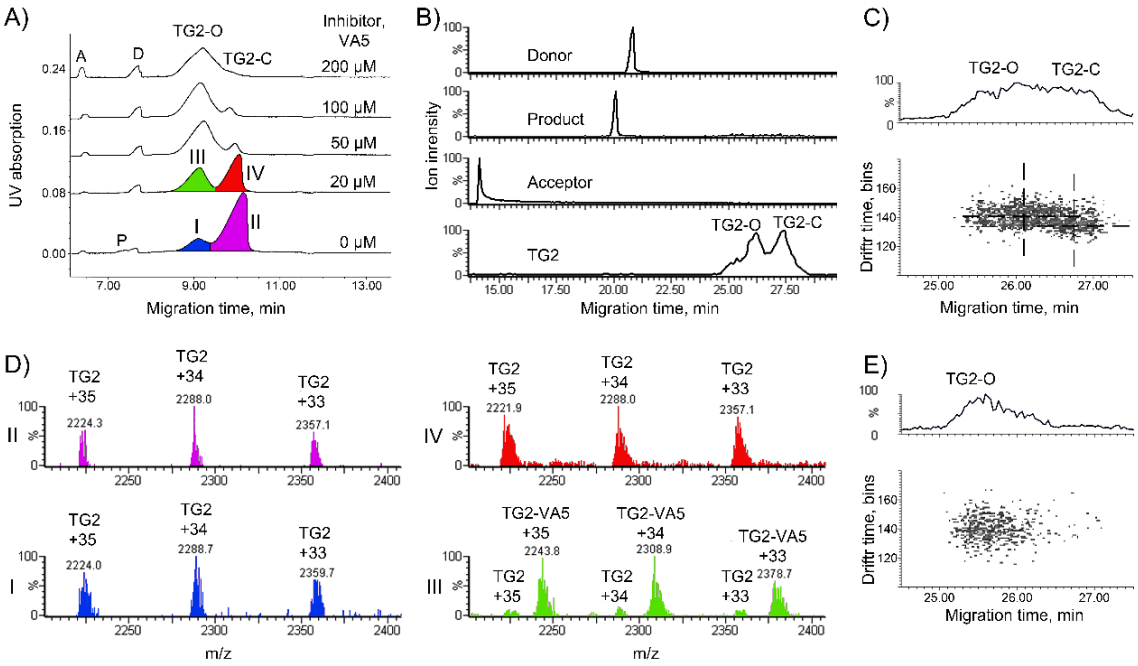

Figure 6.8. CE-UV-ESI-IM-MS experimental data. A) UV data, titration experiment. Incubation - 5 min with inhibitors, then 5 min with substrates. B) MS data at 0 µM inhibitor, acceptor peptide was extracted at m/z=392.28, donor peptide at m/z=854.55, product at m/z=1229.13, TG2 at m/z=2430 Da. C) IMS data at 0 µM inhibitor for TG2 ion m/z=2430. D) Combined spectra for peaks I, II, III and IV. E) IMS data at 200 µM VA5 for TG2-VA5 complex ion m/z=2454.

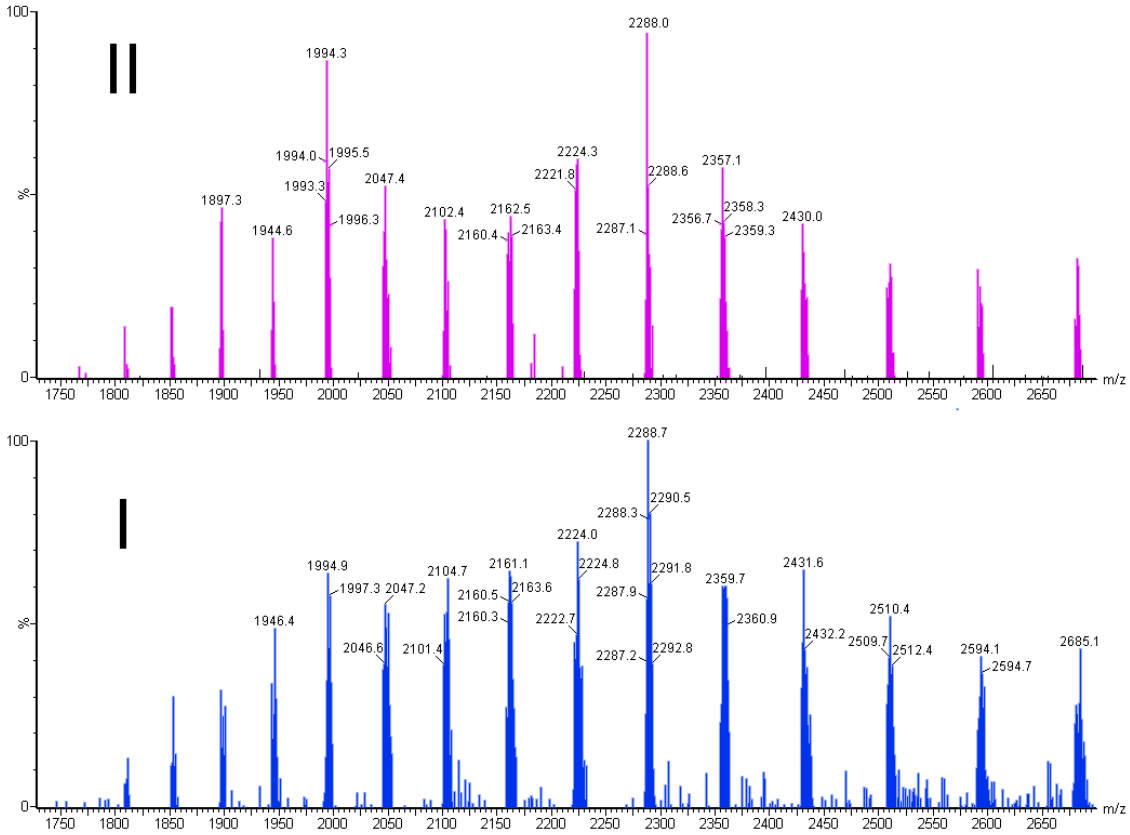

Figure 6.9. MS spectra of TG2 for peak I (TG2-O) and peak II (TG2-C). Please refer to **Figure 6.8A**.

As mentioned above, it is impossible to directly compare the sizes of two analytes (in this case two protein conformations) if their charges in solution are unknown. In the IM experiment it was possible to study equally charged ions for both conformations (m/z (TG2+32H$^+$)=2430 Da), giving an opportunity to compare their cross section areas. It can be seen from **Figure 6.8C** that poor ionization efficiency and the loss of ions in the ion mobility chamber prevented baseline separation of the two conformers on an extracted ion electropherogram, but it was observed that the latter portion of the merged peak had a smaller cross sectional area and drifted faster through the ion mobility chamber. After inhibition with 200 µM VA5, a novel irreversible TG2 inhibitor, the latter portion

disappeared (**Figure 6.8E**). A subsequent inhibitor titration experiment revealed that the TG2-inhibitor complex could be detected only in the TG2-O peak (**Figure 6.8A III**); its combined MS spectrum is presented in **Figure 6.8D III**. The TG2-C peak (**Figure 6.8A IV**) did not indicate the presence of any TG2-inhibitor complex on the MS spectrum (**Figure 6.8D IV**). These results were observed for all three irreversible inhibitors studied (NC9, VA5 and AA10), leading us to the important conclusion that after inhibition, *the TG2-inhibitor complex is stabilized exclusively in the open conformation* and TG2-O can be spatially separated from TG2-C by CE.

The titration experiment also revealed that increasing the concentration of inhibitors caused both a shift in the conformational distribution to the open form and a decrease in the enzymatic activity of TG2 (**Figure 6.10**). UV absorbance data were used to calculate the relative proportion of TG2-O (see Experimental). The ratio between TG2-O and TG2-C was calculated using UV data. Peaks for both conformers were analyzed with Beckman 32 Karate (Beckman, USA) software and the summed area of both peaks was assumed to be 100% of TG2. The proportion of TG2-O is the area of the open form peak relative to the total area of the protein.

$$TG2\ open\ portion = \frac{TG2\ open\ area}{total\ TG2\ area} \tag{6.1}$$

The proportion of TG2 open conformer was then treated as an inhibitor response in subsequent dose-response analysis, as shown in **Figure 6.10A,** for GraphPad Prism 6 software. It can be seen that after 5 min of incubation, VA5 was the only inhibitor able to completely convert TG2 to the open conformation, at the highest concentrations studied.

All inhibitors in this experiment showed different potency and apparent efficacy for conformational displacement, with VA5 being the most potent and efficacious (Table 6.1).

In the same inhibitor titration experiments, MS detection allowed the semi-quantitative monitoring of both added substrates (donor and acceptor) and the product generated by the TG2-mediated transamidation reaction (**Figure 6.8B**). Following 5 min incubation with inhibitor, substrates were added to the incubation solution and cross-linking was allowed to occur for an additional 5 min. The relative activity of TG2 was then calculated by MS detection of the product after this incubation. Peaks for the product (m/z=1229.13) were integrated using QuanLynx software (Waters, USA). In the absence of inhibitors the activity of TG2 was treated as 100%. The relative residual activity (RRA) was defined as the ratio of the amount of product observed at a given concentration of an inhibitor to the amount of product observed in the absence of inhibitor.

$$RRA = \frac{product\ response\ at\ tested\ concentration\ of\ inhibitor}{product\ response\ at\ 0\ \mu M\ of\ inhibitor} \qquad (6.2)$$

Obtained numbers were analyzed in GraphPad Prism 6 software These RRA data were then subjected to the same dose-response analysis as shown in **Figure 6.10B**. Significant inhibition was observed after 5 min incubation at the concentrations studied, allowing EC_{50} values to be determined for activity antagonism (Table 6.1). Inhibition constants were also determined independently by a continuous spectrophotometric assay method (see Experimental) and are also shown in Table 6.1. Comparison of EC_{50} and K_I values shows that the EC_{50} values are slightly higher than K_I values for VA5 and AA10, as expected for a competitive inhibitor. However, this was not the case for NC9, suggesting

a certain imprecision in the values determined from the fitting of the data of Figure 6.10B. This may be due to incomplete coverage of the sigmoidal curve, particularly at [I] < EC_{50}.

Comparison of the two plots of Figure 6.10 and the values shown in Table 6.1 reveals that there is no direct correlation between the potency of inhibitors to favour the open conformation of TG2 and to inhibit its transamidation activity. To account for this significant difference between the effect on conformation and the effect on activity, it is important to consider what conformational forms are present during the inhibition experiment. Previously the half-lives for TG2 opening and closing were determined to be 5.0 min and 13.9 min, respectively. This signifies that the interconversion between these conformers occurs over the time scale of our inhibition experiments (5 min incubation time in the presence of inhibitors). From Figure 6.8A we can infer that at the moment of addition of inhibitor, approximately 20% of TG2 was present in the catalytically competent open form and therefore available for inhibition. Upon the addition of 20 µM inhibitor, the three inhibitors studied showed dramatically different abilities to bind to TG2 and to promote a conformational change (**Figure 6.10A**). This may be due to the structural differences of inhibitors (**Figure 6.11**). VA5 may be able to bind stronger to the open state, thereby diminishing the proportion of the closed form, *without necessarily favoring the fully open and catalytically competent form*, from which irreversible covalent inhibition can occur. However, AA10 and NC9 have a weaker effect on the conformational equilibrium, perhaps due to their lesser ability to bind an intermediate conformational state.

A

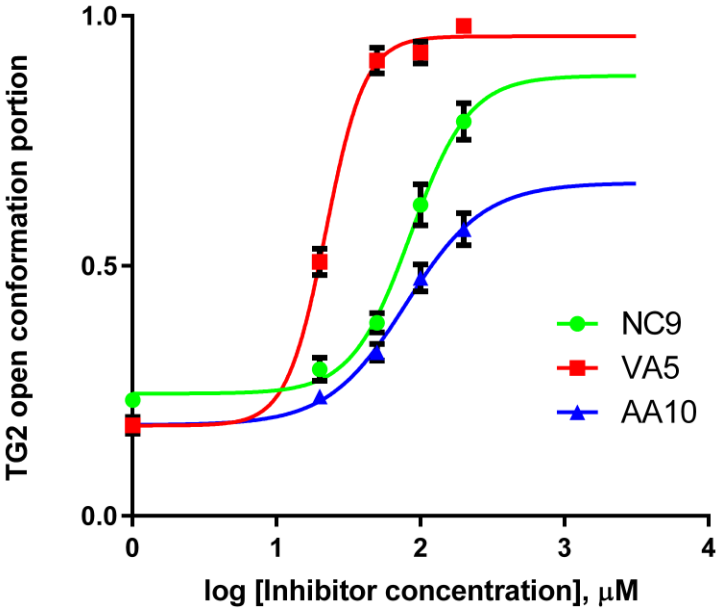
1.0
0.5
0.0
TG2 open conformation portion
0
1
2
3
4
log [Inhibitor concentration], μM
NC9
VA5
AA10

B

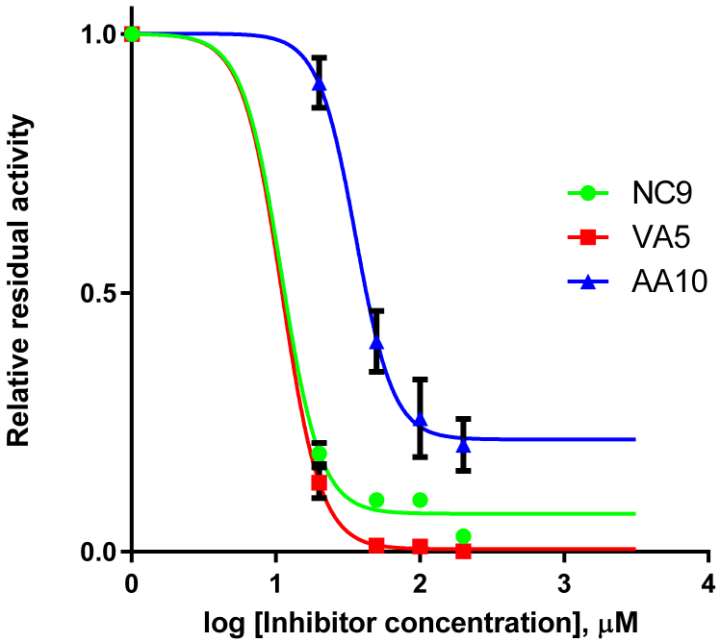
1.0
0.5
0.0
Relative residual activity
0
1
2
3
4
log [Inhibitor concentration], μM
NC9
VA5
AA10

Figure 6.10. Titration experiment, GraphPad Prism 6 four parameter fitment. Concentrations: inhibitors - 0 µM, 20 µM, 50 µM, 100 µM, 200 µM; TG2 - 30 µM, substrates - 100 µM each, $CaCl_2$ - 200 µM. Incubation - 5 min with inhibitors, then 5 min with substrates.

Table 6.1. Combined CE-UV-MS and independent kinetic data.

CE-UV-MS	NC9	VA5	AA10
EC_{50} for open proportion (µM) [a]	70.8	19.7	119
EC_{50} for Activity (µM) [a]	11.5	11.0	42.5
k_{inact} (min^{-1})	0.41 [b]	0.86 ± 0.11 [c]	1.29 ± 0.24 [c]
K_I (µM)	29 [b]	6.3 ± 1.6 [c]	7.9 ± 2.6 [c]
k_{inact}/K_I ($\mu M^{-1}\ min^{-1}$)	0.014 [b]	0.13 ± 0.04 [c]	0.16 ± 0.06 [c]

[a] Determined from the fitting of data shown in Figure 6.10 (see Experimental).

[b] Taken from reference [233]

[c] Measured herein (see Experimental).

NC9

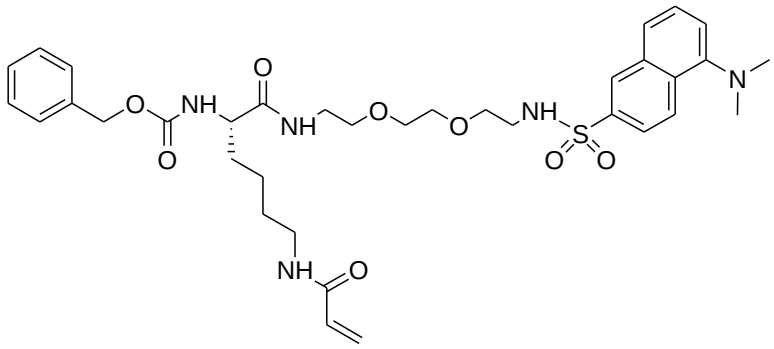

$C_{35}H_{47}N_5O_8S$
Exact Mass: 697.3145

VA5

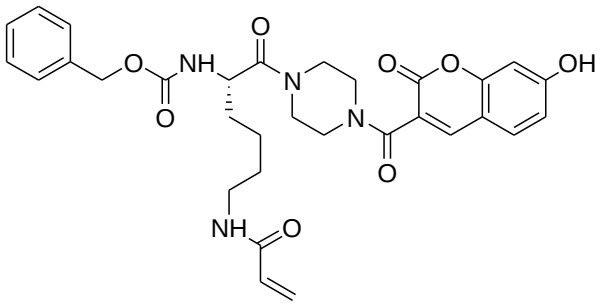

$C_{31}H_{34}N_4O_8$
Exact Mass: 590.2377

AA10

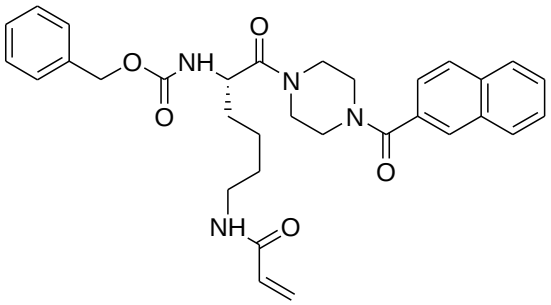

$C_{32}H_{36}N_4O_5$
Exact Mass: 556.2686

Figure 6.11. Structural and molecular formulas of tested inhibitors.

This study showed that it was possible to track both conformational changes of the enzyme and its enzymatic activity in a single experiment. The data suggested that enzymatic activity relies not only on the portion of "chemically-inhibited" enzyme but as well on the distribution of active and inactive conformations of the enzyme. It is an important link in the chain of understanding and characterizing inhibitors: while VA5 can be used to rapidly convert TG2 into an open inhibited form, AA10 is more suitable for slow inhibition without any significant interference into TG2 natural conformational switching.

6.5. Conclusion

In summary, we have shown for the first time that KCE can be used to separate and detect the slowly interconverting open and closed conformations of human TG2. The addition of effector ligands affects this conformational equilibrium, in a manner consistent with previous structural data[203, 205, 218, 219] and allowed the first direct measurement of the K_d value for calcium binding. These results provide important insight into the role of the slow conformational change in the functional regulation of TG2. The time scale of these conformational changes (seconds), compared to those associated with TG2 catalysis (milliseconds to microseconds) and those known for protein side-chain movement (nanoseconds to picoseconds) illustrate the complexity of the conformational landscape of TG2 and its relation to TG2 function.

We believe this study firmly establishes the broad utility of KCE as a powerful, complementary method for studying protein structure and function. While the slow

conformational changes studied herein give rise to separate peaks on the electropherogram, faster conformational changes of other proteins could also be detected through peak broadening. Furthermore, this method could be extended to include detection of the in situ catalytic activity of separate conformers and their susceptibility to inhibitor binding.

6.6. Acknowledgments

This work was funded by the Natural Sciences and Engineering Research Council of Canada, the University of Ottawa and the Canada Foundation for Innovation. G.G.M was a recipient of Ontario Graduate Scholarship.

Chapter 7: Substrate screening

7.1. Objectives

My objectives were to develop a method for automated substrate screening and enzyme profiling by CE-MS. I was in charge of all CE-MS experiments and experimental MS data analysis.

Antony St.-Jacques was responsible for aminotransferases production and coupled assays. Alexander Mungham assisted in MINISEP development. Matthew Eason was responsible for expression vectors. Dr. Roberto Chica provided supervision for the experimental part. Dr. Maxim Berezovski provided technical guidelines and supervision in performing all CE experiments.

7.2. Introduction

Enzymes are the most efficient catalysts known. They can accelerate chemical reactions by up to 26 orders of magnitude[235] and display exquisite regio-, chemo-, and stereoselectivities[236]. In addition, enzymes generate few byproducts and operate at moderate temperature in water, which makes them highly desirable as an environmentally friendly alternative to conventional chemical catalysts for many industrial applications. For example, enzymes are used for the production of food[237], pharmaceuticals[238], and fine and bulk chemicals[239] as well as biofuels[240], and this number is expected to grow as industry demand for sustainability continues to increase[241].

In order to be applicable as a biocatalyst for a desired reaction, an enzyme must efficiently perform the required chemistry under the necessary conditions and transform the correct molecules to produce the desired compound(s). This last property is called substrate specificity and is defined as the range of molecules that an enzyme can use as substrates. For many applications, enzymes that display the required substrate specificity may already exist in nature and need only to be identified and isolated[242, 243]. Alternatively, in the absence of a natural enzyme that possesses the required substrate specificity, rational protein design or directed evolution can be used to create enzymes that can transform the desired compounds[244]. In both instances, it is crucial to assess the substrate specificity of the candidate enzyme to determine if it is suitable for the intended application. Thus, substrate specificity profiling is often a prerequisite to the application of enzymes for biocatalysis as it can provide information on potential uses for a specific enzyme that would otherwise be unknown.

Enzyme substrate specificity is evaluated using enzymatic assays, which can be either continuous or discontinuous. Continuous or "real-time" assays monitor enzymatic reactions by detecting the disappearance of substrates or the appearance of products, as the reaction is occurring. The advantage of using a continuous assay is the ability to monitor an enzymatic reaction in real-time. However, this leads to the disadvantage of significantly limiting the number of reactions that can be simultaneously studied. Examples of continuous enzymatic assays include spectrophotometric[245, 246] and fluorometric[247, 248] methods. Discontinuous or "fixed-time" assays also monitor enzymatic reactions by quantifying the disappearance or appearance of substrates and

products, respectively. However, unlike continuous assays, this is done at specific times during the reaction by quenching it and analyzing the composition of the reaction mixture at that given time. Discontinuous assays have the advantage of allowing simultaneous analysis of multiple reactions but have the disadvantage of requiring postreaction steps, such as quenching and separation or extraction of reaction components. Examples of discontinuous assays include electrophoresis-[249, 250] and chromatography[251]-based methods.

Most enzyme activities cannot be monitored directly because they do not produce chromogenic or fluorescent products, complicating detection. Common strategies to overcome this limitation involve derivatization of products for easier detection[251] or use of coupled assays in which the product of interest is involved in a further enzymatic reaction to produce a compound that can then be easily detected[246]. These additional steps can introduce measurement errors, complicate data analysis, and increase the number of false positives and negatives. Recently, mass spectrometry (MS) has been developed as a detection method for enzyme assays[252-255] due to its advantages of high sensitivity, low reactant quantity requirement, direct detection of product without derivatization, and the ability to multiplex[256]. However, MS-based enzyme assays require multiple steps, such as premixing and quenching, which have the disadvantages of requiring microliter amounts of solutions to be handled and of potentially causing the degradation or chemical modification of analytes in the reaction mixture, respectively. Thus, there is still a need for the development of new MS-based methods for enzyme

analysis that require minute amounts of reagents (<1 μL) and no quenching, allowing automation and multiplexing.

In this work, we introduce an entirely automated enzyme assay based on capillary electrophoresis coupled to electrospray ionization mass spectrometry termed MINISEP-MS for multiple interfluent nanoinjections–incubation–separation–enzyme profiling using mass spectrometry. MINISEP-MS requires only nanoliters of reagent solutions and uses the separation capillary as a microreactor, allowing multiple substrates to be assayed simultaneously. The method can be used to rapidly profile the substrate specificity of any enzyme and to measure steady-state kinetics in an automated fashion. We used the MINISEP-MS assay to profile the substrate specificity of three aminotransferases (*E. coli* aspartate aminotransferase, *E. coli* branched-chain amino acid aminotransferase, and *Bacillus sp.* YM-1 d-amino acid aminotransferase) for 33 potential amino acid substrates and to measure steady-state kinetics. Using MINISEP-MS, we were able to recapitulate the known substrate specificities and to discover new amino acid substrates for these industrially relevant enzymes. Additionally, we were able to measure the apparent K_M and k_{cat} parameters for amino acid donor substrates of these aminotransferases.

7.3. Materials and methods

Chemical and reagents. All reagents used were of the highest available purity. Restriction enzymes and DNA-modifying enzymes were from New England Biolabs. Amino and keto acids were purchased from Sigma-Aldrich, and Ni-NTA agarose resin was

obtained from Promega. All aqueous solutions were prepared using deionized water purified with a Barnstead Nanopure Diamond system.

Plasmids. Codon-optimized E. coli branched-chain amino acid aminotransferase (BCAT) and Bacillus sp. D-amino acid aminotransferase (DAAT) genes obtained from Integrated DNA Technologies were subcloned into pET11-a (Novagen) via NdeI/BamHI. The plasmids were then transformed into Escherichia coli XL-1 Blue. The E. coli aspartate aminotransferase gene cloned into plasmid pET-45b (Novagen) was a generous gift from Michael D. Toney (University of California, Davis).

Protein expression and purification. Expression vectors containing the aminotransferase genes were transformed into E. coli BL21(DE3) cells. The transformed cells were grown in 500 mL Luria-Bertani medium containing 100 μg/mL ampicillin at 37°C until they reached an OD600 of 0.6. 1 mM of isopropyl β-D-1-thiogalactopyranoside was added to the flasks to induce protein expression followed by shaking for an additional 3 hours at 37°C. The cells were harvested by centrifugation and then lysed using an EmulsiFlex-B15 cell disruptor (Avestin). The proteins were then extracted and purified by immobilized metal affinity chromatography, according to manufacturer's protocol. Elution fractions containing the aminotransferases were desalted using Econo-Pac 10DG columns (Bio-Rad). Protein concentrations were quantified via a modified version of the Bradford assay, where the calibration curve is constructed as a plot of the ratio of the absorbance measurements at 590 nm and 450 nm versus concentration[257].

GDH assays. Activities are reported in units (U), which are μmols of product produced by the enzymatic reaction per minute. The aminotransferase catalyzed reaction was

coupled to L-glutamate dehydrogenase (GDH) from bovine liver (Sigma). For substrate specificity profiling, the reaction mixtures contained 10 mU of aminotransferase, 2-10 mM of amino acid donor substrate, 0.1-5 mM of α-keto acid acceptor substrate, 16 µM of pyridoxal phosphate (PLP), 1 U of GDH, and 0.5 mM of NAD+ in 100 mM potassium phosphate buffer (pH 8). For the DAAT reactions, NAD+ was replaced by NADH and 15 mM of ammonium chloride was also added. For steady-state kinetics, L-valine (donor substrate) concentrations varied between 0.03 and 7 mM, while the α-ketoglutarate concentration was 0.5 mM. PLP, GDH, and NAD+ quantities were the same as above. All kinetic measurements were performed in 96-well plates with a SpectraMax 384 Plus plate reader (Molecular Devices). Triplicates of 200 µL reactions in separate wells of 96-well plates (Greiner) were incubated for 60 minutes at 37 °C with continuous absorbance measurements at 340 nm, the absorption wavelength of NADH (ε = 6220 M-1 cm-1)[258]. Path lengths for each well were calculated ratiometrically using the difference in absorbance of potassium phosphate buffer at 900 nm and 998 nm. Separate reactions for each amino acid/enzyme pair, in which the aminotransferase was replaced by buffer, were used as blanks. Substrate specificity profiles were performed with two independent enzyme purification batches, while the steady-state kinetics were performed using BCAT from three independent purification batches.

MINISEP-MS. Amino acid substrate stock solutions were each prepared to a concentration of 100 mM. Glycine, L-lysine, L-serine, L-arginine, L-histidine, L-proline, L-aspartate, L-alanine, and L-tert-leucine were all dissolved in deionized water. L-leucine, L-isoleucine, L-threonine, L-methionine, L-glutamine, L-valine, L-tryptophan, β-alanine, L-2-

aminobutyrate, D-threonine, D-serine, D-leucine, D-alanine, D-lysine, D-valine, D-2-aminobutyrate, D-methionine, and D-phenylglycine were all dissolved in 10 mM ammonium bicarbonate buffer pH 8. L-tyrosine, L-asparagine, L-glutamate, L-phenylalanine, L-5-hydroxytryptophan, L-3,4-dihydroxyphenylalanine, and D-phenylalanine all had small amounts of 1 mM NaOH added until they were entirely dissolved, and then were diluted with deionized water. A 100 mM stock solution of α-ketoglutarate in 10 mM ammonium bicarbonate buffer pH 8 was used as the universal acceptor substrate for all enzymatic reactions. All solutions were filtered through 0.22-µm pore size membrane filters (Millipore, Nepean, ON, Canada).

CE-MS conditions were as follows unless otherwise stated. SYNAPT G2 High Definition Mass Spectrometer from Waters (Milford, MA, USA) was coupled on-line with PA800 plus Pharmaceutical Analysis CE system from Beckman Coulter (Brea, CA, USA) through the CE-ESI sprayer from Micromass (Manchester, UK). Experimental conditions were as follows: capillary voltage of 3.50 kV, sample cone voltage of 65 V, extractor cone voltage of 4.0 V and source temperature of 100°C. Cone gas, nano flow gas and purge gas flows were 5 L/h, 0.50 Bar and 3 L/h, respectively. Sheath-liquid flow composed of 80:20 isopropanol:water with 5 mM trimethylamine[259] was used to increase ionization efficiency of the sample and was introduced at 2.0 µL/min. Fused silica separation capillary from Polymicro (Phoenix, AZ, USA) was 150 cm long with inner diameter of 50 µm and outer diameter of 365 µm and was preconditioned before usage by rinsing with 100 mM NaOH for 25 minutes at 75 psi and deionized water for 25 minutes at 75 psi. Before each run the capillary was rinsed for 3 min at 75 psi with 100 mM NaOH, deionized

water and 30 mM ammonium bicarbonate buffer. 30 mM ammonium bicarbonate buffer was used as a separation buffer. The capillary temperature for all experiments was kept at 37°C.

Off-line incubation experiment. The sample mixtures for off-line incubation containing both substrates and enzyme had the following compositions: 1 mM of each amino acid, 5 mM α-ketoglutarate, 0.15 U/mL enzyme of interest, and 100 μM PLP in 10 mM ammonium bicarbonate buffer pH 8. Incubation was performed at 37°C for 10 min with shaking (500 rpm). The sample was injected by 2 psi for 12 sec following by a spacer injection of 30 mM ammonium bicarbonate buffer pH 8 by 10 psi for 60 sec and a control containing only amino acids by 2 psi for 12 sec. 30 kV potential with an anode at the injection end was applied for separation for 22 min following by 5 psi pressure for 30 min.

MINISEP conditions. Each subplug of buffer, substrates or enzymes was introduced in the capillary by pressure of 2 psi for 12 sec. A spacer of 30 mM ammonium bicarbonate buffer pH 8 was injected between plugs by pressure of 10 psi for 60 sec. Pressure-vacuum mixing was performed by applying pressure of 2 psi for 12 sec and then vacuum of 2 psi for 12 sec. The mixing was repeated two times. A 30 kV potential with an anode at the injection end was applied for separation for 3 min following by 5 psi pressure for 20 min. Concentrations of all compounds were the same as for the off-line experiment.

7.4. Results and discussion

MINISEP-MS assay development

In this work, we aimed to develop an assay for automated enzyme substrate specificity profiling that 1) could be applied to the study of any enzyme activity, 2) could

allow simultaneous analysis of many candidate substrates, and 3) would require very small quantities of reagents. To meet these requirements, capillary electrophoresis (CE) coupled to mass spectrometry (MS) was selected because of several of its features. Firstly, CE uses water-based buffers for separation instead of organic solvents, as is the case in HPLC, which makes it possible to use the separation capillary as a microreactor for an enzymatic reaction, decreasing the amounts of reagents required. Secondly, CE separation efficiency for small molecules is high, reaching more than 500,000 theoretical plates[260], improving selectivity and sensitivity. Thirdly, an important feature of CE is that it is easily interfaced with electrospray ionization (ESI) MS, providing a comprehensive detection method that eliminates the need for product derivatization or coupled assays, simplifying the experimental procedure. Lastly, ESI-MS provides the ability to multiplex, which allows multiple substrate candidates to be tested simultaneously, increasing the rapidity of analysis.

Herein, we developed an enzyme assay that we termed MINISEP-MS. This method, which employs a fused silica capillary that acts as both microreactor and separation column, consists of several steps (**Figure 7.1**). Initially, substrate mixtures (SM) and enzymes with cofactors (E1, E2, E3) are placed in separate vials (**Figure 7.1**, top). Then, subplugs of SM and incubation buffer (B) are loaded into the capillary (**Figure 7.1**, Step 1) to create the first plug. This first plug does not contain any enzyme and serves as an internal control. In the next step, subplugs of SM and enzymes with cofactors are injected into the capillary (**Figure 7.1**, Step 2) to create additional plugs that are spaced with a running buffer. After all components are injected individually, they are mixed together

inside the capillary by impulses of forward and backward pressure (vacuum) (**Figure 7.1**, Step 3). These short impulses facilitate the Poiseuille flow that stretches subplugs, and diffusion in lateral (transverse) direction completes mixing within the 50-µm diameter capillary. The mixing of multiple components by transverse diffusion of laminar flow profiles (TDLFP) inside a capillary was comprehensively described and modeled mathematically by Krylov's group[261-263].

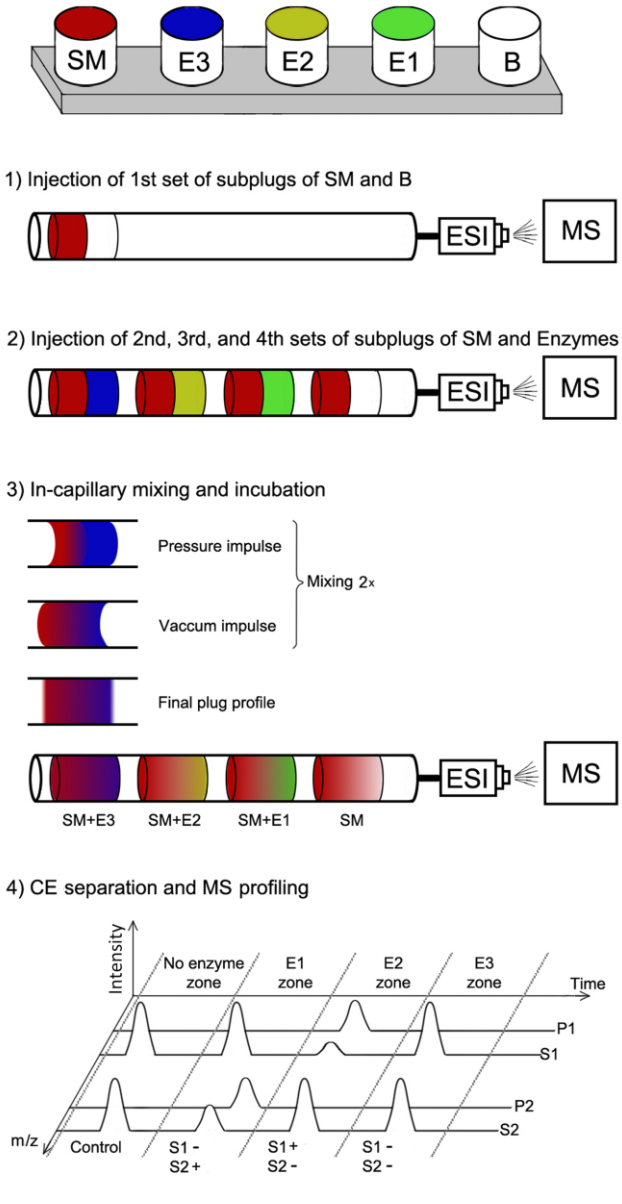

Figure 7.1. Schematic representation of MINISEP-MS assay. In this assay, capillary electrophoresis (CE) is interfaced with electrospray ionization (ESI) mass spectrometry (MS). 1) Subplugs of substrate mixture (SM) and buffer (B) are injected into the capillary. 2) Subplugs of SM and various enzymes (E) are injected, resulting in plugs separated by a running buffer. 3) In-capillary mixing is performed by applying two pressure and vacuum impulses. The mixing step is followed by incubation to allow enzymatic reactions to occur. 4) CE separation and MS detection of substrates (S) and products (P) is performed. Substrates and products co-migrate in zones corresponding to each plug. "+" and "-" symbols indicate the presence or absence of reactivity with the corresponding enzyme, respectively.

It should be noted that mixing of reaction components occurs only within the same plug; no interplug mixing of components was observed. This is due to the fact that the space between plugs is 20 times longer than the plug length. Next, the mixed components are incubated to allow the enzymatic reaction to occur. Following incubation, the components are separated by applying an electric potential along the capillary and are analyzed by MS (**Figure 7.1**, Step 4). Separation quenches the enzyme reactions due to the different mobilities of enzymes, substrates, and cofactors, which are pulled apart by an electrophoretic force. The separation is specifically adjusted to constrain the migration of analytes within the boundaries of a plug. To do so, the inter-plug distance (Δx) should meet the condition $\Delta x > \Delta v \times tsep$, where Δv is the velocity difference between the fastest and slowest components in adjacent plugs, and tsep is the CE separation time. Our protocol was optimized for use with a Beckman PA800 Plus CE instrument and a Waters Synapt G2 MS. It is important to note that each MINISEP-MS assay included a control plug containing all substrates and no enzyme (**Figure 7.1**, step 1), allowing inter-plug contamination to be monitored. If pressure-assisted injection was replaced with

electrokinetic injection, no efficient mixing was observed and no product of an enzymatic reaction was detected.

To demonstrate the power and usefulness of the MINISEP-MS method, we were interested in analyzing enzymes that synthesize valuable molecules that are difficult to detect by absorbance or fluorescence spectroscopies. For this purpose, we selected three aminotransferases: E. coli aspartate aminotransferase (AAT), E. coli branched-chain amino acid aminotransferase (BCAT) and Bacillus sp. YM-1 D-amino acid aminotransferase (DAAT). Aminotransferases, also called transaminases, are pyridoxal phosphate dependent enzymes involved in the biosynthesis of amino acids and amino acid derived metabolites[264]. They catalyze the transfer of the amino group from an amino acid donor to a keto acid acceptor, generating a new amino acid/keto acid pair (**Figure 7.2**). AAT, BCAT, and DAAT were selected because they all utilize the α-ketoglutarate acceptor substrate, while displaying very different amino acid donor specificities: AAT reacts preferentially with L-aspartate and L-aromatic amino acids[265], BCAT reacts preferentially with branched-chain aliphatic L-amino acids such as L-leucine, L-valine and L-isoleucine[266], while DAAT reacts with many D-amino acids having aliphatic, aromatic, charged, or polar side chains[267]. The markedly different substrate specificities of these enzymes provided us with a suitable test set to adequately validate the MINISEP-MS assay as a tool for enzyme substrate specificity profiling.

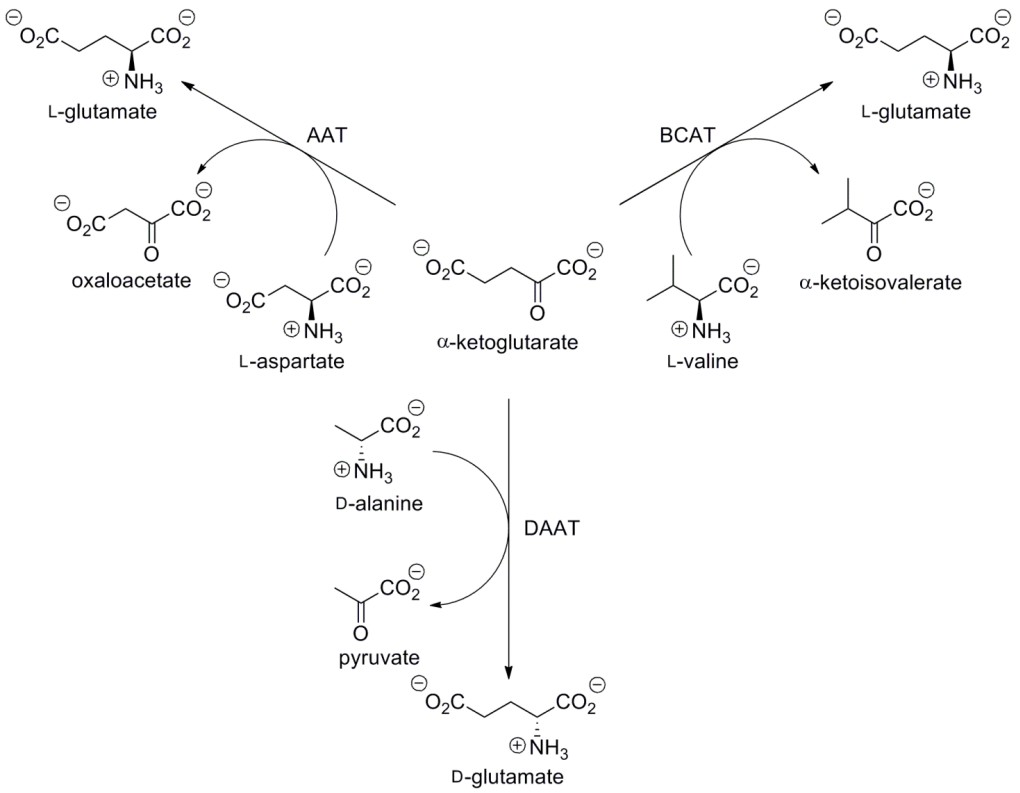

Figure 7.2. Reactions catalyzed by aminotransferases. Aspartate aminotransferase (AAT), branched-chain amino acid aminotransferase (BCAT) and D-amino acid aminotransferase (DAAT) catalyze transamination reactions where the amino group of a donor α-amino acid substrate is transferred to an α-keto acid acceptor substrate, yielding a new α-amino acid and α-keto acid pair. These reactions are dependent on the pyridoxal phosphate cofactor. AAT, BCAT, and DAAT all utilize the α-ketoglutarate acceptor substrate but react with different α-amino acid donors.

During development of the MINISEP-MS assay, experimental conditions of the enzymatic reactions, CE separation, and MS detection were optimized. For the enzymatic reactions, a temperature of 37°C and a pH of 8 were chosen to maximize enzyme activity. An incubation period of 20 minutes was chosen to minimize differences in reaction times for each enzyme since sets of subplugs of enzymes and substrate mixtures that are injected earlier would have slightly longer reaction times. Furthermore, this incubation time was selected because it resulted in insignificant differences in peak width arising

from longitudinal diffusion in a capillary. To increase CE separation efficiency, the ionic strength of the separation buffer was higher (30 mM) than that of the incubation buffer (10 mM) in order to compensate for Taylor dispersion and longitudinal diffusion during the incubation by the application of field-amplified sample stacking. Furthermore, the incubation buffer pH was equal to or higher than that of the separation buffer so as to create pH-mediated sample stacking. As MS detection requires volatile buffers to facilitate ionization of analytes, ammonium bicarbonate buffer was used for both incubation and separation, instead of the typical potassium phosphate[268] or tris-hydrochloride[269] buffers used for aminotransferase reactions. The CE separation time was optimized to eliminate inter-plug contamination and to satisfy the following requirement: tsep < 20 × plug length / Δv. For optimization of MS detection, parameters were adjusted to visually obtain the most stable spray when ions of interest were detectable and total ion current was stable, and electrospray ionization potentials were lowered to prevent parent ion fragmentation. Additionally, the 33 amino acid substrate candidates were divided into

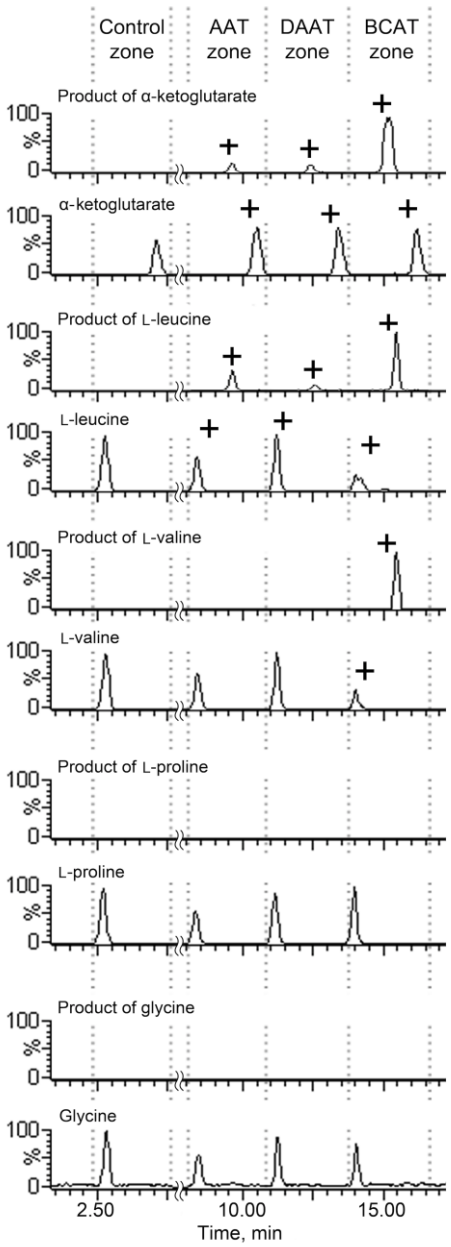

Figure 7.3. Example of experimental data obtained with the MINISEP-MS assay. Aspartate aminotransferase (AAT), branched-chain amino acid aminotransferase (BCAT) and D-amino acid aminotransferase (DAAT) were assayed with a substrate mixture consisting of the α-ketoglutarate acceptor, and potential donors L-leucine, L-valine, L-proline, and glycine. Buffer was also tested with the substrate mixture, as a control. Following incubation, electropherograms were extracted for $[M\text{-}1H^{+}]^{-1}$ ions with a detection window of 0.05 Da. A "+" sign indicates the presence of reactivity for a specific enzyme/amino acid combination. Experimental conditions are described in the text. The X-axes shows travel time to a MS detector after the CE voltage is turned off and pressure applied.

seven groups according to their molecular weights (**Table 7.1**). These groups were selected to prevent any potential overlap in m/z ratios for substrates and products. It is possible to decrease the number of groups by combining more amino acids together but this can lead to false positives and negatives due to overlaps in substrate or product m/z ratios. MS detection was performed in negative mode for a m/z range of 50-300, and electropherograms were extracted for [M-1H+]-1 ions with a detection window of 0.05 Da.

Table 7.1. Amino acid mixtures tested with the MINISEP-MS assay.

Mixture	Amino acid	Amino Acid, Monoisotopic molecular weights (g/mol)	Amino acid, $[M-1H^+]^{-1}$, m/z	Product, $[M-1H^+]^{-1}$, m/z
SM1	glycine	75.032	74.0242	72.9926
	L-proline	115.0633	114.0555	113.0239
	L-lysine	146.1055	145.0977	144.0661
	L-valine	117.079	116.0712	115.0396
	L-leucine	131.0946	130.0868	129.0552
SM2	L-alanine	89.0477	88.0399	87.0083
	L-serine	105.0426	104.0348	103.0032
	L-tyrosine	181.0739	180.0661	179.0345
	L-isoleucine	131.0946	130.0868	129.0552

SM3	L-glutamine	146.0691	145.0613	144.0297
	L-histidine	155.0695	154.0617	153.0301
	L-phenylalanine	165.079	164.0712	163.0396
	L-threonine	119.0582	118.0504	117.0188
	L-asparagine	132.0535	131.0457	130.0141
SM4	L-arginine	174.1117	173.1039	172.0723
	L-aspartate	133.0375	132.0297	130.9981
	L-tryptophan	204.0899	203.0821	202.0505
	β-alanine	89.0477	88.0399	87.0083
SM5	L-2-aminobutyrate	103.0633	102.0555	101.0239
	L-*tert*-leucine	131.0946	130.0868	129.0552
	L-methionine	149.0432	148.0354	147.0038
	L-3,4-dihydroxyphenylalanine	197.0688	196.061	195.0294
SM6	D-alanine	89.0477	88.0399	87.0083
	D-2-aminobutyrate	103.0633	102.0555	101.0239
	D-threonine	119.0582	118.0504	117.0188
	D-phenylglycine	151.0633	150.0555	149.0239
	D-phenylalanine	165.079	164.0712	163.0396
SM7	D-methionine	149.0432	148.0354	147.0038
	D-serine	105.0426	104.0348	103.0032
	D-valine	117.079	116.0712	115.0396

D-leucine	131.0946	130.0868	129.0552
D-lysine	146.1055	145.0977	144.0661
L-5-hydroxytryptophan	220.0848	219.077	218.0454

Figure 7.3 shows experimental data for a MINISEP-MS experiment for the reactions of AAT, BCAT, and DAAT with a substrate mixture containing the α-ketoglutarate acceptor and potential donors L-leucine, L-valine, L-proline, and glycine. Because aminotransferases catalyze transamination reactions, the products of these amino acids are α-keto acids, and vice-versa (**Figure 7.2**). Replacement of the amino group on the donor substrate with oxygen via transamination makes the overall charge of the product more negative compared to the substrate, resulting in a slower migration during CE separation. On the other hand, the product of α-ketoglutarate, L-glutamate, displayed the opposite behavior because its keto oxygen atom was replaced with an amino group, increasing its positive charge. These variations in migration time are readily observed in the electropherograms of **Figure 7.3**. However, to simplify analysis of experimental data, separation time was adjusted specifically to allow substrates and products from each plug to migrate together in non-overlapping zones.

As can be seen in **Figure 7.3**, BCAT showed enzymatic activity towards L-leucine and L-valine. AAT and DAAT also showed enzymatic activity for L-leucine but at a lower level, as illustrated by smaller peaks for α-ketoisocaproate, the product of L-leucine. L-proline and glycine did not react with any of the tested enzymes. Also, the first plug, containing buffer

instead of enzyme, did not yield any products (**Figure 7.3**, control zone), as expected. Since all of the enzymes were incubated under identical conditions, it was possible to perform a semi-quantitative comparison of their enzymatic activities which clearly showed that BCAT converted L-leucine with a much faster rate than AAT or DAAT, as expected, since L-leucine is a native substrate of BCAT[266] but not AAT[270] or DAAT. For confirmation, the same experiment was repeated with reversed enzyme injection order and gave identical results, as did off-line incubation experiments.

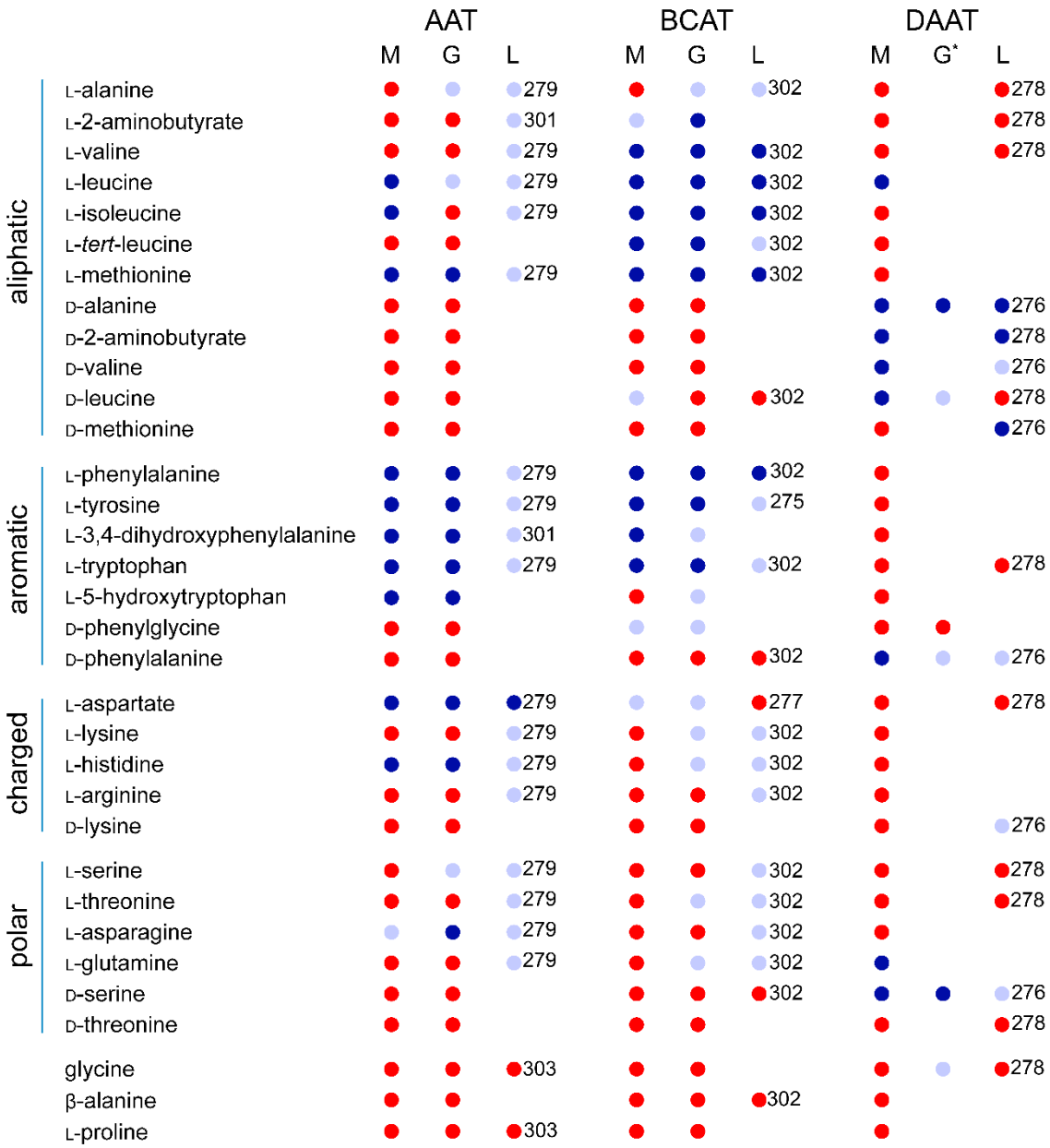

Figure 7.4. Substrate specificity profiles of aminotransferases. Amino acid substrate specificities of *E. coli* aspartate aminotransferase (AAT), *E. coli* branched-chain amino acid aminotransferase (BCAT), and *Bacillus sp.* YM-1 D-amino acid aminotransferase (DAAT) were evaluated using the MINISEP-MS (M) or L-glutamate dehydrogenase (G) assays. Results from the literature (L) are also included, for comparison[271-273]. Each circle, representing a specific enzyme/amino acid combination, is coloured based on its activity relative to the native substrate for each enzyme (L-aspartate, L-leucine, and D-alanine for AAT, BCAT, and DAAT, respectively), using the following scheme: red, light blue, and dark blue indicate no detectable activity, low activity (<10%) or high activity (>10%), respectively. *: These results were obtained for the corresponding α-keto acid, which

were tested with D-glutamate as the amino donor. Numbers correspond to literature references.

Substrate specificity profiles obtained by MINISEP-MS are reported in **Figure 7.4**. Each circle represents a specific enzyme/amino acid pair, and is colored based on its activity relative to that of the native amino acid substrate for that specific enzyme (L-aspartate, L-leucine, and D-alanine for AAT, BCAT, and DAAT, respectively), which is expected to give a high activity. In the case of MINISEP-MS, activities correspond to the MS intensities for the corresponding α-keto acid product. Since MS response cannot be directly correlated with concentrations as it depends on ionization efficiency of compounds and on the number of analytes, we sorted the MS intensities into three arbitrarily chosen bins to facilitate analysis: no activity, low activity (<10%), and high activity (>10%), represented by red, light blue, and dark blue circles, respectively. A 10% cut-off was selected because the kcat/KM values for two natural substrates of BCAT (L-leucine and L-isoleucine) are known to vary 5-fold[266]. While there is no correlation of MS response for different molecules, our binning system allowed us to qualitatively assess whether an amino acid was a poor or a good substrate for each aminotransferase.

The substrates that gave the highest activity for AAT and BCAT were for the most part as expected, since these enzymes are known to be highly active towards L-aromatic and L-aliphatic amino acids, respectively. However, the fact that L-amino acids such as L-leucine, and L-glutamine were good substrates of DAAT was unexpected, as high activity of DAAT towards L-amino acids has not been reported. To confirm these surprising results, off-line experiments were performed and provided identical results. Additionally, L-aliphatic

amino acids such as L-leucine, L-isoleucine, and L-methionine were found to be good substrates of AAT, even though literature results suggest that these are poor substrates[270]. This discrepancy with literature is likely due to differences in experimental conditions between studies. Nonetheless, using the MINISEP-MS assay, we were able to recapitulate the known substrate specificities of AAT, BCAT, and DAAT.

MINISEP-MS also allowed us to discover previously unknown substrates for each of these aminotransferases. To the best of our knowledge, the reactions catalyzed by AAT with L-5-hydroxytryptophan, BCAT with L-2-aminobutyrate, L-3,4-dihydroxyphenylalanine, D-leucine, and D-phenylglycine, as well as DAAT with L-leucine and L-glutamine, have not been previously reported. It is interesting that our MINISEP-MS results demonstrate that BCAT and DAAT, which are specific towards L- and D-amino acids, respectively, can react with amino acids of the opposite stereochemistry. This can be explained by the fact that these two enzymes share highly similar aminotransferase fold type IV backbone structures, with an RMSD of ~1.3 Å[274, 275], presumably allowing some activity towards these unnatural substrates in vitro. Additionally, our results contradict previous reports where BCAT was shown to be inactive towards L-aspartate[268] and DAAT towards D-leucine[269]. A potential cause for these discrepancies can be differences in the specific assay conditions used. For example, Rudman and Meister[268] assayed BCAT with 75 µM of L-aspartate, which resulted in no detectable activity, while we tested an L-aspartate concentration approximately 13-fold higher (1 mM). Although we were able to detect BCAT activity towards L-aspartate at this higher concentration, our results indicate that it is a poor substrate as its relative activity was less than 10% that of L-leucine, the natural

substrate of BCAT. Similarly, Jenkins and coworkers[269] performed all their DAAT assays with amino acid concentrations of 20 μM, 50-fold lower than the ones we used, which would make detection of poor substrates more difficult as enzyme activity decreases at lower substrate concentrations.

As indicated above, MINISEP-MS allowed us to discover that AAT can perform transamination of L-5-hydroxytryptophan, a precursor of the neurotransmitters serotonin and melatonin[276, 277]. L-5-hydroxytryptophanhas been shown to effectively treat fibromyalgia[278], obesity-related binge eating[279], Friedreich's ataxia[280], depression[281], and insomnia[281]. While this amino acid can be synthesized via catalytic hydrogenation using a palladium catalyst[282, 283], or extracted from plants[284], neither process is environmentally-benign. Biocatalytic production of L-5-hydroxytryptophan with AAT could potentially present an environmentally-friendly alternative to these current methods.

Validation of MINISEP-MS results

In order to validate the results obtained by the MINISEP-MS assay, we tested all of the enzyme/amino acid combinations with a coupled enzyme assay based on the use of L-glutamate dehydrogenase (GDH)[285]. GDH catalyzes the NAD+-dependent oxidative deamination of L-glutamate, yielding α-ketoglutarate and ammonia. GDH uses the L-glutamate synthesized by the various aminotransferases that will transfer the amino group from the amino acid donor substrate to the α-ketoglutarate acceptor. This reaction can be followed spectrophotometrically by measuring the increase in absorbance at 340 nm due to the formation of NADH by GDH. It should be noted that for DAAT, D-glutamate is the donor substrate and various α-keto acids are acceptors. Thus, generation of α-

ketoglutarate from D-glutamate by DAAT leads to a decrease in absorbance at 340 nm in the presence of GDH, NADH, and ammonia.

Specific activities measured with the GDH assay for each enzyme/amino acid pair are reported in Figure 4 as percentages of the activity observed with the native substrates for each aminotransferase, using the same color scheme as for MINISEP-MS. There is generally good agreement between the results obtained by the MINISEP-MS and the GDH assays. All enzyme/substrate combinations that displayed >10% relative activity (**Figure 7.4**, dark blue circles) with the GDH assay also displayed activity when assayed with MINISEP-MS. Additionally, the GDH assay allowed us to identify 11 low activity (<10%) donor substrates for these aminotransferases that the MINISEP-MS assay did not detect. Detection of these low activity substrates by the GDH assay and not by MINISEP-MS likely resulted from the fact that the multiplexing nature of MINISEP-MS creates inherent competitive inhibition as many substrates are tested in the same reaction, leading to false negatives when low activity substrates are tested in the presence of higher activity substrates. Therefore, it is expected that the GDH assay will allow the identification of an increased number of low activity substrates that will not be detected by the MINISEP-MS method. In addition, differences in reaction conditions between the two assays including buffer used as well as substrate concentrations, likely accentuated these differences as it is known that enzymes have different dissociation constants for substrates in different buffers at the same pH and temperature[286], and substrate concentration affects enzyme reaction rate. MINISEP-MS also allowed the detection of two substrates that were not identified with the GDH assay. These are L-isoleucine for AAT and D-leucine for BCAT.

Although the GDH assay allowed the identification of an increased number of poor substrates for these enzymes, it presents many disadvantages compared to the MINISEP-MS method. First, as the GDH assay is a coupled assay, conditions have to be optimized to ensure that the coupling enzyme reaction does not become the rate-limiting step, under all conditions tested. Another disadvantage of coupled enzyme assays such as the GDH assay is that they are specific to a single product that is generated by the enzyme reaction of interest. For example, the GDH assay requires production of L-glutamate or α-ketoglutarate by the aminotransferases, as GDH is specific to these compounds. This disadvantage is illustrated by the fact that we could not test any amino acid other than D-glutamate for DAAT, and instead, had to vary the α-keto acid acceptor to infer activity towards its corresponding D-amino acid. In order to analyze the reactivity of DAAT towards other amino acid donors, other coupling enzymes specific to the α-keto acid product of these amino acids would be required. However, the MINISEP-MS is not limited to reactions that produce specific amino or keto acids.

Another advantage of MINISEP-MS over the GDH assay is the small quantity requirement: MINISEP requires nanoliters of reagent solutions while the GDH assay, even when performed in microplates, requires microliters of reagent solutions, a quantity several orders of magnitude higher. Finally, the MINISEP-MS assay is not hindered by substrates or products that contribute a high background absorbance at the wavelength used for the coupled assay. This is the case with L-3,4-dihydroxyphenylalanine, which absorbs significantly at 340 nm. For our GDH assays with L-3,4-dihydroxyphenylalanine,

the concentration was lowered from 7.5 mM to 2 mM in order to decrease the background signal sufficiently to be able to measure activities accurately.

Kinetic experiments

In addition to automated enzyme substrate specificity profiling, MINISEP-MS can also be used to measure steady-state kinetics. For this application, however, only one amino acid donor substrate is studied at a time to eliminate competitive enzyme inhibition, which can occur in the presence of other amino acids. Using MINISEP-MS, we determined apparent kcat and KM parameters of AAT, BCAT, and DAAT for their natural donor substrates L-aspartate, L-valine, and D-glutamate, respectively. The experimental setup was identical to that described in **Figure 7.1**, except that different substrate concentrations were injected as subplugs instead of different enzymes. Incubation times were 800, 640, 480, 320 and 160 seconds for the 1st, 2nd, 3rd, 4th and 5th plugs, respectively. The 1st plug did not contain enzyme and served as a control.

For any aminotransferase reaction, the stoichiometry of product:substrate is 1:1, since an amino acid/keto acid pair is converted to another amino acid/keto acid pair by the transamination reaction (**Figure 7.2**). Thus, it is possible to quantify the α-keto acid product using the amino acid product and vice versa, since the stoichiometry between these molecules is also 1:1. In order to do this, we used L-glutamate, the amino acid resulting from transamination with α-ketoglutarate, as a standard for quantification of oxaloacetate and α-ketovalerate, the α-keto acid products of AAT and BCAT, respectively. For DAAT, the standard was α-ketoglutarate, as this is the α-keto acid product that results

from transamination of D-glutamate with pyruvate. The calibration curve for L-glutamate is presented on **Figure 7.5**. Quantification of products was done with the Waters QuanLynx software (Milford, MA, USA).Enzyme activity was calculated using the following equation:

$$v=P/t \quad (7.1)$$

where v is the product formation rate, P is the concentration of product, and t is the incubation time.

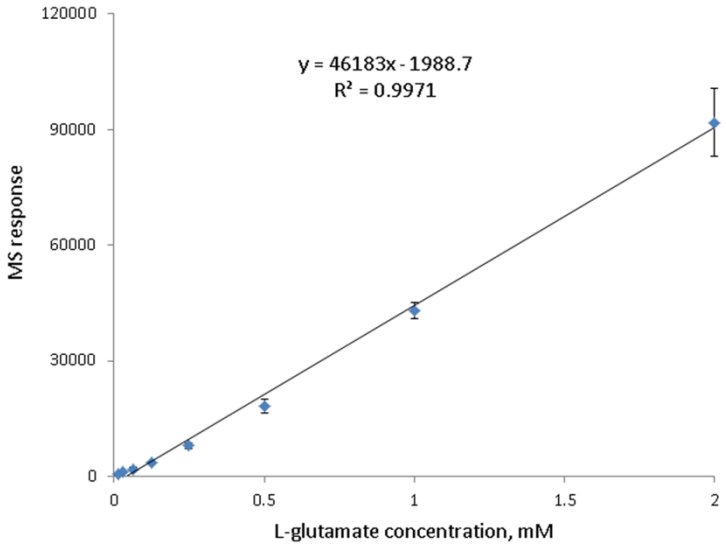

Figure 7.5. Calibration curve for L-glutamate standards. Mass spectrometry (MS) response corresponds to the area under the curve of the L-glutamate peaks. Experimental conditions were identical to the MINISEP-MS experiments, as described under Methods.

As can be seen on **Figure 7.6A**, a linear correlation between the accumulation of the α-keto acid product and incubation time was observed. This is expected since the longer the enzyme reaction is allowed to run, the more product is made. Using the calibration curves that were prepared, we were able to obtain initial rates, which were plotted against substrate concentrations in Michaelis–Menten graphs (**Figure 7.6B** and **Figure**

7.7). Non-linear regression analysis of the data fit to the Michaelis–Menten equation was performed and yielded apparent KM and kcat values (**Table 7.2**). To validate these results, we performed enzyme kinetics of the aminotransferases using the GDH assay. The apparent KM and kcatvalues that we obtained with the GDH assay were in agreement with those obtained with MINISEP-MS (**Table 7.2**). Although the kinetic parameters obtained with the MINISEP-MS and GDH assays were similar to each other, they differed significantly from those reported in the literature (**Table 7.2**). These discrepancies can be attributed to significant differences in experimental conditions such as buffer, temperature (25°Cvs 37°C), and enzyme purity.

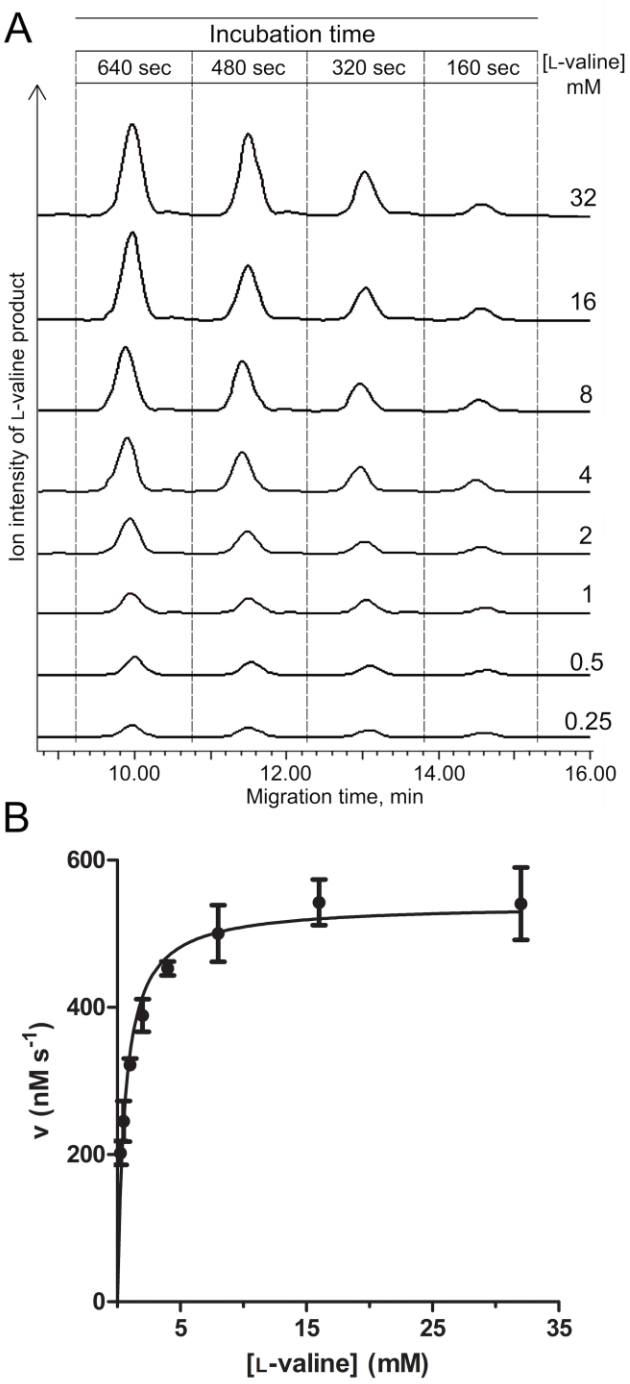

Figure 7.6. Steady-state kinetics of the transamination reaction of L-valine and α-ketoglutarate catalyzed by branched-chain amino acid aminotransferase (BCAT). A) Electropherograms for four incubation times (640 sec, 480 sec, 320 sec, and 160 sec) are shown for 0.25-32 mM of L-valine. Electropherograms were extracted for $[M\text{-}1H^+]^{-1}$ ions with a detection window of 0.05 Da. Plugs consisted of 1 mM α-ketoglutarate, 0.25-32 mM L-valine, 100 µM pyridoxal phosphate, and 50 mU of BCAT. B) Michaelis-Menten plot obtained by fitting the MINISEP-MS data.

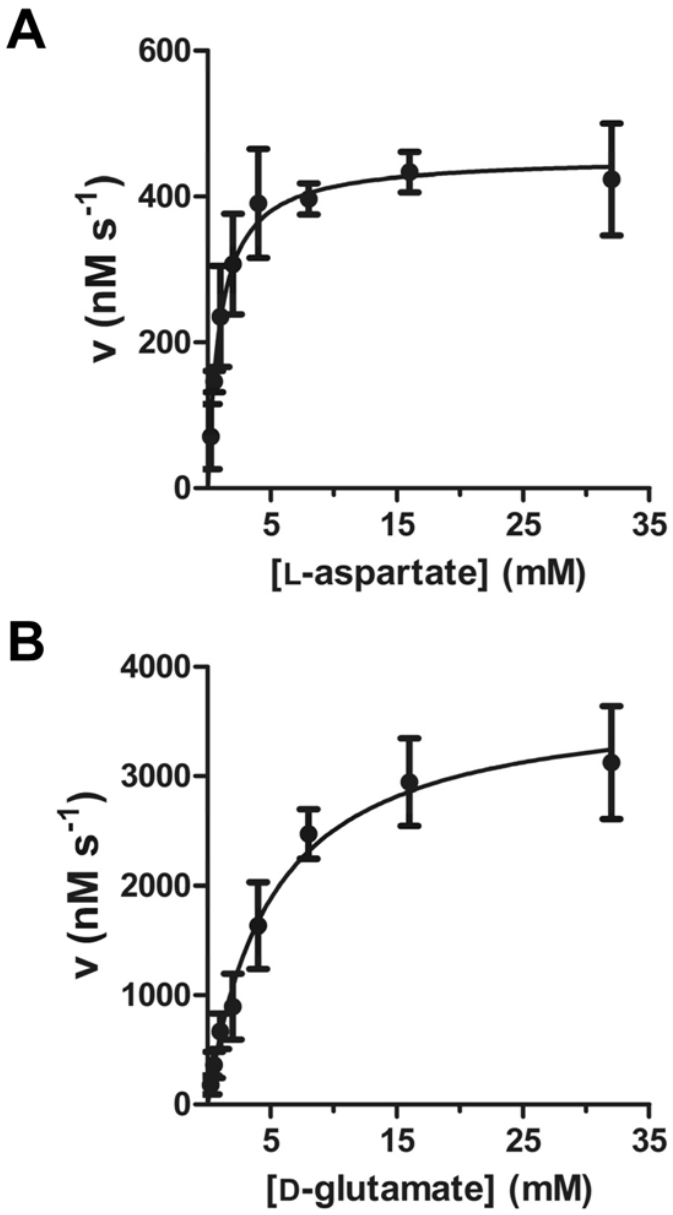

Figure 7.7. Steady-state kinetics of aminotransferase reactions using the MINISEP-MS assay. Michaelis-Menten plots of initial rates versus L-aspartate concentrations for the aspartate aminotransferase reaction (A), or D-glutamate concentrations for the D-amino acid aminotransferase reaction (B). All experiments were performed in triplicate.

Table 7.2. Apparent kinetic parameters of aminotransferases

	AAT[a]		BCAT[b]		DAAT[c]	
	L-aspartate		L-valine		D-glutamate	
Assay	K_M (mM)	k_{cat} (s^{-1})	K_M (mM)	k_{cat} (s^{-1})	K_M (mM)	k_{cat} (s^{-1})
MINISEP-MS[d]	1.1 ± 0.7	1.4 ± 0.2	0.5 ± 0.1	1.5 ± 0.6	5.0 ± 0.5	24 ± 5
GDH[e]	0.32 ± 0.03	2.0 ± 0.2	0.44 ± 0.06	1.14 ± 0.05	4.2 ± 0.8	40 ± 10
Literature	1.9[f]	259[f]	2.7[g]	19[g]	N.A.[h]	N.A.[h]

[a] *E. coli* aspartate aminotransferase

[b] *E. coli* branched-chain amino acid aminotransferase

[c] *Bacillus sp.* YM-1 D-amino acid aminotransferase

[d] Multiple Interfluent Nanoinjections-Incubation-Separation-Enzyme Profiling using Mass Spectrometry assay, 1 mM α-ketoglutarate (for AAT and BCAT) or pyruvate (for DAAT), 100-500 mU of aminotransferase, 100 µM pyridoxal phosphate, 10 mM ammonium bicarbonate buffer, pH 8.0, 37°C. Experiments were performed in triplicate using aminotransferases from three independent protein preparations. Our data.

[e] Glutamate dehydrogenase coupled assay, 0.2 mM (for AAT) or 0.5 mM (for BCAT) α-ketoglutarate , 5 mM pyruvate (for DAAT), 10 mU of aminotransferase, 16 µM pyridoxal phosphate, 0.5 mM NAD^+ (for AAT and BCAT) or NADH (for DAAT), 1 U GDH, 100 mM potassium phosphate buffer, pH 8.0, 37°C. For DAAT, 15 mM of ammonium chloride was also added. Experiments were performed in triplicate using aminotransferases from three independent protein preparations. Our data.

[f] Malate dehydrogenase coupled assay, 0.25-10 × K_M α-ketoglutarate, 5 nM aminotransferase, 20 µM pyridoxal phosphate, 150 µM NADH, 8 U/mL malate dehydrogenase, 100 mM KCl, 200 mM TAPS-KOH buffer, pH 8.4, 25°C. From Deu *et al*.[287]

[g] Glutamate dehydrogenase coupled assay, 10 mM α-ketoglutarate, 2.5 mM NAD^+, 0.2 mg/mL GDH, 0.1 M KCl, 50 mM HEPES-NaOH buffer, pH 8, 25°C. From Kagamiyama *et al*.[266]

[h] Not available.

Comparison with other MS-based enzyme assays

The MINISEP-MS method addresses many issues arising from other MS-based enzyme assays[288, 289]. For example, in typical direct infusion ESI-MS techniques, difficulties in discriminating false positives can arise due to the presence of buffer impurities with masses overlapping those of the analytes. While these problems can be solved using separation-based techniques such as HPLC or CE, conventional HPLC-MS and CE-MS methods are not designed to perform on-line multiplex studies and require a premixing step or reaction quenching before the analysis[256]. In contrast, the MINISEP-MS method does not require premixing, which is advantageous because it allows automation and reduces reagent consumption, an important benefit when studying expensive or difficult to synthesize enzymes and substrates. Furthermore, reaction quenching with solvents or harsh chemicals, which can lead to analyte degradation or chemical modification, is not required in MINISEP-MS since quenching results from application of an electric potential to create an electroosmotic flow. Because of these advantages, the MINISEP-MS assay has the potential of becoming a useful tool for researchers studying enzymes and their use in specific biocatalytic applications.

7.5. Conclusion

In this study, we developed an automated online assay for rapid enzyme substrate specificity profiling and for steady-state kinetics. The MINISEP-MS assay presents many advantages over traditional enzyme assays, such as comprehensive detection of products, low reagent quantity requirement, and the ability to multiplex. Using the MINISEP-MS

assay, we were able to discover new amino acid substrates for three aminotransferases, whose biocatalytic potential is increasingly recognized[290-292]. In the future, substrate specificity profiling with MINISEP-MS could be used to rapidly gain functional information for enzymes found by genome database mining[243], accelerating the discovery of useful biocatalysts for the development of novel industrial processes.

7.6. Acknowledgments

This work was funded by the Natural Sciences and Engineering Research Council of Canada, the University of Ottawa and the Canada Foundation for Innovation. G.G.M and A.D.S. were recipients of Ontario Graduate Scholarships.

Conclusion

At the very end of my thesis I would like to summarize what was done in this five year period and provide a personal opinion about possible future directions where my research can go.

There were two goals for me to achieve: 1) develop methods of bioanalysis by CE-MS to study interactions between biomolecules and their conformational changes as well as enzymatic activity screening and virus quality control and 2) use these methods to produce scientific data which can broaden our understanding of this world. Both goals were successfully achieved.

All necessary methodological information is available in my published articles, as well as instrumental method and excel analysis files. There were some home-made improvements done by me to commercially available CE instruments which increased their usability to study biomolecules, e.g. sample volume limit was decreased from 50 µl to 5 µl, cooling of the whole capillary from UV to MS detector was introduced. I hope that these improvements and methodological approaches will serve well to future generations of scientists not only in the Berezovski lab but also throughout the world.

These methods allowed to reveal new facts about biomolecules and added novel data to the bank of the mankind knowledge. For the best of my knowledge, kinetic parameters for TG2 and thrombin G-quadruplex folding were reported for the first time, as well as for non-covalent complex formation between β-cyclodextrin and flurbiprofen, ibuprofen and salicylic acid. I developed a homogeneous method to determine k_{on}, k_{off} and K_d of fast and weak noncovalent interactions between multiple unlabeled ligands (small molecule drugs)

and an oligosaccharide (α- or β-cyclodextrin) simultaneously in one capillary microreactor. The availability of commercial instrumentation for capillary electrophoresis and high-performance liquid chromatography with all of the previously listed detection approaches suggests that ECEEM can be practiced immediately. ECEEM can potentially facilitate kinetic studies of noncovalent interactions with complicated stoichiometry (different from 1:1) involving proteins and nucleic acids. It has been shown for the first time that KCE can be used to separate and detect the slowly interconverting open and closed conformations of human TG2. The addition of effector ligands affects this conformational equilibrium, in a manner consistent with previous structural data[203, 205, 218, 219] and allowed the first direct measurement of the K_d value for calcium binding. These results provide important insight into the role of the slow conformational change in the functional regulation of TG2. The time scale of these conformational changes (seconds), compared to those associated with TG2 catalysis (milliseconds to microseconds) and those known for protein side-chain movement (nanoseconds to picoseconds) illustrate the complexity of the conformational landscape of TG2 and its relation to TG2 function.

Sixteen new substrates were discovered for three aminotransferases (AAT, BCAT, and DAAT). qCE showed a feasibility to analyse both the count of intact viral particles and sample nucleic acid contamination.

Next logical step would be to apply my methods for more complex systems. It has been shown that the formation of G-quadruplexes in untranslated regions (UTR) of mRNA can regulate its translation into proteins[293]. It may be important to know not only the

thermodynamics of G-quadruplex formation in UTR but the kinetics of folding as well to fully understand how translation regulation works.

TG2 is not the only member of transglutaminase family. Other enzymes include factor XIII (fibrin-stabilizing factor), keratinocyte transglutaminase and others. Factor XIII is an enzyme of the blood coagulation system. It plays a crucial role in blood clot stabilization[294]. So far it is not known if factor XIII can undergo identical conformational changes as TG2. CE-MS technique can be used to investigate this topic.

Another possible application for CE-MS which was not mentioned in my thesis is direct aptamer selection to small molecules. Aptamer selection to small molecules (SM) is challenging due to the fact that the aptamer-SM complex doesn't show any significantly different physicochemical properties relating to free aptamers to perform chromatography based tag-free separation[295]. I performed proof of concepts experiments and showed that aptamer-SM complex formation causes stabilization of a distinct structure of aptamer and can be separated in CE from an unfolded aptamer fraction. Using CE-MS can possibly allow a direct sequencing of aptamers, eliminating an amplification step.

There can be many more potential applications of CE-MS technique for bioanalysis such as analysis of microsomes in human blood, microRNA profiling of blood and cell samples with direct identification of microRNA without amplification steps required and

List of publications

12) Shahrokh M. Ghobadloo, Anna K. Balcerzak, Ana Gargaun, Darija Muharemagic, **Gleb G. Mironov**, Chantelle J. Capicciotti, Jennie G. Briard, Robert N. Ben, and Maxim V. Berezovski (2014) "Carbohydrate-Based Ice Recrystallization Inhibitors Increase Infectivity and Thermostability of Viral Vectors". Scientific Reports, 4.

11) **Gleb G. Mironov**; Okhonin, V.; Khan, N.; Clouthier, C.M.; Berezovski, M.V. (2014) "Conformational Dynamics of DNA G-Quadruplex in Solution Studied by Kinetic Capillary Electrophoresis Coupled On-line with Mass Spectrometry". ChemistryOpen, 3(2), 1-8. Cover page.

10) **Gleb G. Mironov**, Antony D. St.-Jacques, Alexander Mungham, Matthew G. Eason, Roberto A. Chica and Maxim V. Berezovski (2013) "Bioanalysis for Biocatalysis: Multiplexed Capillary Electrophoresis–Mass Spectrometry Assay for Aminotransferase Substrate Discovery and Specificity Profiling". Journal of the American Chemical Society, 135 (37), 13728-13736. DOI: 10.1021/ja407486z

9) Rance Nault; Hiba Abdul-Fattah; **Gleb G Mironov**; Maxim V Berezovski; Thomas W Moon. (2013) "Assessment of Energetic Costs of AhR Activation by β-Naphthoflavone in Rainbow Trout (Oncorhynchus mykiss) Hepatocytes Using Metabolic Flux Analysis". Toxicology and Applied Pharmacology, 271(1), 86-94.

8) Christopher M. Clouthier, **Gleb G. Mironov**, Victor Okhonin, Maxim V. Berezovski and Jeffrey W. Keillor (2012) “Real-time monitoring of protein conformational dynamics in solution using kinetic capillary electrophoresis”. Angewandte Chemie International Edition, 51(50), 12464-12468.

7) Afnan Azizi, **Gleb G. Mironov**, Darija Muharemagic, Mohamed Wehbe, John C. Bell and Maxim V. Berezovski (2012) “Viral Quantitative Capillary Electrophoresis for Counting and Quality Control of RNA Virus”. Analytical Chemistry, 84 (21), 9585–9591.

6) Maxim V. Berezovski and **Gleb G. Mironov** (2012) “Utility of Kinetic Capillary Electrophoresis – Mass Spectrometry to study protein dynamics and affinity interactions”. Expert Review of Proteomics 9(5), 477–479.

5) **Gleb G. Mironov**; Logie, J.; Okhonin, V.; Renaud, J.B.; Mayer, P.M.; Berezovski, M.V. (2012) “Comparative Study of Three Methods for Affinity Measurements: Capillary Electrophoresis Coupled with UV Detection and Mass Spectrometry, and Direct Infusion Mass Spectrometry”. Journal of The American Society for Mass Spectrometry, 23 (7), 1232-1240.

4) Amanda N.Comeau, Justin B. Renaud, **Gleb G. Mironov**, Maxim V. Berezovski, Paul M. Mayer. “Investigating the relationship between the gas-phase conformations and

dissociation energetics of gas-phase specific, peptide–saccharide complexes." International Journal of Mass Spectrometry, 2012, 316-318, pp 31-39.

3) J. B. Renaud, E. Martineau, **Gleb G. Mironov**, M. Berezovski and P.M. Mayer, "The collaborative role of molecular conformation and energetics in the binding of gas-phase non-covalent polymer/amine complexes". Physical Chemistry Chemical Physics, 2012, 14, 165-172.

2) **Gleb G. Mironov**, Alexey V. Chechik, Rachel Ozer, John C. Bell, and Maxim V. Berezovski, "Viral Quantitative Capillary Electrophoresis for Counting Intact Viruses". Anal. Chem., 2011, 83 (13), pp 5431–5435.

1) **Gleb G. Mironov**, Victor Okhonin, Serge I. Gorelsky, and Maxim V. Berezovski, "Revealing Equilibrium and Rate Constants of Weak and Fast Noncovalent Interactions". Anal. Chem., 2011, 83 (6), pp 2364–2370.

References

1 Tallarek, U.; Rapp, E.; Seidel-Morgenstern, A.; Van As, H. *J Phys Chem B.* **2002**, *106*, 12709-12721.

2 Kemp, G. *Biotechnol.Appl.Biochem.* **1998**, *27*, 9-17.

3 Kraly, J.; Fazal, M.; Schoenherr, R.; Bonn, R.; Harwood, M.; Turner, E.; Jones, M.; Dovichi, N. *Anal.Chem.* **2006**, *78*, 4097-4110.

4 Haselberg, R.; de Jong, G. J.; Somsen, G. W. *J.Chromatogr.A.* **2007**, *1159*, 81-109.

5 Nollet, J. A. **1749**,

6 Vonnegut, B.; Neubauer, R. L. *J.Colloid Sci.* **1952**, *7*, 616-622.

7 Nawab, M. A.; Mason, S. G. *J.Colloid Sci.* **1958**, *13*, 179-187.

8 Drozin, V. G. *J.Colloid Sci.* **1955**, *10*, 158-164.

9 Vanberkel, G. J.; Zhou, F. M. *Anal.Chem.* **1995**, *67*, 2916-2923.

10 Gomez, A.; Tang, K. Q. *Phys.Fluids.* **1994**, *6*, 404-414.

11 Kebarle, P.; Tang, L. *Anal.Chem.* **1993**, *65*, A972-A986.

12 Bruins, A. P. *Journal of Chromatography A.* **1998**, *794*, 345-357.

13 Fenn, J. B. *J.Am.Soc.Mass Spectrom.* **1993**, *4*, 524-535.

14 Schmelzeisen-Redeker, G.; Bütfering, L.; Röllgen, F. W. *International Journal of Mass Spectrometry and Ion Processes.* **1989**, *90*, 139-150.

15 Chernushevich, I.; Loboda, A.; Thomson, B. *J.Mass Spectrom.* **2001**, *36*, 849-865.

16 STEPHENS, W. *Physical Review.* **1946**, *69*, 691-691.

17 Mamyrin, B. A. *International Journal of Mass Spectrometry.* **2001**, *206*, 251-266.

18 Pringle, S. D.; Giles, K.; Wildgoose, J. L.; Williams, J. P.; Slade, S. E.; Thalassinos, K.; Bateman, R. H.; Bowers, M. T.; Scrivens, J. H. *International Journal of Mass Spectrometry.* **2007**, *261*, 1-12.

19 Pringle, S. D.; Giles, K.; Wildgoose, J. L.; Williams, J. P.; Slade, S. E.; Thalassinos, K.; Bateman, R. H.; Bowers, M. T.; Scrivens, J. H. *International Journal of Mass Spectrometry.* **2007**, *261*, 1-12.

20 Schmitt-Kopplin, P.; Frommberger, M. *Electrophoresis.* **2003**, *24*, 3837-3867.

21 Haselberg, R.; de Jong, G. J.; Somsen, G. W. *J.Chromatogr.A.* **2007**, *1159*, 81-109.

22 Muller-Dethlefs, K.; Hobza, P. *Chem.Rev.* **2000**, *100*, 143-167.

23 Mironov, G. G.; Okhonin, V.; Gorelsky, S. I.; Berezovski, M. V. *Anal.Chem.* **2011**, *83*, 2364-2370.

24 Foote, J.; Eisen, H. N. *Proc.Natl.Acad.Sci.U.S.A.* **2000**, *97*, 10679-10681.

25 Neuhauser, W.; Haltrich, D.; Kulbe, K. D.; Nidetzky, B. *Biochemistry (N.Y.).* **1998**, *37*, 1116-1123.

26 Benkovic, S.; Hammes-Schiffer, S. *Science.* **2003**, *301*, 1196-1202.

27 Russell, S. J.; Peng, K. *Trends Pharmacol.Sci.* **2007**, *28*, 326-333.

28 Dock, G. *Am.J.Med.Sci.* **1904**, *127*, 563-592.

29 Southam, C. M. *Trans.N.Y.Acad.Sci.* **1960**, *22*, 657-73.

30 Asada, T. *Cancer.* **1974**, *34*, 1907-1928.

31 Martuza, R. L.; Malick, A.; Markert, J. M.; Ruffner, K. L.; Coen, D. M. *Science.* **1991**, *252*, 854-856.

32 Russell, S. J.; Peng, K.; Bell, J. C. *Nat.Biotechnol.* **2012**, *30*, 658-670.

33 Liu, T.; Galanis, E.; Kirn, D. *Nature Clinical Practice Oncology.* **2007**, *4*, 101-117.

34 Russell, S. J. *Semin.Cancer Biol.* **1994**, *5*, 437-443.

35 Miest, T. S.; Cattaneo, R. *Nature Reviews Microbiology.* **2014**, *12*, 23-34.

36 Breitbach, C. J.; Burke, J.; Jonker, D.; Stephenson, J.; Haas, A. R.; Chow, L. Q. M.; Nieva, J.; Hwang, T.; Moon, A.; Patt, R.; Pelusio, A.; Le Boeuf, F.; Burns, J.; Evgin, L.; De Silva, N.; Cvancic, S.; Robertson, T.; Je, J.; Lee, Y.; Parato, K.; Diallo, J.; Fenster, A.; Daneshmand, M.; Bell, J. C.; Kirn, D. H. *Nature.* **2011**, *477*, 99-U102.

37 Mironov, G. G.; Chechik, A. V.; Ozer, R.; Bell, J. C.; Berezovski, M. V. *Anal.Chem.* **2011**, *83*, 5431-5435.

38 Parato, K. A.; Senger, D.; Forsyth, P. A. J.; Bell, J. C. *Nature Reviews Cancer.* **2005**, *5*, 965-976.

39 Aghi, M.; Martuza, R. L. *Oncogene.* **2005**, *24*, 7802-7816.

40 Liu, T.; Hwang, T.; Park, B.; Bell, J.; Kirn, D. H. *Molecular Therapy.* **2008**, *16*, 1637-1642.

41 Park, B.; Hwang, T.; Liu, T.; Sze, D. Y.; Kim, J.; Kwon, H.; Oh, S. Y.; Han, S.; Yoon, J.; Hong, S.; Moon, A.; Speth, K.; Park, C.; Ahn, Y.; Daneshmand, M.; Rhee, B. G.; Pinedo, H. M.; Bell, J. C.; Kirn, D. H. *Lancet Oncology.* **2008**, *9*, 533-542.

42 Niwa, O.; Decleve, A.; Lieberma.M; Kaplan, H. S. *J.Virol.* **1973**, *12*, 68-73.

43 Saliba, G. S.; Franklin, S. L.; Jackson, G. G. *J.Clin.Invest.* **1968**, *47*, 1303-&.

44 Payne, A. F.; Binduga-Gajewska, I.; Kauffman, E. B.; Kramer, L. D. *J.Virol.Methods.* **2006**, *134*, 183-189.

45 Garrison, A. R.; Alakbarova, S.; Kulesh, D. A.; Shezmukhamedova, D.; Khodjaev, S.; Endy, T. P.; Paragas, J. *Am.J.Trop.Med.Hyg.* **2007**, *77*, 514-520.

46 Hara, S.; Terauchi, K.; Koike, I. *Appl.Environ.Microbiol.* **1991**, *57*, 2731-2734.

47 Marie, D.; Brussaard, C. P. D.; Thyrhaug, R.; Bratbak, G.; Vaulot, D. *Appl.Environ.Microbiol.* **1999**, *65*, 45-52.

48 Driskell, J. D.; Kwarta, K. M.; Lipert, R. J.; Porter, M. D.; Neill, J. D.; Ridpath, J. F. *Anal.Chem.* **2005**, *77*, 6147-6154.

49 Crowther, J.; Reckziegel, P. O.; Prado, J. A. *Vaccine.* **1995**, *13*, 1064-1075.

50 McQuaig, S. M.; Scott, T. M.; Lukasik, J. O.; Paul, J. H.; Harwood, V. J. *Appl.Environ.Microbiol.* **2009**, *75*, 3379-3388.

51 World Health Organization: Geneva, Switzerland. **2004**,

52 Jacobs, B. L.; Langland, J. O.; Kibler, K. V.; Denzier, K. L.; White, S. D.; Holechek, S. A.; Wong, S.; Huynh, T.; Baskin, C. R. *Antiviral Res.* **2009**, *84*, 1-13.

53 Auzanneau, I.; Barreau, C.; Salome, L. *Comptes Rendus De L Academie Des Sciences Serie Iii-Sciences De La Vie-Life Sciences.* **1993**, *316*, 459-462.

54 Hilz, H.; Wiegers, U.; Adamietz, P. *European Journal of Biochemistry.* **1975**, *56*, 103-108.

55 Filipe, V.; Hawe, A.; Jiskoot, W. *Pharm.Res.* **2010**, *27*, 796-810.

56 Du, S.; Kendall, K.; Morris, S.; Sweet, C. *Journal of Chemical Technology and Biotechnology.* **2010**, *85*, 1223-1228.

57 Azizi, A.; Mironov, G. G.; Muharemagic, D.; Wehbe, M.; Bell, J. C.; Berezovski, M. V. *Anal.Chem.* **2012**, *84*, 9585-9591.

58 Kamimura, K.; Suda, T.; Zhang, G.; Liu, D. *Pharm.Med.* **2011**, *25*, 293-306.

59 Galanis, E. *Nature.* **2011**, *477*, 40-41.

60 Breitbach, C. J.; Burke, J.; Jonker, D.; Stephenson, J.; Haas, A. R.; Chow, L. Q. M.; Nieva, J.; Hwang, T. -.; Moon, A.; Patt, R.; Pelusio, A.; Le Boeuf, F.; Burns, J.; Evgin, L.; De Silva, N.; Cvancic, S.; Robertson, T.; Je, J. -.; Lee, Y. -.; Parato, K.; Diallo, J. -.; Fenster, A.; Daneshmand, M.; Bell, J. C.; Kirn, D. H. *Nature.* **2011**, *477*, 99-104.

61 Nguyen, T. L.; Tumilasci, V. F.; Singhroy, D.; Arguello, M.; Hiscott, J. *Cell.Microbiol.* **2009**, *11*, 889-897.

62 Mahy, B. W. J.; Kangro, H. O. *Virology Methods Manual.* **1996**,

63 Dulbecco, R.; Freeman, G. *Virology.* **1959**, *8*, 396-397.

64 Mocé-Llivina, L.; Lucena, F.; Jofre, J. *Appl.Environ.Microbiol.* **2004**, *70*, 2801-2805.

65 Lambeth, C. R.; White, L. J.; Johnston, R. E.; De Silva, A. M. *J.Clin.Microbiol.* **2005**, *43*, 3267-3272.

66 Borsheim, K. Y.; Bratbak, G.; Heldal, M. *Appl.Environ.Microbiol.* **1990**, *56*, 352-356.

67 Schwille, P.; Bieschke, J.; Oehlenschläger, F. *Biophys.Chem.* **1997**, *66*, 211-228.

68 Bustin, S. A. *J.Mol.Endocrinol.* **2002**, *29*, 23-39.

69 Van Aken, W. G.; Dobbelaer, R.; Fuchs, F.; Grachev, V.; Homma, A.; Kurata, T.; Löwer, J.; Minor, P.; Reigel, F.; Vyas, G. N. *WHO Tech.Rep.Ser.* **2007**, *941*

70 Mironov, G. G.; Chechik, A. V.; Ozer, R.; Bell, J. C.; Berezovski, M. V. *Anal.Chem.* **2011**, *83*, 5431-5435.

71 Cary, Z. D.; Willingham, M. C.; Lyles, D. S. *J.Virol.* **2011**, *85*, 5708-5717.

72 Barber, G. N. *Oncogene.* **2005**, *24*, 7710-7719.

73 Lyles, D. S.; Rupprecht, C. E. *Fields Virology.* **2007**, , 1363-1408.

74 Russell, S. J. *Encyclopedia of Life Sciences.* **2001**,

75 Cureton, D. K.; Massol, R. H.; Whelan, S. P. J.; Kirchhausen, T. *PLoS Pathog.* **2010**, *6*

76 Balachandran, S.; Barber, G. N. *IUBMB Life.* **2000**, *50*, 135-138.

77 Russell, S. J. *Cancer Gene Ther.* **2002**, *9*, 961-966.

78 Stojdl, D. F.; Lichty, B. D.; TenOever, B. R.; Paterson, J. M.; Power, A. T.; Knowles, S.; Marius, R.; Reynard, J.; Poliquin, L.; Atkins, H.; Brown, E. G.; Durbin, R. K.; Durbin, J. E.; Hiscott, J.; Bell, J. C. *Cancer Cell.* **2003**, *4*, 263-275.

79 Anonymous **2008**, *Recombinant DNA Advisory Committee, U. S. Department of Health and Human Services: Rockville, MD*

80 Anonymous **2008**, *Recombinant DNA Advisory Committee, U. S. Department of Health and Human Services: Rockville, MD*

81 Clarke, D. K.; Cooper, D.; Egan, M. A.; Hendry, R. M.; Parks, C. L.; Udem, S. A. *Springer Semin.Immunopathol.* **2006**, *28*, 239-253.

82 Cobleigh, M. A.; Buonocore, L.; Uprichard, S. L.; Rose, J. K.; Robek, M. D. *J.Virol.* **2010**, *84*, 7513-7522.

83 Majid, A. M.; Ezelle, H.; Shah, S.; Barber, G. N. *J.Virol.* **2006**, *80*, 6993-7008.

84 Diallo, J. -.; Vähä-Koskela, M.; Le Boeuf, F.; Bell, J. *Methods in Molecular Biology.* **2012**, *797*, 127-140.

85 Sotelo-Silveira, J. R.; Calliari, A.; Cárdenas, M.; Koenig, E.; Sotelo, J. R. *J.Neurobiol.* **2004**, *60*, 187-196.

86 Cosa, G.; Focsaneanu, K. -.; McLean, J. R. N.; McNamee, J. P.; Scaiano, J. C. *Photochem.Photobiol.* **2001**, *73*, 585-599.

87 Krylova, S. M.; Rozenberg, D.; Coulton, J. W.; Krylov, S. N. *Analyst.* **2004**, *129*, 1234-1237.

88 Kremser, L.; Okun, V. M.; Nicodemou, A.; Blaas, D.; Kenndler, E. *Anal.Chem.* **2004**, *76*, 882-887.

89 Johnson, I.; Spence, M. T. Z. *The Molecular Probes Handbook.* **2010**,

90 Ebeling, W.; Hennrich, N.; Klockow, M.; Metz, H.; Orth, H. D.; Lang, H. *European Journal of Biochemistry.* **1974**, *47*, 91-97.

91 Rainsford, E. W.; Harouaka, D.; Wertz, G. W. *J.Virol.* **2010**, *84*, 1741-1751.

92 Thompson, K. A. S.; Yin, J. *Virology Journal.* **2010**, *7*

93 Fields, B. N.; Knipe, D. M.; Howley, P. M. *Fields Virology.* **1996**,

94 Wu, Y.; Zhou, J.; Zhang, X.; Zheng, X.; Jiang, X.; Shi, L.; Yin, W.; Wang, J. *Proteome Science.* **2009**, *7*, 38.

95 Mironov, G. G.; Okhonin, V.; Gorelsky, S. I.; Berezovski, M. V. *Anal.Chem.* **2011**, *83*, 2364-2370.

96 Govern, C. C.; Paczosa, M. K.; Chakraborty, A. K.; Huseby, E. S. *Proc.Natl.Acad.Sci.U.S.A.* **2010**, *107*, 8724-8729.

97 Berezhkovskiy, L. M. *Expert Opinion on Drug Metabolism and Toxicology.* **2008**, *4*, 1479-1498.

98 Goyal, M.; Rizzo, M.; Schumacher, F.; Wong, C. F. *J.Med.Chem.* **2009**, *52*, 5582-5585.

99 Berezhkovskiy, L. M. *J.Pharm.Sci.* **2006**, *95*, 834-848.

100 Brissette, P.; Ballou, D. P.; Massey, V. *Anal.Biochem.* **1989**, *181*, 234-238.

101 Wild, M. K.; Huang, M. -.; Schulze-Horsel, U.; Van der Merwe, P. A.; Vestweber, D. *J.Biol.Chem.* **2001**, *276*, 31602-31612.

102 Fabian, H.; Naumann, D. *Methods.* **2004**, *34*, 28-40.

103 Piliarik, M.; Vaisocherová, H.; Homola, J. *Methods Mol.Biol.* **2009**, *503*, 65-88.

104 Bujalowski, W. *Chem.Rev.* **2006**, *106*, 556-606.

105 Drabovich, A.; Berezovski, M.; Krylov, S. N. *J.Am.Chem.Soc.* **2005**, *127*, 11224-11225.

106 Petrov, A.; Okhonin, V.; Berezovski, M.; Krylov, S. N. *J.Am.Chem.Soc.* **2005**, *127*, 17104-17110.

107 Drabovich, A. P.; Berezovski, M.; Okhonin, V.; Krylov, S. N. *Anal.Chem.* **2006**, *78*, 3171-3178.

108 Drabovich, A. P.; Berezovski, M. V.; Musheev, M. U.; Krylov, S. N. *Anal.Chem.* **2009**, *81*, 490-494.

109 Berezovski, M.; Krylov, S. N. *J.Am.Chem.Soc.* **2002**, *124*, 13674-13675.

110 Okhonin, V.; Petrov, A. P.; Berezovski, M.; Krylov, S. N. *Anal.Chem.* **2006**, *78*, 4803-4810.

111 Cole, J. D. *Quart.Appl.Math.* **1951**, *9*, 225-236.

112 Hopf, E. *Comm.Pure Appl.Math.* **1950**, *3*, 201-230.

113 Li, D. X.; Han, M. J.; Balakrishnan, P.; Yan, Y. D.; Oh, D. H.; Joe, J. H.; Seo, Y.; Kim, J. O.; Park, S. M.; Yong, C. S.; Choi, H. -. *Arch.Pharm.Res.* **2010**, *33*, 95-101.

114 Loftsson, T.; Vogensen, S. B.; Brewster, M. E.; Konráosdóttir, F. *J.Pharm.Sci.* **2007**, *96*, 2532-2546.

115 Loftsson, T.; Magnúsdóttir, A.; Másson, M.; Sigurjónsdóttir, J. F. *J.Pharm.Sci.* **2002**, *91*, 2307-2316.

116 Musheev, M. U.; Javaherian, S.; Okhonin, V.; Krylov, S. N. *Anal.Chem.* **2008**, *80*, 6752-6757.

117 Chu, Y. -.; Avila, L. Z.; Biebuyck, H. A.; Whitesides, G. M. *J.Med.Chem.* **1992**, *35*, 2915-2917.

118 Avila, L. Z.; Chu, Y. -.; Blossey, E. C.; Whitesides, G. M. *J.Med.Chem.* **1993**, *36*, 126-133.

119 Chu, Y. -.; Avila, L. Z.; Gao, J.; Whitesides, G. M. *Acc.Chem.Res.* **1995**, *28*, 461-468.

120 Mironov, G. G.; Logie, J.; Okhonin, V.; Renaud, J. B.; Mayer, P. M.; Berezovski, M. V. *J.Am.Soc.Mass Spectrom.* **2012**, *23*, 1232-1240.

121 Petrov, A.; Okhonin, V.; Berezovski, M.; Krylov, S. N. *J.Am.Chem.Soc.* **2005**, *127*, 17104-17110.

122 Sloat, A. L.; Roper, M. G.; Lin, X.; Ferrance, J. P.; Landers, J. P.; Colyer, C. L. *Electrophoresis.* **2008**, *29*, 3446-3455.

123 Yang, P.; Mao, Y.; Lee, A. W. -.; Kennedy, R. T. *Electrophoresis.* **2009**, *30*, 457-464.

124 Berezovski, M.; Krylov, S. N. *Anal.Chem.* **2005**, *77*, 1526-1529.

125 Berezovski, M.; Drabovich, A.; Krylova, S. M.; Musheev, M.; Okhonin, V.; Petrov, A.; Krylov, S. N. *J.Am.Chem.Soc.* **2005**, *127*, 3165-3171.

126 Drabovich, A. P.; Berezovski, M. V.; Musheev, M. U.; Krylov, S. N. *Anal.Chem.* **2009**, *81*, 490-494.

127 Chu, Y. -.; Avila, L. Z.; Biebuyck, H. A.; Whitesides, G. M. *J.Med.Chem.* **1992**, *35*, 2915-2917.

128 Avila, L. Z.; Chu, Y. -.; Blossey, E. C.; Whitesides, G. M. *J.Med.Chem.* **1993**, *36*, 126-133.

129 Chu, Y. -.; Avila, L. Z.; Gao, J.; Whitesides, G. M. *Acc.Chem.Res.* **1995**, *28*, 461-468.

130 Olivares, J. A.; Nguyen, N. T.; Yonker, C. R.; Smith, R. D. *Anal.Chem.* **1987**, *59*, 1230-1232.

131 Chen, Z.; Weber, S. G. *TrAC - Trends in Analytical Chemistry.* **2008**, *27*, 738-748.

132 Ušelová-Velcláková, K.; Zusková, I.; Gaš, B. *Electrophoresis.* **2007**, *28*, 2145-2152.

133 Lomsadze, K.; Salgado, A.; Calvo, E.; Antonio López, J.; Chankvetadze, B. *Electrophoresis.* **2011**, *32*, 1156-1163.

134 Vega, E. D.; Lomsadze, K.; Chankvetadze, L.; Salgado, A.; Scriba, G. K. E.; Calvo, E.; López, J. A.; Crego, A. L.; Marina, M. L.; Chankvetadze, B. *Electrophoresis.* **2011**, *32*, 2640-2647.

135 Arancibia, J. A.; Escandar, G. M. *Analyst.* **1999**, *124*, 1833-1838.

136 Nair, T. M.; Myszka, D. G.; Davis, D. R. *Nucleic Acids Res.* **2000**, *28*, 1935-1940.

137 Olson, S. T.; Srinivasan, K. R.; Bjork, I.; Shore, J. D. *J.Biol.Chem.* **1981**, *256*, 11073-11079.

138 Schiel, J. E.; Hage, D. S. *Journal of Separation Science.* **2009**, *32*, 1507-1522.

139 Mironov, G. G.; Okhonin, V.; Gorelsky, S. I.; Berezovski, M. V. *Anal.Chem.* **2011**, *83*, 2364-2370.

140 Li, D. X.; Han, M. J.; Balakrishnan, P.; Yan, Y. D.; Oh, D. H.; Joe, J. H.; Seo, Y.; Kim, J. O.; Park, S. M.; Yong, C. S.; Choi, H. -. *Arch.Pharm.Res.* **2010**, *33*, 95-101.

141 Loftsson, T.; Vogensen, S. B.; Brewster, M. E.; Konráosdóttir, F. *J.Pharm.Sci.* **2007**, *96*, 2532-2546.

142 Drabovich, A.; Berezovski, M.; Krylov, S. N. *J.Am.Chem.Soc.* **2005**, *127*, 11224-11225.

143 López-Nicolás, J. M.; García-Carmona, F. *Food Chem.* **2008**, *109*, 868-875.

144 López-Nicolás, J. M.; Núñez-Delicado, E.; Pérez-López, A. J.; Barrachina, A. C.; Cuadra-Crespo, P. *Journal of Chromatography A.* **2006**, *1135*, 158-165.

145 Frycák, P.; Schug, K. A. *Anal.Chem.* **2008**, *80*, 1385-1393.

146 Ueda, H.; Perrin, J. H. *J.Pharm.Biomed.Anal.* **1986**, *4*, 107-110.

147 Cirri, M.; Maestrelli, F.; Orlandini, S.; Furlanetto, S.; Pinzauti, S.; Mura, P. *J.Pharm.Biomed.Anal.* **2005**, *37*, 995-1002.

148 Manzoori, J. L.; Amjadi, M. *Spectrochimica Acta - Part A: Molecular and Biomolecular Spectroscopy.* **2003**, *59*, 909-916.

149 Mura, P.; Bettinetti, G. P.; Manderioli, A.; Faucci, M. T.; Bramanti, G.; Sorrenti, M. *Int.J.Pharm.* **1998**, *166*, 189-203.

150 Orienti, I.; Zecchi, V.; Bertasi, V.; Fini, A. *Arch.Pharm.(Weinheim).* **1991**, *324*, 943-947.

151 Wei, W.; Ju, H. X. *Chromatographia.* **2003**, *58*, 449-453.

152 Vilarnovo, B. P.; Penin, S. S.; Perez-Marcos, M. B.; Vila-Jato, J. L.; Torres-Labandeira, J. J. *Proceedings of the 9th International Symposium on Cyclodextrins.* **1999**, , 441-444.

153 Guo, M.; Song, F.; Liu, Z.; Liu, S. *Journal of Mass Spectrometry.* **2004**, *39*, 594-599.

154 Mayer, P. M.; Martineau, E. *Physical Chemistry Chemical Physics.* **2011**, *13*, 5178-5186.

155 Berezovski, M.; Krylov, S. N. *J.Am.Chem.Soc.* **2002**, *124*, 13674-13675.

156 Mironov, G. G.; Okhonin, V.; Khan, N.; Clouthier, C. M.; Berezovski, M. V. *ChemistryOpen.* **2014**, *3*, 58-64.

157 Wang, Q.; Liu, J. -.; Chen, Z.; Zheng, K. -.; Chen, C. -.; Hao, Y. -.; Tan, Z. *Nucleic Acids Res.* **2011**, *39*, 6229-6237.

158 Simonsson, T.; Pecinka, P.; Kubista, M. *Nucleic Acids Res.* **1998**, *26*, 1167-1172.

159 Dai, J.; Chen, D.; Jones, R. A.; Hurley, L. H.; Yang, D. *Nucleic Acids Res.* **2006**, *34*, 5133-5144.

160 Rankin, S.; Reszka, A. P.; Huppert, J.; Zloh, M.; Parkinson, G. N.; Todd, A. K.; Ladame, S.; Balasubramanian, S.; Neidle, S. *J.Am.Chem.Soc.* **2005**, *127*, 10584-10589.

161 Cogoi, S.; Quadrifoglio, F.; Xodo, L. E. *Biochemistry (N.Y.).* **2004**, *43*, 2512-2523.

162 Sun, D.; Guo, K.; Rusche, J. J.; Hurley, L. H. *Nucleic Acids Res.* **2005**, *33*, 6070-6080.

163 Drygin, D.; Siddiqui-Jain, A.; O'Brien, S.; Schwaebe, M.; Lin, A.; Bliesath, J.; Ho, C. B.; Proffitt, C.; Trent, K.; Whitten, J. P.; Lim, J. K. C.; Von Hoff, D.; Anderes, K.; Rice, W. G. *Cancer Res.* **2009**, *69*, 7653-7661.

164 Morris, M. J.; Negishi, Y.; Pazsint, C.; Schonhoft, J. D.; Basu, S. *J.Am.Chem.Soc.* **2010**, *132*, 17831-17839.

165 Paramasivan, S.; Rujan, I.; Bolton, P. H. *Methods.* **2007**, *43*, 324-331.

166 Zhang, A. Y. Q.; Balasubramanian, S. *J.Am.Chem.Soc.* **2012**, *134*, 19297-19308.

167 Henderson, E.; Hardin, C. C.; Walk, S. K.; Tinoco Jr., I.; Blackburn, E. H. *Cell.* **1987**, *51*, 899-908.

168 Ying, L.; Green, J. J.; Li, H.; Klenerman, D.; Balasubramanian, S. *Proc.Natl.Acad.Sci.U.S.A.* **2003**, *100*, 14629-14634.

169 Adrian, M.; Heddi, B.; Phan, A. T. *Methods.* **2012**, *57*, 11-24.

170 Zhao, Y.; Kan, Z. -.; Zeng, Z. -.; Hao, Y. -.; Chen, H.; Tan, Z. *J.Am.Chem.Soc.* **2004**, *126*, 13255-13264.

171 Campbell, N. H.; Parkinson, G. N. *Methods.* **2007**, *43*, 252-263.

172 Li, Y.; Xu, F.; Liu, C.; Xu, Y.; Feng, X.; Liu, B. -. *Analyst.* **2013**, *138*, 4475-4482.

173 Li, Y.; Xu, Y.; Feng, X.; Liu, B. -. *Anal.Chem.* **2012**, *84*, 9025-9032.

174 Olivares, J. A.; Nguyen, N. T.; Yonker, C. R.; Smith, R. D. *Anal.Chem.* **1987**, *59*, 1230-1232.

175 Drabovich, A.; Berezovski, M.; Krylov, S. N. *J.Am.Chem.Soc.* **2005**, *127*, 11224-11225.

176 Petrov, A.; Okhonin, V.; Berezovski, M.; Krylov, S. N. *J.Am.Chem.Soc.* **2005**, *127*, 17104-17110.

177 Berezovski, M.; Krylov, S. N. *J.Am.Chem.Soc.* **2002**, *124*, 13674-13675.

178 Okhonin, V.; Petrov, A. P.; Berezovski, M.; Krylov, S. N. *Anal.Chem.* **2006**, *78*, 4803-4810.

179 Cole, J. D. *Quart.Appl.Math.* **1951**, *9*, 225-236.

180 Hopf, E. *Comm.Pure Appl.Math.* **1950**, *3*, 201-230.

181 Mironov, G. G.; Okhonin, V.; Gorelsky, S. I.; Berezovski, M. V. *Anal.Chem.* **2011**, *83*, 2364-2370.

182 Musheev, M. U.; Javaherian, S.; Okhonin, V.; Krylov, S. N. *Anal.Chem.* **2008**, *80*, 6752-6757.

183 Hong, E. S.; Yoon, H. -.; Kim, B.; Yim, Y. -.; So, H. -.; Shin, S. K. *J.Am.Soc.Mass Spectrom.* **2010**, *21*, 1245-1255.

184 Vairamani, M.; Gross, M. L. *J.Am.Chem.Soc.* **2003**, *125*, 42-43.

185 Balthasart, F.; Plavec, J.; Gabelica, V. *J.Am.Soc.Mass Spectrom.* **2013**, *24*, 1-8.

186 Avila, L. Z.; Chu, Y. -.; Blossey, E. C.; Whitesides, G. M. *J.Med.Chem.* **1993**, *36*, 126-133.

187 Chu, Y. -.; Avila, L. Z.; Gao, J.; Whitesides, G. M. *Acc.Chem.Res.* **1995**, *28*, 461-468.

188 Clouthier, C. M.; Mironov, G. G.; Okhonin, V.; Berezovski, M. V.; Keillor, J. W. *Angewandte Chemie - International Edition.* **2012**, *51*, 12464-12468.

189 Arora, K.; Brooks III, C. L. *Proc.Natl.Acad.Sci.U.S.A.* **2007**, *104*, 18496-18501.

190 Haspel, N.; Moll, M.; Baker, M. L.; Chiu, W.; Kavraki, L. E. *BMC Struct.Biol.* **2010**, , 1.

191 Boehr, D. D.; Dyson, H. J.; Wright, P. E. *Chem.Rev.* **2006**, *106*, 3055-3079.

192 Boehr, D. D.; McElheny, D.; Dyson, H. J.; Wrightt, P. E. *Science.* **2006**, *313*, 1638-1642.

193 Boehr, D. D.; Nussinov, R.; Wright, P. E. *Nature Chemical Biology.* **2009**, *5*, 789-796.

194 Fanucci, G. E.; Cafiso, D. S. *Curr.Opin.Struct.Biol.* **2006**, *16*, 644-653.

195 Grant, B. J.; Gorfe, A. A.; McCammon, J. A. *Curr.Opin.Struct.Biol.* **2010**, *20*, 142-147.

196 Imamoto, Y.; Kamikubo, H.; Harigai, M.; Shimizu, N.; Kataoka, M. *Biochemistry (N.Y.).* **2002**, *41*, 13595-13601.

197 Kajihara, D.; Abe, R.; Iijima, I.; Komiyama, C.; Sisido, M.; Hohsaka, T. *Nature Methods.* **2006**, *3*, 923-929.

198 Taraban, M.; Zhan, H.; Whitten, A. E.; Langley, D. B.; Matthews, K. S.; Swint-Kruse, L.; Trewhella, J. *J.Mol.Biol.* **2008**, *376*, 466-481.

199 Berezovski, M.; Krylov, S. N. *J.Am.Chem.Soc.* **2002**, *124*, 13674-13675.

200 Petrov, A.; Okhonin, V.; Berezovski, M.; Krylov, S. N. *J.Am.Chem.Soc.* **2005**, *127*, 17104-17110.

201 De Kort, B. J.; De Jong, G. J.; Somsen, G. W. *Electrophoresis.* **2010**, *31*, 2861-2868.

202 De Kort, B. J.; Ten Kate, G. A.; De Jong, G. J.; Somsen, G. W. *Anal.Chem.* **2011**, *83*, 6060-6067.

203 Begg, G. E.; Carrington, L.; Stokes, P. H.; Matthews, J. M.; Wouters, M. A.; Husain, A.; Lorand, L.; Iismaa, S. E.; Graham, R. M. *Proc.Natl.Acad.Sci.U.S.A.* **2006**, *103*, 19683-19688.

204 Begg, G. E.; Holman, S. R.; Stokes, P. H.; Matthews, J. M.; Graham, R. M.; Iismaa, S. E. *J.Biol.Chem.* **2006**, *281*, 12603-12609.

205 Di Venere, A.; Rossi, A.; De Matteis, F.; Rosato, N.; Finazzi Agrò, A.; Mei, G. *J.Biol.Chem.* **2000**, *275*, 3915-3921.

206 Colak, G.; Keillor, J. W.; Johnson, G. V. W. *PLoS ONE.* **2011**, *6*

207 Griffin, M.; Casadio, R.; Bergamini, C. M. *Biochem.J.* **2002**, *368*, 377-396.

208 Gundemir, S.; Colak, G.; Tucholski, J.; Johnson, G. V. W. *Biochimica et Biophysica Acta - Molecular Cell Research.* **2012**, *1823*, 406-419.

209 Lorand, L.; Graham, R. M. *Nature Reviews Molecular Cell Biology.* **2003**, *4*, 140-156.

210 Mastroberardino, P. G.; Piacentini, M. *J.Intern.Med.* **2010**, *268*, 419-431.

211 Munsie, L.; Caron, N.; Atwal, R. S.; Marsden, I.; Wild, E. J.; Bamburg, J. R.; Tabrizi, S. J.; Truant, R. *Hum.Mol.Genet.* **2011**, *20*, 1937-1951.

212 Norlund, M. A.; Lee, J. M.; Zainelli, G. M.; Muma, N. A. *Brain Res.* **1999**, *851*, 154-163.

213 Selkoe, D. J.; Abraham, C.; Ihara, Y. *Proc.Natl.Acad.Sci.U.S.A.* **1982**, *79*, 6070-6074.

214 Piper, J. L.; Gray, G. M.; Khosla, C. *Biochemistry (N.Y.).* **2002**, *41*, 386-393.

215 Chhabra, A.; Verma, A.; Mehta, K. *Anticancer Res.* **2009**, *29*, 1909-1919.

216 Choi, K.; Siegel, M.; Piper, J. L.; Yuan, L.; Cho, E.; Strnad, P.; Omary, B.; Rich, K. M.; Khosla, C. *Chemistry and Biology.* **2005**, *12*, 469-475.

217 Mehta, K. *Amino Acids.* **2009**, *36*, 709-716.

218 Pinkas, D. M.; Strop, P.; Brunger, A. T.; Khosla, C. *PLoS biology.* **2007**, *5*

219 Mariani, P.; Carsughi, F.; Spinozzi, F.; Romanzetti, S.; Meier, G.; Casadio, R.; Bergamini, C. M. *Biophys.J.* **2000**, *78*, 3240-3251.

220 Pardin, C.; Roy, I.; Chica, R. A.; Bonneil, E.; Thibault, P.; Lubell, W. D.; Pelletier, J. N.; Keillor, J. W. *Biochemistry (N.Y.).* **2009**, *48*, 3346-3353.

221 Király, R.; Cssz, E.; Kurtán, T.; Antus, S.; Szigeti, K.; Simon-Vecsei, Z.; Korponay-Szabó, I. R.; Keresztessy, Z.; Fésüs, L. *FEBS Journal.* **2009**, *276*, 7083-7096.

222 Roy, I.; Smith, O.; Clouthier, C. M.; Keillor, J. W. *Protein Expr.Purif.* **2013**, *87*, 41-46.

223 Leblanc, A.; Gravel, C.; Labelle, J.; Keillor, J. W. *Biochemistry (N.Y.).* **2001**, *40*, 8335-8342.

224 Keillor, J. W.; Chica, R. A.; Chabot, N.; Vinci, V.; Pardin, C.; Fortin, E.; Gillet, S. M. F. G.; Nakano, Y.; Kaartinen, M. T.; Pelletier, J. N.; Lubell, W. D. *Canadian Journal of Chemistry.* **2008**, *86*, 271-276.

225 Mironov, G. G.; Okhonin, V.; Gorelsky, S. I.; Berezovski, M. V. *Anal.Chem.* **2011**, *83*, 2364-2370.

226 Chu, Y. -.; Avila, L. Z.; Biebuyck, H. A.; Whitesides, G. M. *J.Med.Chem.* **1992**, *35*, 2915-2917.

227 Liu, S.; Cerione, R. A.; Clardy, J. *Proc.Natl.Acad.Sci.U.S.A.* **2002**, *99*, 2743-2747.

228 Keillor, J. W.; Chica, R. A.; Chabot, N.; Vinci, V.; Pardin, C.; Fortin, E.; Gillet, S. M. F. G.; Nakano, Y.; Kaartinen, M. T.; Pelletier, J. N.; Lubell, W. D. *Canadian Journal of Chemistry.* **2008**, *86*, 271-276.

229 Caron, N. S.; Munsie, L. N.; Keillor, J. W.; Truant, R. *PLoS ONE.* **2012**, *7*

230 Pavlyukov, M. S.; Antipova, N. V.; Balashova, M. V.; Shakhparonov, M. I. *Biochem.Biophys.Res.Commun.* **2012**, *421*, 773-779.

231 Lortat-Jacob, H.; Burhan, I.; Scarpellini, A.; Thomas, A.; Imberty, A.; Vivès, R. R.; Johnson, T.; Gutierrez, A.; Verderio, E. A. M. *J.Biol.Chem.* **2012**, *287*, 18005-18017.

232 Okhonin, V.; Berezovski, M. V.; Krylov, S. N. *J.Am.Chem.Soc.* **2010**, *132*, 7062-7068.

233 Keillor, J. W.; Chica, R. A.; Chabot, N.; Vinci, V.; Pardin, C.; Fortin, E.; Gillet, S. M. F. G.; Nakano, Y.; Kaartinen, M. T.; Pelletier, J. N.; Lubell, W. D. *Canadian Journal of Chemistry-Revue Canadienne De Chimie.* **2008**, *86*, 271-276.

234 Mironov, G. G.; St-Jacques, A. D.; Mungham, A.; Eason, M. G.; Chica, R. A.; Berezovski, M. V. *J.Am.Chem.Soc.* **2013**, *135*, 13728-13736.

235 Edwards, D. R.; Lohman, D. C.; Wolfenden, R. *J.Am.Chem.Soc.* **2012**, *134*, 525-531.

236 García-Urdiales, E.; Alfonso, I.; Gotor, V. *Chem.Rev.* **2005**, *105*, 313-354.

237 Casado, V.; Martín, D.; Torres, C.; Reglero, G. *Methods in Molecular Biology.* **2012**, *861*, 495-523.

238 Savile, C. K.; Janey, J. M.; Mundorff, E. C.; Moore, J. C.; Tam, S.; Jarvis, W. R.; Colbeck, J. C.; Krebber, A.; Fleitz, F. J.; Brands, J.; Devine, P. N.; Huisman, G. W.; Hughes, G. J. *Science.* **2010**, *329*, 305-309.

239 Clouthier, C. M.; Pelletier, J. N. *Chem.Soc.Rev.* **2012**, *41*, 1585-1605.

240 Turner, N. J. *Nature Chemical Biology.* **2009**, *5*, 567-573.

241 Sanderson, K. *Nature.* **2011**, *471*, 397-398.

242 Höhne, M.; Schätzle, S.; Jochens, H.; Robins, K.; Bornscheuer, U. T. *Nature Chemical Biology.* **2010**, *6*, 807-813.

243 Luo, X. J.; Yu, H. L.; Xu, J. H. *Enzyme Eng.* **2012**, *1*

244 Raj, H.; Szymanski, W.; De Villiers, J.; Rozeboom, H. J.; Veetil, V. P.; Reis, C. R.; De Villiers, M.; Dekker, F. J.; De Wildeman, S.; Quax, W. J.; Thunnissen, A. -. W. H.; Feringa, B. L.; Janssen, D. B.; Poelarends, G. J. *Nature Chemistry.* **2012**, *4*, 478-484.

245 Dorgan, K. M.; Wooderchak, W. L.; Wynn, D. P.; Karschner, E. L.; Alfaro, J. F.; Cui, Y.; Zhou, Z. S.; Hevel, J. M. *Anal.Biochem.* **2006**, *350*, 249-255.

246 Cooper, A. J. L.; Conway, M.; Hutson, S. M. *Anal.Biochem.* **2002**, *308*, 100-105.

247 Palamakumbura, A. H.; Trackman, P. C. *Anal.Biochem.* **2002**, *300*, 245-251.

248 Miners, J. S.; Verbeek, M. M.; Rikkert, M. O.; Kehoe, P. G.; Love, S. *J.Neurosci.Methods.* **2008**, *167*, 229-236.

249 Zhang, R. -.; Xu, X. -.; Chen, T. -.; Li, L.; Rao, P. -. *Anal.Biochem.* **2000**, *280*, 286-290.

250 Iqbal, J.; Jirovsky, D.; Lee, S. -.; Zimmermann, H.; Müller, C. E. *Anal.Biochem.* **2008**, *373*, 129-140.

251 Anumula, K. R. *Glycobiology.* **2012**, *22*, 912-917.

252 Liesener, A.; Perchuc, A. -.; Schöni, R.; Wilmer, M.; Karst, U. *Rapid Communications in Mass Spectrometry.* **2005**, *19*, 2923-2928.

253 Partserniak, I.; Werstuck, G.; Capretta, A.; Brennan, J. D. *ChemBioChem.* **2008**, *9*, 1065-1073.

254 Pi, N.; Leary, J. A. *J.Am.Soc.Mass Spectrom.* **2004**, *15*, 233-243.

255 Forsberg, E. M.; Green, J. R. A.; Brennan, J. D. *Anal.Chem.* **2011**, *83*, 5230-5236.

256 Scheerle, R. K.; Grassmann, J.; Letzel, T. *Analytical Sciences.* **2012**, *28*, 607-612.

257 Ernst, O.; Zor, T. *Journal of Visualized Experiments.* **2010**,

258 Xie, T.; Ren, R.; Zhang, Y. -.; Pang, Y.; Yan, C.; Gong, X.; He, Y.; Li, W.; Miao, D.; Hao, Q.; Deng, H.; Wang, Z.; Wu, J. -.; Yan, N. *J.Biol.Chem.* **2012**, *287*, 794-802.

259 Kok, M. G. M.; de Jong, G. J.; Somsen, G. W. *Electrophoresis.* **2011**, *32*, 3016-3024.

260 Yang, Y.; Boysen, R. I.; I-Chen Chen, J.; Keah, H. H.; Hearn, M. T. W. *Journal of Chromatography A.* **2003**, *1009*, 3-14.

261 Okhonin, V.; Liu, X.; Krylov, S. N. *Anal.Chem.* **2005**, *77*, 5925-5929.

262 Krylova, S. M.; Okhonin, V.; Krylov, S. N. *Journal of Separation Science.* **2009**, *32*, 742-756.

263 Okhonin, V.; Wong, E.; Krylov, S. N. *Anal.Chem.* **2008**, *80*, 7482-7486.

264 Eliot, A. C.; Kirsch, J. F. *Annual Review of Biochemistry.* **2004**, *73*, 383-415.

265 Yagi, T.; Kagamiyama, H.; Motosugi, K.; Nozaki, M.; Soda, K. *FEBS Lett.* **1979**, *100*, 81-84.

266 Kagamiyama, H.; Hayashi, H. *Methods in Enzymology.* **2000**, *324*, 103-113.

267 Fuchikami, Y.; Yoshimura, T.; Gutierrez, A.; Soda, K.; Esaki, N. *J.Biochem.* **1998**, *124*, 905-910.

268 RUDMAN, D.; MEISTER, A. *The Journal of biological chemistry.* **1953**, *200*, 591-604.

269 Martinez-Carrion, M.; Jenkins, W. T. *The Journal of biological chemistry.* **1965**, *240*, 3538-3546.

270 Hayashi, H.; Inoue, K.; Nagata, T.; Kuramitsu, S.; Kagamiyama, H. *Biochemistry (N.Y.).* **1993**, *32*, 12229-12239.

271 Onuffer, J. J.; Ton, B. T.; Klement, I.; Kirsch, J. F. *Protein Science.* **1995**, *4*, 1743-1749.

272 Bommer, M.; Ward, J. M. *Enzyme Microb.Technol.* **2013**, *52*, 218-225.

273 Powell, J. T.; Morrison, J. F. *European Journal of Biochemistry.* **1978**, *87*, 391-400.

274 Goto, M.; Miyahara, I.; Hayashi, H.; Kagamiyama, H.; Hirotsu, K. *Biochemistry (N.Y.).* **2003**, *42*, 3725-3733.

275 Peisach, D.; Chipman, D. M.; Van Ophem, P. W.; Manning, J. M.; Ringe, D. *Biochemistry (N.Y.).* **1998**, *37*, 4958-4967.

276 Gartside, S. E.; Cowen, P. J.; Sharp, T. *Neuropharmacology.* **1992**, *31*, 9-14.

277 Murch, S. J.; KrishnaRaj, S.; Saxena, P. K. *Plant Cell Rep.* **2000**, *19*, 698-704.

278 Sarzi Puttini, P.; Caruso, I. *J.Int.Med.Res.* **1992**, *20*, 182-189.

279 Cangiano, C.; Ceci, F.; Cascino, A.; Del Ben, M.; Laviano, A.; Muscaritoli, M.; Antonucci, F.; Rossi-Fanelli, F. *Am.J.Clin.Nutr.* **1992**, *56*, 863-867.

280 Trouillas, P.; Serratrice, G.; Laplane, D.; Rascol, A.; Augustin, P.; Barroche, G.; Clanet, M.; Degos, C. F.; Desnuelle, C.; Dumas, R.; Michel, D.; Viallet, F.; Warter, J. M.; Adeleine, P. *Arch.Neurol.* **1995**, *52*, 456-460.

281 Birdsall, T. C. *Alternative Medicine Review.* **1998**, *3*, 271-280.

282 Koo, J.; Avakian, S.; Martin, G. J. *J.Org.Chem.* **1959**, *24*, 179-183.

283 Frangatos, G.; Chubb, F. L. *Can.J.Chem.* , *37*

284 Turner, E. H.; Blackwell, A. D. *Med.Hypotheses.* **2005**, *65*, 138-144.

285 Day, N.; Keillor, J. W. *Anal.Biochem.* **1999**, *274*, 141-144.

286 Baici, A.; Luisi, P. L.; Olomucki, A.; Doublet, M. O.; Klincak, J. *European Journal of Biochemistry.* **1974**, *46*, 59-66.

287 Deu, E.; Koch, K. A.; Kirsch, J. F. *Protein Science.* **2002**, *11*, 1062-1073.

288 Cutillas, P. R.; Khwaja, A.; Graupera, M.; Pearce, W.; Gharbi, S.; Waterfield, M.; Vanhaesebroeck, B. *Proc.Natl.Acad.Sci.U.S.A.* **2006**, *103*, 8959-8964.

289 Tholey, A.; Zabet-Moghaddam, M.; Heinzle, E. *Anal.Chem.* **2006**, *78*, 291-297.

290 Hwang, B. -.; Cho, B. -.; Yun, H.; Koteshwar, K.; Kim, B. -. *J Molec Catal B.* **2005**, *37*, 47-55.

291 Panke, S.; Held, M.; Wubbolts, M. *Curr.Opin.Biotechnol.* **2004**, *15*, 272-279.

292 Schulze, B.; Wubbolts, M. G. *Curr.Opin.Biotechnol.* **1999**, *10*, 609-615.

293 Bhattacharyya, D.; Nguyen, K.; Basu, S. *Biochemistry (N.Y.).* **2014**, *53*, 5461-5470.

294 Muszbek, L.; Ariëns, R. A.; Ichinose, A. *Journal of Thrombosis and Haemostasis.* **2007**, *5*, 181-183.

295 McKeague, M.; Derosa, M. C. *Journal of Nucleic Acids.* **2012**, *2012*